DOE/ID/13320-3

Improved Life of Die Casting Dies of H13 Steel by Attaining Improved Mechanical Properties and Distortion Control During Heat Treatment

Final Report

J. F. Wallace
D. Schwam

October 1998

Work Performed Under Contract No. DE-FC07-94ID13320

For
U.S. Department of Energy
Assistant Secretary for
Energy Efficiency and Renewable Energy
Washington, DC

By
Case Western Reserve University
Cleveland, OH

DOE/ID/13320-3

IMPROVED LIFE OF DIE CASTING DIES OF H13 STEEL BY ATTAINING IMPROVED MECHANICAL PROPERTIES AND DISTORTION CONTROL DURING HEAT TREATMENT

FINAL REPORT

J. F. Wallace
D. Schwam

October 1998

Work Performed Under Contract No. DE-FC07-94ID13320

Prepared for the
U.S. Department of Energy
Assistant Secretary for
Energy Efficiency and Renewable Energy
Washington, DC

Prepared by
Case Western Reserve University
Cleveland, OH

DISCLAIMER

DISCLAIMER

Portions of this document may be illegible in electronic image products. Images are produced from the best available original document.

ABSTRACT

Optimum heat treatment of dies, quenching in particular, are critical in ensuring satisfactory performance in service. Rapid cooling rates increase the thermal fatigue or heat checking resistance of the steel. However, very fast cooling rates can also lead to distortion, and lower fracture toughness values, increasing the danger of catastrophic fracture.

The ultimate goal of this project is to increase die life by using fast enough quenching rates (more than 30°F/min average cooling rate from 1750°F to 550°F - 1/2" below working surfaces) to obtain good toughness and fatigue resistance in Premium Grade H-13 steel dies. The main tasks of the project were:

- Compile database on physical and mechanical properties of H-13.
- Conduct gas quenching experiments to determine cooling rates of dies in different vacuum furnaces.
- Measure the as-quenched distortion of dies and the residual stresses.
- Generate Finite Element Analysis models to predict cooling rates, distortion and residual stress of gas quenched dies.
- Establish rules and create PC-based expert system for prediction of cooling rates, distortion and residual stress in vacuum/gas quenched H-13 dies.

An iterative approach of computer modeling validated by experimental measurements was taken, as illustrated in figure 1. In the first cycle a simple shape, rectangular block, was used for the computer model and the experiments. Subsequently, modeling of a more intricate die shape was undertaken.

Cooling curves during gas quenching of H-13 blocks and die shapes have been measured under a variety of gas pressures, i.e. 2 bar, 5 bar, 7.5, 10 bar nitrogen, 4 bar argon, 20 bar nitrogen + helium and oil. Dimensional changes caused by the above gas quenching processes have been determined by accurate mapping of all surfaces with Coordinate Measuring Machines before and after the quench. Residual stresses were determined by the ASTM E837 hole-drilling strain gage method. To facilitate the computer modeling work, a comprehensive database of H-13 mechanical and physical properties has been compiled. Finite Element Analysis of the heat treated shapes has been conducted using the TRAST/ABAQUS codes.

AN ITERATIVE PROCESS OF DEVELOPING RULES FOR QUENCHING DISTORTION OF H-13 DIES

COMPUTER MODELING	EXPERIMENTAL
1. Build thermal FEA model for simple (block) H-13 shape.	2. Validate model prediction by quenching experiment; fine tune parameters.
3. Build distortion FEA model for H-13 block.	4. Measure distortion (CMM) of the H-13 block.

5. Compare predicted to measured block distortion; Refine model and parameters to improve fit.

6. Build thermal FEA model for H-13 die.	7. Validate model prediction by quenching experiment; fine tune parameters.
8. Build distortion FEA model for H-13 die.	9. Measure distortion (CMM) of the H-13 die.

10. Compare predicted to measured die distortion; Refine model and parameters to improve fit.

The project has successfully completed all the experimental goals. Detailed distortion mapping of large H13 blocks and dies was conducted with a CMM machine. Concomitantly, the cooling curves at different locations in the block/die were measured. This procedure was repeated for different quenching gas pressures, utilizing stateof the art vacuum heat treating furnaces. A quantitative correlation was established for the block shaped parts between the cooling rate from austenitizing temperature and the cooling rate. Essentially, in the experimental window of 10degrees F/min to 150 degrees F/min measured in these large blocks and dies, the higher cooling rates yield more distortion. The main sources of distortion are the plastic deformation occurring early on in the quench and the volume changes induced by the phase transformation. As the outside of the part cools and contracts, it applies large stresses on the inside that is still hot, hence causing plastic deformation. Ultimately, the distortion is determined by how thick and strong the colder outside "shell" is. If the "shell" is strong enough to resist the internal stresses applied by the hot core, the part will not distort excessively. Industrial heat treating practice includes means to control excessive distortion by interrupting the quench before the onset of the martensitic transformation. This interruption slows down the cooling rate around 750 degrees F-1000 degrees F. This stabilizes the internal stresses and allows the surface and core temperatures to equalize. The nitrogen gas quench is normally continued after these temperatures are within 200°F. The interrupted quench combines the benefits of a fast cooling rate in the critical range with an acceptable distortion level. The controlled experiments conducted by this project demonstrate a significant decrease in distortion of 30-40% facilitated by the interrupted quench procedure.

The computer modeling part of the project was successful in handling the temperature distribution in the part during the quench. Good fit of modeled vs. measured quenched rates has been demonstrated for simple die shapes. The models also predict well the phase transformation products resulting from the quench. These models assume no distortion during heating to the austenitizing temperature, which is the case with slow heating. The models account for latent heat, thermal and phase transformation strains as well as plastic deformation.

There is a good fit between the predicted and measured distortion contours. However, the magnitude of the predicted distortion and residual stresses does not match well the measured values. Further fine tuning of the model is required before it can be used to predict distortion and residual stress in a quantitative manner. This last step is a prerequisite to generating rules for a reliable expert system.

LIST OF CONTENTS

I. INTRODUCTION

This report outlines work done under CWRU Subproject OPE-R&D-95-212 "Improved Life of Die Castings of H-13 by Attaining Improved Mechanical Properties and Distortion Control During Heat Treatment", sponsored by the Department of Energy, under the Metal Casting Competitiveness Research Program. It is part of the a larger project on "Research, Development and Demonstration of Die Casting Research to Increase the Competitiveness of the U.S. Foundry Industry". The larger project was submitted by Ohio State University, that subsequently coordinated and monitored the subprojects.

Finite Element Analysis and computer simulation are revolutionizing design and manufacturing processes. Application of these techniques results in significant time and money savings. Prototyping and preliminary designs of products that used to take months, and involve expensive iterative trial and error runs can be shortened or eliminated. A critical aspect of using these methods in die fabrication is availability of reliable material data. In addition, the computer predictions need to be carefully validated on select models, before using them on a wider scale.

The report includes a compilation of material properties for H-13 and related steels. A format similar to the Aerospace Structural Metals Handbook was adopted for this compilation to facilitate comparison with H-11, covered by this source. A bibliography of publications on these steels is also included in the report. These are provided in print as well as Procite files.

Control of distortion during heat treating of die steels is a critical aspect of die fabrication, with major technical and economic implications. Currently, dies can be brought to final dimensions within the tight required tolerances only after final heat treatment. This behooves die makers to leave generous feedstock to be removed in the hard, tough, hardened condition by expensive grinding or to utilize Elecro-Discharge Machining (EDM) methods, followed by more heat treatment. Ideally, die makers would prefer to machine dies to final dimensions before heat treatment. In the present generation of die steels, some heat treating distortion is unavoidable if the best mechanical properties are to be attained. It follows that the only practical way to minimize post-heat treatment machining would be to predict distortion and offset it in advance by allowing the right amount of material at the right locations.

Many attempts have been made over the years to predict and control quenching distortion. The few successful cases were limited to very specific part geometries and processing conditions. The multitude of parameters that affect distortion makes this task extremely difficult to accomplish. A fascinating example is the effect of quenchant flow direction on the distortion. Everything else being identical, the distortion measured off round cylinders under such cooling conditions shows a remarkable dependency on the direction of the flow.

Two recent developments are turning prediction of heat treating die distortion by die makers into a more feasible task:

(a) Vacuum/pressure gas quenching of dies. As this method becomes more common, there is a better chance to achieve improved, reproducible control over the quenching process.

(b) Availability of lower cost Finite Element Analysis computer software, and the necessary computer hardware to run it. At the time of this writing, the availability of FEA codes for heat treating distortion is very limited, and requires relatively expansive workstations. However, many FEA software houses are beginning to offer PC versions of their codes and the Pentium PC computers are capable of running such applications.

1. Literature Review *

The distortion that accompanies heat treatment has been a problem to the heat treaters over the years. Factors affecting distortion and the different means to control it has been the subject of various literature. These factors include the structure and composition of the steel, the properties, residual stress, cross-section, and surface condition [1,2,3,4]. Another important factor is the heat treatment process itself; the furnace characteristics, the quenching operation [1,2,3,5,6,7] and even the racking operation [3,7] contribute to the distortion.

---

* - Based on "Prediction of Heat-up and Distortion in the Heat Treatment of Steels", M.Sc. Thesis by Melrex Ordillas, Case Western Reserve University, May 1994. Adviser, Prof. J.F. Wallace.

In the area of materials control, heat treaters and their customers are now more aware of the effect of materials quality on distortion. Many keep track of the steel grades as well as requiring a controlled and "clean" steel. Efforts are exerted to provide a steel with "low and stable distortion". For example, Fukuzumi et al [4] of Mitsubishi Steel studied the effects of impurities. In a recent publication, Fukuzumi noted that addition of aluminum to steel as a deoxidizer and a grain refiner, has a marked effect on distortion. He has shown that a controlled amount of aluminum and nitrogen, which form aluminum nitride in the austenite phase will minimize distortion.

Different aspects of the quenching process are being studied. Quench bath flow analysis has been done by Lally and Kearny [8]. These studies, however, were conducted using a quench tank in the unloaded condition and could not be extended to tanks with actual parts. The primary reason for the narrow focus of the project is the complexity of the fluid flow and fluid flow analysis. Different types of quenchants and quenching methods were evaluated. These include the use of variable agitation [9], spray cooling [10], fluidized bed [11], salt bath [12], PAG [13], martempering [14], interrupted quench [15], inert gas quenching [16], and vacuum quenching [17].

Computer systems for process controls and on-line monitors for the heat treating process have been developed. Marathon and Honeywell have developed systems that can monitor the furnace and the quench bath temperature, check the carbon potential, and even alert the operator of possible processing abnormalities. Equipment has also been developed to obtain experimental information on the cooling and quenching rate. Segerberg and Bodin [18] have developed the "Quenchotest" - an equipment used for plotting cooling curves during quenching.

With the advent of improved computers and the development of the finite element method, as well as the popularity of modeling and simulation, a number of studies have modeled the quenching process and distortion in steels. One of the earlier finite element analysis of the quenching process was conducted by Burnett [19] in 1977, who studied the development of the

residual stress in carburized 8620 steel cylinders. The cylinders were 0.5 inch in diameter and 8 inches long. The focus of this research was on the residual stress, not distortion nor its relation to the residual stress. By the mid 1980's and onward, more studies were conducted on heat treatment stresses and the accompanying phase transformation including studies on the internal and quenching stresses by Denis [20], Sjostrom [21], LeBlond [22], and Li [23,24].

More recent studies have dealt with distortion, its prediction and the mechanisms that control it. Henrikson [25] et al modeled the distortion of thin strips of 4023 and 4620 steels of varying thicknesses and carburized on 1 side, using finite element method. The prediction of his model did not agree with experimental data. The authors stated that distortion and residual stress are sensitive to constitutive parameters and carbon contents. Buckmayr and Kirkaldy [26] built a coupled FEM model for the holistic determination of the temperature field, microstructure and residual stress. The software included a calculation of the transient temperature, phase transformation, microstructural evolution, mechanical response (distortion and residual stresses), and hardenability. No equations were presented in the paper nor were there any comparison made to actual data. Ramakrishnan [27] modeled the heat treatment of nickel-based superalloys. The experimental part included a test run with 13 thermocouples to determine the cooling rate at the interior of the alloy, from which an inverse heat conduction code was used to calculate the surface heat flux distribution. Thus, the thermal history of the locations inside the part were calculated, experimentally verified and the thermally induced stresses as well as the distortion were calculated. However, the distortion results were not compared to the actual parts. Other studies of the same nature were done by Saboury [28] and Petrus [29].

Inoue [30] of Kyoto University in Japan has developed a Metallo-thermo mechanical theory that considers the interaction between metallurgical, thermal and the mechanical aspects during heat treatment to predict distortion. Kamamoto et al [31] used the finite element method to calculate the transient stresses occurring during quenching. From this, the residual stresses were determined and distortion effects were estimated. The emphasis was on the residual stress calculation. No comparison to real distortion data was presented in this study. Persampieri [32]

developed a methodology for predicting the final microstructure, residual stress and deformation of a steel during heat treatment. This approach led to a better understanding of the process, and allows for a sensitivity analysis of the operation, but no distortion results were presented. A study which compares the actual distortion against the simulated or calculated distortion was done by Askel [33]. Aluminum (commercial purity) and aluminum alloys were used in this experiment. Askel employed FEM to model and simulate the distortion of the bar from experimental data.

The quenching experiment is not realistic because a 12" X 3" aluminum block was used, and only the first quarter inch of the width was quenched, leaving the 2 3/4 inch above the water. Simulation results were 30% different from the actual measured distortion values. The practicality of employing these studies, however is limited.

In the above distortion simulations, the finite element method has been used extensively because it is the only means that can simulate distortion. Research is in the direction of specializing finite element codes to suit particular applications. Finite element programs that incorporate microstructural evolution and transformation effects into thermal stress calculations are under development. Of these, HEARTS from CRC Corp. in Japan, TRAST (runs in ABAQUS) from Linkoping University in Sweden, and SYSWELD from Framasoft in France are the most well developed and closest to commercialization.

REFERENCES

1. Howes, M.A. Factors Affecting Distortion in Hardened Steel Components. Conference Proceeding: Quenching and Distortion Control, G.E. Totten, ed. September 1992. pp 251 - 258.

2. Krauss, G. Heat Treatment, Microstructures, and Residual Stresses in Carburized Steels. Factors Affecting Distortion in Hardened Steel Components. Conference Proceeding: Quenching and Distortion Control, G.E. Totten, ed., September 1992. pp 181 - 191.

3. Walton, H. Dimensional Changes During hardening and Tempering of Through-Hardened Bearing Steels. Conference Proceeding: Quenching and Distortion Control, G.E. Totten, ed. September 1992. pp 265 - 273.

4. Fukuzumi, T. and T. Yoshimura. Reduction of Distortion Caused by Heat Treatment on Automobile Gear Steels. Conference Proceeding: Quenching and Distortion Control, G.E. Totten, ed., September 1992. pp 199 - 203.

5. Mikita, Yoshio, Ichiro Nakabayashi, and Kiyoshi Sakamaki. How Quench Conditions affect Cracking in Tapered Cylinders. Heat Treating. December 1989. pp 21 - 24.

6. Moerdijk, W.A. Effects of Process Parameters on Distortion. Conference Proceeding: Quenching and Distortion Control, G.E. Totten, ed., September 1992. pp 287 - 296.

7. Von Bergen, R.T. The Effects of Quenchant Media Selection and Control on the Distortion of Engineered Steel Parts. Conference Proceeding: Quenching and Distortion Control, G.E. Totten, ed. September 1992. pp 275 - 282.

8. Lally, K.S., M.W. Kearny, and G.E. Totten. Quench Tank Agitation. Conference Proceeding: Quenching and Distortion Control, G.E. Totten, ed., September 1992. pp 95 - 105.

9. Han, S.W., S.G. Yun, and G.E. Totten. Continuously Variable Agitation in Quench System Design. Conference Proceeding: Quenching and Distortion Control,G.E. Totten,ed. September 1992. pp 119-126.

10. Hodgson, P.D., K.M. Browne, R.K. Gibbs, T.T. Pham, and D.C. Collinson. The Mathematical Modeling of Temperature and Microstructure During Spray Cooling. Conference Proceeding: Quenching and Distortion Control, G.E. Totten, September 1992. pp 41 - 49.

11. Dinunzi, A. Advances in Fluidized Bed Quenching. Conference Proceeding: Quenching and Distortion Control,G.E. Totten,ed. September 1992. pp 74 - 78.

12. Foreman, R. W. Salt Bath Quenching. Conference Proceeding: Quenching and Distortion Control,G.E. Totten,ed. September 1992. pp 119-126.

13. Howard, R.D. and L.F. Comb. Poly(Alkylene Glycol) Concentration Control and Reclamation Using Membrane Technology as Applied to Steel Heat Treatment. Conference Proceeding: Quenching and Distortion Control,G.E. Totten,ed. September 1992. pp 107-112.

14. Brennan, R. J. Distortion Control With Martempering Oils. Conference Proceeding:Quenching and Distortion Control, G.E. Totten, ed., September 1992. pp 83 - 86.

15. Mikita, Yoshio, Ichiro Nakabayashi, and Kiyoshi Sakamaki. How Quench Conditions affect Cracking in Tapered Cylinders. Heat Treating. December 1989. pp 21 - 24.

16. Karpov, L.P. Low-Distortion Quenching in Inert Gases. Material Science and Heat Treatment, Vol 15. September 1973. pp 857 - 862.

17. Holoboff, R., B. Lhote, R. Speri, and O. Delcourt. Vacuum Quenching Improvements Through Controlled Atmospheres. Conference Proceeding: Quenching and Distortion Control, G.E. Totten, ed. September 1992. pp 113 - 117.

18. Segerberg,S and J. Bodin. Variation in the Heat Transfer Coefficient Around Components of Different Shapes During Quenching. Conference Proceeding: Quenching and Distortion Control, G.E. Totten, ed. September 1992. pp 165 - 170.

19. Burnett, J.A. Evaluation of Elastic-Plastic Stresses in Quenched Carburized Cylinders by FEM. Ph.D. Thesis, University of Akron. 1977.

20. Denis, S, E. Gautier, A. Simon, and G. Beck. Stress-Phase-Transformation Interactions - Basic Principles, Modelling, and Calculation of Internal Stresses. Materials Science and Technology, Vol. 1. October 1985. pp 805 - 814.

21. Sjostrom, S. Interactions and Constitutive Models for Calculating Quench Stresses In Steel. Materials Science and Technology. Vol 1. October 1985. pp 823 - 829.

22. Leblond, J.B., Mattle, G., Devaus, J., and J.C. Devaux. Mathematical Models of Anisothermal Phase Transformations in Steels, and Predicted Plastic Behavior. Materials Science and Technology. October 1985. Vol 1. pp 815-822.

23. Li, Y.Y. and Y. Chen. Modeling Quenching to Predict Residual Stress and Microstructure Distribution. Transactions of the ASME. Vol 110, October 1988. pp 372 - 379.

24. Li, Y.Y. Modeling Quenching to Predict Residual Stress and Microstructure Distribution. Ph.D. Thesis. October 1988

25. Henrikson, M., D.B. Larson and C.J. Van Tyne. Modeling Distortion and Residual Stress in Carburized Steels. Conference Proceeding: Quenching and Distortion Control, G.E. Totten, ed., September 1992. pp 213 - 219.

26. Buchmayr, B. and J.S. Kirkaldy. A Fundamental Based Microstructural Model for the Optimization of Heat Treatment Processes. Conference Proceeding: Quenching and Distortion Control, G.E. Totten, ed., September 1992. pp 221 - 227.

27. Ramakrishnan, R.I. Quench Analysis of Aerospace Components Using FEM. Conference Proceeding: Quenching and Distortion Control, G.E. Totten, September 1992. pp 235-242.

28. Saboury, S. Effect of Carburizing Process Parameters on Distortion of AISI 4118 Gears. Conference Proceeding: Quenching and Distortion Control, G.E. Totten, September 1992. pp 259 - 264.

29. Petrus, G. T. Krauss, and B.L. Ferguson. Distortion Prediction Using the Finite Element Method. Conference Proceeding: Quenching and Distortion Control, G.E. Totten, ed., September 1992. pp 283 - 286.

30. Inoue, T.,D-Y. Ju, and K. Arimoto. Metallo-Thermo-Mechanical Simulation of Quenching Process - Theory and Implementation of Computer Code "HEARTS". Conference Proceeding: Quenching and Distortion Control, G.E. Totten, September 1992. pp 205-212.

31. Kamamoto, S., T. Nishimori and S. Kinoshita. Analysis of Residual Stress and Distortion Resulting from Quenching in Large Low-Alloy Steel Shafts. Materials Science and Technology, Vol 1. October 1985. pp 798 - 804

32. Persampieri, David, Arturo San Roman and Peter Hilton, Improved Heat Treating of Critical Parts Via Numerical Modeling. Industrial Heating. November 1990. pp 20 - 24.

33. Askel, B., W.R. Arthur, and S. Mukherjee. A Study of Quenching: Experiment and Modeling. Journal of Engineering for Industry. Vol 114, August 1992. pp 309 - 313.

34. Beer, Ferdinand P. and Russell Johnston, Jr. Vector Mechanics for Engineers, 4th Ed. McGraw-Hill Book Co. 1984. pp 159 - 160.

35. Wallace J.F. and Michal G.M. "Quench Calculator" for H-13 Die Steels for Aluminum Die Casting, May 1986.

2. Prediction of Cooling Curves and Microstructures

2.1 Calculation of Cooling Rates

A computer program was developed to calculate the cooling rates of arbitrary size blocks of H13 steel [35]. The k and h values used in this program were derived from experimental cooling curves obtained under different quenching conditions. Table I lists the quench media for which the h parameter was calculated. Also listed is the corresponding value for the surface heat transfer coefficient which was obtained from each h.

The program was tested against experimentally determined curves, and proved that it could accurately track experimentally determined cooling curves for H13 steel. A comparison between calculated and experimentally determined cooling curves for a 10 inch cube of H13 steel quenched in helium at 2 atmospheres pressure is shown in Figure 2. The calculated and experimentally determined cooling curves are essentially identical over the entire range of temperatures measured at the center of the block. For the surface of the block, the initial cooling curves differ, but then converge over the temperature range of importance for determining the microstructure i.e. 1750 to 750°F. Thus, the heat transfer model was shown to successfully simulate the cooling rates of the H13 steel die blocks.

The heat transfer model was used to calculate the cooling rates for a variety of die block shapes. These block sizes are summarized in Table II. For shapes that differ substantially from a parallepiped, the key section thickness combined with the surface to volume ratio shown in table II for that section can be used to find the equivalent rectangular parallepiped block shape. Cooling rates were computed at the block surface and at a depth of one quarter of the section thickness below the surface, i.e. the mid-radius position. The various quenching media and conditions for which cooling rates were determined are listed in table I. All cooling rates were computed based upon an initial block temperature of 1900°F. For each combination of block

thickness, shape, location and quench media, an average cooling rate over two temperature ranges was computed. The first range was from 1750 to 1550°F. The cooling rate over that range of temperatures was used to assess the amount of MC precipitation formed on austenite grain boundaries. The second range was from 1550 to 750°F. The cooling rate over this range of temperature was used to determine the matrix phases and their amounts that would form due to the particular quench conditions.

2.2 Prediction of Microstructures

The model is based on work in the literature, showing that for a given austenizing temperature and subsequent cooling rate, a specific H13 microstructure is developed. The correlation between cooling rate and microstructure is summarized in the continuous cooling diagram for H13 steel shown in figure 3. The amounts of martensite, bainite and pearlite developed for several specific cooling rates are indicated in the figure. Interpolation of these results yielded figure 4 which shows the amounts of martensite, bainite and pearlite formed as continuous function of cooling rate.

The cooling rates for the range of H13 block sizes listed in Table II quenched in the ten quenchants listed in Table I were correlated, through the use of figures 4 and 5, with the type and amount of each phase in the matrix microstructure. These results are summarized in Tables III Through IIIj. The percentage of pearlite P, bainite b, and martensite M are listed for the surface and quarter thickness positions for each H13 block size, shape and quenchant employed.

The matrix microstructures are predicted in table III depending upon the H13 block size, shape and quenchant employed. The extremes in block geometry are the 2 inch cube at the small end and the 14 inch cube at the large end. The constituents of the matrix microstructure for the 2 and 14 inch blocks as a function of quenchant are listed in Table V. The microstructures at the surface and mid-radius positions of the 2 inch block are essentially identical. The slow vacuum quench produced a 28% bainite/ 72% martensite structure, while the rapid polymeric quenchants

were able to produce essentially 100% martensite at both positions for the 2 inch block. The 14 inch cube shows a much wider variation in matrix microstructures. The cooling rate in vacuum is so slow that pearlite is formed. Only the very rapid quench of the 10% UCON A polymeric solution could produce a 100% martensite structure on the surface of the 14 inch cube. At the mid-radius position of the 14 inch cube the matrix microstructure observed is relatively insensitive to the quench employed. Again, this is due to the heat extraction through the H13 steel controlling the cooling rate, and thus the microstructure.

The microstructural constituents listed in Tables III and IIIc are based upon nitrogen and helium gas quenches run at 2 atm. pressure, and a gas velocity of 3,400 ft/min. The microstructural constituents expected for quenches run at other pressures and gas velocities can be estimated through knowledge of the relationship between pressure P, gas velocity v and the surface heat transfer coefficient H. For a given type of gas, these parameters are related by the equation:

$$H = a\sqrt{Pv}$$

In this equation, a is a constant of proportionality that is unique for a particular gas. For helium gas at a temperature of about 100°F, a is equal to 0.23, with P in atmospheres, v in ft/min and H in BTU/hr-ft^2-°F. The equivalent value of a for nitrogen is 0.17. By using these constants in the equation, H can be estimated for helium or nitrogen gas quenching at any values of P and v. Once H is determined for a given gas quenching condition, values for the microstructural constituents predicted can be obtained by a linear interpolation of microstructural component as function of H. This is done by looking up the microstructures predicted in Table III for an H just below the one calculated. The results of such an interpolation procedure are listed in Table VI. This example shows both the effect of decreasing nitrogen gas pressure to 1.5 atm. and velocity to 1,500 ft/min and increasing helium gas pressure to 5 atm. and velocity to 5,000 ft/min.

TABLE I: The Average Convective Heat-Transfer Coefficient Determined For Various Quench Procedures

QUENCHANT	H(BTU/HR-FT^2-°F)
Vacuum at 100°F	3.6
Nitrogen at 100°F, 2 atm. and 3,400 ft/min.	13.9
Helium at 100°F, 2 atm. and 3,400 ft/min.	19.2
Low Speed Oil - at 100°F	47.1
Fluidized Alumina at 100°F	61.7
High Speed Rape/Parafin Oil at 100°F	104.5
Salt at 750°F	105.9
Salt at 575°F	122.2
30% UCON A Solution at 100°F	159.2
10% UCON A Solution at 100°F	293.3

TABLE II: RANGE OF GEOMETRIES FOR THE H13 STEEL BLOCKS

Thickness (Inch)	Width X Length (Inch X Inch): Numbers in parentheses are the surface area to volume ratios for the blocks												
2"	2x14 (2.14)	2x10 (2.20)	2x8 (2.25)	2x6 (2.33)	2x4 (2.5)	2x3 (2.67)	2x2 (3.00)	3x3 (2.33)	4x4 (2.00)	6x6 (1.67)	8x8 (1.50)	10x10 (1.40)	14x14 (1.29)
3"	3x14 (1.48)	3x10 (1.53)	3x8 (1.58)	3x6 (1.67)	3x4 (1.83)	3x3 (2.00)	4x4 (1.67)	6x6 (1.33)	8x8 (1.17)	10x10 (1.07)	14x14 (0.95)		
4"	4x14 (1.14)	4x10 (1.20)	4x8 (1.25)	4x6 (1.33)	4x4 (1.50)	6x6 (1.17)	8x8 (1.00)	10x10 (0.90)	14x14 (0.79)				
6"	6x14 (0.81)	6x10 (0.87)	6x8 (0.92)	6x6 (1.00)	8x8 (0.83)	10x10 (0.73)	14x14 (0.62)						
8"	8x14 (0.64)	8x10 (0.70)	8x8 (0.75)	10x10 (0.65)	14x14 (0.54)								
10"	10x14 (0.54)	10x10 (0.60)	14x14 (0.50)										
14"	14x14 (0.43)												

TABLE III (a)

MICROSTRUCTURAL CONSTITUENTS PRODUCED BY COOLING BLOCKS OF H13 STEEL IN A VACUUM

(Initial Block Temperature 1900°F, Ambient Temperature 100°F, All Block Dimensions in Inches)
(Amount of each microstructural constituent is listed in percent)

THICKNESS													
2	Width X Length	2 X 14	2 X 10	2 X 8	2 X 6	2 X 4	2 X 3	2 X 2	3 X 3	4 X 4	6 X 6	8 X 8	10 X 10	14 X 14
	Surf.Area/Volume	2.14	2.20	2.25	2.33	2.50	2.67	3.00	2.33	2.00	1.67	1.50	1.40	1.29
	MC Precip.-Surf.	94	94	93	93	92	92	91	93	94	94	95	95	96
	" " -Q.Thick.	94	96	93	93	92	93	91	93	94	94	95	96	96
	Microstruc.-Surf.	33B67M	33B67M	32B68M	32B68M	31B69M	30B70M	28B72M	32B68M	34B66M	37B63M	39B61M	40B60M	42B58M
	" -Q.Thick.	33B67M	33B67M	32B68M	32B68M	31B69M	30B70M	28B72M	32B68M	34B66M	37B63M	39B61M	40B60M	42B58M
3	Width X Length	3 X 14	3 X 10	3 X 8	3 X 6	3 X 4	3 X 3	4 X 4	6 X 6	8 X 8	10 X 10	14 X 14		
	Surf.Area/Volume	1.48	1.53	1.58	1.67	1.83	2.00	1.67	1.33	1.17	1.07	0.95		
	MC Precip.-Surf.	95	95	95	94	94	94	94	95	96	96	96		
	" " -Q.Thick.	95	95	95	94	94	94	94	95	96	96	96		
	Microstruc.-Surf.	39B61M	38B62M	37B63M	37B63M	35B65M	33B67M	37B63M	41B59M	43B57M	46B54M	50B50M		
	" -Q.Thick.	39B61M	38B62M	37B63M	37B63M	35B65M	34B66M	37B63M	41B59M	43B57M	46B54M	50B50M		
4	Width X Length	4 X 14	4 X 10	4 X 8	4 X 6	4 X 4	6 X 6	8 X 8	10 X 10	14 X 14				
	Surf.Area/Volume	1.14	1.20	1.25	1.33	1.50	1.17	1.00	0.90	0.79				
	MC Precip.-Surf.	96	96	96	95	95	96	96	96	97				
	" " -Q.Thickness	96	96	96	95	95	96	96	96	97				
	Microstruc.-Surf.	44B56M	43B57M	42B58M	41B59M	38B62M	44B56M	48B52M	53B47M	43B57M				
	" -Q.Thick.	44B56M	43B57M	42B58M	41B59M	38B62M	44B56M	48B52M	53B47M	43B57M				
6	Width X Length	6 X 14	6 X 10	6 X 8	6 X 6	8 X 8	10 X 10	14 X 14						
	Surf.Area/Volume	0.81	0.87	0.92	1.00	0.83	0.73	0.62						
	MC Precip.-Surf.	96	96	96	96	96	97	97						
	" " -Q.Thick.	96	96	96	96	96	97	97						
	Microstruc.-Surf.	43B57M	53B47M	52B47M	48B52M	54B46M	58B42M	3P63B34M						
	" -Q.Thick.	43B57M	53B47M	52B48M	48B52M	48B52M	58B42M	3P63B34M						
8	Width X Length	8 X 14	8 X 10	8 X 8	10 X 10	14 X 14								
	Surf.Area/Volume	0.64	0.70	0.75	0.65	0.54								
	MC Precip.-Surf.	97	97	97	97	97								
	" " -Q.Thick.	97	97	97	97	97								
	Microstruc.-Surf.	3P62B35M	1P60B39M	58B42M	3P62B35M	7P67B26M								
	" -Q.Thick.	3P62B35M	1P60B39M	58B42M	3P62B35M	7P67B26M								
10	Width X Length	10 X 14	10 X 10	14 X 14										
	Surf.Area/Volume	0.54	0.60	0.50										
	MC Precip.-Surf.	97	97	98										
	" " -Q.Thick.	97	97	98										
	Microstruc.-Surf.	7P67B26M	5P64B31M	9P69B22M										
	" -Q.Thick.	7P67B26M	5P64B31M	9P69B22M										
14	Width X Length	14 X 14												
	Surf.Area/Volume	0.43												
	MC Precip.-Surf.	98												
	" " -Q.Thick.	98												
	Microstruc.-Surf.	13P72B15M												

TABLE (b)

MICROSTRUCTURAL CONSTITUENTS PRODUCED BY QUENCHING BLOCKS OF H13 STEEL WITH 2 ATM. PRESSURE OF NITROGEN

(Initial Block Temperature 1900°F, Nitrogen Temperature 100°F, All Block Dimensions in Inches)
(Amount of each microstructural constituent is listed in inches)

THICKNESS

2	Width X Length	2 X 14	2 X 10	2 X 8	2 X 6	2 X 4	2 X 3	2 X 2	3 X 3	4 X 4	6 X 6	8 X 8	10 X 10	14 X 14
	Surf.Area/Volume	2.14	2.20	2.25	2.33	2.50	2.67	3.00	2.33	2.00	1.67	1.50	1.40	1.29
	MC Precip.-Surf.	81	81	81	80	79	77	74	80	83	87	89	89	89
	" " -Q.Thick.	81	81	81	80	79	77	74	80	83	87	89	89	89
	Microstruc.-Surf.	20B80M	19B81M	19B81M	19B81M	18B82M	17B83M	16B84M	18B82M	20B80M	22B78M	23B77M	24B76M	25B75M
	" -Q.Thick.	20B80M	19B81M	19B81M	19B81M	18B82M	17B83M	16B84M	18B82M	20B80M	22B78M	23B77M	24B76M	25B75M

3	Width X Length	3 X 14	3 X 10	3 X 8	3 X 6	3 X 4	3 X 3	4 X 4	6 X 6	8 X 8	10 X 10	14 X 14
	Surf.Area/Volume	1.48	1.53	1.58	1.67	1.83	2.00	1.67	1.33	1.17	1.07	0.95
	MC Precip.-Surf.	87	87	87	86	83	82	85	89	91	92	92
	" " -Q.Thick.	87	87	87	86	83	82	85	89	91	92	92
	Microstruc.-Surf.	23B77M	23B77M	22B78M	22B78M	20B80M	20B80M	21B79M	24B76M	25B75M	27B73M	29B71M
	" -Q.Thick.	23B77M	23B77M	22B78M	22B78M	20B80M	20B80M	21B79M	24B76M	25B75M	27B73M	29B71M

4	Width X Length	4 X 14	4 X 10	4 X 8	4 X 6	4 X 4	6 X 6	8 X 8	10 X 10	14 X 14
	Surf.Area/Volume	1.14	1.20	1.25	1.33	1.50	1.17	1.00	0.90	0.79
	MC Precip.-Surf.	90	90	89	88	86	90	92	93	94
	" " -Q.Thick.	90	90	89	88	86	90	92	93	94
	Microstruc.-Surf.	26B74M	25B75M	24B76M	24B76M	22B78M	24B76M	27B71M	29B71M	31B69M
	" -Q.Thick.	26B74M	25B75M	24B76M	24B76M	23B77M	24B76M	27B73M	29B71M	31B69M

6	Width X Length	6 X 14	6 X 10	6 X 8	6 X 6	8 X 8	10 X 10	14 X 14
	Surf.Area/Volume	0.81	0.87	0.92	1.00	0.83	0.73	0.62
	MC Precip.-Surf.	92	92	92	91	93	94	94
	" " -Q.Thick.	93	93	92	91	93	94	95
	Microstruc.-Surf.	30B70M	29B71M	28B72M	26B74M	29B71M	32B68M	35B65M
	" -Q.Thick.	30B70M	29B71M	28B72M	27B73M	29B71M	32B68M	35B65M

8	Width X Length	8 X 14	8 X 10	8 X 8	10 X 10	14 X 14
	Surf.Area/Volume	0.64	0.70	0.75	0.65	0.54
	MC Precip.-Surf.	94	93	93	94	94
	" " -Q.Thick.	94	94	93	94	96
	Microstruc.-Surf.	34B66M	32B68M	31B69M	33B67M	37B63M
	" -Q.Thick.	34B66M	32B68M	31B69M	33B67M	37B63M

10	Width X Length	10 X 14	10 X 10	14 X 14
	Surf.Area/Volume	0.54	0.60	0.50
	MC Precip.-Surf.	94	94	94
	" " -Q.Thick.	95	95	96
	Microstruc.-Surf.	37B63M	34B66M	39B61M
	" -Q.Thick.	37B63M	34B66M	39B61M

14	Width X Length	14 X 14
	Surf.Area/Volume	0.43
	MC Precip.-Surf.	94
	" " -Q.Thick.	96
	Microstruc.-Surf.	42B58M
	" -Q.Thick.	42B58M

TABLE III (c)

MICROSTRUCTURAL CONSTITUENTS PRODUCED BY QUENCHING BLOCKS OF H13 STEEL WITH 2 ATM. PRESSURE OF HELIUM

(Initial Block Temperature 1900°F, Helium Temperature 100°F, All Block Dimensions in Inches)
(Amount of each microstructural constituent is listed in percent)

THICKNESS													
2	Width X Length	2 X 14	2 X 10	2 X 8	2 X 6	2 X 4	2 X 3	2 X 2	3 X 3	4 X 4	6 X 6	8 X 8	10 X 10	14 X 14
	Surf.Area/Volume	2.14	2.20	2.25	2.33	2.50	2.67	3.00	2.33	2.00	1.67	1.50	1.40	1.29
	MC Precip.-Surf.	76	75	75	75	74	71	68	74	79	84	85	86	86
	" " -Q.Thick.	76	76	76	75	74	71	68	74	79	84	85	86	86
	Microstruc.-Surf.	17B83M	17B83M	17B83M	16B84M	15B85M	14B86M	13B87M	16B84M	17B83M	19B81M	21B79M	22B78M	23B77M
	" -Q.Thick.	17B83M	17B83M	17B83M	16B84M	15B85M	14B86M	13B87M	16B84M	17B83M	19B81M	21B79M		
3	Width X Length	3 X 14	3 X 10	3 X 8	3 X 6	3 X 4	3 X 3	4 X 4	6 X 6	8 X 8	10 X 10	14 X 14		
	Surf.Area/Volume	1.48	1.53	1.58	1.67	1.83	2.00	1.67	1.33	1.17	1.07	0.95		
	MC Precip.-Surf.	83	82	82	82	79	77	81	86	89	89	89		
	" " -Q.Thick.	83	83	83	82	79	77	81	86	89	90	90		
	Microstruc.-Surf.	20B80M	20B80M	20B80M	19B81M	18B82M	17B83M	19B81M	21B79M	23B77M	24B76M	26B74M		
	" -Q.Thick.	20B80M	20B80M	20B80M	19B81M	18B82M	17B83M	19B81M	21B79M	23B77M	24B76M	26B74M		
4	Width X Length	4 X 14	4 X 10	4 X 8	4 X 6	4 X 4	6 X 6	8 X 8	10 X 10	14 X 14				
	Surf.Area/Volume	1.14	1.20	1.25	1.33	1.50	1.17	1.00	0.90	0.79				
	MC Precip.-Surf.	86	86	85	85	83	88	89	90	90				
	" " -Q.Thick.	87	87	87	85	83	88	90	92	92				
	Microstruc.-Surf.	23B77M	22B78M	22B78M	21B79M	20B80M	22B78M	24B76M	26B74M	28B72M				
	" -Q.Thick.	23B77M	22B78M	22B78M	21B79M	20B80M	22B78M	24B76M	26B74M	28B72M				
6	Width X Length	6 X 14	6 X 10	6 X 8	6 X 6	8 X 8	10 X 10	14 X 14						
	Surf.Area/Volume	0.81	0.87	0.92	1.00	0.83	0.73	0.62						
	MC Precip.-Surf.	89	89	89	88	90	90	90						
	" " -Q.Thick.	92	91	90	89	91	93	94						
	Microstruc.-Surf.	27B73M	26B74M	25B75M	24B76M	26B74M	28B72M	32B68M						
	" -Q.Thick.	27B73M	26B74M	25B75M	24B76M	26B74M	28B72M	32B68M						
8	Width X Length	8 X 14	8 X 10	8 X 8	10 X 10	14 X 14								
	Surf.Area/Volue	0.64	0.70	0.75	0.65	0.54								
	MC Precip.-Surf.	90	90	90	90	91								
	" " -Q.Thick.	94	93	92	94	95								
	Microstruc.-Surf.	30B70M	29B71M	28B72M	30B70M	34B66M								
	" -Q.Thick.	30B70M	29B71M	28B72M	30B70M	34B66M								
10	Width X Length	10 X 14	10 X 10	14 X 14										
	Surf.Area/Volume	0.54	0.60	0.50										
	MC Precip.-Surf.	90	90	91										
	" " -Q.Thick.	94	94	95										
	Microstruc.-Surf.	33B67M	31B69M	36B64M										
	" -Q.Thick.	33B67M	31B69M	36B64M										
14	Width X Length	14 X 14												
	Surf.Area/Volume	0.43												
	MC Precip.-Surf.	92												
	" " -Q.Thick.	96												

TABLE I d)

MICROSTRUCTURAL CONSTITUENTS PRODUCED BY COOLING BLOCKS OF H13 STEEL IN A FLUIDIZED BED

(Initial Block Temperature 1900°F, Alumina Temperature 100°F, All Block Dimensions in Inches)
(Amount of each microstructural constituent is listed in percent)

THICKNESS

2	Width X Length	2 X 14	2 X 10	2 X 8	2 X 6	2 X 4	2 X 3	2 X 2	3 X 3	4 X 4	6 X 6	8 X 8	10 X 10	14 X 14
	Surf.Area/Volume	2.14	2.20	2.25	2.33	2.50	2.67	3.00	2.33	2.00	1.67	1.50	1.40	1.29
	MC Precip.-Surf.	48	47	47	47	47	47	44	47	49	49	49	49	49
	" " -Q.Thick.	55	55	55	55	54	52	50	57	64	68	68	68	68
	Microstruc.-Surf.	9B91M	8B92M	8B92M	8B92M	7B93M	6B94M	5B95M	7B93M	9B91M	12B88M	13B87M	13B87M	14B86M
	" -Q.Thick.	9B91M	8B92M	8B92M	8B92M	7B93M	7B93M	5B95M	7B93M	9B91M	12B88M	13B87M	14B86M	14B86M

3	Width X Length	3 X 14	3 X 10	3 X 8	3 X 6	3 X 4	3 X 3	4 X 4	6 X 6	8 X 8	10 X 10	14 X 14
	Surf.Area/Volume	1.48	1.53	1.58	1.67	1.83	2.00	1.67	1.33	1.17	1.07	0.95
	MC Precip.-Surf.	49	49	49	49	49	47	48	49	49	49	49
	" " -Q.Thick.	68	66	66	66	64	60	68	76	77	77	77
	Microstruc.-Surf.	12B88M	11B89M	12B88M	11B89M	10B90M	9B91M	11B89M	14B86M	16B84M	17B83M	17B83M
	" -Q.Thick.	12B88M	12B88M	12B88M	11B89M	10B90M	9B91M	11B89M	14B86M	16B84M	17B83M	18B82M

4	Width X Length	4 X 14	4 X 10	4 X 8	4 X 6	4 X 4	6 X 6	8 X 8	10 X 10	14 X 14
	Surf.Area/Volume	1.14	1.20	1.25	1.33	1.50	1.17	1.00	0.90	0.79
	MC Precip.-Surf.	49	49	49	49	48	48	49	49	49
	" " -Q.Thick.	74	74	74	73	69	79	82	83	83
	Microstruc.-Surf.	15B85M	15B85M	14B86M	13B87M	12B88M	15B85M	17B83M	18B82M	19B81M
	" -Q.Thick.	15B85M	15B85M	14B86M	13B87M	12B88M	15B85M	17B83M	19B81M	20B80M

6	Width X Length	6 X 14	6 X 10	6 X 8	6 X 6	8 X 8	10 X 10	14 X 14
	Surf.Area/Volume	0.81	0.87	0.92	1.00	0.83	0.73	0.62
	MC Precip.-Surf.	49	49	49	48	49	49	50
	" " -Q.Thick.	84	84	83	80	86	88	89
	Microstruc.-Surf.	18B82M	18B82M	17B83M	16B84M	18B82M	20B80M	21B79M
	" -Q.Thick.	20B80M	19B81M	18B82M	17B83M	19B81M	21B79M	24B76M

8	Width X Length	8 X 14	8 X 10	8 X 8	10 X 10	14 X 14
	Surf.Area/Volume	0.64	0.70	0.75	0.65	0.54
	MC Precip.-Surf.	50	50	49	50	50
	" " -Q.Thick.	89	88	86	90	92
	Microstruc.-Surf.	20B80M	19B81M	19B81M	20B80M	22B78M
	" -Q.Thick.	23B77M	21B79M	20B80M	23B77M	26B74M

10	Width X Length	10 X 14	10 X 10	14 X 14
	Surf.Area/Volume	0.54	0.60	0.50
	MC Precip.-Surf.	50	49	50
	" " -Q.Thick.	91	90	93
	Microstruc.-Surf.	21B79M	20B80M	22B78M
	" -Q.Thick.	25B75M	24B76M	28B72M

14	Width X Length	14 X 14
	Surf.Area/Volume	0.43
	MC Precip.-Surf.	51
	" " -Q.Thick.	94
	Microstruc.-Surf.	23B77M
	" -Q.Thick.	29B71M

TABL .I (e)

MICROSTRUCTURAL CONSTITUENTS PRODUCED BY COOLING BLOCKS OF H13 STEEL IN A SALT BATH

(Initial Block Temperature 1900°F, Salt Temperature 750°F, All Block Dimensions in Inches)
(Amount of each microstructural constituent is listed in percent)

THICKNESS

2	Width X Length	2 X 14	2 X 10	2 X 8	2 X 6	2 X 4	2 X 3	2 X 2	3 X 3	4 X 4	6 X 6	8 X 8	10 X 10	14 X 14
	Surf.Area/Volume	2.14	2.20	2.25	2.33	2.50	2.67	3.00	2.33	2.00	1.67	1.50	1.40	1.29
	MC Precip.-Surf.	50	48	48	48	45	50	51	51	51	51	51	51	52
	" " -Q.Thick.	57	57	57	57	56	54	48	60	66	70	70	71	72
	Microstruc.-Surf.	100B	100B	100B	100B	100B	100B	100B	100B	100B	100B	100B	100B	100B
	" -Q.Thick.	100B	100B	100B	100B	100B	100B	100B	100B	100B	100B	100B	100B	100B

3	Width X Length	3 X 14	3 X 10	3 X 8	3 X 6	3 X 4	3 X 3	4 X 4	6 X 6	8 X 8	10 X 10	14 X 14
	Surf.Area/Volume	1.48	1.53	1.58	1.67	1.83	2.00	1.67	1.33	1.17	1.07	0.95
	MC Precip.-Surf.	51	51	51	50	50	49	50	51	51	51	52
	" " -Q.Thick.	69	69	69	69	66	62	70	78	80	80	80
	Microstruc.-Surf.	100B	100B	100B	100B	100B	100B	100B	100B	100B	100B	100B
	" -Q.Thick.	100B	100B	100B	100B	100B	100B	100B	100B	100B	100B	100B

4	Width X Length	4 X 14	4 X 10	4 X 8	4 X 6	4 X 4	6 X 6	8 X 8	10 X 10	14 X 14
	Surf.Area/Volume	1.14	1.20	1.25	1.33	1.50	1.17	1.00	0.90	0.79
	MC Precip.-Surf.	51	51	50	50	50	50	51	51	52
	" " -Q.Thick.	77	77	77	76	72	81	84	85	86
	Microstruc.-Surf.	100B	100B	100B	100B	100B	100B	100B	100B	100B
	" -Q.Thick.	100B	100B	100B	100B	100B	100B	100B	100B	100B

6	Width X Length	6 X 14	6 X 10	6 X 8	6 X 6	8 X 8	10 X 10	14 X 14
	Surf.Area/Volume	0.81	0.87	0.92	1.00	0.83	0.73	0.62
	MC Precip.-Surf.	51	50	50	50	50	51	52
	" " -Q.Thick.	86	86	85	83	88	90	91
	Microstruc.-Surf.	100B	100B	100B	100B	100B	100B	100B
	" -Q.Thick.	100B	100B	100B	100B	100B	100B	100B

8	Width X Length	8 X 14	8 X 10	8 X 8	10 X 10	14 X 14
	Surf.Area/Volume	0.64	0.70	0.75	0.65	0.54
	MC Precip.-Surf.	52	52	51	52	52
	" " -Q.Thick.	91	90	88	91	93
	Microstruc.-Surf.	100B	100B	100B	100B	100B
	" -Q.Thick.	100B	100B	100B	100B	100B

10	Width X Length	10 X 14	10 X 10	14 X 14
	Surf.Area/Volume	0.54	0.60	0.50
	MC Precip.-Surf.	53	52	53
	" " -Q.Thick.	93	92	94
	Microstruc.-Surf.	100B	100B	100B
	" -Q.Thick.	100B	100B	100B

14	Width X Length	14 X 14
	Surf.Area/Volume	0.43
	MC Precip.-Surf.	55
	" " -Q.Thick.	94
	Microstruc.-Surf.	100B
	" -Q.Thick.	100B

TABLE ... (g)

MICROSTRUCTURAL CONSTITUENTS PRODUCED BY QUENCHING BLOCKS OF H13 STEEL IN A LOW SPEED OIL

(Initial Block Temperature 1900°F, Oil Temperature 100°F, All Block Dimensions in Inches)
(Amount of each microstructural constituent is listed in percent)

THICKNESS

2	Width X Length	2 X 14	2 X 10	2 X 8	2 X 6	2 X 4	2 X 3	2 X 2	3 X 3	4 X 4	6 X 6	8 X 8	10 X 10	14 X 14
	Surf.Area/Volume	2.14	2.20	2.25	2.33	2.50	2.67	3.00	2.33	2.00	1.67	1.50	1.40	1.29
	MC Precip.-Surf.	56	55	55	55	55	55	50	60	60	60	62	73	62
	" " -Q.Thick.	59	59	59	59	59	55	52	61	68	72	73	73	73
	Microstruc.-Surf.	10B90M	10B90M	9B91M	9B91M	8B92M	8B92M	7B93M	9B91M	10B90M	13B87M	15B85M	15B85M	16B84M
	" -Q.Thick.	10B90M	10B90M	9B91M	9B91M	8B92M	8B92M	7B93M	9B91M	10B90M	13B87M	15B85M	15B85M	16B84M

3	Width X Length	3 X 14	3 X 10	3 X 8	3 X 6	3 X 4	3 X 3	4 X 4	6 X 6	8 X 8	10 X 10	14 X 14
	Surf.Area/Volume	1.48	1.53	1.58	1.67	1.83	2.00	1.67	1.33	1.17	1.07	0.95
	MC Precip.-Surf.	61	61	61	60	60	60	61	62	62	62	62
	" " -Q.Thick.	70	70	70	70	67	64	71	79	84	86	86
	Microstruc.-Surf.	14B86M	14B86M	13B87M	13B87M	11B89M	10B90M	12B88M	15B85M	17B83M	18B82M	19B81M
	" -Q.Thick.	14B86M	14B86M	13B87M	13B87M	11B89M	10B90M	12B88M	15B85M	17B83M	18B82M	19B81M

4	Width X Length	4 X 14	4 X 10	4 X 8	4 X 6	4 X 4	6 X 6	8 X 8	10 X 10	14 X 14
	Surf.Area/Volume	1.14	1.20	1.25	1.33	1.50	1.17	1.00	0.90	0.79
	MC Precip.-Surf.	62	62	61	61	60	61	61	62	62
	" " -Q.Thick	78	78	77	76	72	81	84	86	86
	Microstruc.-Surf.	16B84M	16B84M	16B84M	15B85M	13B87M	17B83M	19B81M	20B80M	22B78M
	" -Q.Thick.	17B83M	16B84M	16B84M	15B85M	13B87M	17B83M	19B81M	20B80M	22B78M

6	Width X Length	6 X 14	6 X 10	6 X 8	6 X 6	8 X 8	10 X 10	14 X 14
	Surf.Area/Volume	0.81	0.87	0.92	1.00	0.83	0.73	0.62
	MC Precip.-Surf.	62	61	61	61	61	62	62
	" " -Q.Thick.	86	86	85	82	87	90	90
	Microstruc.-Surf.	20B80M	20B80M	19B81M	18B82M	20B80M	22B78M	24B76M
	" -Q.Thick.	21B79M	20B80M	19B81M	18B82M	21B79M	22B78M	25B75M

8	Width X Length	8 X 14	8 X 10	8 X 8	10 X 10	14 X 14
	Surf.Area/Volume	0.64	0.70	0.75	0.65	0.54
	MC Precip.-Surf.	62	62	61	62	62
	" " -Q.Thick.	90	89	88	90	93
	Microstruc.-Surf.	23B77M	22B78M	21B79M	23B77M	25B75M
	" -Q.Thick.	24B76M	23B77M	22B78M	24B76M	27B73M

10	Width X Length	10 X 14	10 X 10	14 X 14
	Surf.Area/Volume	0.54	0.60	0.50
	MC Precip.-Surf.	62	62	63
	" " -Q.Thick.	92	91	94
	Microstruc.-Surf.	24B76M	22B78M	26B74M
	" -Q.Thick.	26B74M	24B76M	29B71M

14	Width X Length	14 X 14
	Surf.Area/Volume	0.43
	MC Precip.-Surf.	64
	" " -Q.Thick.	94

MICROSTRUCTURAL CONSTITUENTS PRODUCED BY QUENCHING BLOCKS OF H13 STEEL
IN A POLYMERIC QUENCHANT (UCON A 30% CONCENTRATION

(Initial Block Temperature 1900°F, Quenchant Temperature 100°F, All Block Dimensions in Inches)
(Amount of each microstructural constituent is listed in percent)

THICKNESS

2	Width X Length	2 X 14	2 X 10	2 X 8	2 X 6	2 X 4	2 X 3	2 X 2	3 X 3	4 X 4	6 X 6	8 X 8	10 X 10	14 X 14
	Surf.Area/Volume	2.14	2.20	2.25	2.33	2.50	2.67	3.00	2.33	2.00	1.67	1.50	1.40	1.29
	MC Precip.-Surf.	0	0	0	0	0	0	0	0	0	0	0	0	0
	" " -Q.Thick.	36	36	36	36	35	34	27	43	49	50	50	50	50
	Microstruc.-Surf.	2B98M	3B97M	1B99M	1B99M	1B99M	100M	100M	3B97M	4B96M	5B95M	5B95M	5B95M	5B95M
	" -Q.Thick.	3B97M	3B97M	3B97M	2B98M	2B98M	2B98M	1B99M	3B97M	5B95M	7B93M	8B92M	8B92M	8B92M

3	Width X Length	3 X 14	3 X 10	3 X 8	3 X 6	3 X 4	3 X 3	4 X 4	6 X 6	8 X 8	10 X 10	14 X 14
	Surf.Area/Volume	1.48	1.53	1.58	1.67	1.83	2.00	1.67	1.33	1.17	1.07	0.95
	MC Precip.-Surf.	0	0	0	0	0	0	0	0	0	0	0
	" " -Q.Thick.	54	54	54	53	52	48	58	62	63	63	63
	Microstruc.-Surf.	4B96M	4B96M	4B96M	4B96M	4B96M	3B97M	5B95M	7B93M	7B93M	7B93M	7B93M
	" -Q.Thick.	7B93M	7B93M	7B93M	7B93M	5B95M	4B96M	7B93M	10B90M	11B89M	12B88M	12B88M

4	Width X Length	4 X 14	4 X 10	4 X 8	4 X 6	4 X 4	6 X 6	8 X 8	10 X 10	14 X 14
	Surf.Area/Volume	1.14	1.20	1.25	1.33	1.50	1.17	1.00	0.90	0.79
	MC Precip.-Surf.	0	0	0	0	0	0	0	0	0
	" " -Q.Thick.	64	64	64	64	59	69	71	71	71
	Microstruc.-Surf.	6B94M	6B94M	6B94M	6B94M	5B95M	7B93M	7B93M	8B92M	8B92M
	" -Q.Thick.	10B90M	10B90M	10B90M	9B91M	7B93M	11B89M	14B86M	15B85M	16B84M

6	Width X Length	6 X 14	6 X 10	6 X 8	6 X 6	8 X 8	10 X 10	14 X 14
	Surf.Area/Volume	0.81	0.87	0.92	1.00	0.83	0.73	0.62
	MC Precip.-Surf.	0	0	0	0	0	0	0
	" -Q.Thick.	77	77	76	74	80	81	82
	Microstruc.-Surf.	7B93M	7B93M	7B93M	6B94M	7B93M	8B92M	8B92M
	" -Q.Thick.	16B84M	15B85M	14B86M	13B87M	16B84M	18B82M	21B79M

8	Width X Length	8 X 14	8 X 10	8 X 8	10 X 10	14 X 14
	Surf.Area/Volume	0.64	0.70	0.75	0.65	0.54
	MC Precip.-Surf.	0	0	0	0	0
	" " -Q.Thick.	84	84	82	86	87
	Microstruc.-Surf.	7B93M	9B92M	7B93M	8B92M	8B92M
	" -Q.Thick.	20B80M	18B82M	17B83M	19B81M	23B77M

10	Width X Length	10 X 14	10 X 10	14 X 14
	Surf.Area/Volume	0.54	0.60	0.50
	MC Precip.-Surf.	0	0	0
	" " -Q.Thick.	89	87	90
	Microstruc.-Surf.	8B92M	8B92M	8B92M
	" -Q.Thick.	22B78M	21B79M	25B75M

14	Width X Length	14 X 14
	Surf.Area/Volume	0.43
	MC Precip.-Surf.	0
	" " -Q.Thick.	92
	Microstruc.-Surf.	8B92M

TABLE . (h)

MICROSTRUCTURAL CONSTITUENTS PRODUCED BY QUENCHING BLOCKS OF H13 STEEL IN A HIGH SPEED OIL (RAPE SEED)

(Initial Block Temperature 1900°F, Oil Temperature 100°F, All Block Dimensions in Inches)
(Amount of each microstructural constituent is listed in percent)

THICKNESS

2	Width X Length	2 X 14	2 X 10	2 X 8	2 X 6	2 X 4	2 X 3	2 X 2	3 X 3	4 X 4	6 X 6	8 X 8	10 X 10	14 X 14
	Surf.Area/Volume	2.14	2.20	2.25	2.33	2.50	2.67	3.00	2.33	2.00	1.67	1.50	1.40	1.29
	MC Precip.-Surf.	16	14	13	13	13	13	13	13	14	15	15	15	15
	" " -Q.Thick.	44	44	44	44	43	42	35	50	57	59	59	59	59
	Microstruc.-Surf.	5B95M	5B95M	5B95M	5B95M	4B96M	3B97M	2B98M	5B95M	7B93M	8B92M	9B91M	9B91M	9B91M
	" -Q.Thick.	5B95M	5B95M	5B95M	5B95M	4B96M	3B97M	2B98M	5B95M	7B93M	9B91M	10B90M	10B90M	10B90M

3	Width X Length	3 X 14	3 X 10	3 X 8	3 X 6	3 X 4	3 X 3	4 X 4	6 X 6	8 X 8	10 X 10	14 X 14
	Surf.Area/Volume	1.48	1.53	1.58	1.67	1.83	2.00	1.67	1.33	1.17	1.07	0.95
	MC Precip.-Surf.	14	14	14	13	13	13	14	15	15	15	15
	" " -Q.Thick.	59	59	59	60	57	53	62	68	69	69	69
	Microstruc.-Surf.	8B92M	7B93M	7B93M	7B93M	7B93M	6B94M	8B92M	10B90M	12B88M	12B88M	11B89M
	" -Q.Thick.	9B91M	9B91M	9B91M	8B92M	9B91M	6B94M	8B92M	11B89M	13B87M	14B80M	14B86M

4	Width X Length	4 X 14	4 X 10	4 X 8	4 X 6	4 X 4	6 X 6	8 X 8	10 X 10	14 X 14
	Surf.Area./Volume	1.14	1.20	1.25	1.33	1.50	1.17	1.00	0.90	0.79
	MC Precip.-Surf.	14	14	12	12	12	13	14	15	15
	" " -Q.Thick	68	68	68	67	63	74	76	77	77
	Microstruc.-Surf.	10B90M	10B90M	9B91M	9B91M	8B92M	11B89M	12B88M	13B87M	13B87M
	" -Q.Thick.	12B88M	12B88M	12B88M	11B89M	9B91M	13B87M	15B85M	17B85M	18B82M

6	Width X Length	6 X 14	6 X 10	6 X 8	6 X 6	8 X 8	10 X 10	14 X 14
	Surf.Area/Volume	0.81	0.87	0.92	1.00	0.83	0.73	0.62
	MC Precip.-Surf.	14	12	12	12	13	14	15
	" " -Q.Thick.	80	80	79	76	82	84	85
	Microstruc.-Surf.	12B88M	12B88M	12B88M	11B89M	13B87M	14B86M	14B86M
	" -Q.Thick.	17B83M	17B83M	16B84M	14B86M	17B83M	19B81M	22B78M

8	Width X Length	8 X 14	8 X 10	8 X 8	10 X 10	14 X 14
	Surf.Area/Volume	0.64	0.70	0.75	0.65	0.54
	MC Precip.-Surf.	15	14	13	14	15
	" " -Q.Thick.	86	86	84	87	90
	Microstruc.-Surf.	13B87M	13B87M	13B87M	14B86M	15B85M
	" -Q.Thick.	21B79M	20B80M	18B82M	21B79M	24B76M

10	Width X Length	10 X 14	10 X 10	14 X 14
	Surf.Area/Volume	0.54	0.60	0.50
	MC Precip.-Surf.	15	14	15
	" " -Q.Thick.	90	88	92
	Microstruc.-Surf.	14B86B	18B82M	15B85M
	" -Q.Thick	23B77M	22B78M	26B74M

14	Width X Length	14 X 14
	Surf.Area/Volume	0.43
	MC Precip.-Surf	16
	" " -Q.Thick.	93

MICROSTRUCTURAL CONSTITUENTS PRODUCED BY QUENCHING BLOCKS OF H13 STEEL IN A POLYMERIC QUENCHANT (UCON A 10% CONCENTRATION)

(Initial Block Temperature 1900°F, Quenchant Temperature 100°F, All Block Dimensions in Inches)
(Amount of each microstructural constituent is listed in percent)

THICKNESS

2	Width X Length	2 X 14	2 X 10	2 X 8	2 X 6	2 X 4	2 X 3	2 X 2	3 X 3	4 X 4	6 X 6	8 X 8	10 X 10	14 X 14
	Surf.Area/Volume	2.14	2.20	2.25	2.33	2.50	2.67	3.00	2.33	2.00	1.67	1.50	1.40	1.29
	MC Precip.-Surf.	0	0	0	0	0	0	0	0	0	0	0	0	0
	" " -Q.Thick.	25	24	24	24	24	16	34	36	37	37	37	38	38
	Microstruc.-Surf.	100M	100M	100M	100M	100M	100M	100M	100M	100M	100M	100M	100M	100M
	" -Q.Thick.	1B99M	1B99M	1B99M	1B99M	1B99M	1B99M	100M	1B99M	3B97M	5B95M	5B95M	5B95M	5B95M
3	Width X Length	3 X 14	3 X 10	3 X 8	3 X 6	3 X 4	3 X 3	4 X 4	6 X 6	8 X 8	10 X 10	14 X 14		
	Surf.Area/Volume	1.48	1.53	1.58	1.67	1.83	2.00	1.67	1.33	1.17	1.07	0.95		
	MC Precip.-Surf.	0	0	0	0	0	0	0	0	0	0	0		
	" " -Q.Thick.	46	46	46	46	45	40	51	54	55	55	55		
	Microstruc.-Surf.	100M	100M	100M	100M	100M	100M	100M	100M	100M	100M	100M		
	" -Q.Thick.	5B95M	5B95M	5B95M	5B95M	4B96M	2B98M	5B95M	8B92M	9B91M	10B90M	10B90M		
4	Width X Length	4 X 14	4 X 10	4 X 8	4 X 6	4 X 4	6 X 6	8 X 8	10 X 10	14 X 14				
	Surf.Area/Volume	1.14	1.20	1.25	1.33	1.50	1.17	1.00	0.90	0.79				
	MC Precip.-Surf.	0	0	0	0	0	0	0	0	0				
	" " -Q.Thick.	59	59	59	58	55	64	64	64	64				
	Microstruc.-Surf.	100M	100M	100M	100M	100M	100M	100M	100M	100M				
	" -Q.Thick.	8B92M	8B92M	8B92M	7B93M	6B94M	10B90M	13B87M	13B87M	14B86M				
6	Width X Length	6 X 14	6 X 10	6 X 8	6 X 6	8 X 8	10 X 10	14 X 14						
	Surf.Area/Volume	0.81	0.87	0.92	1.00	0.83	0.73	0.62						
	MC Precip.-Surf.	0	0	0	0	0	0	0						
	" " -Q.Thick.	73	73	73	70	76	77	77						
	Microstruc.-Surf.	100M	100M	100M	100M	100M	100M	100M						
	" -Q.Thick.	14B86M	14B86M	14B86M	13B87M	12B86M	17B83M	19B81M						
8	Width X Length	8 X 14	8 X 10	8 X 8	10 X 10	14 X 14								
	Surf.Area/Volume	0.81	0.70	0.75	0.65	0.54								
	MC Precip.-Surf	0	0	0	0	0								
	" " -Q.Thick.	82	82	80	84	85								
	Microstruc.-Surf.	100M	100M	100M	100M	100M								
	" -Q.Thick.	18B82M	17B83M	16B84M	19B81M	22B78M								
10	Width X Length	10 X 14	10 X 10	14 X 14										
	Surf.Area/Volume	0.54	0.60	0.50										
	MC Precip.-Surf.	0	0	0										
	" " -Q.Thick.	87	86	89										
	Microstruc.-Surf.	100M	100M	100M										
	" -Q.Thick.	22B78M	20B80M	24B76M										
14	Width X Length	14 X 14												
	Surf.Area/Volume	0.43												
	MC Precip.-Surf.	0												
	" " -Q.Thick.	92												
	Microstruc.-Surf.	100M												
	" -Q.Thick.	25B75M												

Table IV: The Variation of MC Grain Boundary Precipitation as a function of Quenchant for the Two Extreme H13 Steel Block Sizes

Quenchant	2 inch Cube		14 inch Cube	
	Surface	Mid-Radius	Surface	Mid-Radius
Vacuum	91	91	98	98
Nitrogen	74	74	94	96
Helium	68	68	92	96
Low Speed Oil	50	52	64	94
Salt at 750°F	45	50	55	94
Fluidized Alumina	44	48	51	94
Salt at 575°F	28	41	32	94
High Speed Oil	13	35	16	93
30% UCON A Solution	0	27	0	92
10% UCON A Solution	0	16	0	92

TABLE V: The Variation of Matrix Microstructures Produced as a Function of Quenchant for the Two Extreme H13 Steel Block Sizes

Quenchant	2 inch Cube		14 inch Cube	
	Surface	Mid-Radius	Surface	Mid-Radius
Vacuum	28B 72M	28B 72M	13P 72B 15M	14P 72B 14M
Nitrogen	16B 84M	16B 84M	42B 58M	42B 58M
Helium	13B 87M	13B 87M	38B 62M	38B 62M
Low Speed Oil	7B 93M	7B 93M	26B 74M	30B 70M
Fluidized Alumina	5B 95M	5B 95M	23B 77M	29B 71M
High Speed Oil	2B 98M	2B 98M	15B 85M	27B 73M
30% UCON A Solution	100M	1B 99M	8B 92M	26B 74M
10% UCON A Solution	100M	100M	100M	25B 75M

TABLE VI Example of Linear Interpolation to Determine Microstructural Constituents for Gas Quench Pressures and Velocities Different Than Those in Tables III b and III c

Quenchant	H	Surface of an 8 inch Cube of H13 MC Precipitation	Microstructure	
Vacuum	3.6	97	58B	42M
Nitrogen at 1.5 atm. and 1,500 ft/min	8.0	95	46B	54M
Nitrogen at 2 atm and 3,400 ft/min	13.9	93	31B	69M
Helium at 2 atm and 3,400 ft/min	19.2	90	28B	72M
Helium at 5 atm and 5,000 ft/min	36.9	71	24B	76M
Low Speed Oil	47.1	61	21B	79M

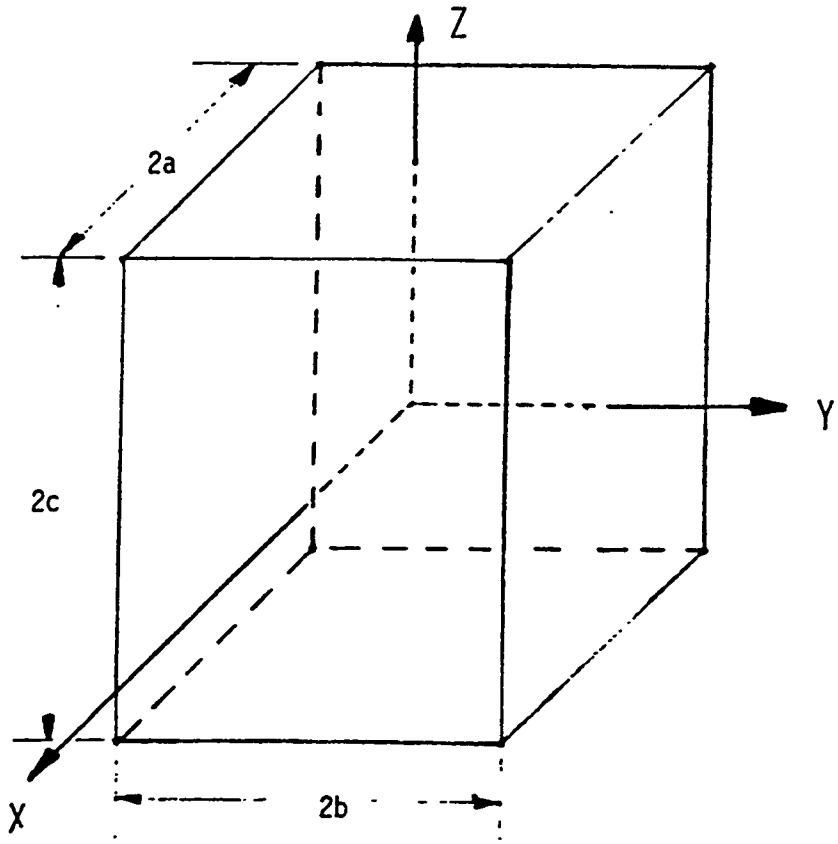

FIGURE 1 - The geometry of an arbitrary rectangular parallelepided shaped die block.

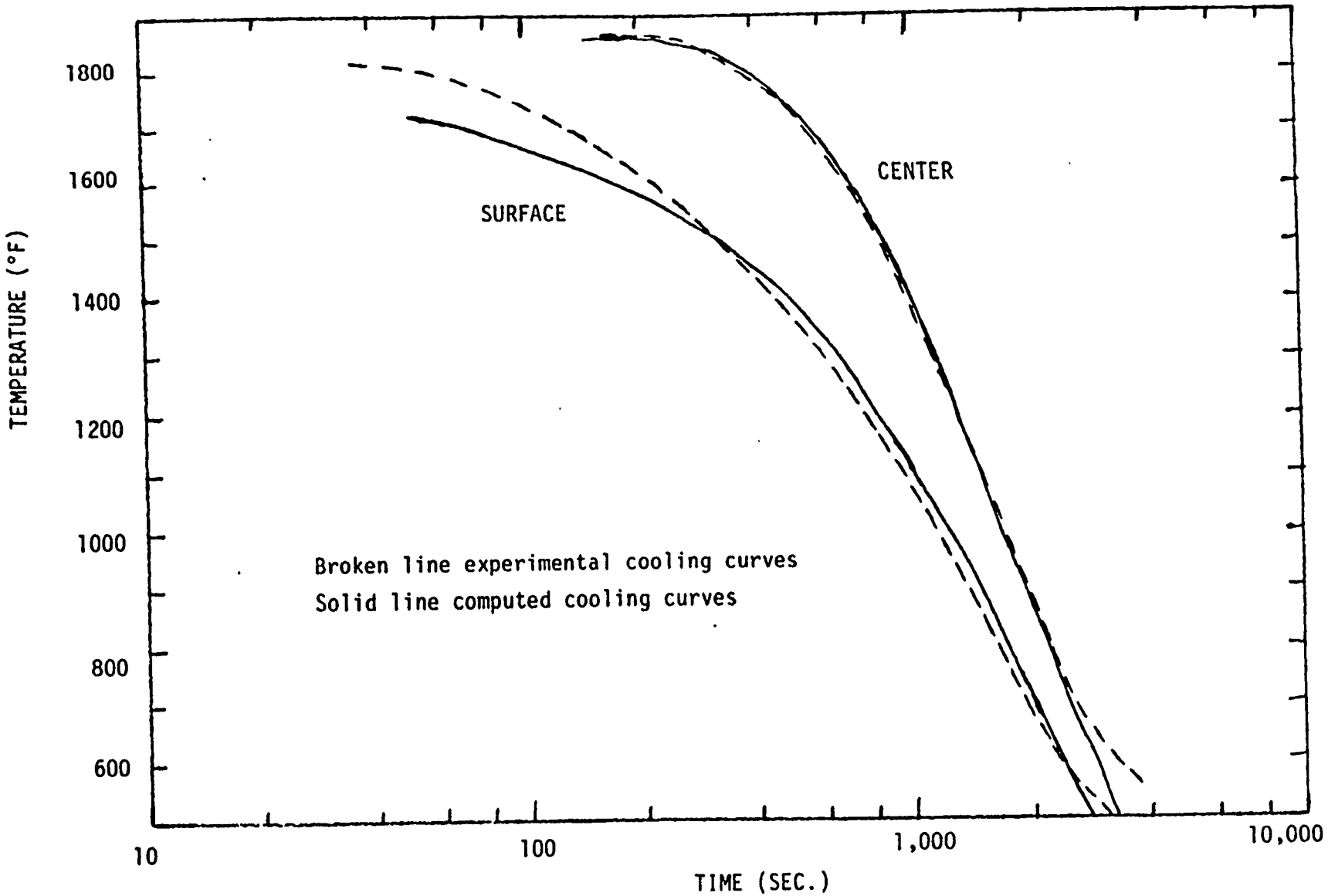

FIGURE 2 - Computed and experimentally determined cooling curves for the center and surface of a 10" cube of H13 quenched in helium at 2 atmospheres pressure.

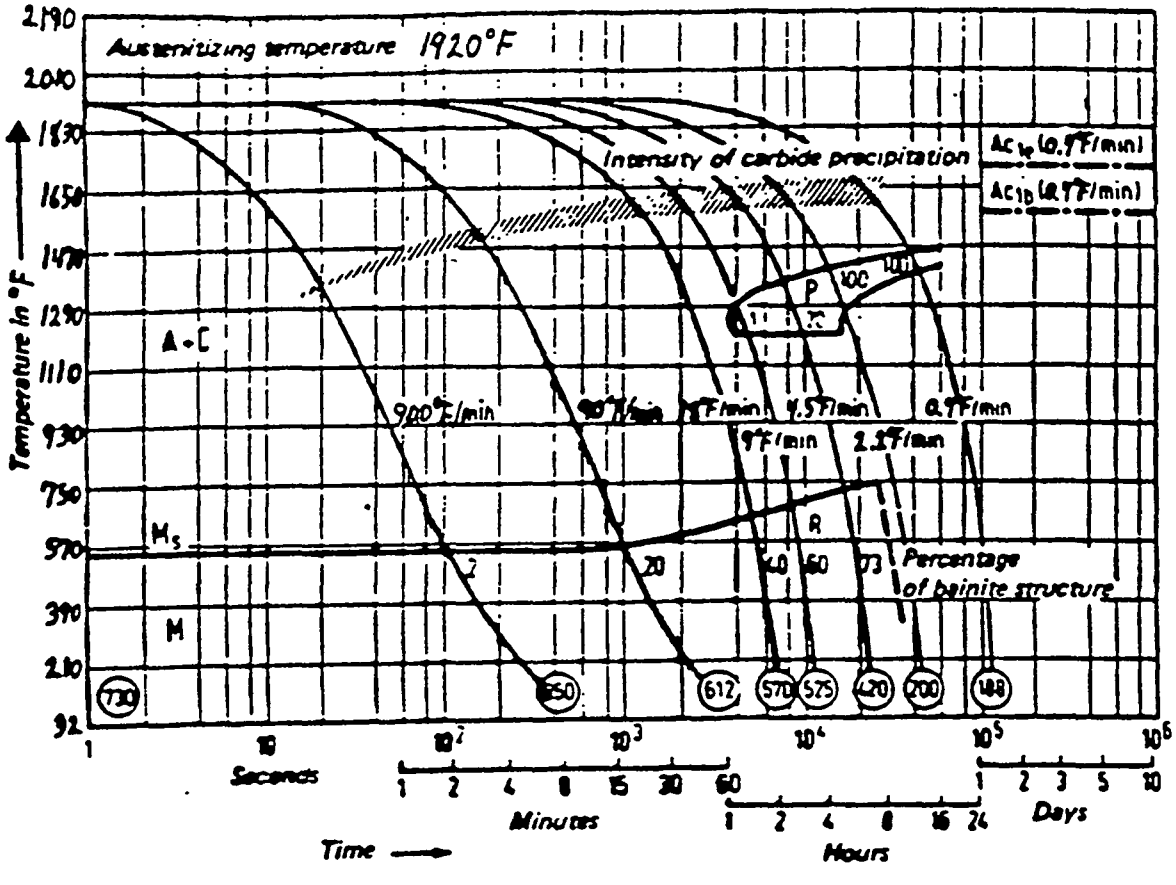

FIGURE 3 - The continuous cooling transformation diagram for H13 steel.

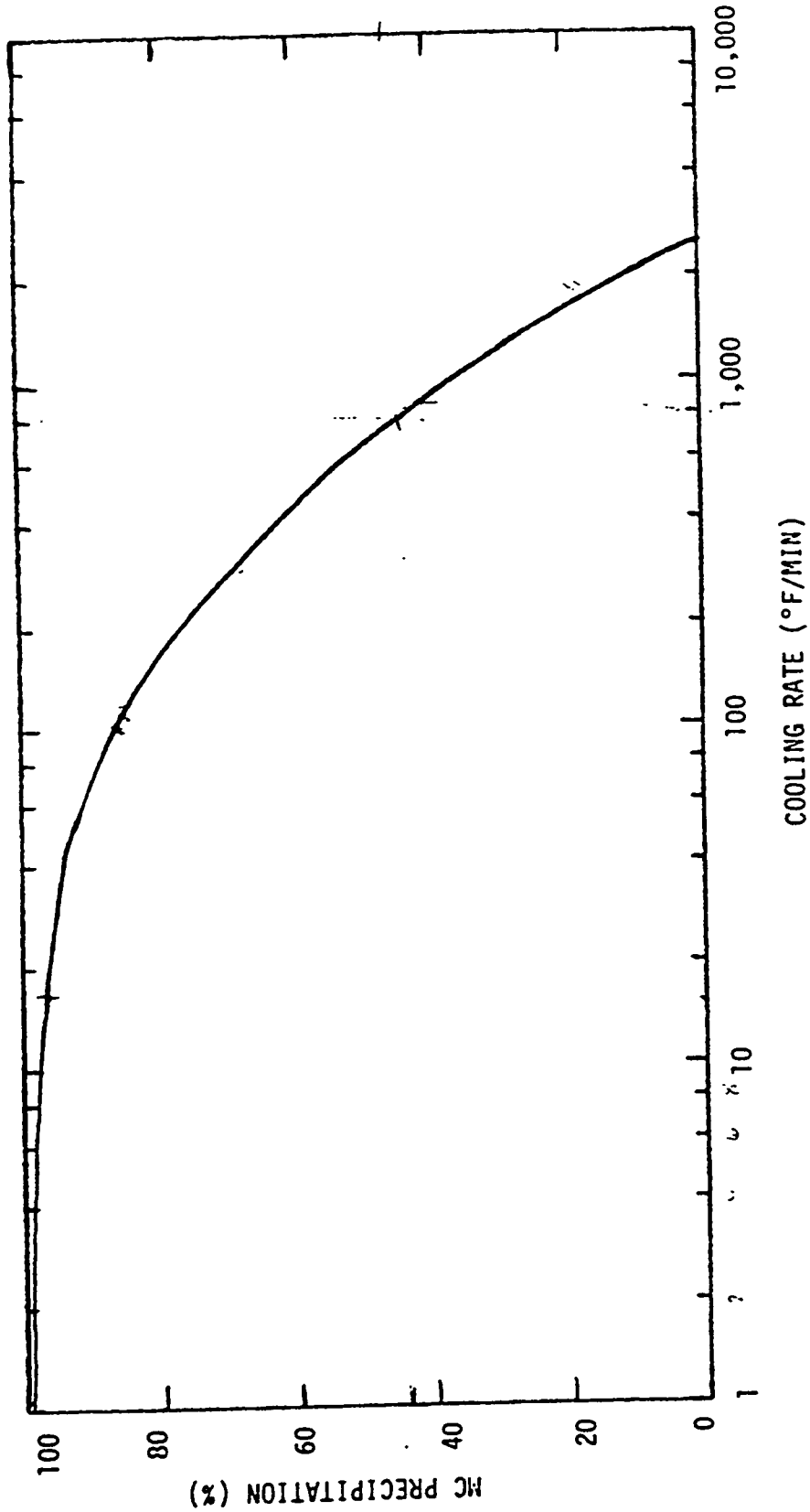

FIGURE 5 - The percentage of MC precipitation in H13 steel as a function of cooling rate.

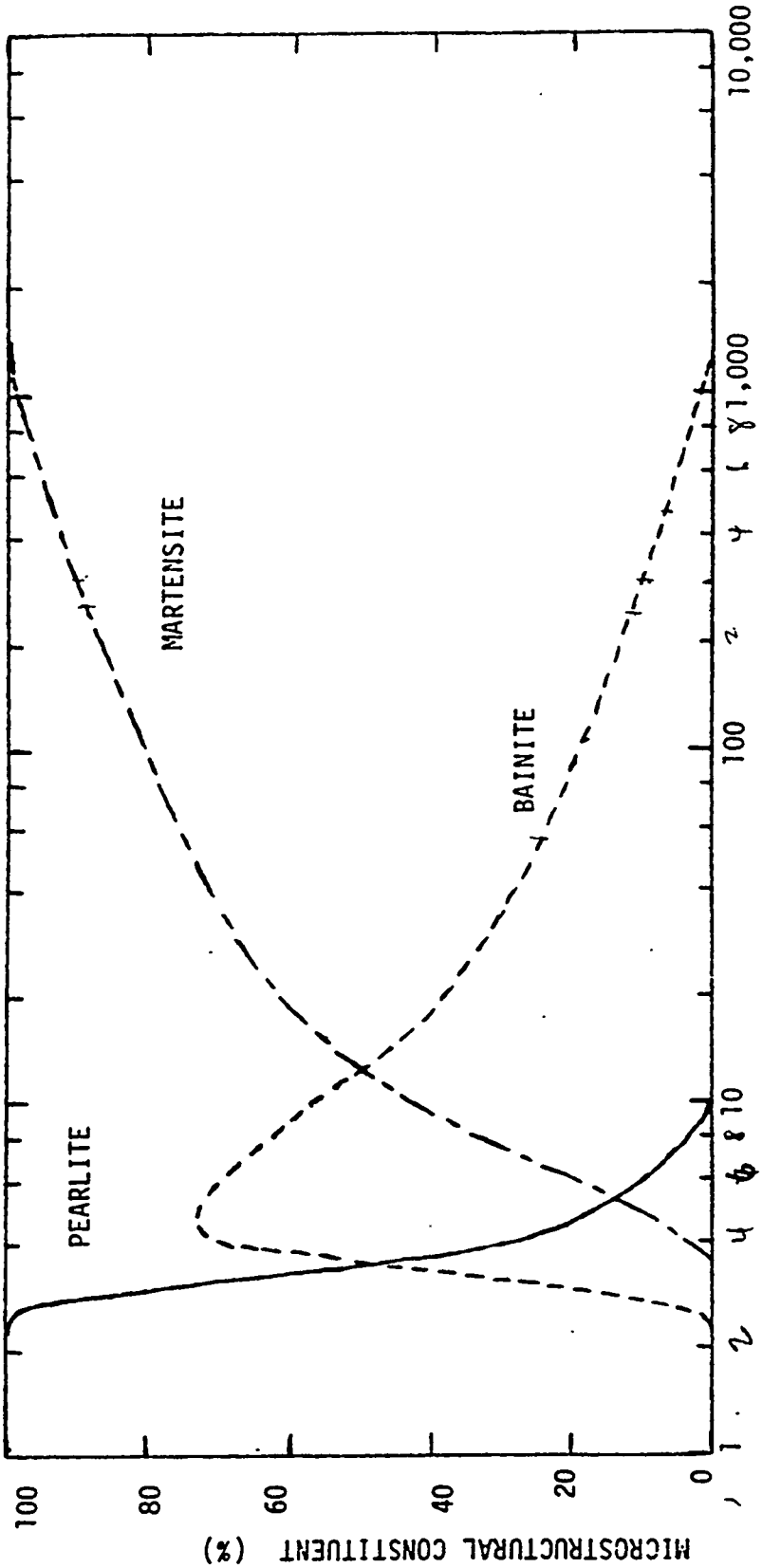

FIGURE 4 - The percentage martensite, bainite and pearlite in H13 steel as a function of cooling rate.

3. Experimental Cooling Rates

Computer prediction of distortion requires calculation of detailed transient temperature changes in the die. In order to increase the confidence level in the calculated values, the results of the calculations have to be validated with measured temperatures in vacuum/gas quench experiments. This section provides information on such experiments from literature sources as well as ours.

3.1 Principles of Vacuum/Gas Quenching

This brief review of gas quenching in vacuum furnaces is based on an article by E. J. Radcliffe [36]. Rapid cooling is achieved in these furnaces by blasting the heat treated parts with an inert gas. A typical setup is shown in figure 3.1.

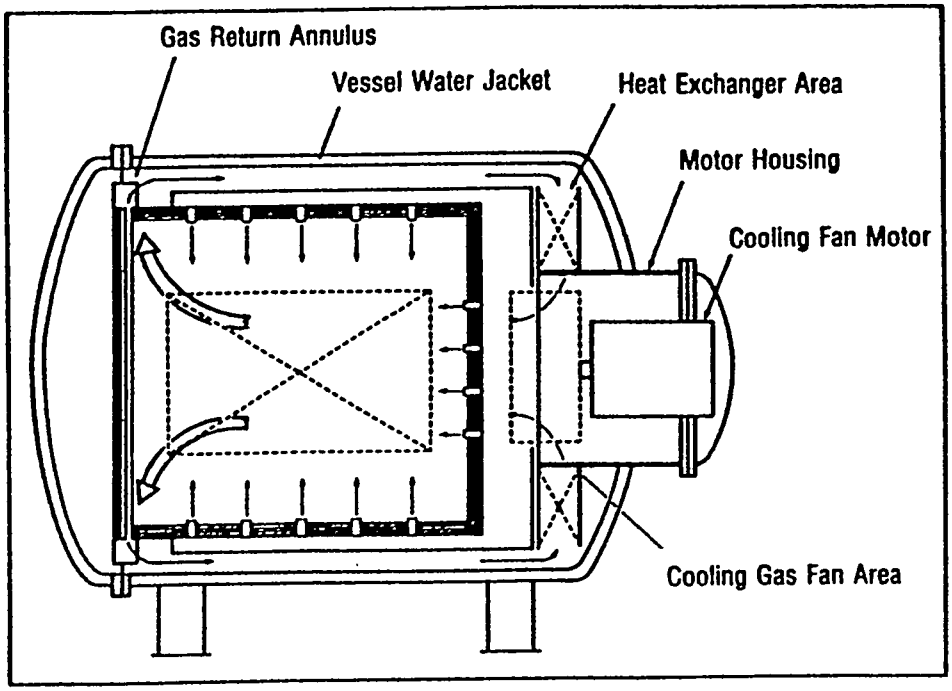

Figure 3.1: Typical vacuum/gas quench furnace

The cooling rates of the heat treated parts is controlled by the gas parameters and the component parameters.

3.1.1 Gas Parameters

The gas parameters control the rate at which heat is removed from the surface of the component. This rate is described by the equation:

$$Q = hA\Delta T$$

A - surface area of the component

h - heat transfer coefficient

T - temperature difference between the gas and the component

The effect of gas temperature and heat transfer coefficient on the cooling rate of a 1 inch dia. slug shown in figure 3.2 is demonstrated in figure 3.3.

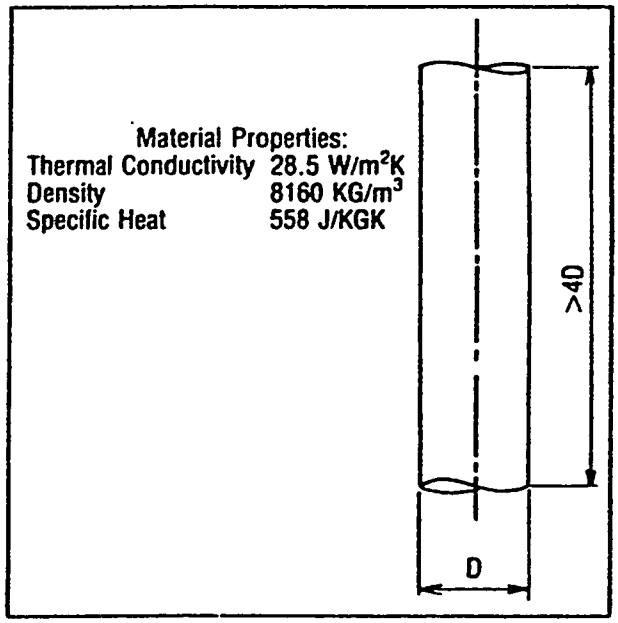

Figure 3.2: Steel cylinder used in the analytical model

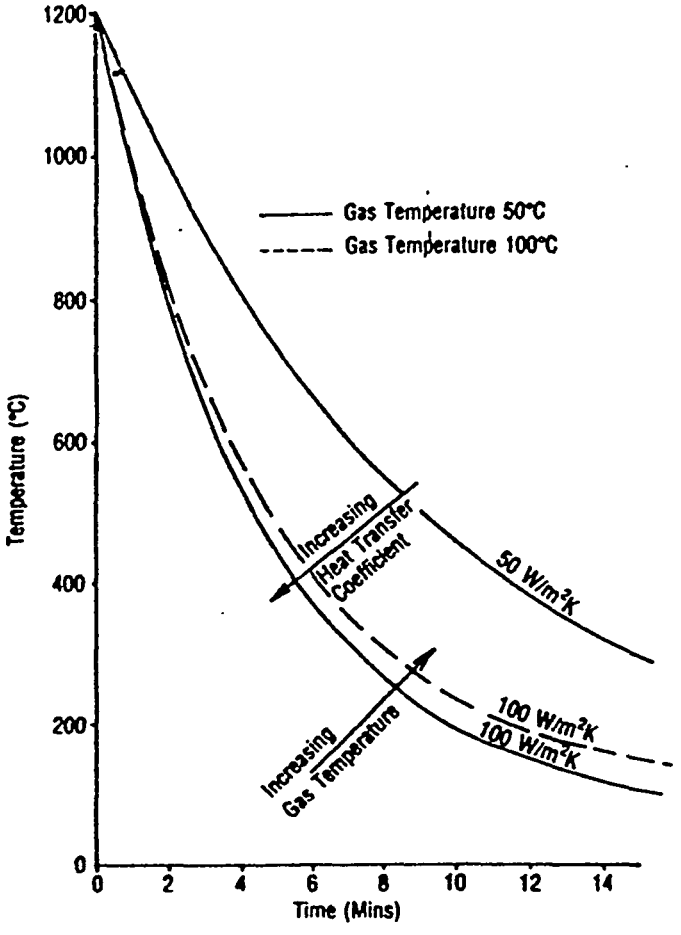

Figure 3.3: Effect of gas temperature and heat transfer on the cooling of a 1 inch dia. cylinder.

Gas temperature during quenching is controlled by the design of the heat exchanger and the flow distribution around the components. The heat transfer coefficient for a given gas, h, is related to the gas velocity V and the gas pressure P by the equation:

$$h = C(VP)^m$$

m and C are constants that depend on the furnace, component size and load configuration. Figures 3.4 and 3.5 show the effect of gas velocity and gas pressure respectively, on cooling the 1 inch diameter steel slug. For this particular situation, it can be shown that m=0.8. This relationship is demonstrated in figure 3.6.

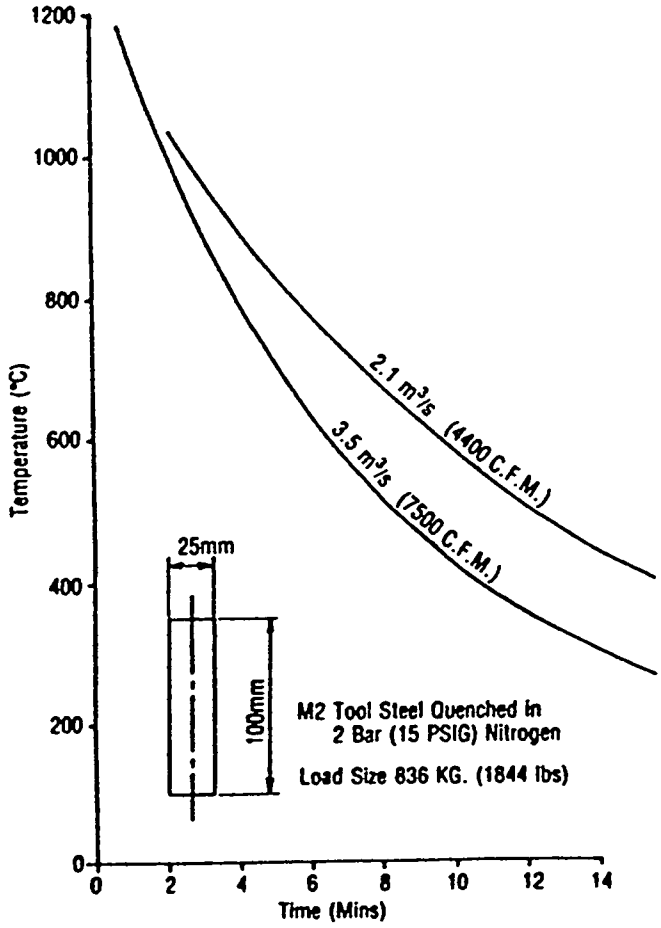

Figure 3.4: Effect of gas velocity

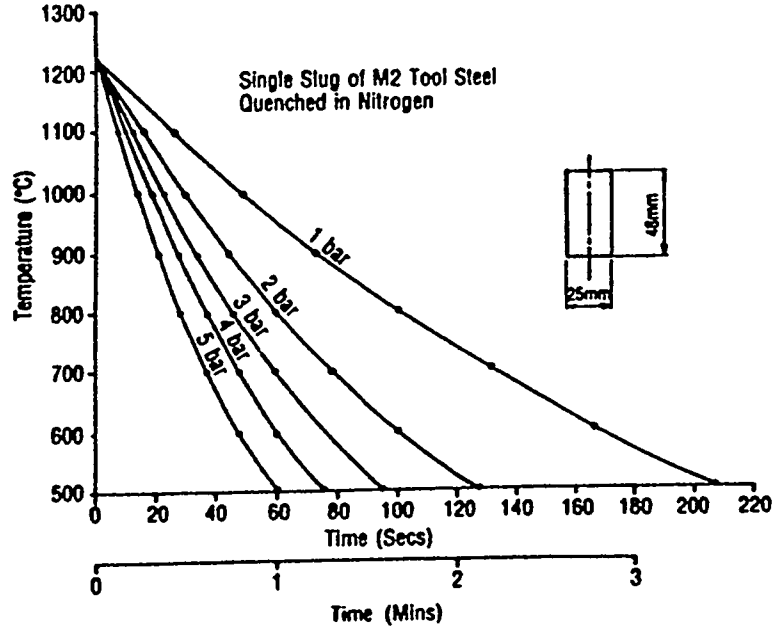

Figure 3.5: Effect of gas pressure

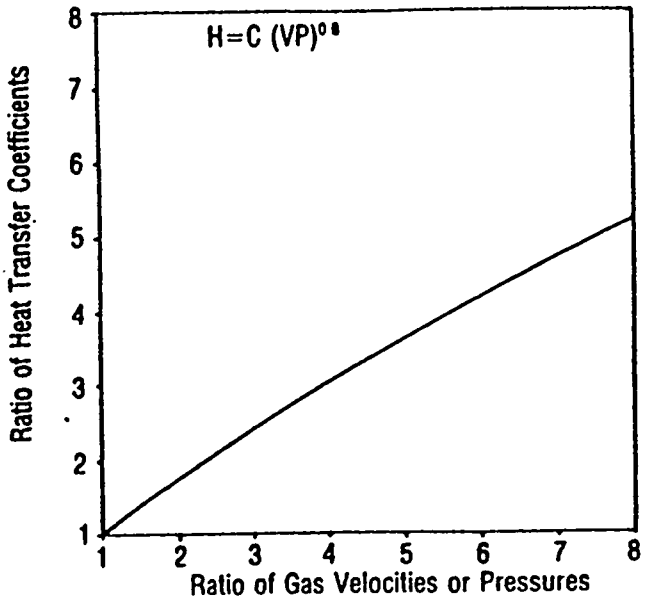

Figure 3.6: Effect of gas velocity/pressure on heat transfer coefficient

Notice the multiple of gas and velocity in the equation. Equal increase in either one has the same effect on h, hence on the cooling rate. However, from a technical standpoint, increasing gas velocity is more demanding on the design of the blower than increasing the pressure: doubling the gas velocity increases the blower power by a factor of eight, while doubling the gas pressure only increases the blower power by a factor of two. The heat transfer is also a function of the gas properties. Shown in figure 3.7 is the effect of gas properties on the cooling of the steel slug. The lower cost of nitrogen makes it the preferred choice in most gas quench applications.

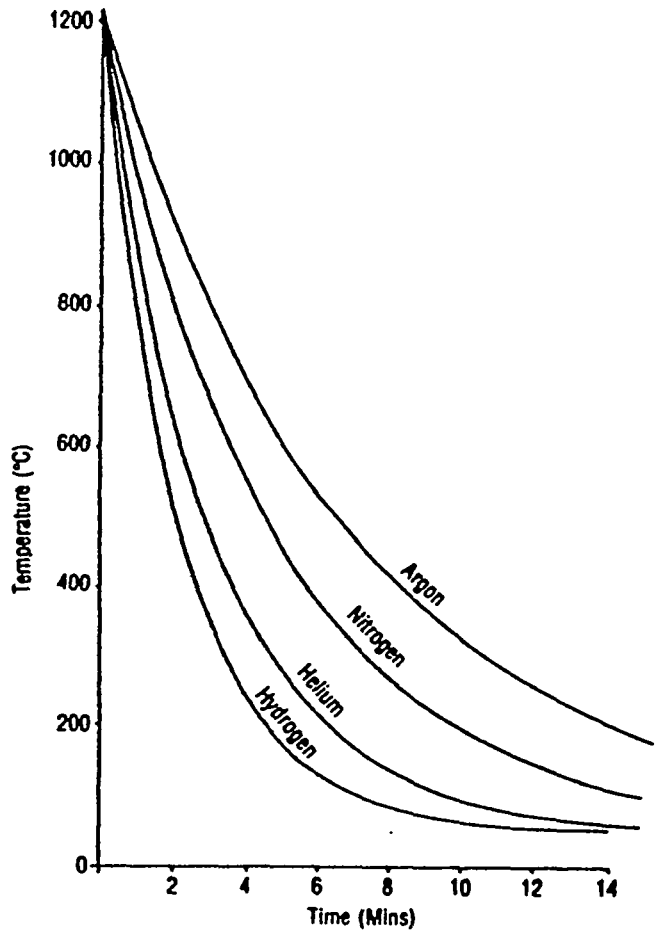

Figure 3.7: Effect of gas properties on the cooling rate

3.1.2 Component Parameters

The rate of heat transfer from the center of the components to the surface is controlled by component size, shape and material properties such as density, specific heat and thermal conductivity. The effect of the slug diameter is shown in figure 3.8. At the surface of the component, the cooling rate is inversly proportional to the component diameter, as demonstrated in figure 3.9. The temperature at the center of the cylinder lags behind the surface as shown in figure 3.10.

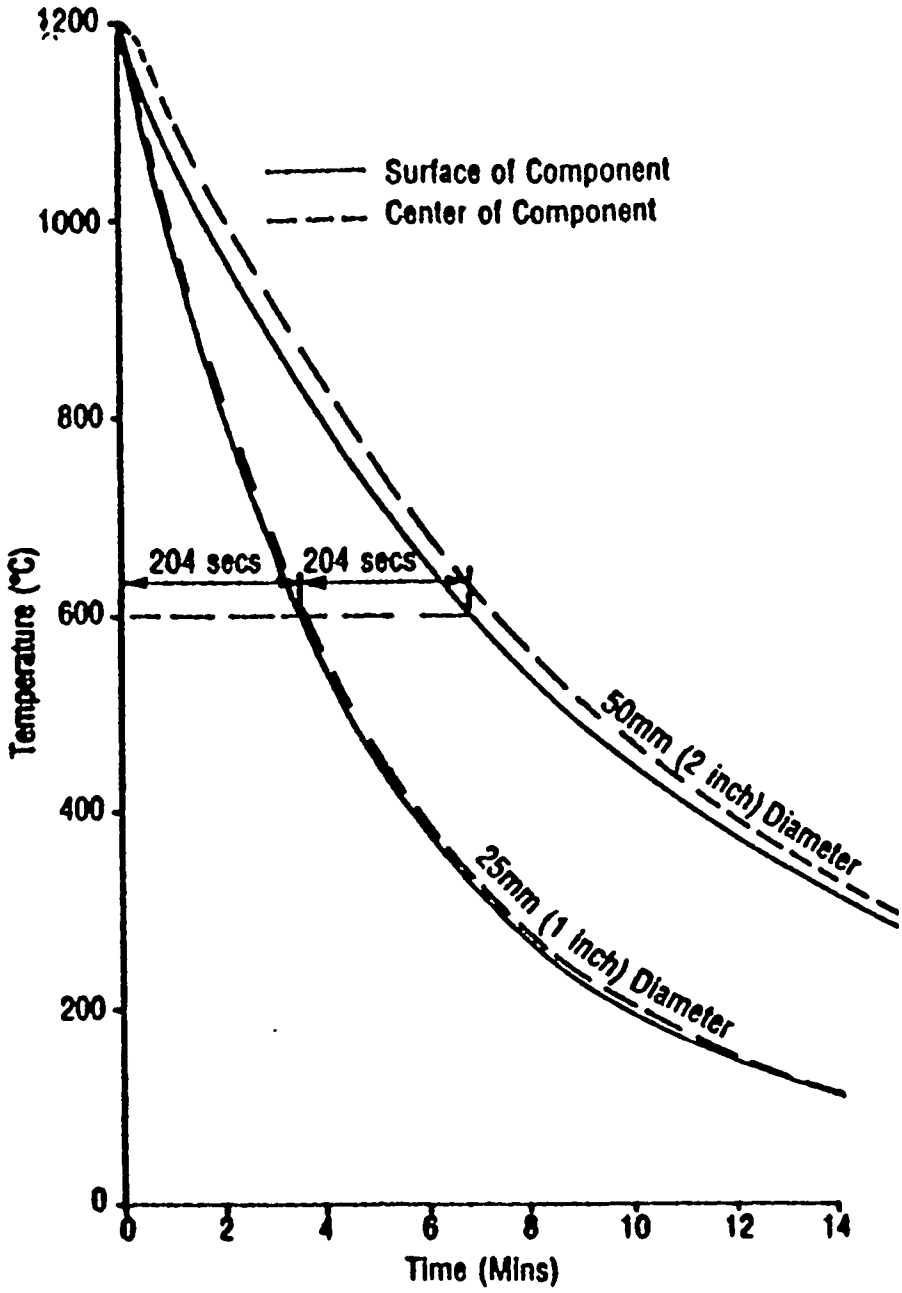

Figure 3.8: Effect of diameter on cooling

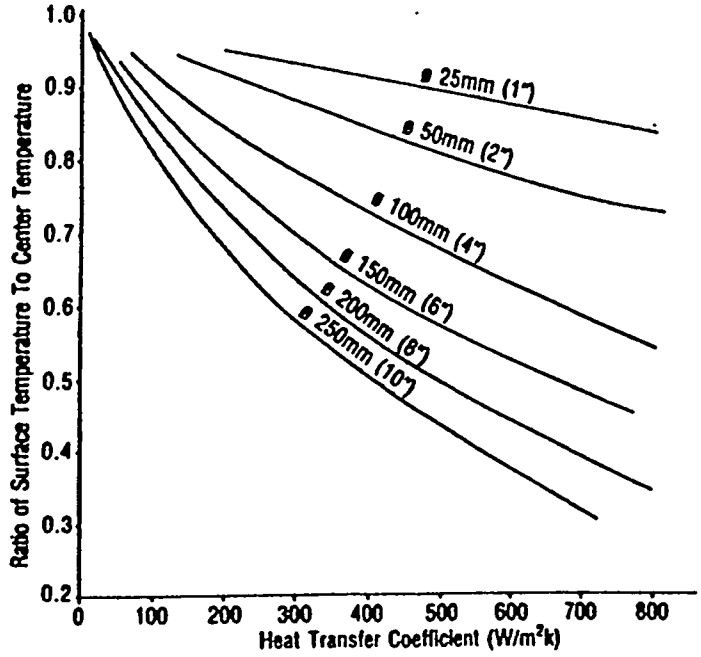

Figure 3.9: Ratio of surface temperature to center temperature

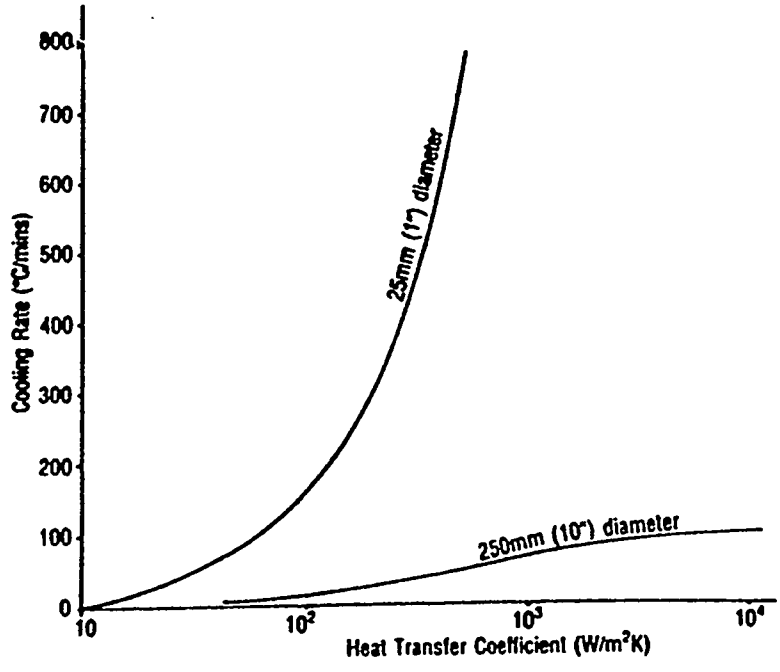

Figure 3.10: Cooling rate at the center of the cylinder

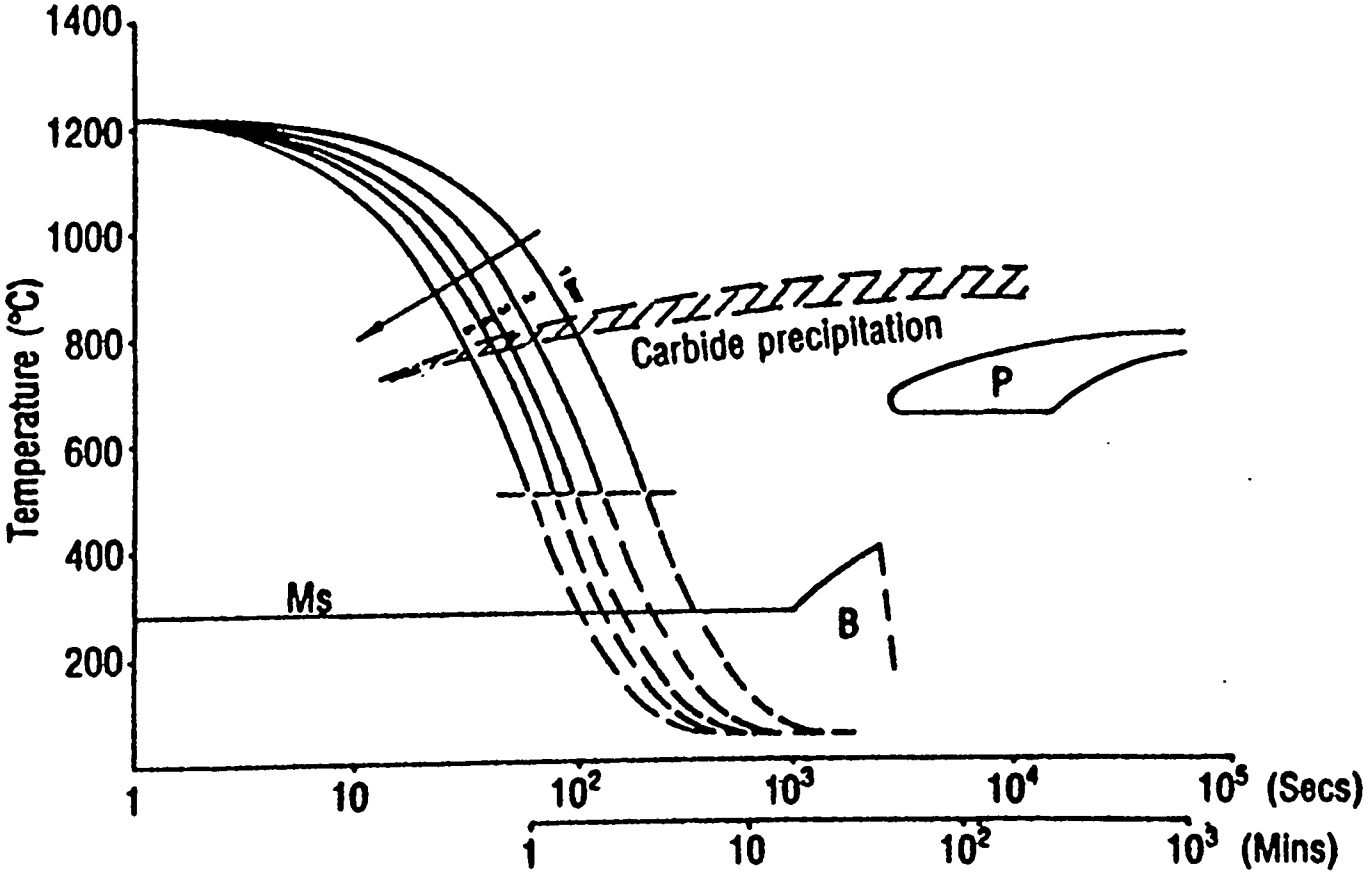

Figure 3.11: CCT diagram for H13; superimposed are cooling curves for a 1 inch dia. component quenched with gas pressures of 1 to 5 bars

As the heat transfer coefficient is increased, the component parameters begin to restrict the cooling rate and large temperature differences begin to develop. Unless controled, these differences can cause distortion and cracking in large diameter components.

3.2 Gas Quenching of Large-section Tool Steels

This section summarizes work done at Solar Atmospheres, Souderton, PA and Ironbound Heat Treating, as reported by William W. Hoke II [37]. Three large blocks of steel were treated with thermocouples attached at different locations. The sizes of the blocks, location of the thermocouples and the respective curves are all shown in figure 3.12. Each block was used three times, in different furnaces: HL-26 (26-inch-dia.hot zone), HL-36 and HL-50. The operating conditions of the furnaces are shown in Table 1.

Furnace	Operating pressure	Current	Conditions	Hardness Rockwell C
HL-24	15 psig	70 amps	center nozzles only	63
HL-36	25 psig	100 amps	outer nozzles closed	63
HL-36	21 psig	100 amps	all nozzles open	63
HL-50	7 psig	60 amps	all nozzles open	61

Table I: Operating conditions and as-quenched hardness

Figure 3.12: Experimental cooling curves for large die blocks

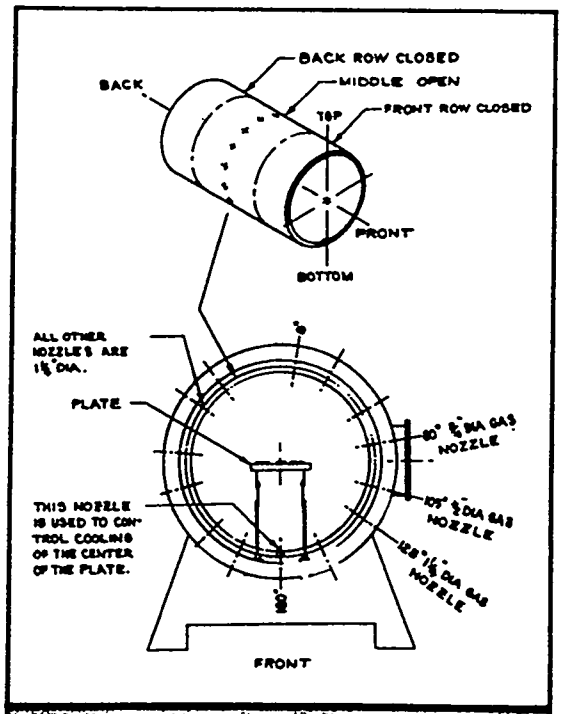

Fig. 1: Modified nozzle pattern

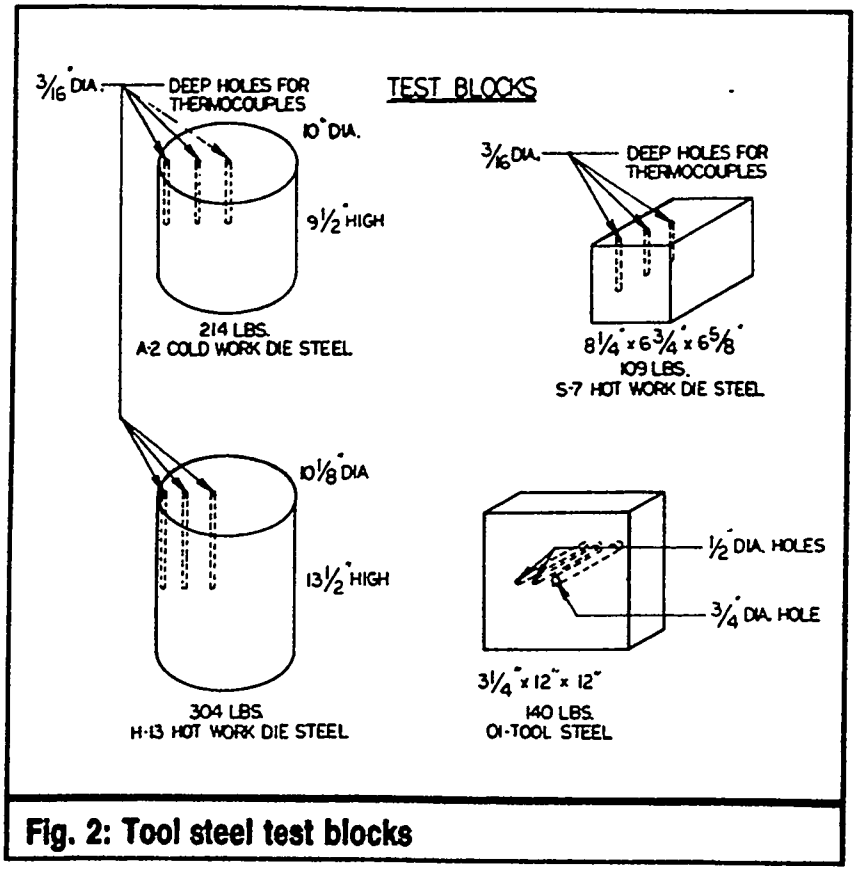

Fig. 2: Tool steel test blocks

Figure 3.12: Experimental cooling curves for large die blocks(cont.)

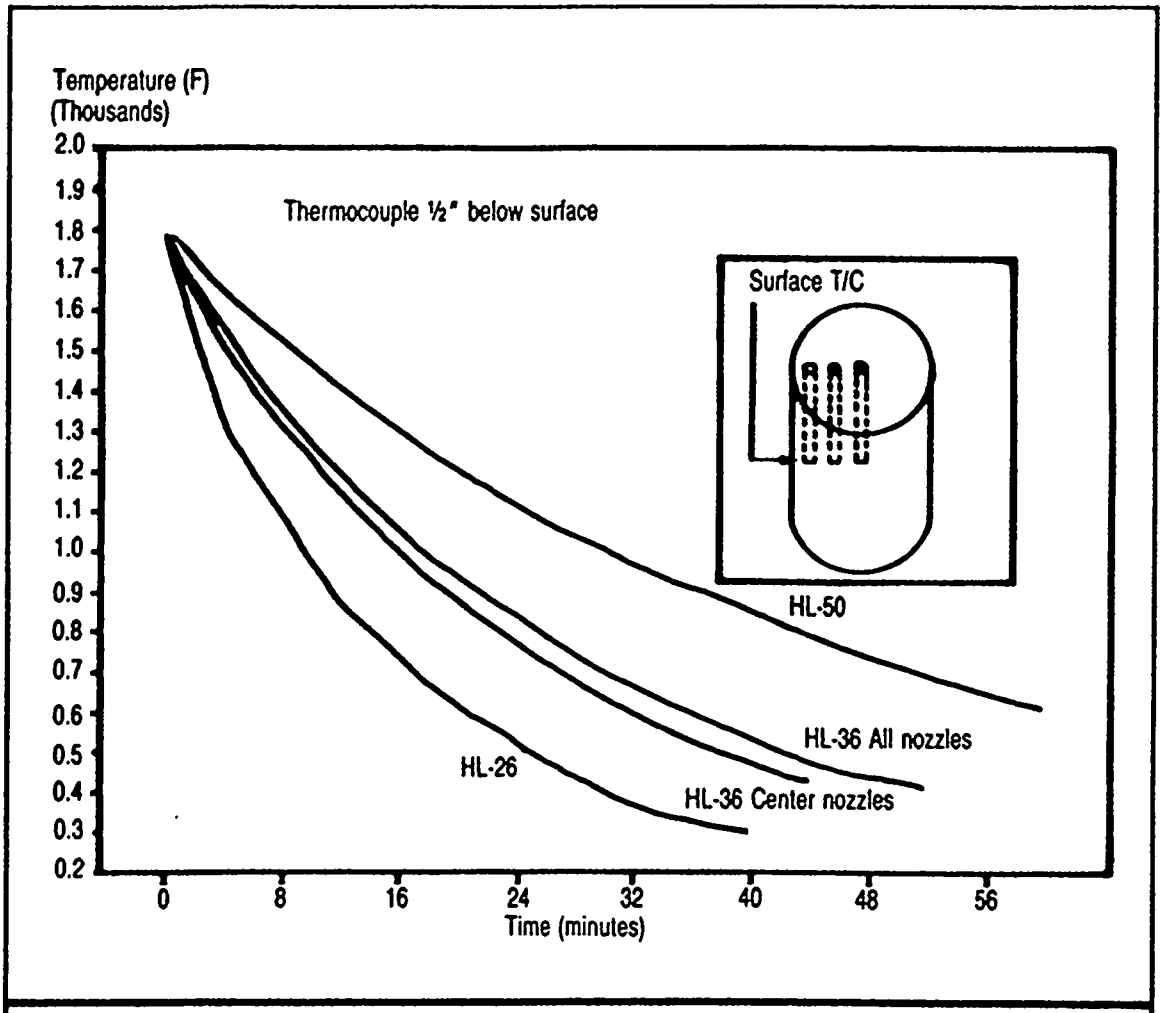

Fig. 3: Cooling curve—A2 block, 214 lbs.

Figure 3.12: Experimental cooling curves for large die blocks(cont.)

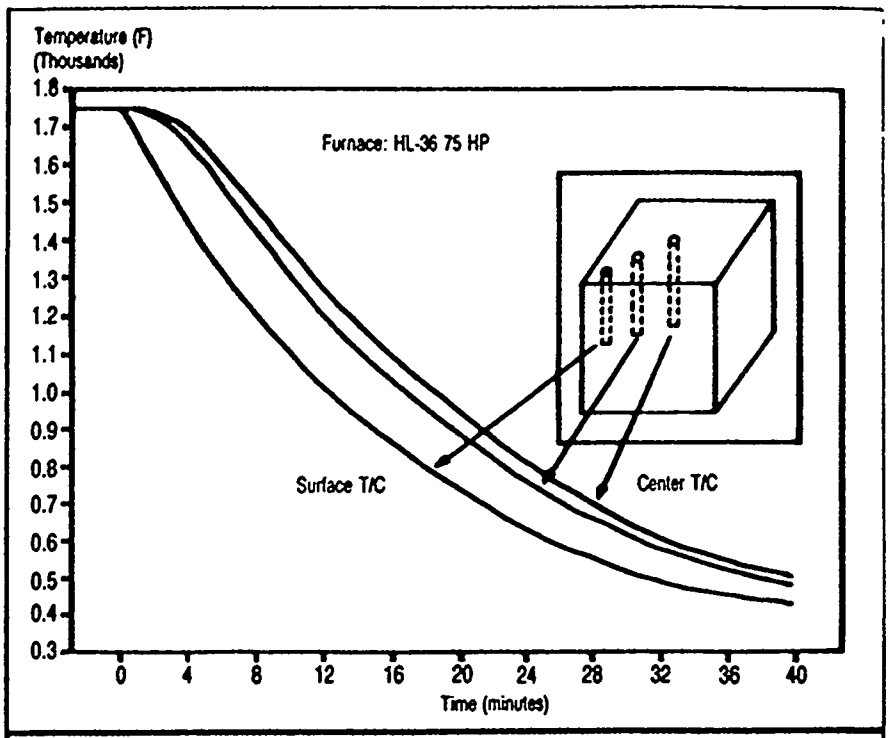

Fig. 4: Cooling curve—S7 Block, 109 lbs.

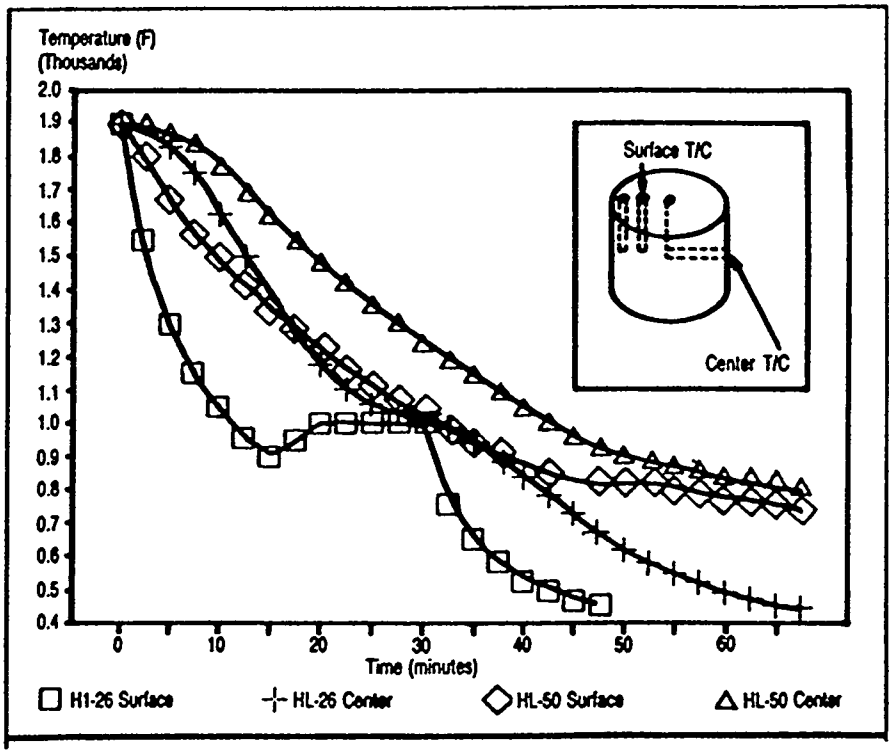

Figure 3.12: Experimental cooling curves for large die blocks(cont.)

3.3 Gas Quenching of Thick Plates

Following are calculated temperature profiles and cooling-rate curves at different locations of a 4 inches thick plate for gas and HIP quenching. The model accounts for a variable h, coefficient of heat transfer, that changes as a function of temperature, as shown in the graph.

1 Dimensional Heat Transfer Model
4 inch Thick Plate

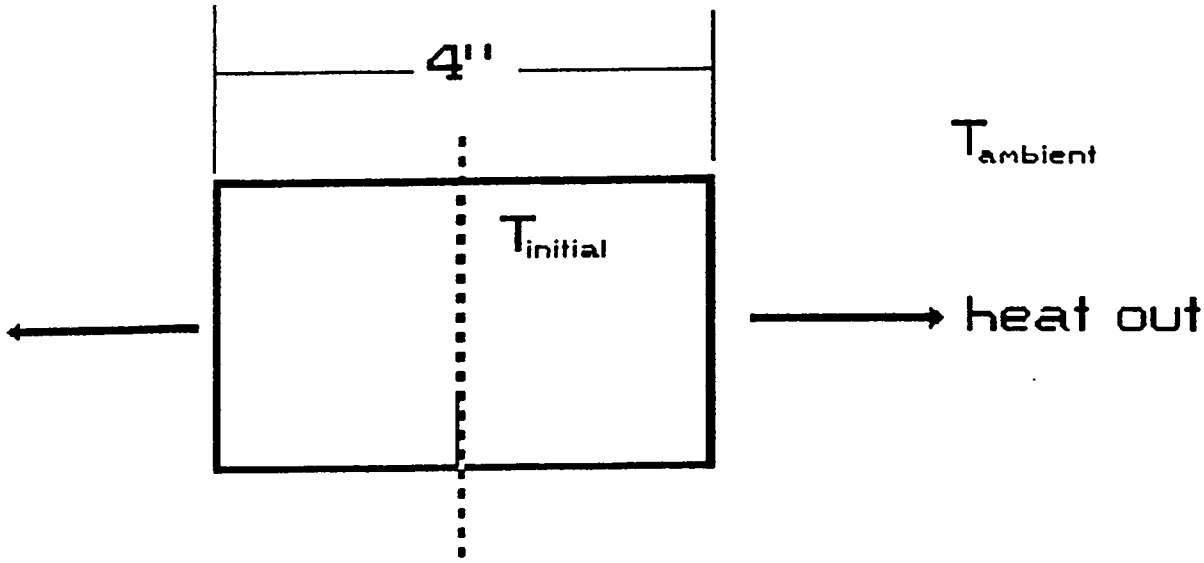

1. heat loss is controlled by the surface heat transfer coefficient
2. h is a function of surface temperature, gas properties and gas flow rate

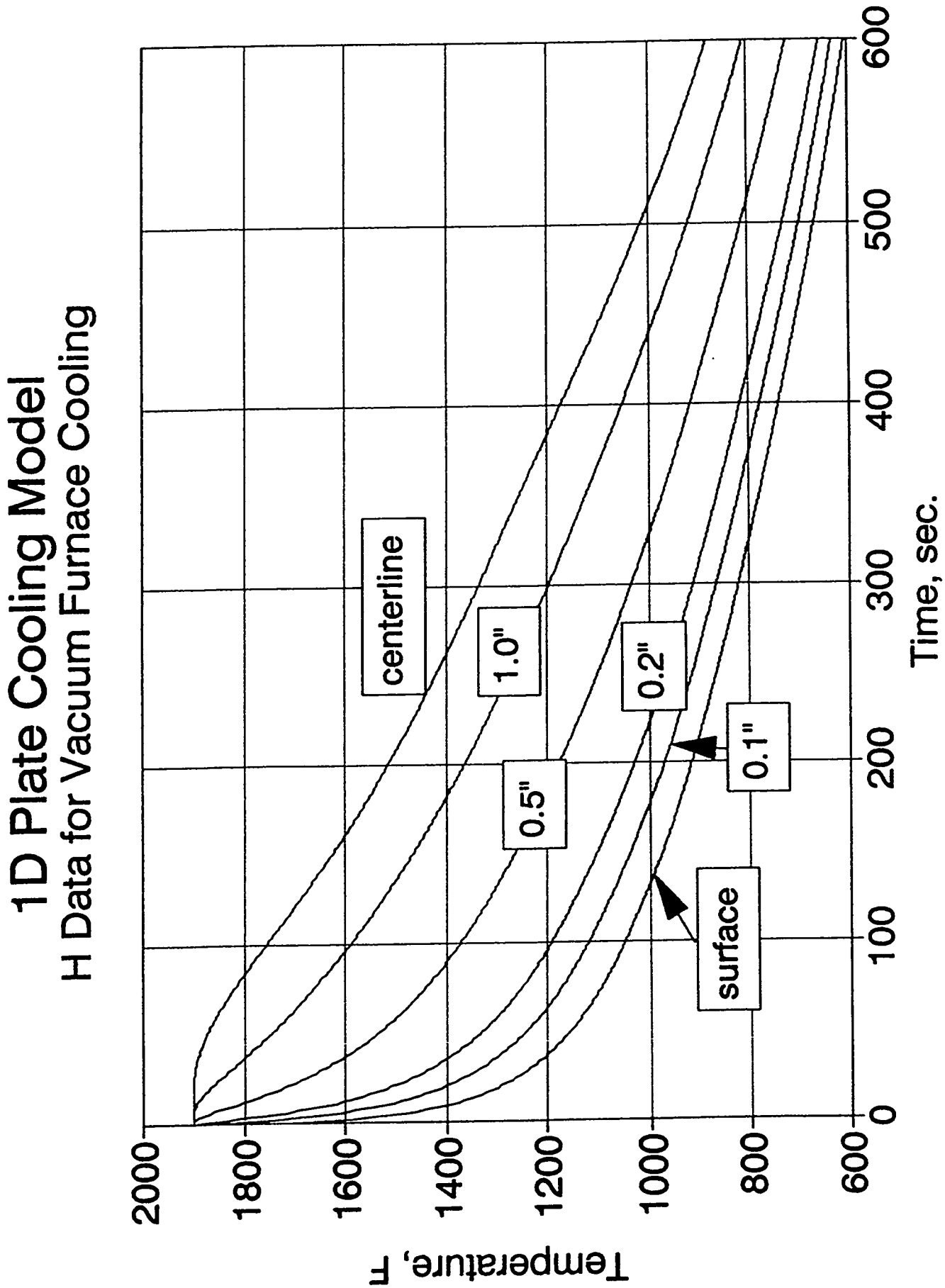
1D Plate Cooling Model
H Data for Vacuum Furnace Cooling
Temperature, F
Time, sec.
2000
1800
1600
1400
1200
1000
800
600
0
100
200
300
400
500
600
centerline
1.0"
0.5"
0.2"
0.1"
surface

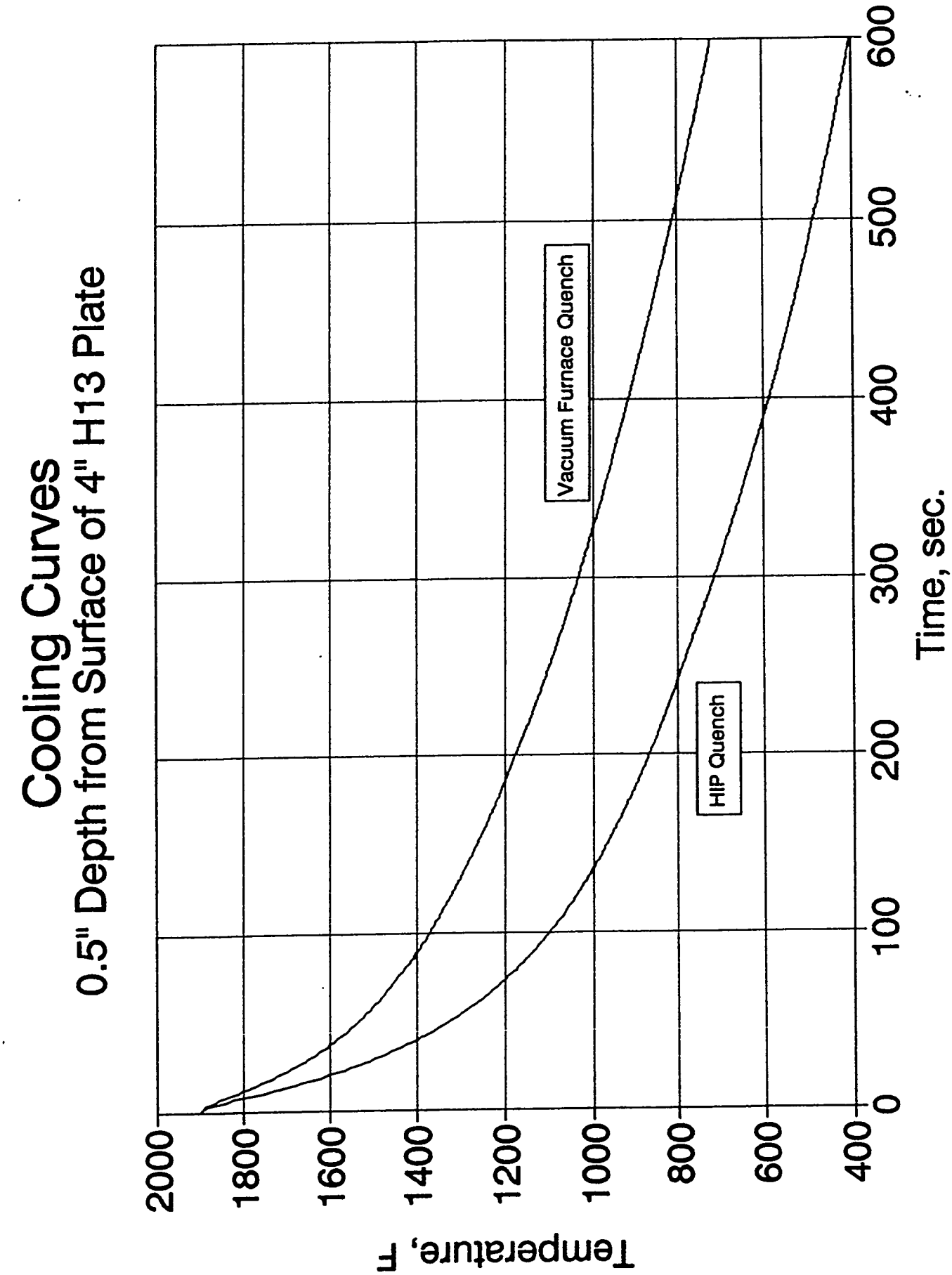
Cooling Curves
0.5" Depth from Surface of 4" H13 Plate
Temperature, °F
2000
1800
1600
1400
1200
1000
800
600
400
0
100
200
300
400
500
600
Time, sec.
Vacuum Furnace Quench
HIP Quench

Cooling Rate Curves

0.5" Depth from Surface of 4" H13 Plate

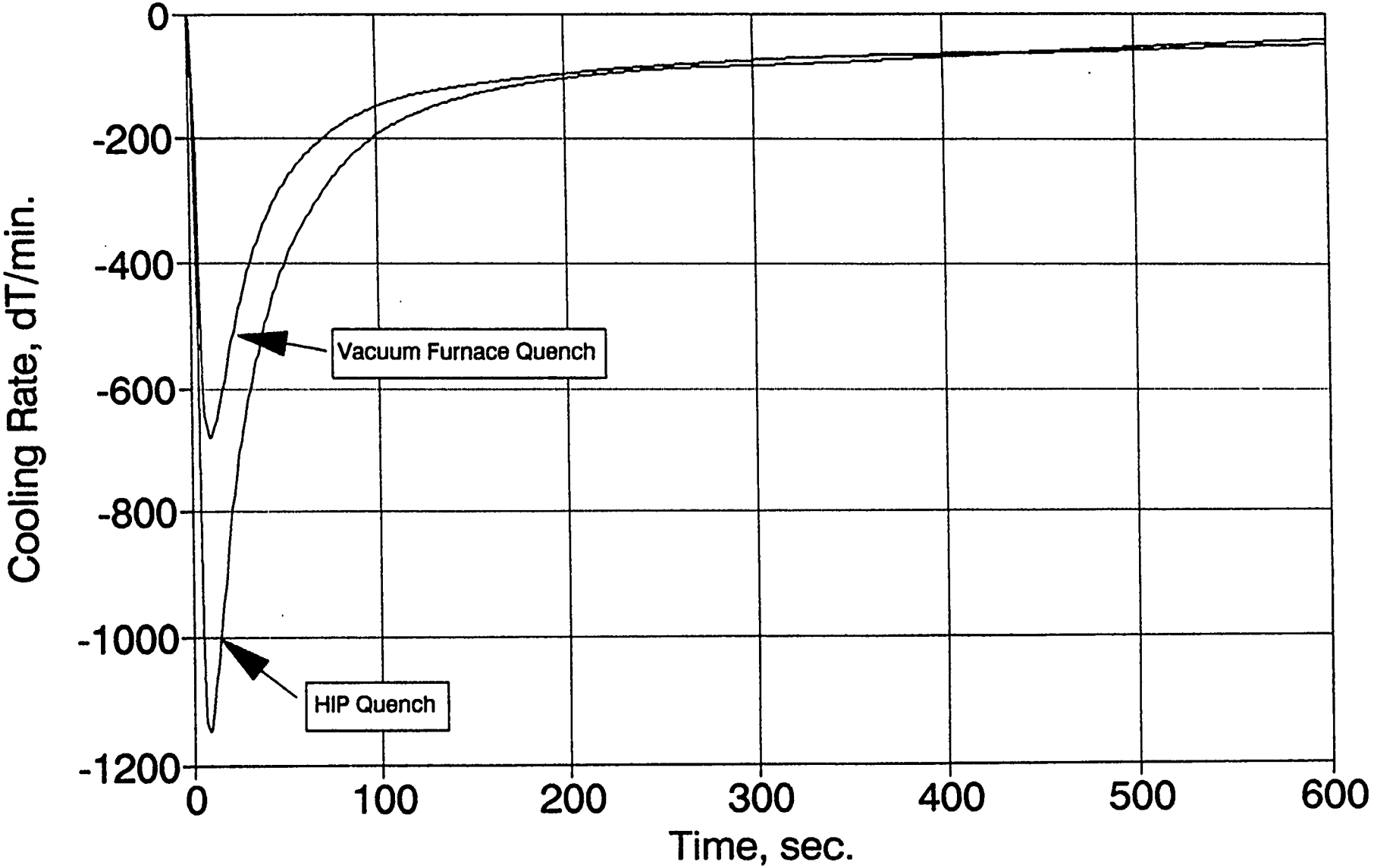

1D Plate Cooling Model
H Data for HIP Gas Quench

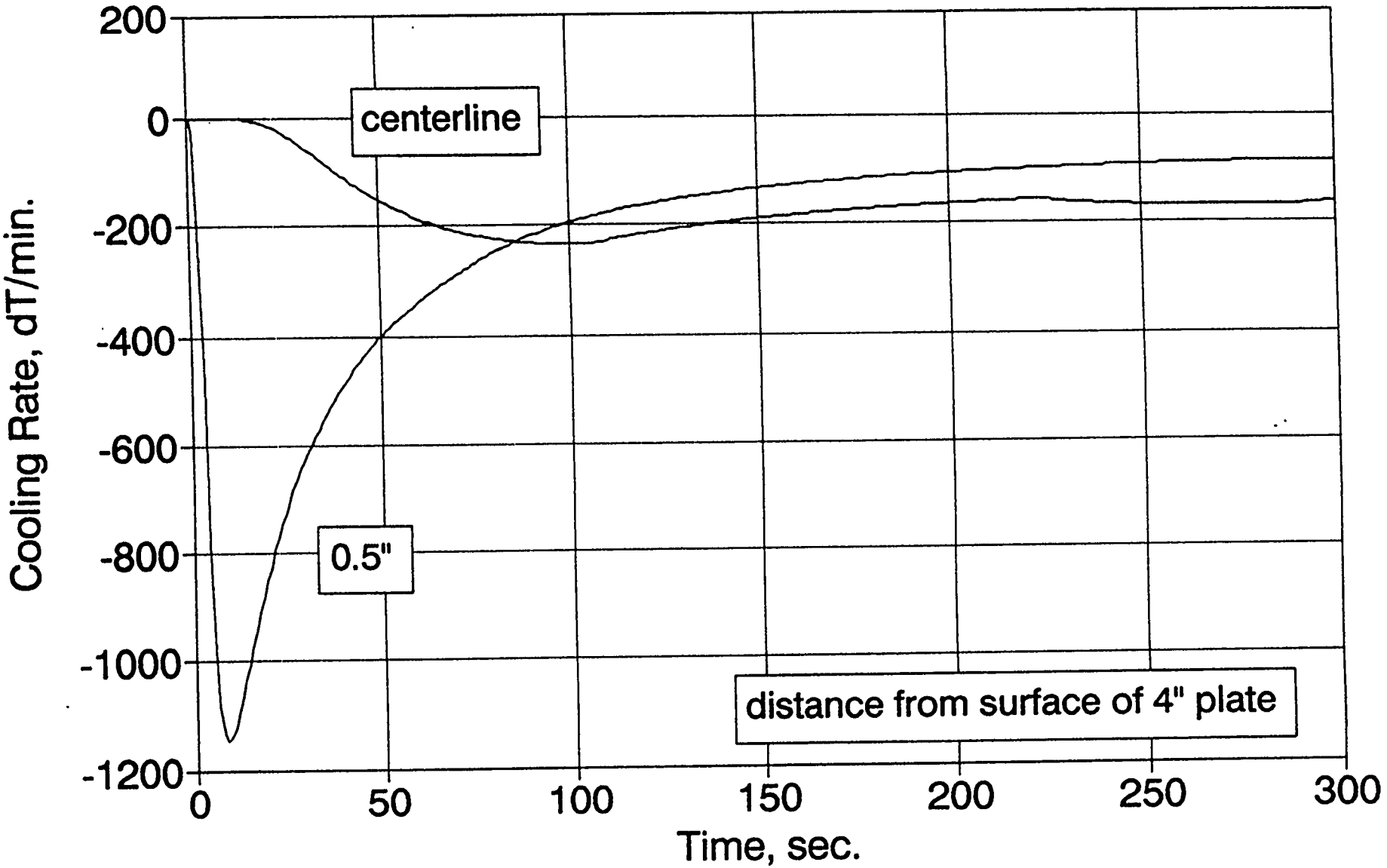

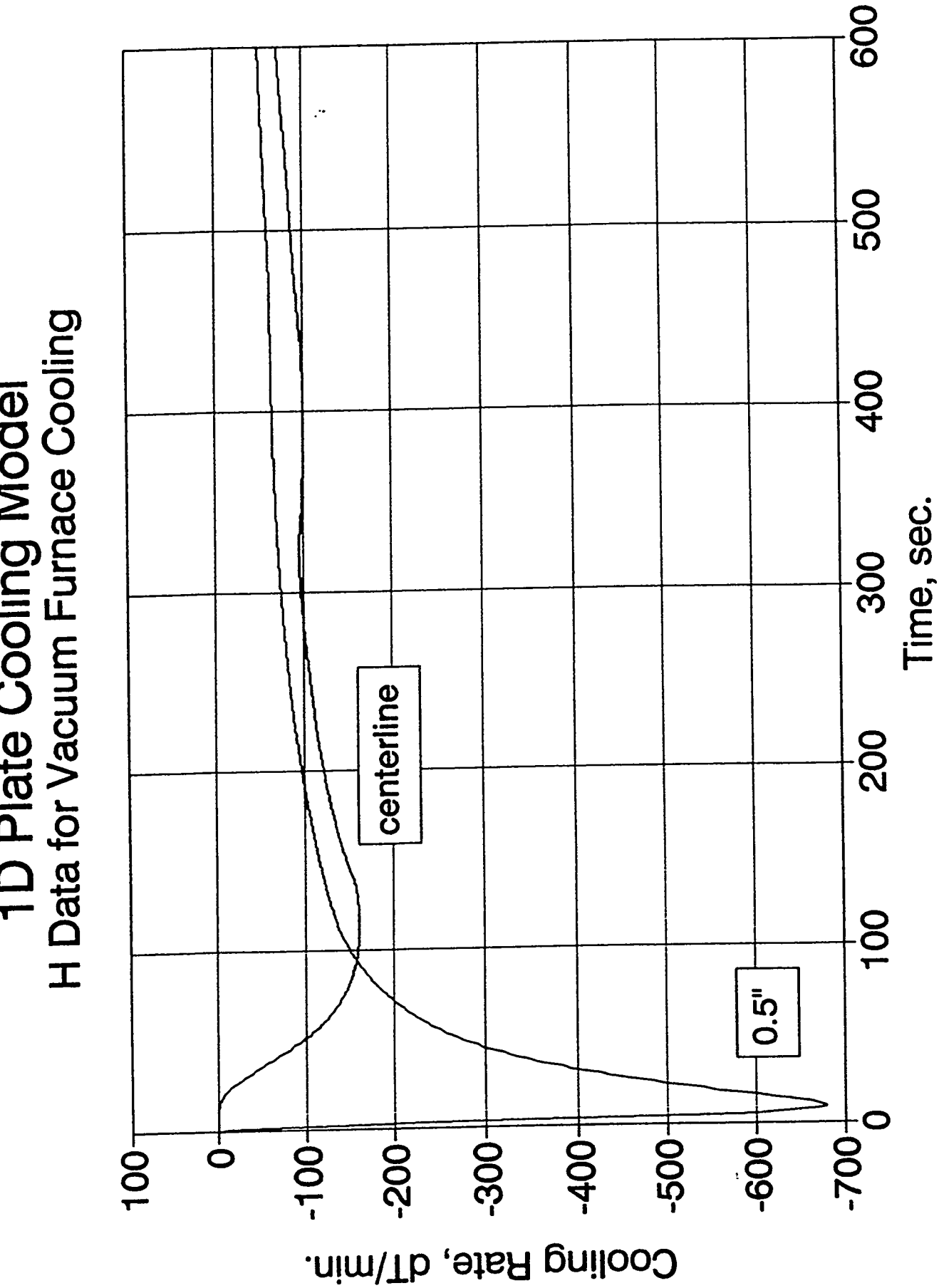
1D Plate Cooling Model
H Data for Vacuum Furnace Cooling
Cooling Rate, dT/min.
100
0
-100
-200
-300
-400
-500
-600
-700
0
100
200
300
400
500
600
Time, sec.
centerline
0.5"

1D Plate Cooling Model
H Data for HIP Gas Quench

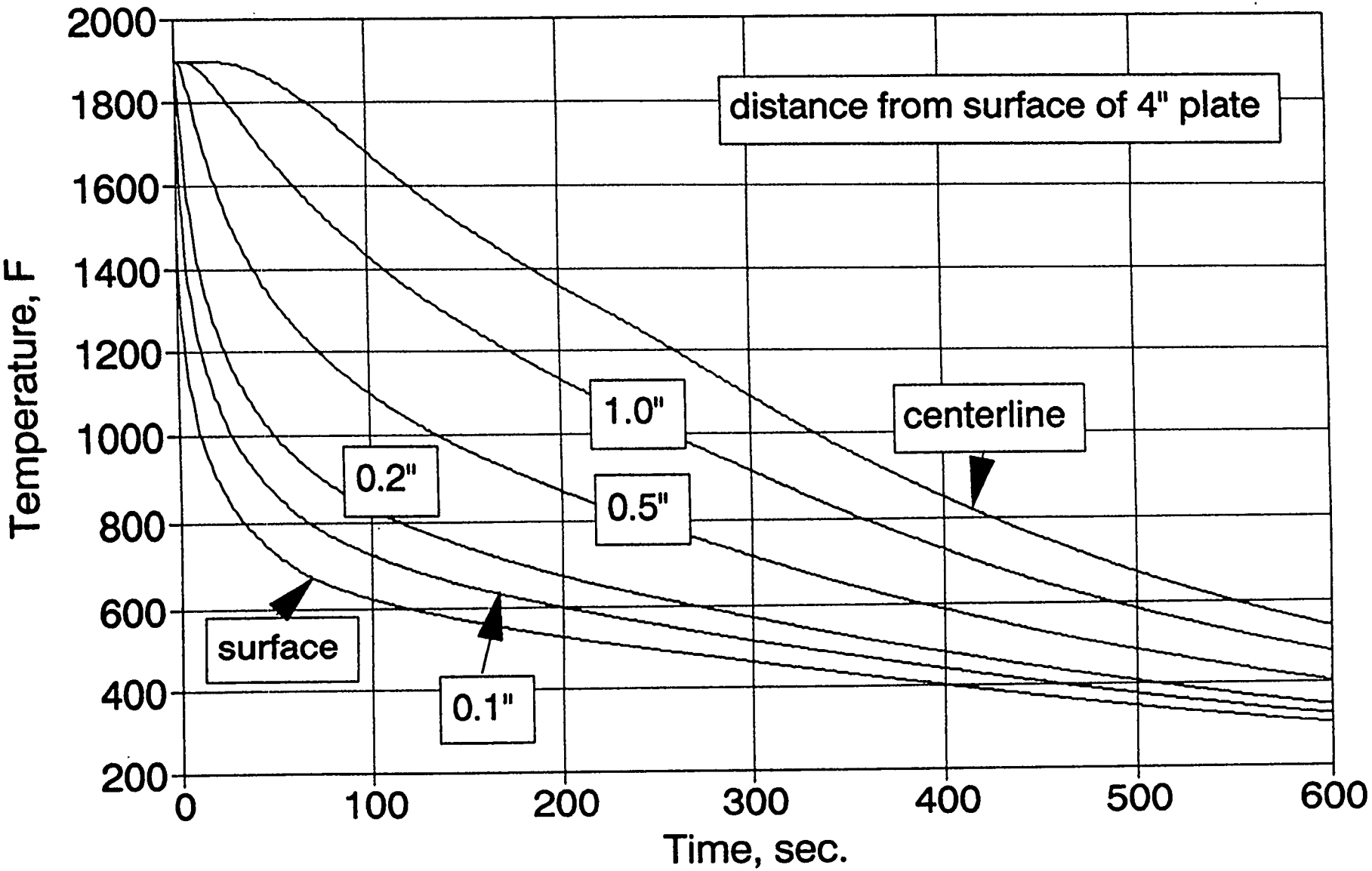

Surface Heat Transfer Coefficient

Bergman & Segerberg Data

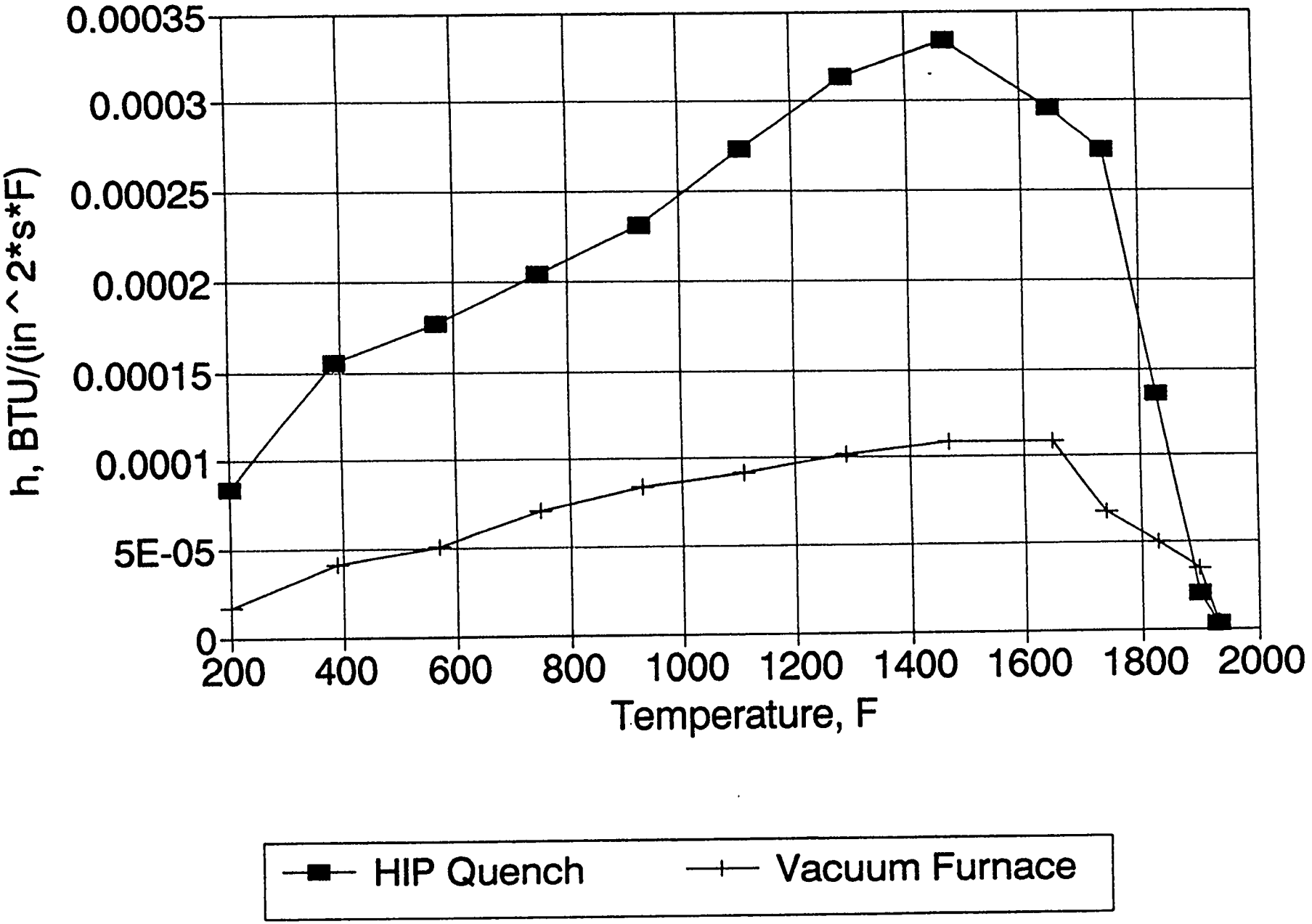

4. Die Materials Properties Data Base

Predicting thermal stresses and distortion caused by heat treatment using finite elements methods, requires inputs of physical and mechanical properties of the die material. This information is not readily available in the literature. Standard mechanical and physical property data is normally concerned with the stable condition of the materials, mostly at room temperature. Properties that change as a function of temperature are also available, though to a lesser extent. The most difficult to obtain are phase dependant properties. The properties of metastable austenite are such an example, that relates to quenching of steel.

The objective of this compilation is to provide relevant material properties for hot die steels, with H13 as the highest priority. Equivalent and related steels have also been included. Rather than excluding redundant data from multiple sources, it has been retained as a means of validating and confirming the information.

4. Die materials properties data base

4.1 General

4.1.1 Commercial Designation

4.1.2 Alternate Designations

4.1.3 Specifications

4.1.4 Composition

Chemical Composition. AISI: Nominal. 0.35 C, 1.50 Mo, 5.00 Cr, 1.00 V. UNS: 0.32 to 0.45 C, 4.75 to 5.50 Cr, 0.20 to 0.50 Mn, 1.10 to 1.75 Mo, 0.030 P max, 0.030 S max, 0.80 to 1.20 Si, 0.80 to 1.20 V

Similar Steels (U.S. and/or Foreign). UNS T20813; ASTM A681 (H-13); FED QQ-T-570 (H-13); SAE J437 (H13), J438 (H13), J467 (H13); (W. Ger.) DIN 1.2344; (Fr.) AFNOR Z 40 COV 5; (Ital.) UNI X 35 CrMoV 05 KU; (Jap.) JIS SKD 61; (Swed.) SS14 2242; (U.K.) B.S. BH13

Characteristics. A very popular and available grade. Is deep hardening and has very high toughness. Has excellent resistance to heat checking and can be water cooled in service. Is suitable for a wide range of applications including extrusion dies, die casting dies, mandrels, hot shears, and hot forging dies and punches. Has medium wear resistance, but can be carburized or nitrided to impart higher surface hardness with some loss in resistance to heat checking. Because of low carbon content, does not exhibit notable secondary hardening during tempering. Hardness begins to drop off rapidly when tempering above 1000 °F (540 °C). Has very low distortion in heat treating and high resistance to softening at elevated temperature. Hardness does not vary up to 800 °F (425 °C), and tools can withstand working temperatures of 1000 °F (540 °C). Has medium to high machinability and medium resistance to decarburization

Hot Work Tool Steels (H): Chemical Composition

Steel type	Chemical composition, % C	Cr	Mo	W	V
Chromium types					
H10	0.35-0.45	3.00-3.75	2.00-3.00	...	0.25-0.75
H11	0.33-0.43	4.75-5.50	1.10-1.60	...	0.30-0.60
H12	0.30-0.40	4.75-5.50	1.25-1.75	1.00-1.70	0.50 max
H13	0.32-0.40	4.75-5.50	1.10-1.75	...	0.80-1.20
H14	0.35-0.45	4.75-5.50	0.20-0.50	4.00-5.25	...
H19(a)	0.32-0.45	4.00-4.50	0.20-0.50	3.75-4.50	1.75-2.20

AISI H13 and Related Hot Tool Steels

#	Source	Designation	C	Mn	Si	S	P	Cr	Mo	V	Ni	W
1	Latrobe Steel	VDC, VDC-RF	.40	.40	1.00			5.25	1.35	1.00		
2	Jessop	Dica B Vanadium	.37	.40	1.00			5.00	1.35			
3	Carpenter	883	.41	.35	1.00			5.35	1.40	0.90		
4	Thyssen	Thyrotherm 2344	.40	.40	1.00			5.30	1.30	1.00		
5	Uddeholm	Ovar Supreme	.39	.49	.93	.001	.020	5.29	1.20	0.84	.15	.02
6	Hitachi Metal	YEM4	.31	.63	.31	.003	.015	5.38	2.57	0.65	.07	.02
7	Daido Steel	DH21	.38	.65	.23	.001	.012	5.34	1.79	0.82	.06	.02
8	Uddeholm	Ovar	.40	.47	1.12	.002max	0.020	5.20	1.30	0.96		

4.1.5 Heat Treatment

Recommended Heat Treating Practice

Normalizing. Do not normalize

Annealing. Heat to 1550 to 1650 °F (845 to 900 °C). Use lower limit for small sections and upper limit for large sections. Surface protection against decarburization by use of pack, controlled atmosphere, or vacuum is required. Heat slowly and uniformly, especially for hardened tools. Holding time varies from about 1 hr for light sections and small furnace charges to about 4 hr for heavy sections and large charges. For pack annealing, hold 1 hr per inch of cross section. Cool slowly in furnace at a rate not exceeding 50 °F (28 °C) per hour until 1000 °F (540 °C) is reached, when a faster cooling rate will not affect final hardness. Typical annealed hardness, 192 to 229 HB

Stress Relieving. Optional. Heat to 1200 to 1250 °F (650 to 675 °C) and hold for 1 hr per inch of cross section (minimum of 1 hr). Cool in air

Hardening. Surface protection against decarburization or carburization is required by utilizing salt, pack, controlled atmosphere or vacuum. For preheating, die blocks or other tools for open furnace treatment should be placed in a furnace that is not over 500 °F (260 °C). Work that is packed in containers may be safely placed in furnaces at 700 to 1000 °F (370 to 540 °C). Once the workpieces (or container) have attained temperature, heat slowly (no faster than 200 °F or 110 °C per hour) to 1500 °F (815 °C). Hold for 1 hr per inch of thickness (or per inch of container thickness if packed). If double preheating facilities, such as salt baths, are available, thermal shock can be reduced by preheating at 1000 to 1200 °F (540 to 650 °C) and further preheating at 1550 to 1600 °F (845 to 870 °C). Austenitize at 1825 to 1900 °F (995 to 1040 °C) for 15 to 40 min. Use shorter time for small sections and longer time for large sections. Quench in air. If blast cooling, air should be dry and blasted uniformly on surface to be hardened. To minimize scale, tools can be flash quenched in oil to cool the surface below scaling temperature (about 1000 °F, 540 °C), but this increases distortion. The procedure is best carried out by quenching from the austenitizing temperature into a salt bath held at 1100 to 1200 °F (595 to 640 °C), holding in the quench until the workpiece reaches the temperature of the bath, and then withdrawing the workpiece and allowing it to cool in air. Quenched hardness, 51 to 54 HRC

Stabilizing. Optional. For intricate shapes, stress relieve temper at 300 to 320 °F (150 to 160 °C) briefly. Refrigerate at −150 to −320 °F (−100 to −195 °C). Temper immediately after part reaches room temperature

Tempering. Temper immediately after tool reaches about 125 °F (52 °C) at 1000 to 1200 °F (540 to 650 °C). Forced convection air tempering furnaces heat tools at a moderately safe rate. Salt baths are acceptable for small parts, but may cause cracking of large or intricate shaped dies due to thermal shock. Temper for 1 hr per inch of thickness, cool to room temperature, and retemper using the same time at temperature. The second temper is essential and a third temper would be beneficial. Approximate tempered hardness, 53 to 38 HRC

Recommended Processing Sequence

- Rough machine
- Stress relieve (optional)
- Finish machine
- Preheat
- Austenitize
- Quench
- Stabilize (optional)
- Temper
- Final grind to size

Hot Work Tool Steels (H): Thermal Treatment Temperatures

Treatment	Temperature range °C	°F
Types H11, H12, H13, H19, H21		
Forging, start	1095-1135	2000-2075
Forging, finish	925 min	1700 min
Annealing	845-870	1550-1600
Stress relieving	650-675	1200-1250
Hardening	1010-1025	1850-1875
Tempering	(a)	(a)

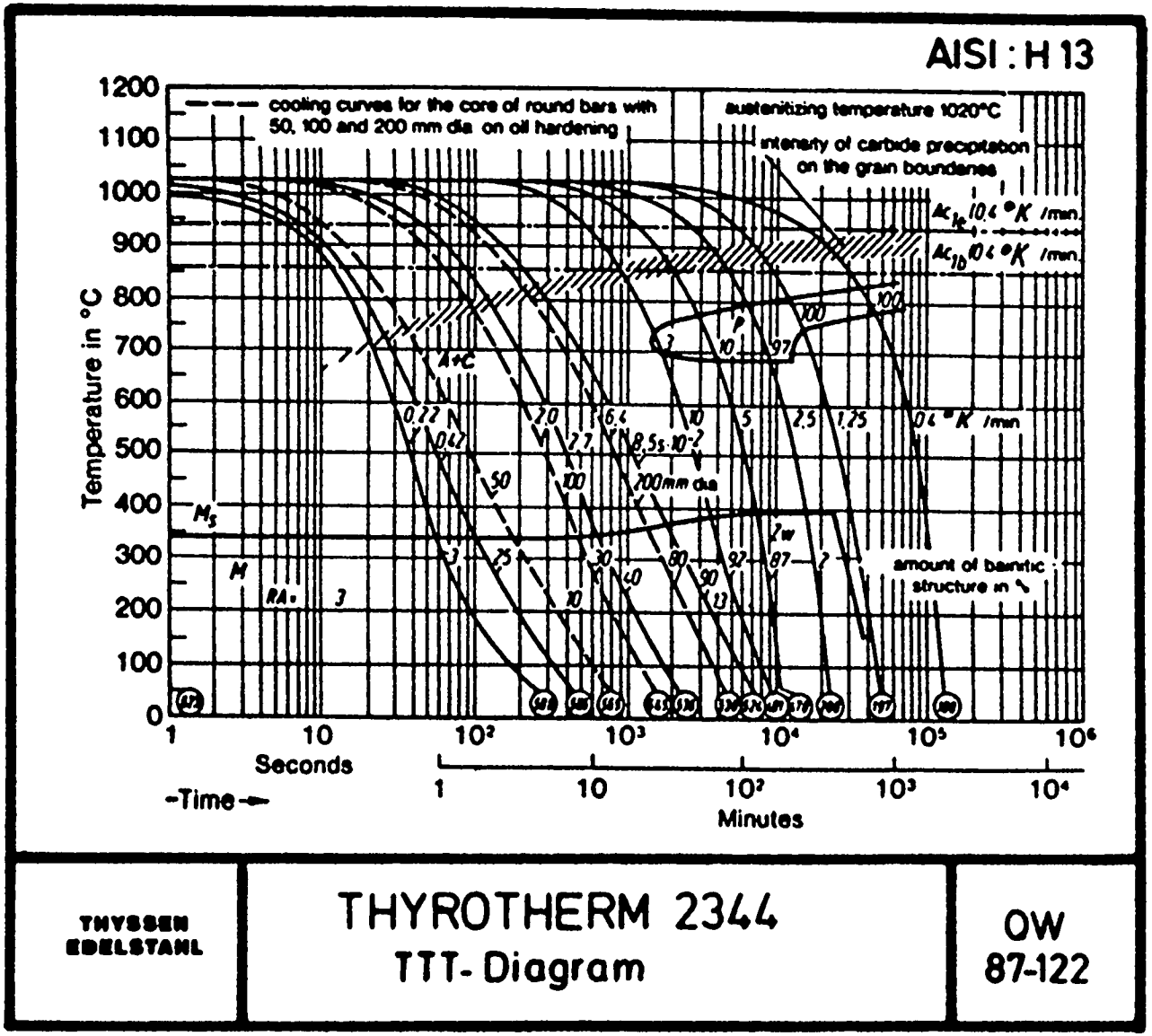
AISI : H 13
cooling curves for the core of round bars with 50, 100 and 200 mm dia on oil hardening
austenitizing temperature 1020°C
intensity of carbide precipitation on the grain boundaries
Temperature in °C
Seconds
Minutes
-Time-
amount of bainitic structure in %
THYSSEN EDELSTAHL
THYROTHERM 2344
TTT-Diagram
OW
87-122

Tool and Die Steels

Composition: 0.37% C - 0.51% Mn - 1.00% Si - 5.10% Cr - 1.26% Mo - 0.97% V Austenitized (a) at 1080°C (1976°F) (b) 1030°C (1886°F)

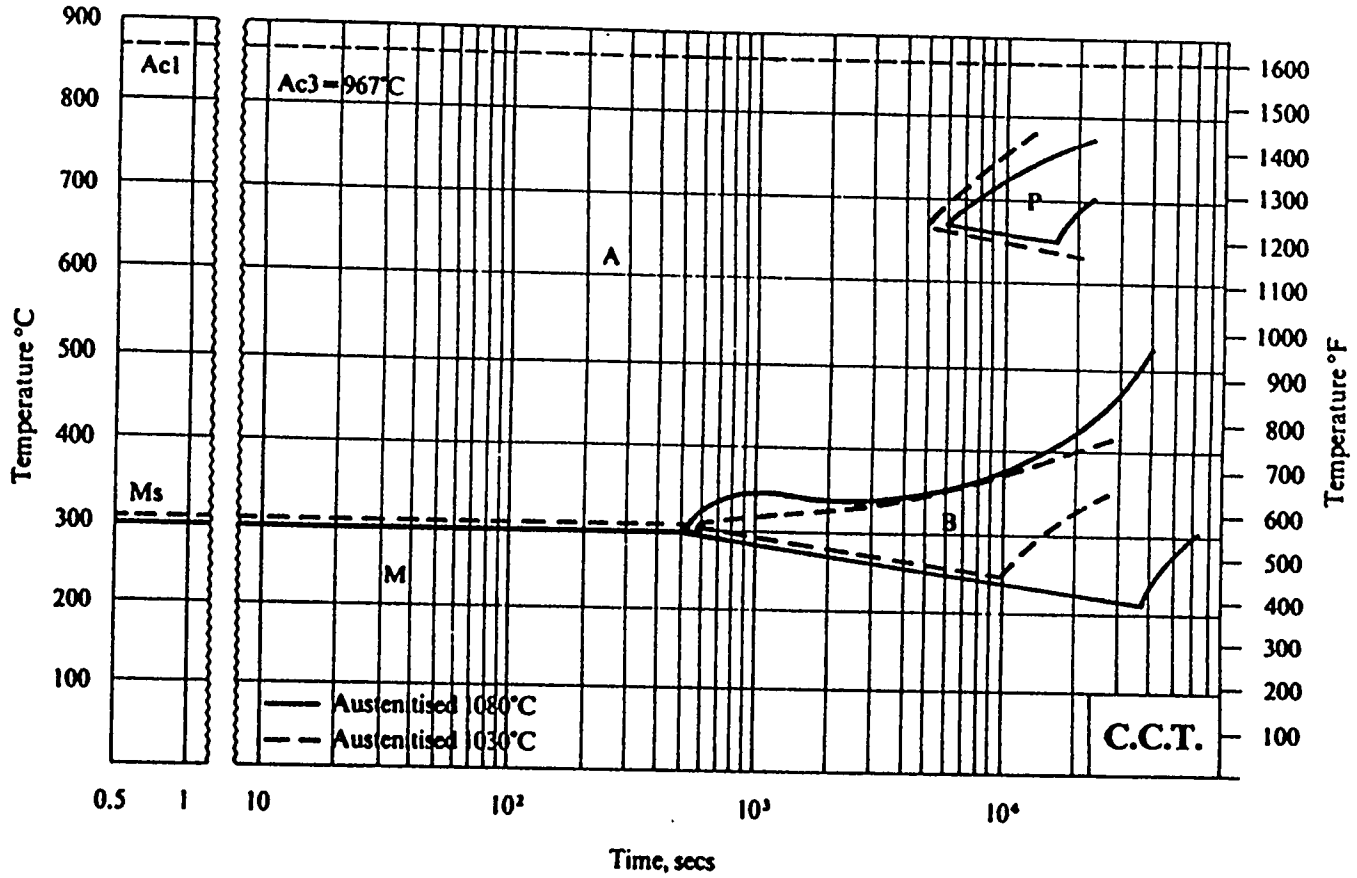

CCT Diagram for H-13, austenitized at (a) 1976°F (b) 1886°F

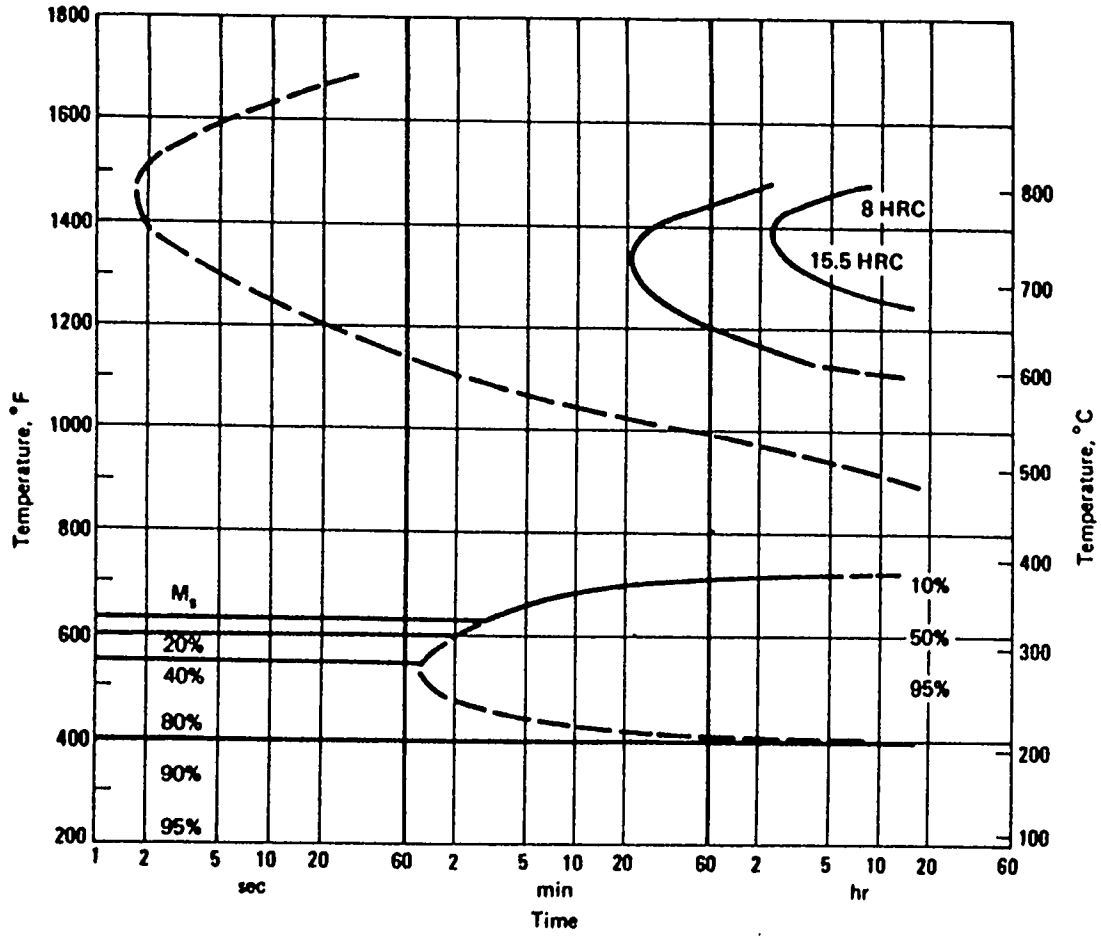

H13: Isothermal Transformation Diagram. Diagram for H13 tool steel, containing 0.40 C, 1.05 Si, 5.00 Cr, 1.35 Mo, 1.10 V. Austenitized at 1850 °F (1010 °C). (Source: Crucible Steel)

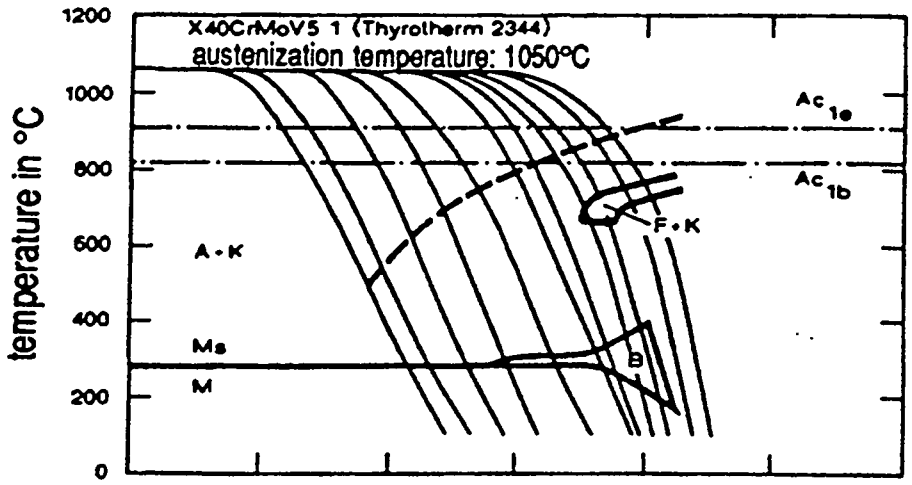

CCT curves for continuous cooling of Thyrotherm 2344 (Schruff)

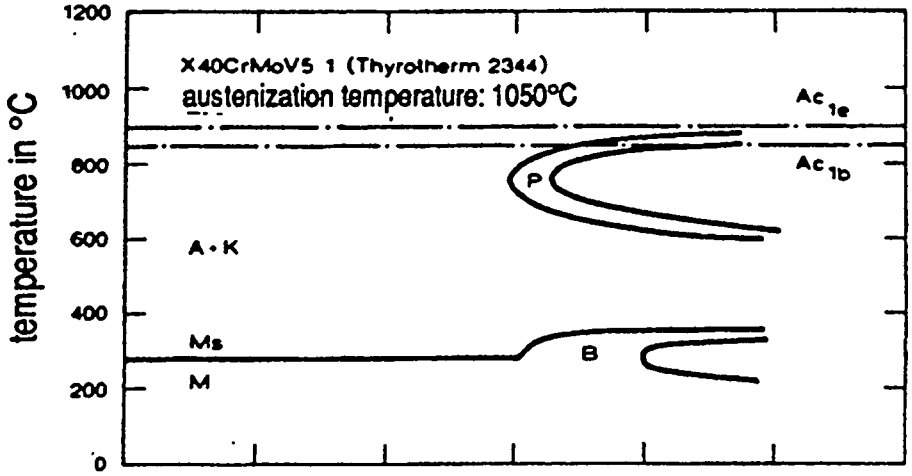

TTT curves for isothermal cooling of Thyrotherm 2344 (Schruff)

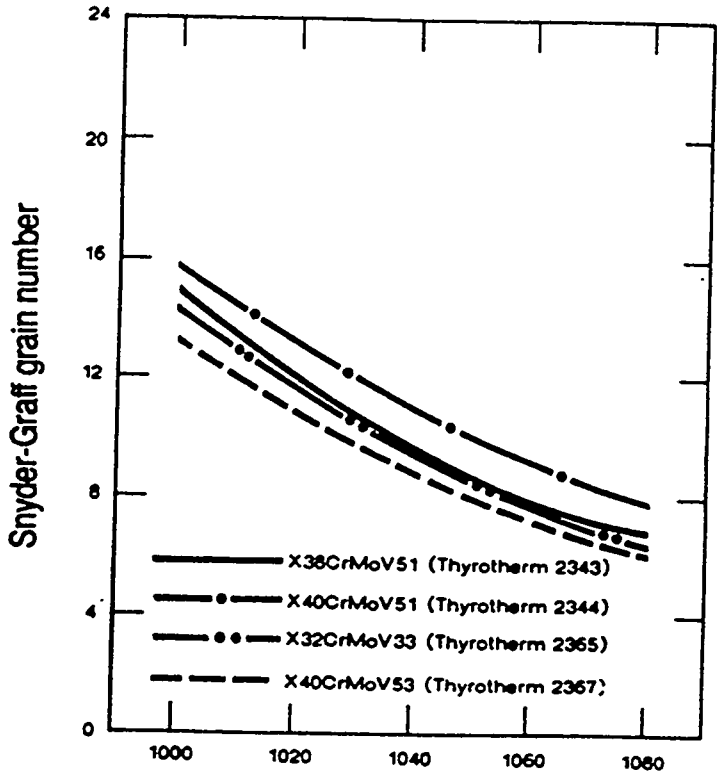

Austenite grain size at different hardening temperatures (Schruff).

Carbide phases in the hot-work tool steels examined

Steel grade	Type of precipitation							
	annealed state				hardened: 1040°C 15 mins/water			
	M_7C_3	$M_{23}C_6$	M_6C	MC	M_7C_3	$M_{23}C_6$	M_6C	MC
X 38 CrMoV 5 1 (Thyrotherm 2343)	x		x	x			x	x
X 40 CrMoV 5 1 (Thyrotherm 2344)	x		x	x			x	x
X 32 CrMoV 3 3 (Thyrotherm 2365)	x	x	x	x			x	x
X 38 CrMoV 5 3 (Thyrotherm 2367)		x	x	x			x	x

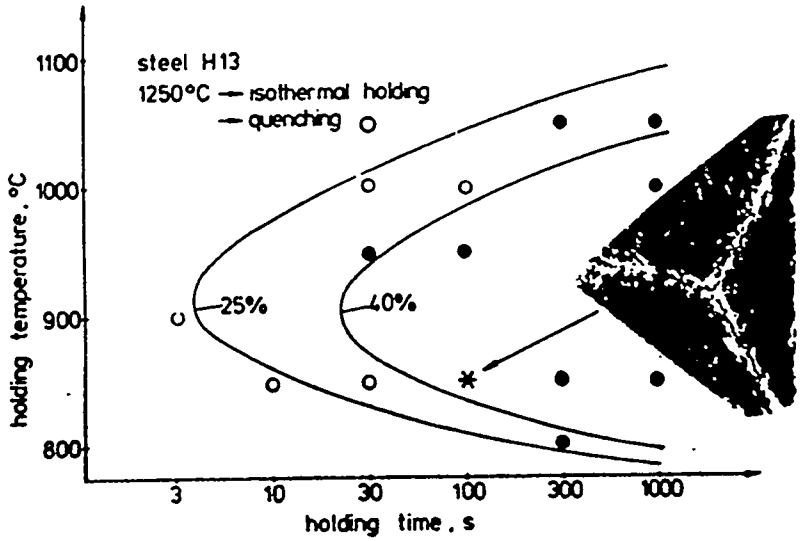

Relative covering of grain boundaries by MC-carbides (see insert) after cooling from forging or diffusion annealing temperatures (5)

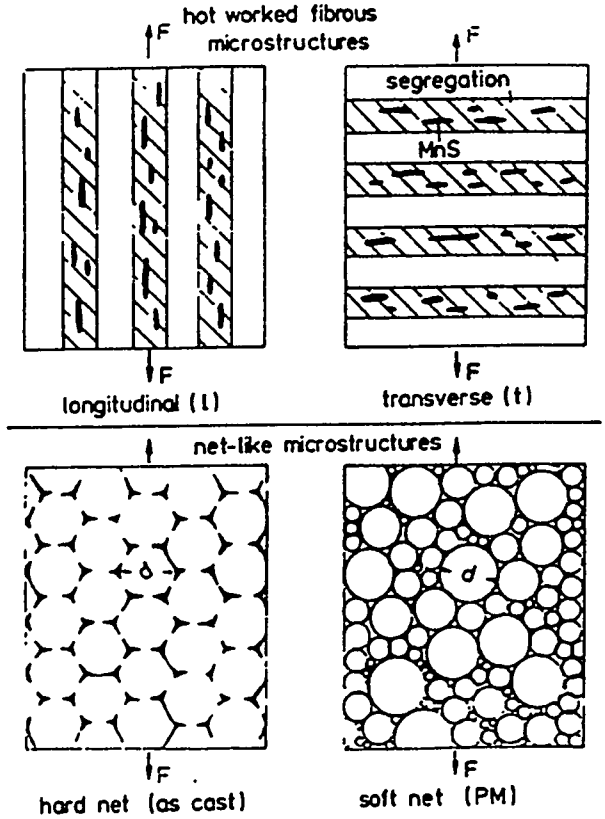

Schematic representation of microstructures (5)

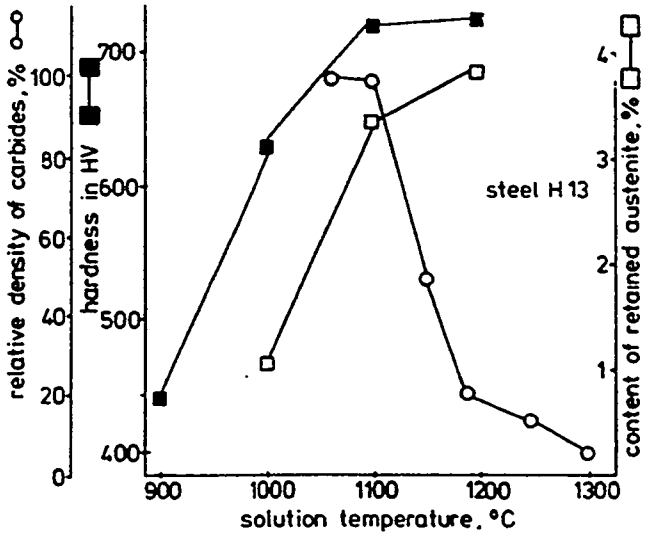

Dissolution of carbides and subsequent hardness and retained austenite after quenching (Berns)

Results of the Grain Size Ratings

Austenitizing Parameters*		ASTM Grain Size**		
Temperature (°C)	Time (min.)	Avg.	σ_{n-1}	95% Confidence Interval+
1024	25	10.1	0.31	9.9 - 10.3
1024	50	9.7	0.21	9.5 - 9.9
1024	80	9.8	0.47	9.5 - 10.1
1066	25	8.8	0.37	8.5 - 9.1
1066	50	8.8	0.27	8.6 - 9.0
1066	80	8.2	0.64	7.7 - 8.7
1107	25	7.1	1.24	6.2 - 8.0
1107	50	6.8	1.31	6.1 - 7.5
1107	80	5.9	2.15	4.4 - 7.4

* Specimens were austenitized in neutral salt, step-quenched to 760°C (salt) - 15 min., A.C.

** Converted from Snyder-Graff intercept grain size.

+ Calculated using the Student's t test statistic.

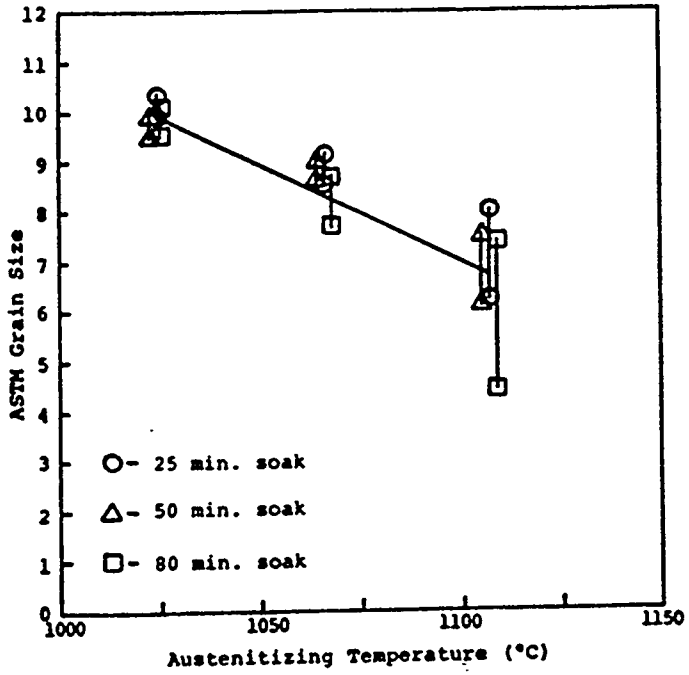

Plot of ASTM grain size (95% confidence interval) versus austenitizing temperature (Schmidt)

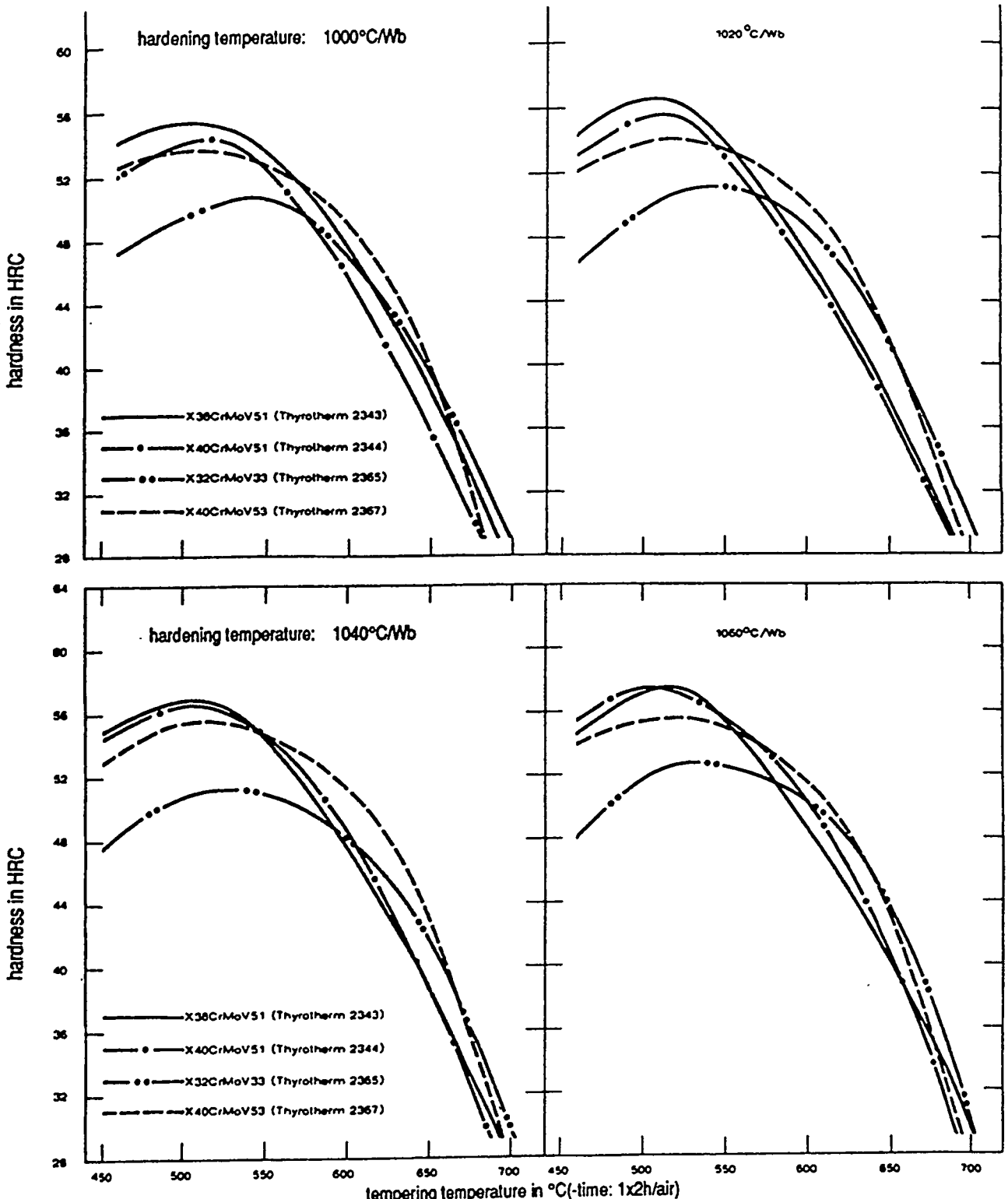

Tempering behaviour of the hot-work tool steels examined (Berns 1990).

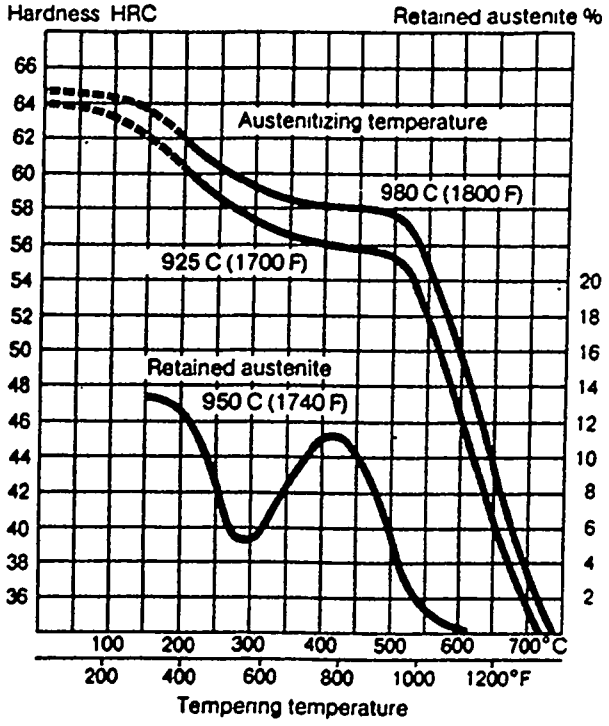

(a)

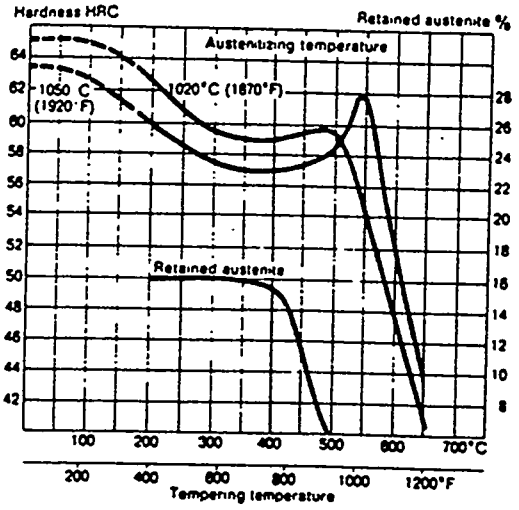

(b)

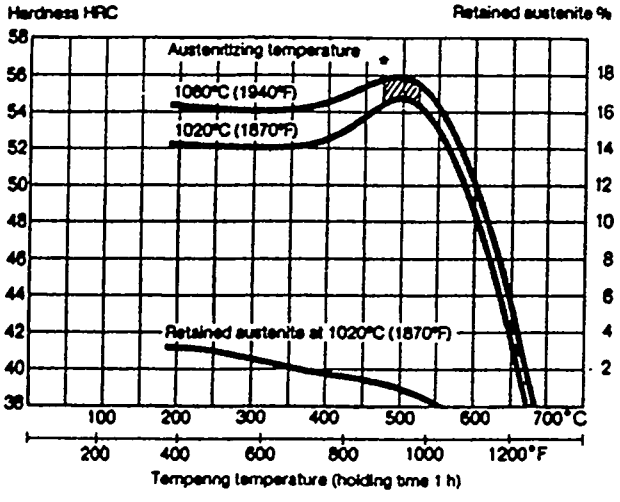

(c)

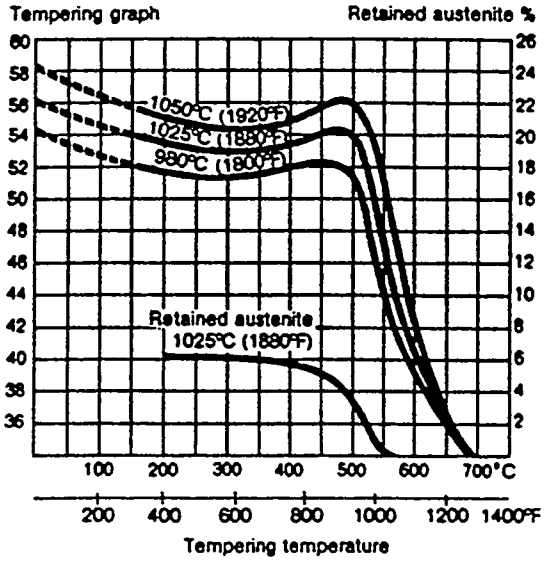

(d)

Curves of hardness and retained austenite as a function of tempering temperature for H-13(Branco et al.)

4.1.6 Hardness

Hot Work Tool Steels (H): Effect of Tempering Temperature on Hardness

Tempering temperature °C	°F	Hardness, HRC H11 (a)	H12 (b)	H13 (c)	H19 (d)	H21 (e)	H21 (f)
As quenched		56-57	54-56	51-53	...	53	52
150	300	55-56	...	...	...	52	51
205	400	55-56	...	...	...	...	...
260	500	55-56	53	...	...	...	...
315	600	54-55	...	51-53	...	...	...
370	700	54-55	...	...	...	48	47
425	800	54-55	53	51-53	...	...	...
480	900	55-56	52-54	51-53	...	49	48
510	950	...	...	52-54	58-59	...	...
540	1000	56-57	55-56	52-54	57-58	51	59
565	1050	...	52	51-53	55-56	52	50
595	1100	45-50	48	49-51	52-53	51	50.5
620	1150	...	44	45-47	50-51	50	51
650	1200	33-38	40	39-41	45-46	48	47
675	1250	...	35	31-33	39-40	39	38
705	1300	25-30	29-30	28-30	34-35	34	34

(a) Air or oil quenched from 995 to 1025 °C (1825 to 1875 °F). (b) Air quenched from 1010 °C (1850 °F); tempered 2 h. (c) Air quenched from 1025 °C (1875 °F) or oil quenched from 1010 °C (1850 °F); tempered 1 h. (d) Oil quenched from 1175 °C (2150 °F); double tempered for 2 h each time. (e) Oil quenched from 1175 °C (2150 °F); tempered 2 h. (f) Air quenched from 1175 °C (2150 °F); tempered 2 h

Hot Work Tool Steels (H): Effect of Hardness and Temperature on Charpy V-Notch Impact Values (Ref 6)

Oversized Charpy specimens were austenitized at 1010 °C (1850 °F) for 1 h; air cooled and double tempered to the indicated hardness, prior to grinding to finished size

Original hardness, HRC	Impact energy at temperature of: 25 °C (80 °F) J	ft·lb	260 °C (500 °F) J	ft·lb	540 °C (1000 °F) J	ft·lb	595 °C (1100 °F) J	ft·lb
Type H11								
54-55	18	13	24	18	27	20	...	...
48-49	24	18	38	28	42	31	41	30
42-44	31	23	58	43	64	47	...	...
Type H12								
50	7	5	16	12	16	12	24	18

Types H11, H13 Hot Work Tool Steels: Effect of Temperature on Hot Brinell Hardness

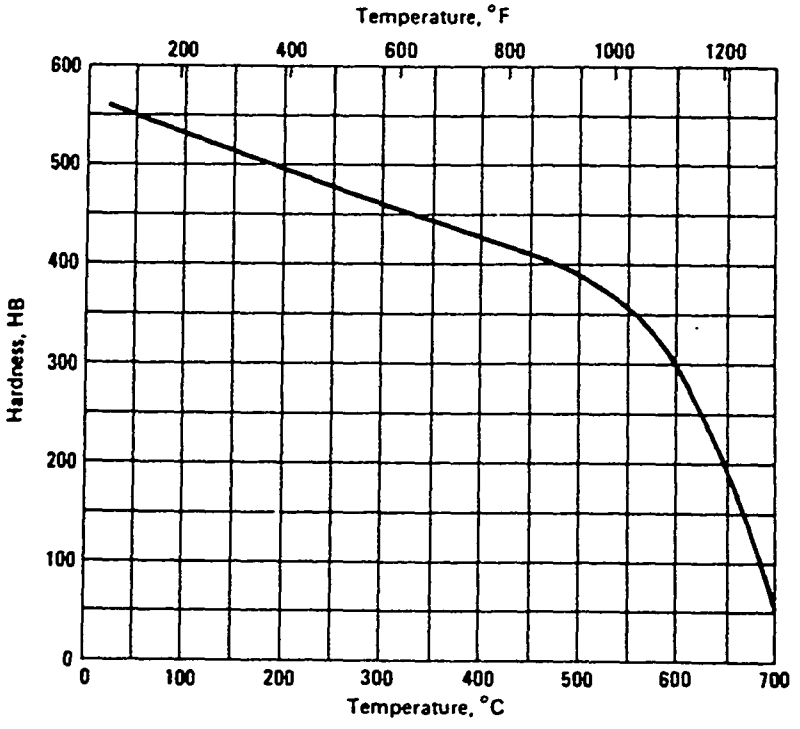

H13: Dimensional Change Versus Tempering Temperature. H13 containing 0.40 C, 1.00 Si, 5.00 Cr, 1.20 Mo, and 1.00 V. Change in a block 1 by 2 by 6 in. (25 by 51 by 152 mm) (Source: Latrobe Steel)

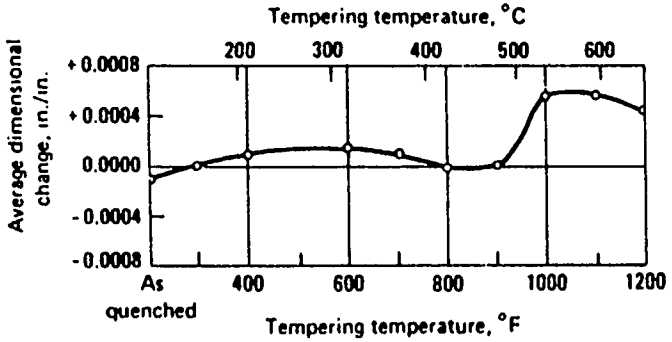

H13: Hardness Versus Tempering Temperature. Hardness and dimensional change for H13 steel, austenitized at 1000 °F (540 °C). (Source: Jessop-Saville and *Tool Steels*, American Society for Metals, 1980)

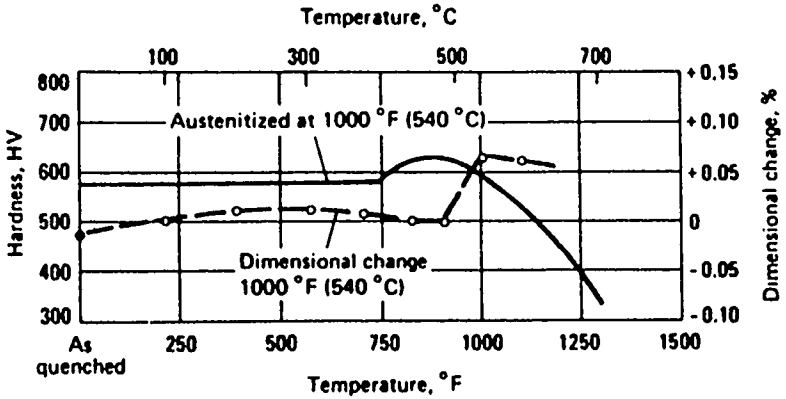

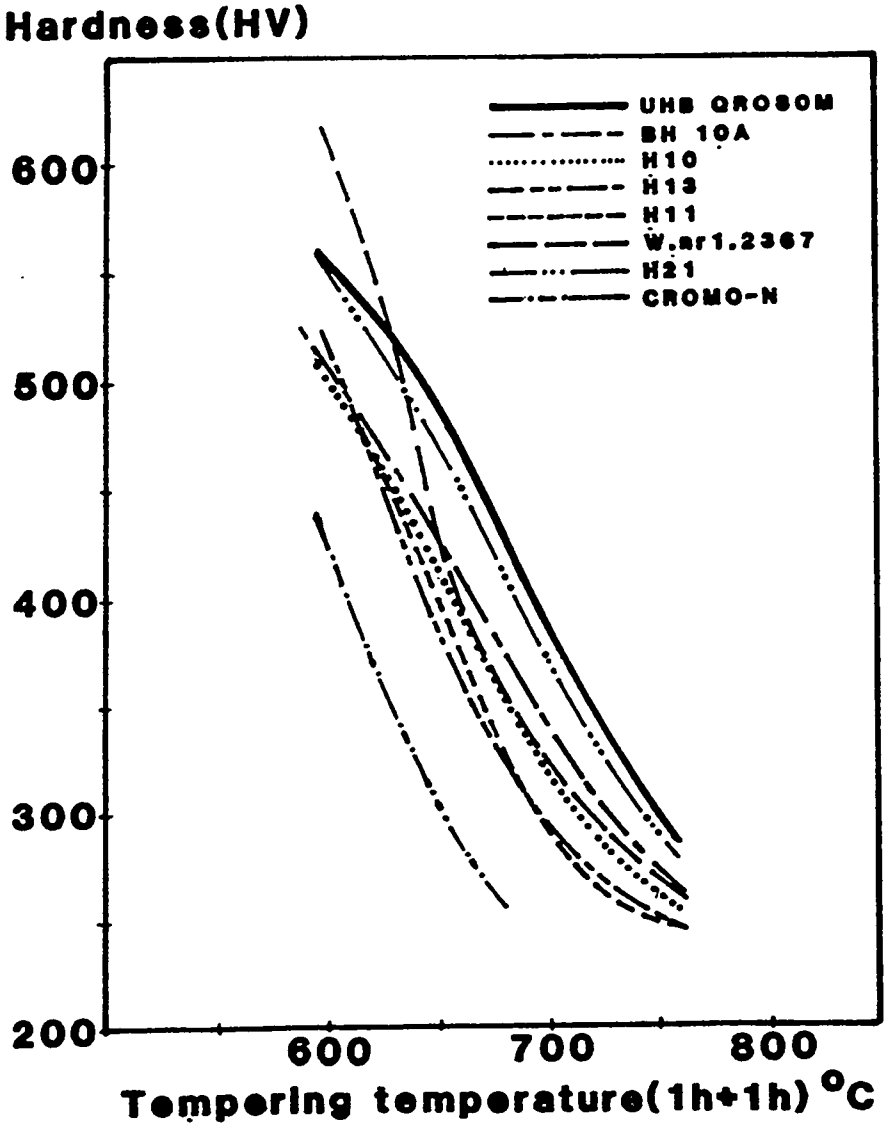

Hardness of H13 as a function of tempering temperature and time after quenching (1050oC, 30 min. oil) and tempering to room temperature hardness of 460 HV (Norstrom).

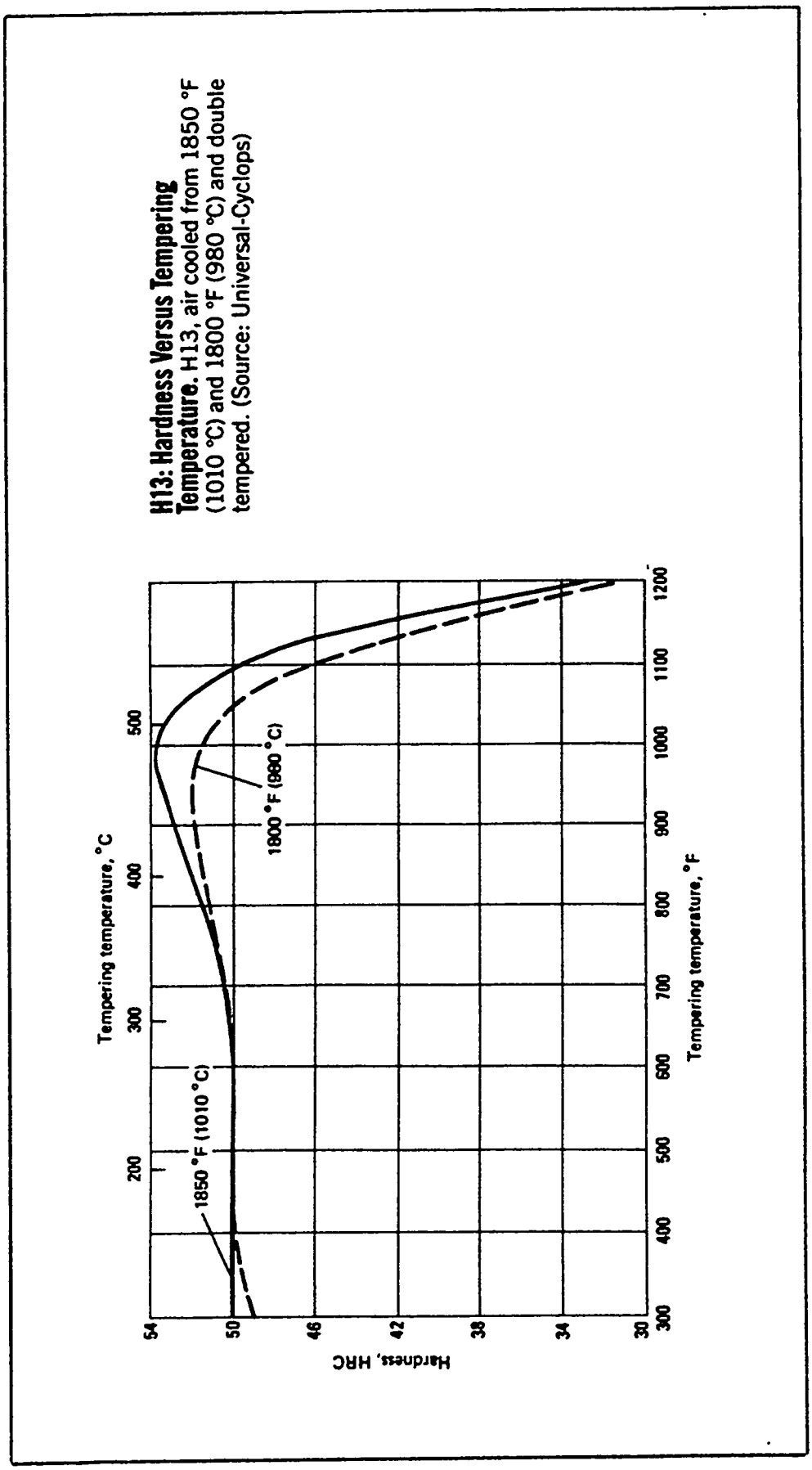

H13: Hardness Versus Tempering Temperature. H13, air cooled from 1850 °F (1010 °C) and 1800 °F (980 °C) and double tempered. (Source: Universal-Cyclops)

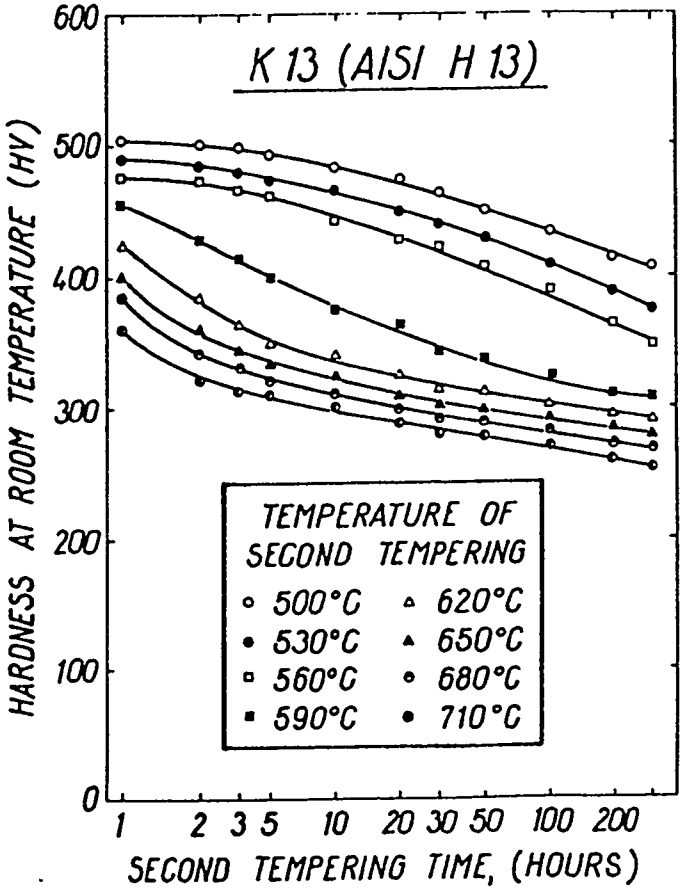
K 13 (AISI H 13)
HARDNESS AT ROOM TEMPERATURE (HV)
600
500
400
300
200
100
0
1
2
3
5
10
20
30
50
100
200
SECOND TEMPERING TIME, (HOURS)
TEMPERATURE OF SECOND TEMPERING
500°C
530°C
560°C
590°C
620°C
650°C
680°C
710°C

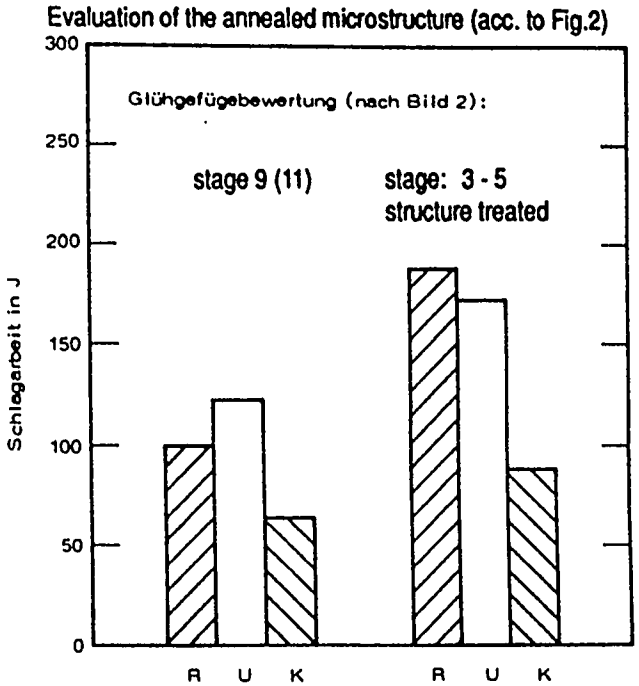

Influence of the structure treatment on the annealed microstructure and the toughness of hot-work tool steels
Material: X40CrMoV51 (Thyrotherm 2344)
Size: 480 mm dia.
(R=edge, Ü=1/4 dia., K=core) **(Berns 1990).**

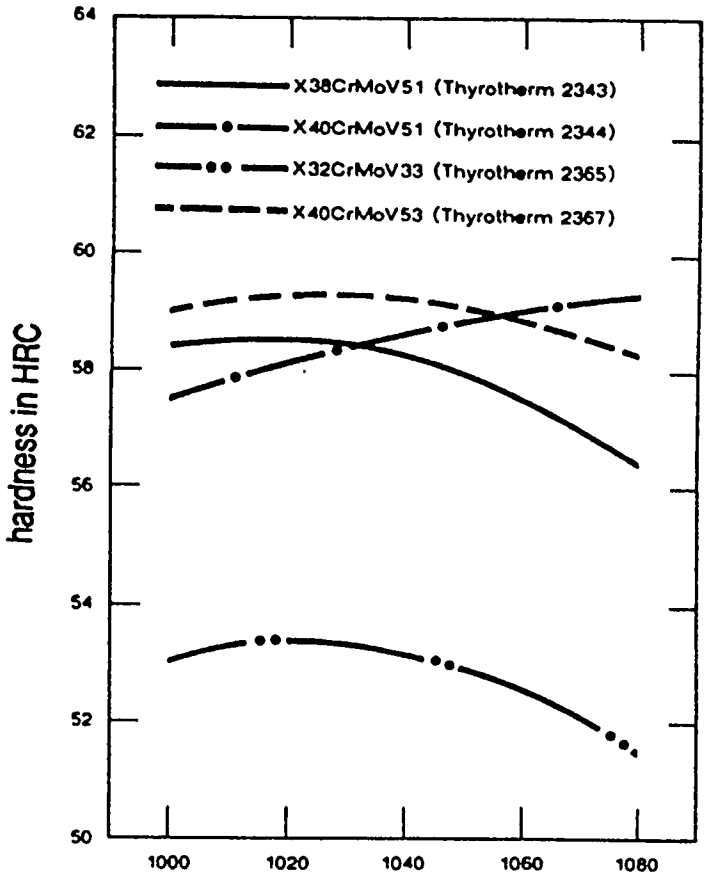

hardening temperature in °C
(-time: 15min/hot bath)

Interrelationship between hardening temperature and hardness **(Schruff).**

4.1.7 Forms and Conditions Available

Processing and service characteristics of tool steels (continued)

AISI designation	Hardening and tempering: Resistance to decarburization	Hardening response	Amount of distortion(a)	Resistance to cracking	Approximate hardness(b), HRC	Fabrication and service: Machinability	Toughness	Resistance to softening	Resistance to wear
Chromium hot work steels									
H10	Medium	Deep	Very low	Highest	39-56	Medium to high	High	High	Medium
H11	Medium	Deep	Very low	Highest	38-54	Medium to high	Very high	High	Medium
H12	Medium	Deep	Very low	Highest	38-55	Medium to high	Very high	High	Medium
H13	Medium	Deep	Very low	Highest	38-53	Medium to high	Very high	High	Medium
H14	Medium	Deep	Low	Highest	40-47	Medium	High	High	Medium
H19	Medium	Deep	A, low; O, medium	High	40-57	Medium	High	High	Medium to high
Tungsten hot work steels									
H21	Medium	Deep	A, low; O, medium	High	36-54	Medium	High	High	Medium to high
H22	Medium	Deep	A, low; O, medium	High	39-52	Medium	High	High	Medium to high
H23	Medium	Deep	Medium	High	34-47	Medium	Medium	Very high	Medium to high
H24	Medium	Deep	A, low; O, medium	High	45-55	Medium	Medium	Very high	High
H25	Medium	Deep	A, low; O, medium	High	35-44	Medium	High	Very high	Medium
H26	Medium	Deep	A or S, low; O, medium	High	43-58	Medium	Medium	Very high	High
Molybdenum hot work steels									
H42	Medium	Deep	A or S, low; O, medium	Medium	50-60	Medium	Medium	Very high	High
Air-hardening medium-alloy cold work steels									
A2	Medium	Deep	Lowest	Highest	57-62	Medium	Medium	High	High
A3	Medium	Deep	Lowest	Highest	57-65	Medium	Medium	High	Very high
A4	Medium to high	Deep	Lowest	Highest	54-62	Low to medium	Medium	Medium	Medium to high
A6	Medium to high	Deep	Lowest	Highest	54-60	Low to medium	Medium	Medium	Medium to high
A7	Medium	Deep	Lowest	Highest	57-67	Low	Low	High	Highest
A8	Medium	Deep	Lowest	Highest	50-60	Medium	High	High	Medium to high
A9	Medium	Deep	Lowest	Highest	35-56	Medium	High	High	Medium to high
A10	Medium to high	Deep	Lowest	Highest	55-62	Medium to high	Medium	Medium	High
High-carbon, high-chromium cold work steels									
D2	Medium	Deep	Lowest	Highest	54-61	Low	Low	High	High to very high
D3	Medium	Deep	Very low	High	54-61	Low	Low	High	Very high
D4	Medium	Deep	Lowest	Highest	54-61	Low	Low	High	Very high
D5	Medium	Deep	Lowest	Highest	54-61	Low	Low	High	High to very high
D7	Medium	Deep	Lowest	Highest	58-65	Low	Low	High	Highest
Oil-hardening cold work steels									
O1	High	Medium	Very low	Very high	57-62	High	Medium	Low	Medium
O2	High	Medium	Very low	Very high	57-62	High	Medium	Low	Medium
O6	High	Medium	Very low	Very high	58-63	Highest	Medium	Low	Medium
O7	High	Medium	W, high; O, very low	W, low; O, very high	58-64	High	Medium	Low	Medium

Adapted from *Tool Steels*, American Iron and Steel Institute. (a) A, air cool; B, brine quench; O, oil quench; S, salt bath quench; W, water quench. (b) After tempering in temperature range normally recommended for this steel. (c) Carburized case hardness. (d) After aging at 510 to 550 °C (950 to 1025 °F). (e) Toughness decreases with increasing carbon content and depth of hardening.

4.1.8 Melting and Casting Practice
4.1.9 Special Considerations

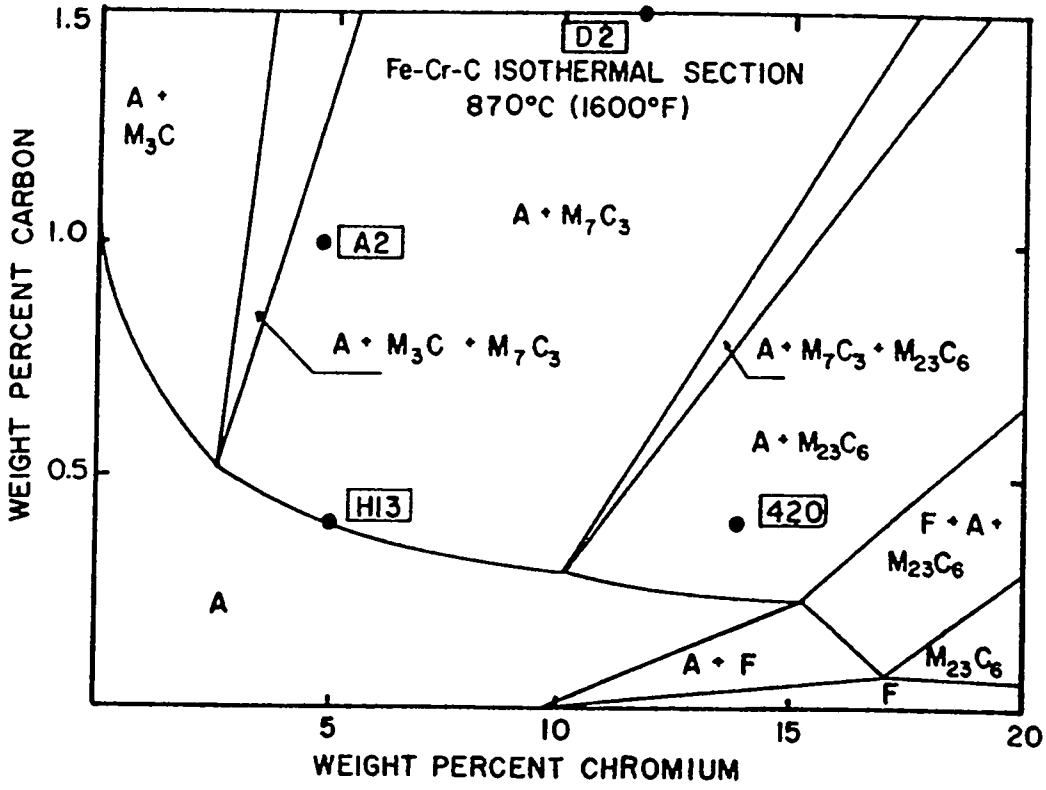

Isothermal section of the Fe-rich corner of the Fe-Cr-C system at 870°C [8]. Compositions of the alloys are indicated based only on their chromium and carbon contents. A and F designate austenite and ferrite, respectively (Branco et al.)

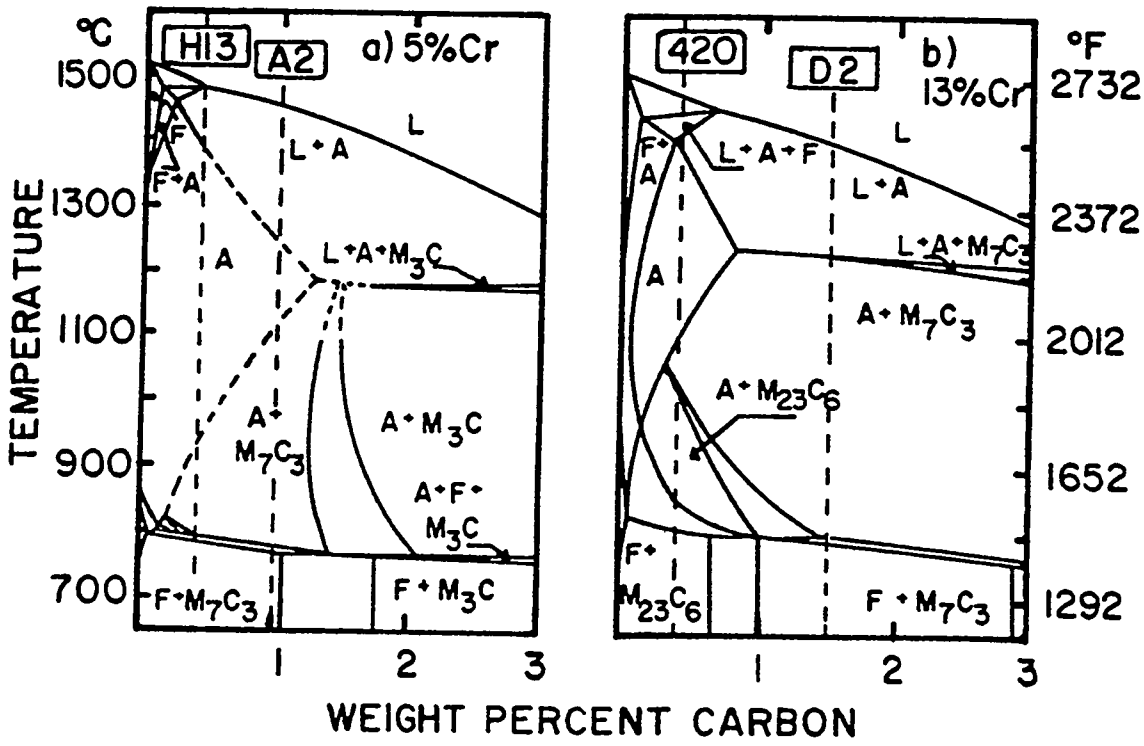

- Vertical sections for (a) 5 pct and (b) 13 pct Cr alloys of the Fe-Cr-C system [11]. Vertical dashed lines indicate phase equilibria of the alloys based only on their chromium carbon contents. A, F and L designate austenite, ferrite and liquid, respectively(Branco et al.)

Density and thermal expansion of selected tool steels

Type	Density Mg/m³	Density lb/in.³	Thermal expansion µm/m·K from 20 °C to 100 °C	200 °C	425 °C	540 °C	650 °C	µin./in. °F from 68 °F to 200 °F	400 °F	800 °F	1000 °F	1200 °F
W1	7.84	0.282	10.4	11.0	13.1	13.8(a)	14.2(b)	5.76	6.13	7.28	7.64(a)	7.90(b)
W2	7.85	0.283	...	...	14.4	14.8	14.9	...	...	8.0	8.2	8.3
S1	7.88	0.255	12.4	12.6	13.5	13.9	14.2	6.9	7.0	7.5	7.7	7.9
S2	7.79	0.281	10.9	11.9	13.5	14.0	14.2	6.0	6.6	7.5	7.8	7.9
S5	7.76	0.280	...	...	12.6	13.3	13.7	...	...	7.0	7.4	7.6
S6	7.75	0.279	...	...	12.6	13.3	...	...	...	7.0	7.4	...
S7	7.76	0.280	...	12.6	13.3	13.7(a)	13.3	...	7.0	7.4	7.6(a)	7.4
O1	7.85	0.283	...	10.6(c)	12.8	14.0(d)	14.4(d)	...	5.9(c)	7.1	7.8(d)	8.0(d)
O2	7.66	0.277	11.2	12.6	13.9	14.6	15.1	6.2	7.0	7.7	8.1	8.4
O7	7.8	0.282	...	...	...	...	...	...	...	...	...	...
A2	7.86	0.284	10.7	10.6(c)	12.9	14.0	14.2	5.96	5.91(c)	7.2	7.8	7.9
A6	7.84	0.283	11.5	12.4	13.5	13.9	14.2	6.4	6.9	7.5	7.7	7.9
A7	7.66	0.277	...	...	12.4	12.9	13.5	...	...	6.9	7.2	7.5
A8	7.87	0.284	...	...	12.0	12.4	12.6	...	...	6.7	6.9	7.0
A9	7.78	0.281	...	...	12.0	12.4	12.6	...	...	6.7	6.9	7.0
D2	7.70	0.278	10.4	10.3	11.9	12.2	12.2	5.8	5.7	6.6	6.8	6.8
D3	7.70	0.278	12.0	11.7	12.9	13.1	13.5	6.7	6.5	7.2	7.3	7.5
D4	7.70	0.278	...	...	12.4	...	...	...	...	6.9	...	...
D5	...	...	...	...	...	12.0	...	...	...	...	6.7	...
H10	7.81	0.281	...	...	12.2	13.3	13.7	...	...	6.8	7.4	7.6
H11	7.75	0.280	11.9	12.4	12.8	12.9	13.3	6.6	6.9	7.1	7.2	7.4
H13	7.76	0.280	10.4	11.5	12.2	12.4	13.1	5.8	6.4	6.8	6.9	7.3
H14	7.89	0.285	11.0	...	...	...	...	6.1	...	...	...	...
H19	7.98	0.288	11.0	11.0	12.0	12.4	12.9	6.1	6.1	6.7	6.9	7.2
H21	8.28	0.299	12.4	12.6	12.9	13.5	13.9	6.9	7.0	7.2	7.5	7.7
H22	8.36	0.302	11.0	...	11.5	12.0	12.4	6.1	...	6.4	6.7	6.9
H26	8.67	0.313	...	...	...	12.4	...	...	...	...	6.9	...
H42	8.15	0.295	...	...	...	11.9	...	...	...	...	6.6	...
T1	8.67	0.313	...	9.7	11.2	11.7	11.9	...	5.4	6.2	6.5	6.6
T2	8.67	0.313	...	...	...	...	...	...	...	...	...	...
T4	8.68	0.313	...	...	...	11.9	...	...	...	...	6.6	...
T5	8.75	0.316	11.2	...	...	11.5	...	6.2	...	...	6.4	...
T6	8.89	0.321	...	...	...	...	...	...	...	...	...	...
T8	8.43	0.305	...	...	...	...	...	...	...	...	...	...
T15	8.19	0.296	...	9.9	11.0	11.5	...	...	5.5(c)	6.1	6.4	...
M1	7.89	0.285	...	10.6(c)	11.3	12.0	12.4	...	5.9(c)	6.3	6.7	6.9
M2	8.16	0.295	10.1	9.4(c)	11.2	11.9	12.2	5.6	5.2(c)	6.2	6.6	6.8
M3, class 1	8.15	0.295	...	...	11.5	12.0	12.2	...	...	6.4	6.7	6.8
M3, class 2	8.16	0.295	...	...	11.5	12.0	12.8	...	...	6.4	6.7	7.1
M4	7.97	0.288	...	9.5(c)	11.2	12.0	12.2	...	5.3(c)	6.2	6.7	6.8
M7	7.95	0.287	...	9.5(c)	11.5	12.2	12.4	...	5.3(c)	6.4	6.8	6.9
M10	7.88	0.255	...	...	11.0	11.9	12.4	...	...	6.1	6.6	6.9
M30	8.01	0.289	...	...	11.2	11.7	12.2	...	...	6.2	6.5	6.8
M33	8.03	0.290	...	...	11.0	11.7	12.0	...	...	6.1	6.5	6.7
M36	8.18	0.296	...	...	...	...	...	...	...	...	...	...
M41	8.17	0.295	...	9.7	10.4	11.2	...	...	5.4	5.8	6.2	...
M42	7.98	0.288	...	...	...	...	...	...	...	...	...	...
M46	7.83	0.283	...	...	...	...	...	...	...	...	...	...
M47	7.96	0.288	10.6	11.0	11.9	...	12.6	5.9	6.1	6.6	...	7.0
L2	7.86	0.284	...	...	14.4	14.6	14.8	...	...	8.0	8.1	8.2
L6	7.86	0.284	11.3	12.6	12.6	13.5	13.7	6.3	7.0	7.0	7.5	7.6
P2	7.86	0.284	...	...	13.7	...	...	...	...	7.6	...	...
P5	7.80	0.282	...	...	...	...	...	...	...	...	...	...
P6	7.85	0.284	...	...	...	...	...	...	...	...	...	...
P20	7.85	0.284	...	...	12.8	13.7	14.2	...	...	7.1	7.6	7.9

(a) From 20 °C to 500 °C (68 °F to 930 °F). (b) From 20 °C to 600 °C (68 °F to 1110 °F). (c) From 20 °C to 260 °C (68 °F to 500 °F). (d) From 38 °C (100 °F).

Input data used in distortion computations and dependence on temperature

Property		Temperature, °C 0	300	600	900
Elastic modulus, GN m^{-2}	A	200	175	150	124
	F+P	210	193	165	120
	B	210	193	165	120
	M	200	185	168	...
Poisson ratio	A	0·291	0·309	0·327	0·345
	F+P	0·280	0·296	0·310	0·325
	B	0·280	0·296	0·310	0·325
	M	0·280	0·296	0·310	...
Coefficient of thermal expansion, K^{-1}	A		$2{\cdot}1 \times 10^{-5}$		
	F+P		$1{\cdot}4 \times 10^{-5}$		
	B		$1{\cdot}4 \times 10^{-5}$		
	M		$1{\cdot}3 \times 10^{-5}$		
Coefficient of thermal conductivity, W m^{-1} K^{-1}	A	15·0	18·0	21·7	25·1
	F+P	49·0	41·7	34·3	27·0
	B	49·0	41·7	34·3	27·0
	M	43·1	36·7	30·1	...
Product of density and specific heat capacity, 10^{-6} J m^{-3} K^{-1}	A	4·15	4·40	4·67	4·90
	F+P	3·78	4·46	5·09	5·74
	B	3·78	4·46	5·09	5·74
	M	3·76	4·45	5·07	...
Yield strength, MN m^{-2}	A	190	110	30	20
	F+P	360	230	140	30
	B	440	330	140	30
	M	1600	1480	1260	...

A austenite, F+P ferrite+pearlite, B bainite, M martensite.

Hot Work Tool Steels (H): Average Coefficients of Linear Thermal Expansion

Temperature range °C	°F	Coefficient µm/m·K	µin./in.·°F
Types H11, H13			
25-95	80-200	11.0	6.1
25-205	80-400	11.5	6.4
25-425	80-800	12.2	6.8
25-540	80-1000	12.4	6.9
25-650	80-1200	13.1	7.3
25-790	80-1450	13.5	7.5
260-650	500-1200	14.0	7.8
260-790	500-1450	14.4	8.0
425-650	800-1200	14.6	8.1
425-790	800-1450	14.8	8.2

Physical properties of hot-work tool steels X 38 CrMoV 5 1 (Thyrotherm 2343), X 40 CrMoV 5 1 (Thyrotherm 2344), X 32 CrMoV 3 3 (Thyrotherm 2365) and X 38 CrMoV 5 3 (Thyrotherm 2367) (Schruff).

1. Specific heat capacity Cp in J/kg K (annealed condition)

Steel grade	Test temperature in °C												
	100	150	200	250	300	350	400	500	600	700	800	900	1000
X 38 CrMoV 5 1 (Thyrotherm 2343)	523	525	530	532	535	540	540	544	544	544	544	536	536
X 40 CrMoV 5 1 (Thyrotherm 2344)	523	545	555	580	595	600	607	615	615	620	624	628	628
X 32 CrMoV 3 3 (Thyrotherm 2365)	481	490	505	520	530	535	545	553	553	553	553	553	553
X 38 CrMoV 5 3 (Thyrotherm 2367)	536	550	565	575	585	595	610	620	607	599	595	582	584

2. Density in $kg/m^3 \times 10^3$

Steel	annealed	hardened	heat-treated
X 38 CrMoV 5 1 (Thyrotherm 2343)	7.751	7.740	7.741
X 40 CrMoV 5 1 (Thyrotherm 2344)	7.735	7.730	7.718
X 32 CrMoV 3 3 (Thyrotherm 2365)	7.847	7.843	7.823
X 38 CrMoV 5 3 (Thyrotherm 2367)	7.817	7.805	7.799

3. Linear coefficient of thermal expansion α in $1/°C \times 10^{-6}$

Steel	State	Temperature interval in °C							
		20-100	20-200	20-300	20-400	20-500	20-600	20-700	20-800
X 38 CrMoV 5 1	annealed	11.2	11.7	12.2	12.3	12.5	12.6	12.6	11.7
(Thyrotherm 2343)	hardened	10.9	11.2	11.7	12.1	12.3	12.4	12.6	12.6
	heat-treat.	11.8	12.4	12.6	12.7	12.8	12.9	12.9	12.8
X 40 CrMoV 5 1	annealed	10.1	11.5	11.9	12.3	12.7	13.0	13.1	13.2
(Thyrotherm 2344)	hardened	10.2	11.1	11.8	12.4	12.7	13.1	13.3	13.5
	heat-treat.	10.9	11.9	12.3	12.7	13.0	13.3	13.5	13.7
X 32 CrMoV 3 3	annealed	11.2	12.0	12.4	12.7	13.1	13.3	13.5	12.6
(Thyrotherm 2365)	hardened	10.9	10.8	10.9	11.1	11.6	12.3	13.0	12.7
	heat-treat.	11.8	12.5	12.7	13.1	13.5	13.6	13.8	13.9
X 38 CrMoV 5 3	annealed	11.0	11.4	12.0	12.5	12.7	13.1	13.3	13.4
(Thyrotherm 2367)	hardened	11.1	11.7	12.6	12.5	12.7	13.3	14.1	14.0
	heat-treat-	11.9	12.5	12.6	12.8	13.1	13.3	13.5	13.8

4. Thermal conductivity λ in $Wm^{-1}K^{-1}$

Steel	State	Temperature in °C						
		100	200	300	400	500	600	700
X 38 CrMoV 5 1	annealed	29.85	30.73	30.98	31.02	31.48	32.32	33.41
(Thyrotherm 2343)	heat-treated	26.80	27.84	27.47	27.30	28.26	29.31	30.35
X 40 CrMoV 5 1	annealed	27.21	28.09	29.22	30.14	31.74	34.08	36.51
(Thyrotherm 2344)	heat-treated	25.47	27.10	28.86	29.89	30.99	32.45	34.25
X 32 CrMoV 3 3	annealed	32.87	34.96	35.50	34.12	32.49	32.24	33.20
(Thyrotherm 2365)	heat-treated	31.40	33.91	33.08	31.40	30.14	29.73	29.31
X 38 CrMoV 5 3	annealed	30.56	31.82	32.66	33.49	34.12	34.75	35.17
(Thyrotherm 2367)	heat-treated	29.94	31.19	32.24	33.08	33.91	34.75	35.17

5. Specific electric resistivity ρ in Ω m
(Test temperature 20°C)

Steel	annealed	heat-treated
X 38 CrMoV 5 1 (Thyrotherm 2343)	$4.71\ 10^{-7}$	$4.81\ 10^{-7}$
X 40 CrMoV 5 1 (Thyrotherm 2344)	$5.20\ 10^{-7}$	$5.32\ 10^{-7}$
X 32 CrMoV 3 3 (Thyrotherm 2365)	$3.03\ 10^{-7}$	$3.08\ 10^{-7}$
X 38 CrMoV 5 3 (Thyrotherm 2367)	$3.66\ 10^{-7}$	$3.97\ 10^{-7}$

6. Modulus of elasticity E in $Nmm^{-2}\ 10^3$ (for 20°C)

Steel	annealed	hardened	heat-treated
X 38 CrMoV 5 1 (Thyrotherm 2343)	217.3	206.6	215.6
X 40 CrMoV 5 1 (Thyrotherm 2344)	216.9	207.8	216.2
X 32 CrMoV 3 3 (Thyrotherm 2365)	217.9	208.0	213.2
X 38 CrMoV 5 3 (Thyrotherm 2367)	227.1	205.8	215.7

7. Dependence of the modulus of elasticity on the test temperature (heat-treated state)

Steel	Test temperature in °C							
	20	100	200	300	400	500	600	700
X38CrMoV51 (Thyrotherm 2343)	215.6	211.2	205.2	198.8	192.2	184.3	173.6	—
X40CrMoV51 (Thyrotherm 2344)	216.2	211.6	205.8	199.5	193.0	184.9	173.6	161.0
X32CrMoV33 (Thyrotherm 2365)	213.2	209.4	202.7	196.5	191.0	183.0	173.1	160.9
X38CrMoV53 (Thyrotherm 2367)	215.7	212.1	205.5	199.4	193.5	185.0	174.4	—

*) "Heat-treated" means quenched and tempered to 43 to 44 HRC".

Thermal, mechanical and phase transformation characteristics of a Cr-Mo-V steel

Table 1 Thermal constants*

Temp., °C	Thermal conductivity, W m^{-1} K^{-1}		Specific heat, J kg^{-1} k^{-1}		Heat transfer coefficient, W m^{-2} K^{-1}
	A	*B*	*A*	*B*	
20	...	44·2	...	481	5250
100	...	43·5	...	490	1750
150	...	43	...	494	1050
200	24·4	42·6	615	502	800
400	24·4	41·9	624	527	700
600	24·4	41·9	632	553	700
800	26·7	...	636	...	700
1000	27·9	...	645	...	700

* *A* austenite; *B* bainite.
Density 7800 kg m^{-3}.

Table 2 Mechanical properties*

Temp., °C	Young's modulus *E*, GN m^{-2}	Yield stress, MN m^{-2}		Thermal expansion coefficient, $\times 10^{-6}$ K^{-1}	
		A	*B*	*A*	*B*
20	205	...	860	...	1·1
100	201	...	860	...	1·1
150	198	...	860	...	1·1
200	194	105	860	2·1	1·1
400	173	95	860	2·1	1·1
600	145	85	860	2·3	1·1
800	115	60	...	2·5	...
1000	85	20	...	2·5	...

* *A* austenite; *B* bainite.
Poisson's ratio 0·3; strain-hardening coefficient 0·05*E*.

Table 3 Characteristics of phase transformation

Start temp., °C	Finish temp., °C	Latent heat, $\times 10^4$ J kg^{-1}	Dilatation, %
520	315	7·53	0·38

Hot Work Tool Steels (H): Average Coefficients of Linear Thermal Expansion

Temperature range °C	Temperature range °F	Coefficient µm/m·K	Coefficient µin./in.·°F
Types H11, H13			
25-95	80-200	11.0	6.1
25-205	80-400	11.5	6.4
25-425	80-800	12.2	6.8
25-540	80-1000	12.4	6.9
25-650	80-1200	13.1	7.3
25-790	80-1450	13.5	7.5
260-650	500-1200	14.0	7.8
260-790	500-1450	14.4	8.0
425-650	800-1200	14.6	8.1
425-790	800-1450	14.8	8.2
Type H12			
25-95	80-200	11.0	6.1
25-205	80-400	11.7	6.5
25-425	80-800	12.6	7.0
25-675	80-1250	13.5	7.5
25-790	80-1450	15.1	8.4
Type H21			
25-95	80-200	10.3	5.7
25-205	80-400	11.0	6.1
25-425	80-800	12.2	6.8
25-650	80-1200	13.1	7.3
25-790	80-1450	13.7	7.6

Hot Work Tool Steels (H): Mean Apparent Specific Heat

Steel type	Temperature range °C	Temperature range °F	Specific heat J/kg·K	Specific heat Btu/lb·°F
H11, H13	0-100	32-212	460	0.11
H21	480	800	628	0.15

Hot Work Tool Steels (H): Density

Steel type	Density g/cm³	Density lb/in.³
H11, H13	7.8	0.28
H12	7.81	0.282
H21	8.19	0.296

4.3. Mechanical Properties

4.3.1 Specified Mechanical Properties

4.3.2 Mechanical Properties at Room Temperature

4.3.3 Mechanical Properties at Various Temperatures

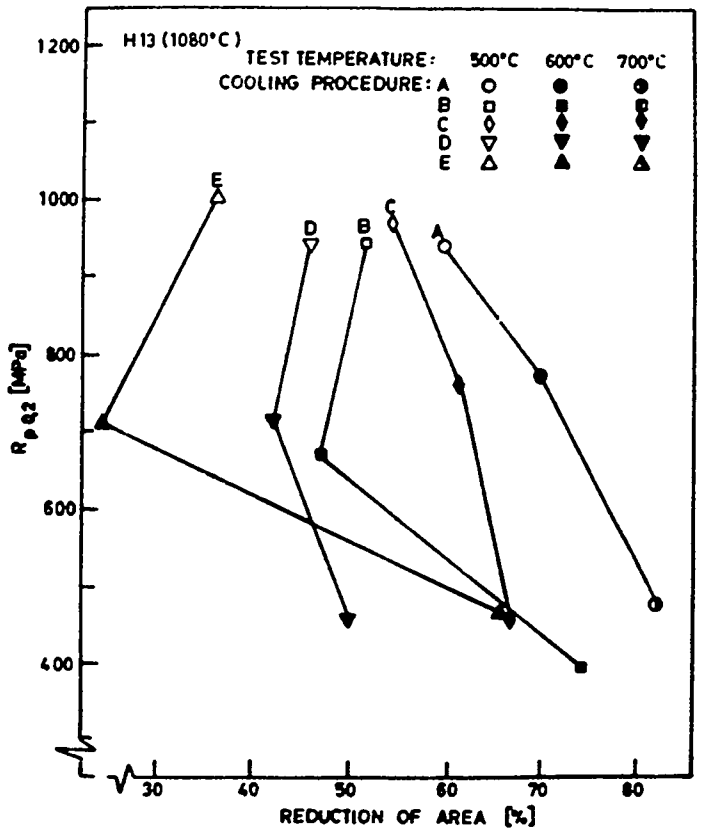

Proof stress (0.2%) and reduction in area obtained in H13 for various cooling procedures following austenitization at 1080°C and various tests temperatures (500-700°C)(Andersen).

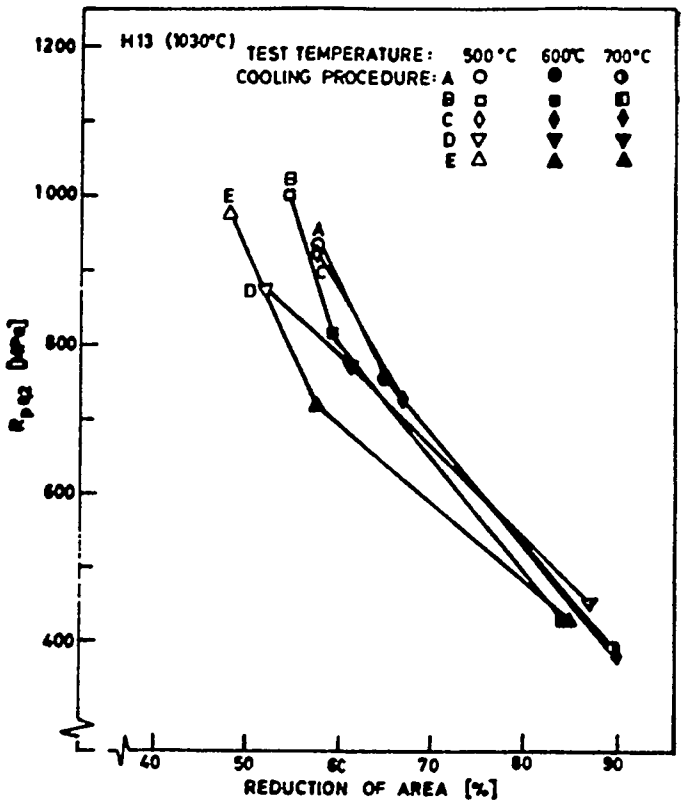

Proof stress (0.2%) and reduction in area obtained in H13 for various cooling procedures following austenitization at 1030°C and various tests temperatures (500-700°C)(Andersen).

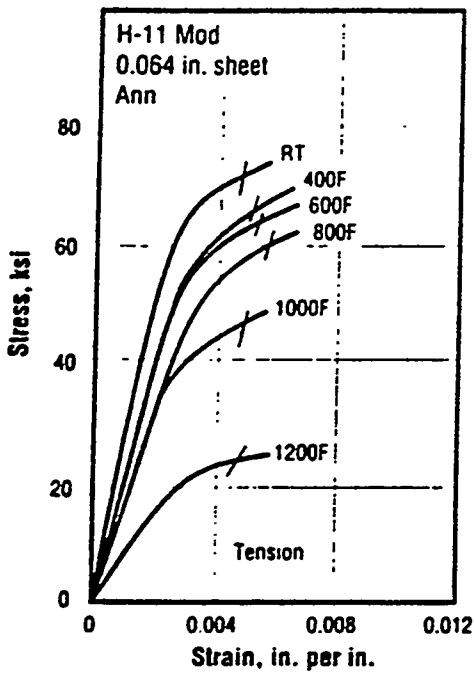

Stress-strain curves at room and elevated temperatures for annealed H11 sheet (Henning).

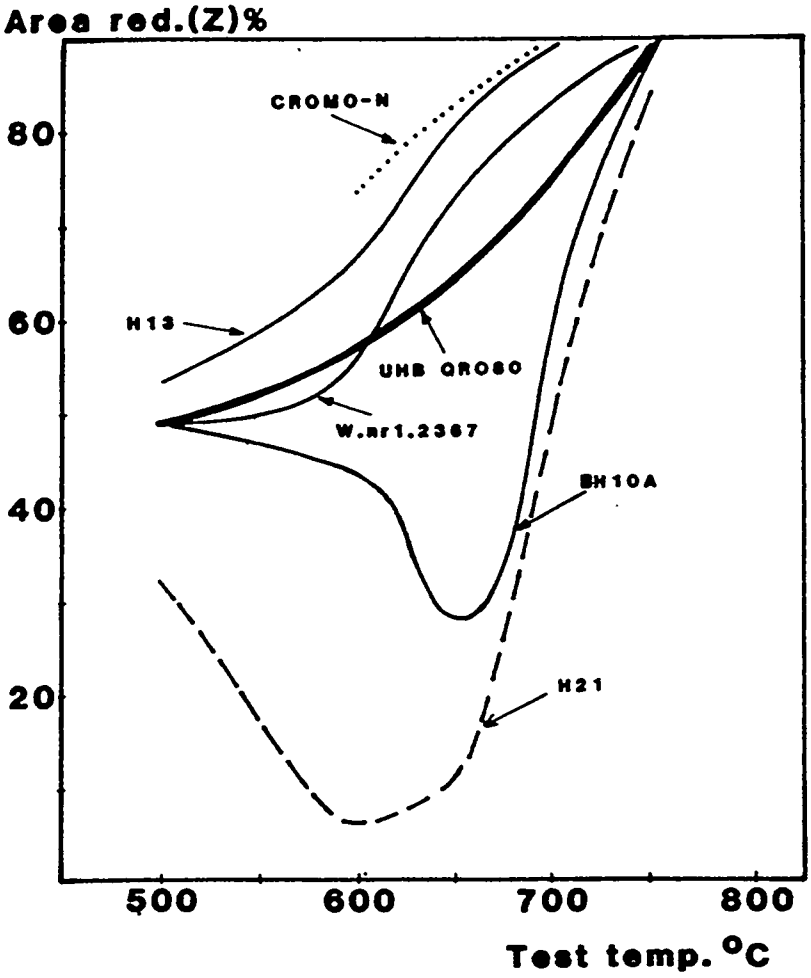

Reduction of area in various die steels after quenching and tempering to 47 HRC (Norstrom)

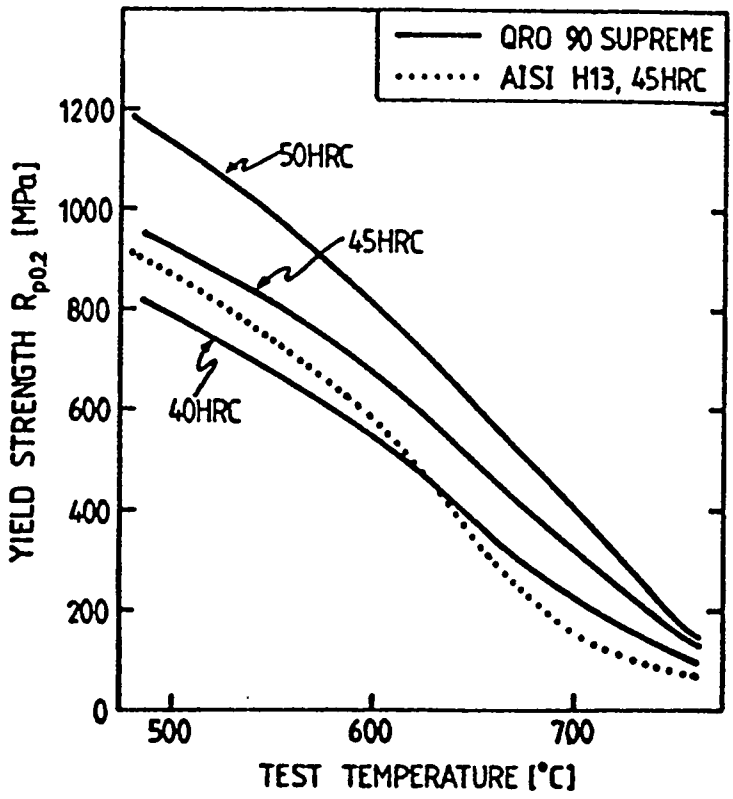

Hot yield strength for UHB QRO 90 SUPREME at different hardnesses and for AISI H13 at 45 HRC. (Sandberg et al.)
Austenitization temperature: 1020°C.

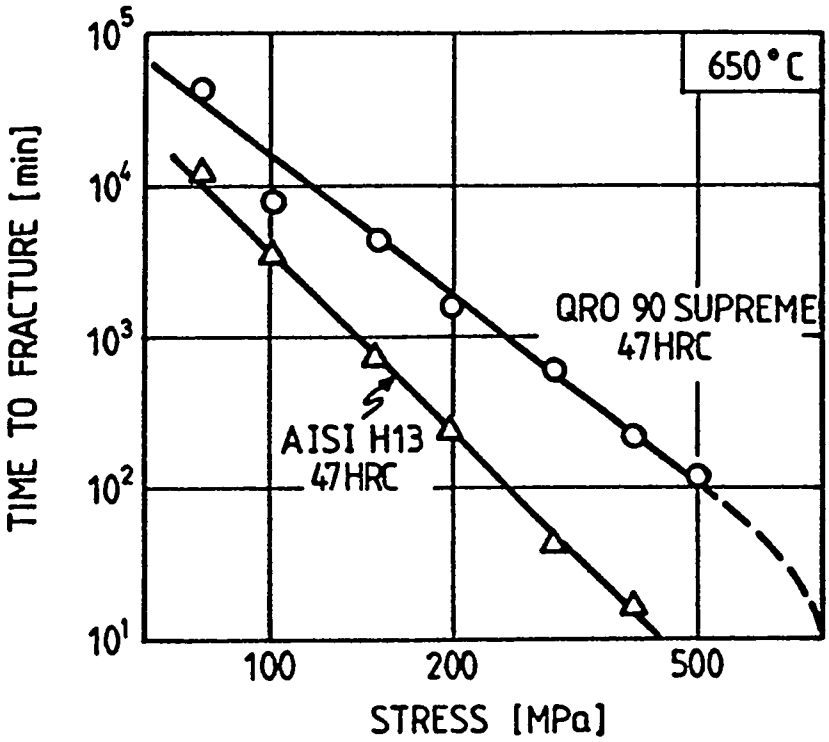

Time to fracture - stress relationships in creep for UHB QRO 90 SUPREME and AISI H13 at 650°C. (Sandberg et al.)
Austenitization temperature: 1020°C.

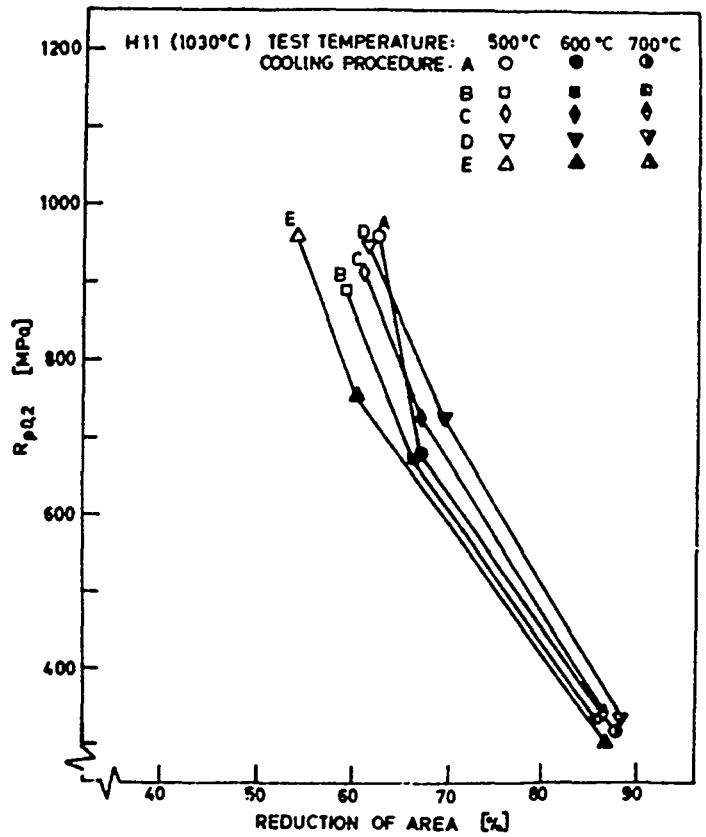

Proof stress (0.2%) and reduction in area obtained in H11 for various cooling procedures following austenitization at various tests temperatures (500-700°C)(Andersen).

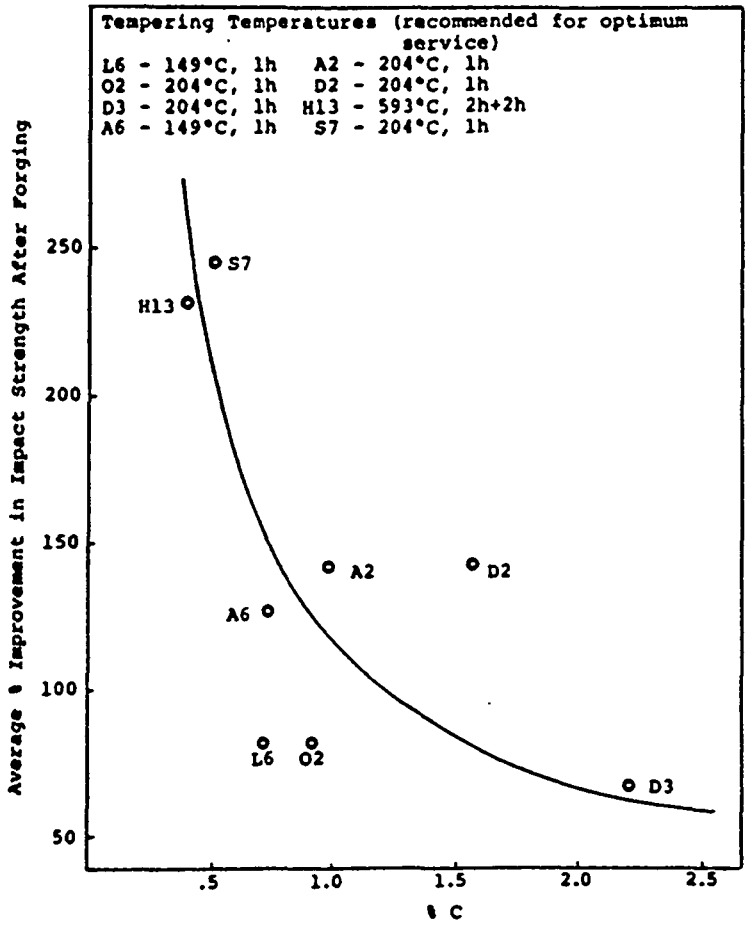

Relationship between %C and average % improvement in impact strength comparing as-cast and forged material. Samples were taken from laboratory heats, austenitized at optimum temperature, and tempered as above(**Hemphill et al.**)

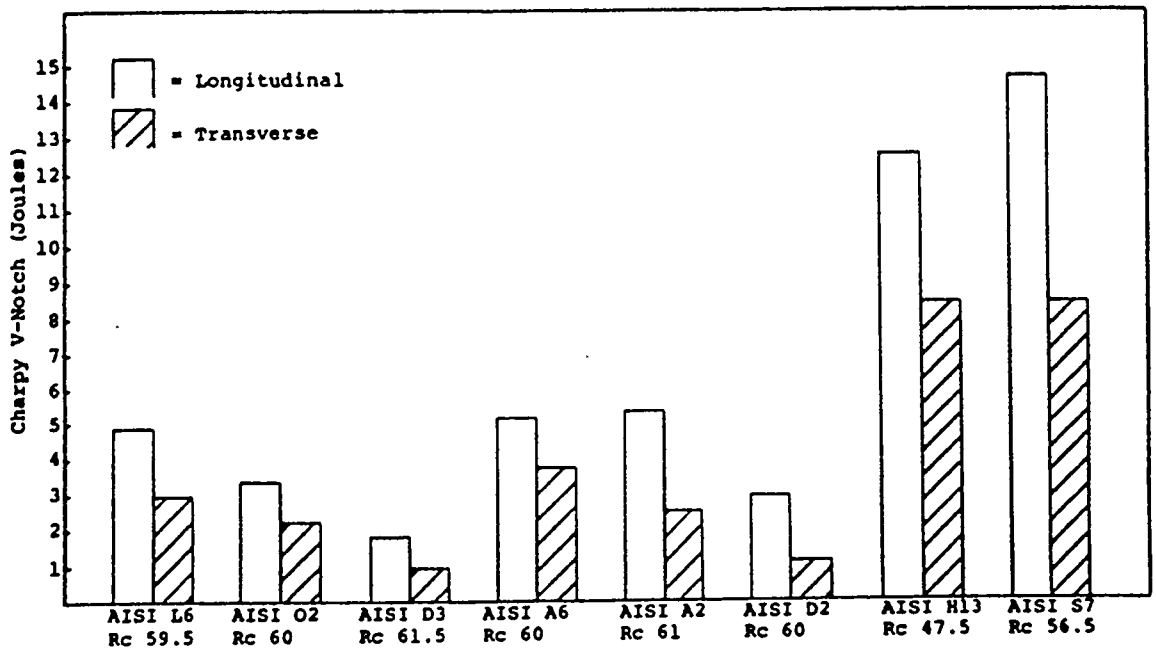

Comparison of longitudinal and transverse Charpy V-notch impact values at typical service hardnesses. Grades were tested at 89 mm square with a forging reduction of approximately 95%.

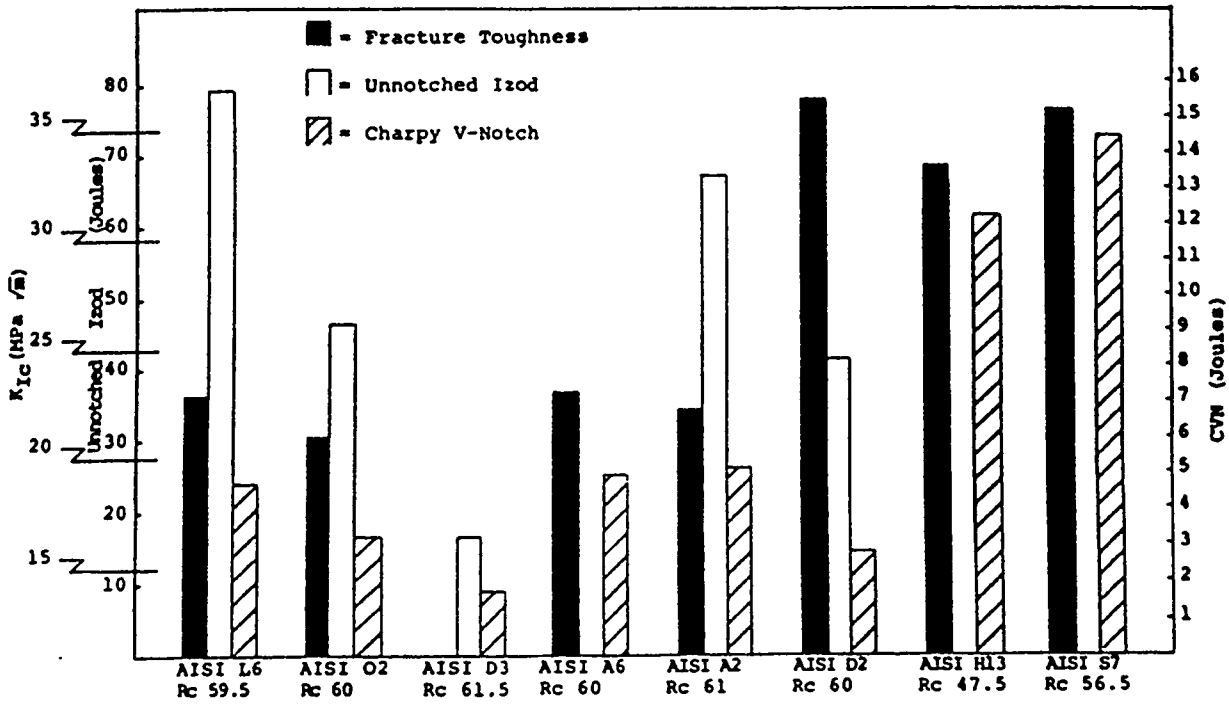

Comparison of fracture toughness, longitudinal unnotched Izod, and longitudinal Charpy V-notch impact results for grades at 89 mm square and at working hardness(**Hemphill et al.**)

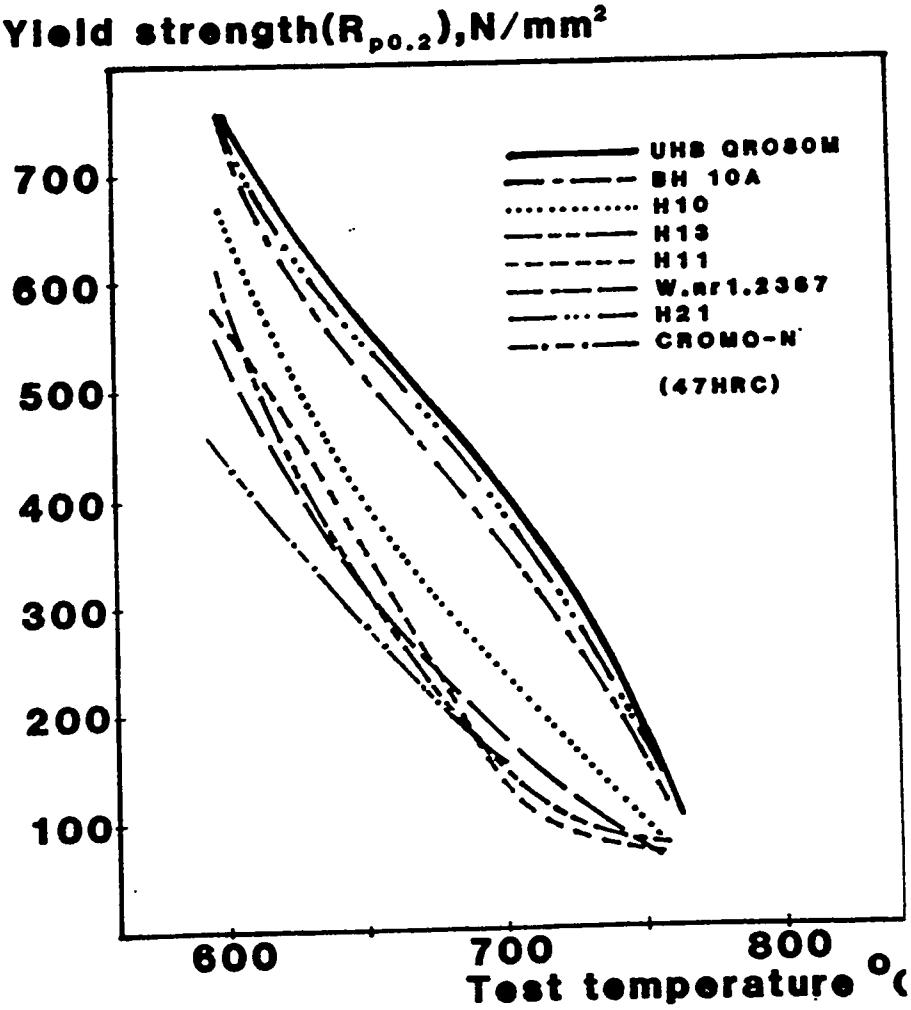

Yield strength of various die steels after quenching and double tempering (1h - 1h) at each temperature (Norstrom).

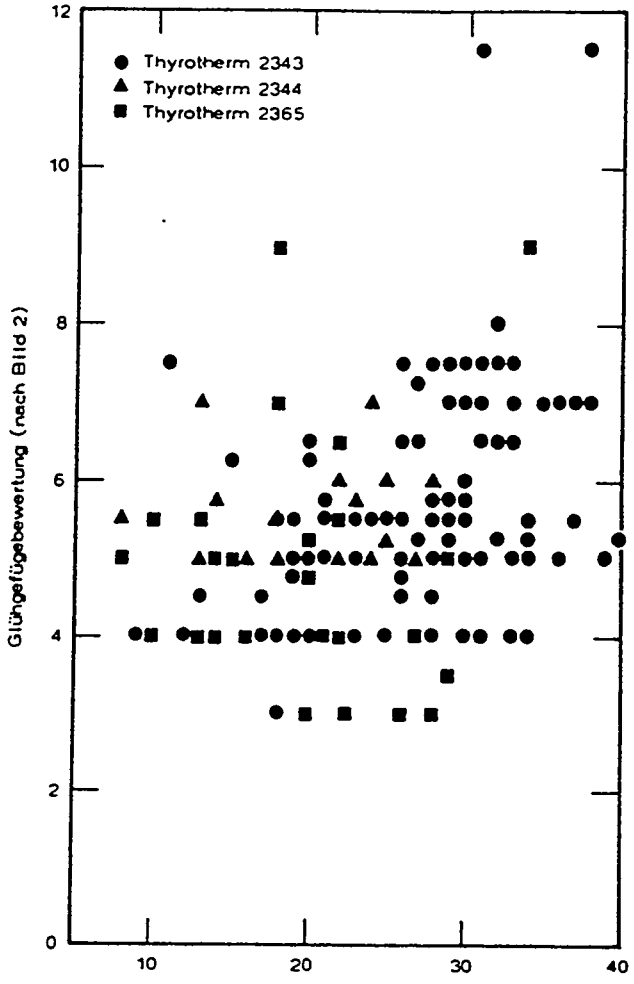

Influence of the annealed microstructure on the notch-impact energy of hot-work tool steels

(Berns 1990).

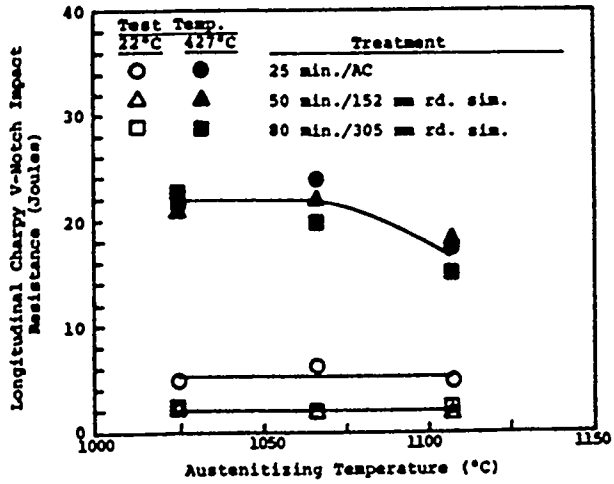

a. 538°C - 2h + 2h temper

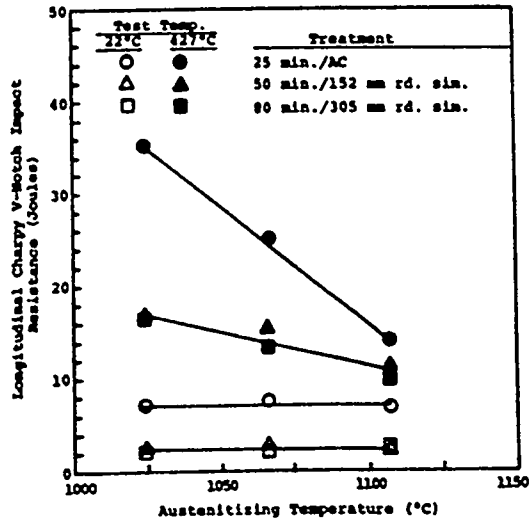

b. 593°C - 2h + 2h temper

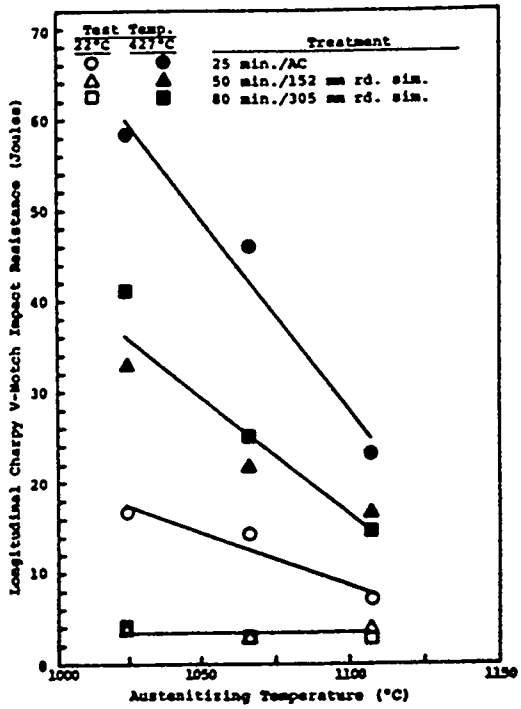

c. 621°C - 2h + 2h temper

Plots of Charpy V-Notch impact toughness versus austenitizing temperature(Schmidt)

Types H11, H13 Hot Work Tool Steels: Relationship of Tensile Properties and Hardness. Impact energy tests used Charpy V-notch specimens. Elongation was measured in 50 mm (2 in.); yield strength at 0.2% offset.

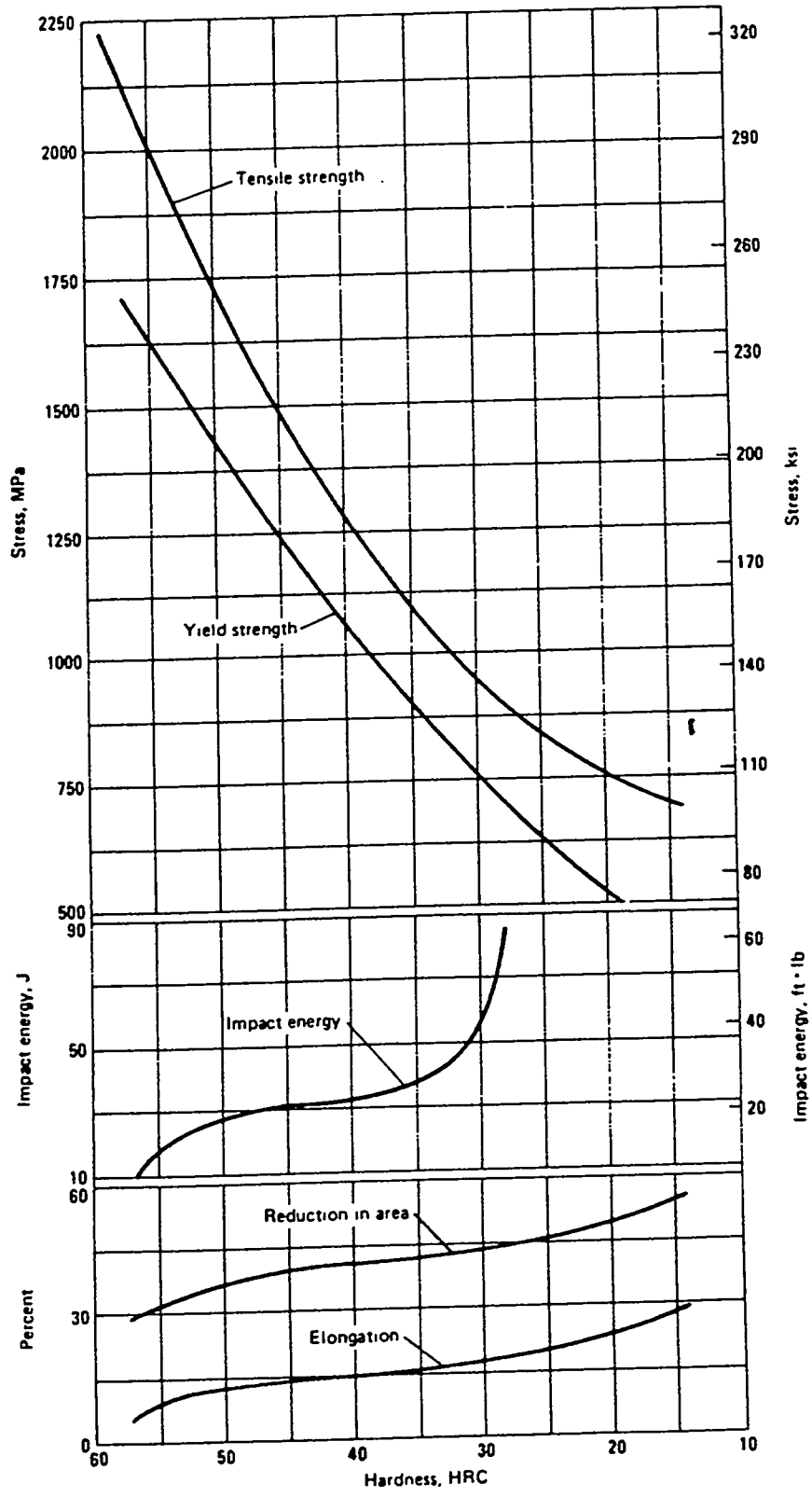

Types H11, H13 Hot Work Tool Steels: Effect of Elevated Temperature on Tensile Strength. Hardness was measured using the Rockwell C hardness test.

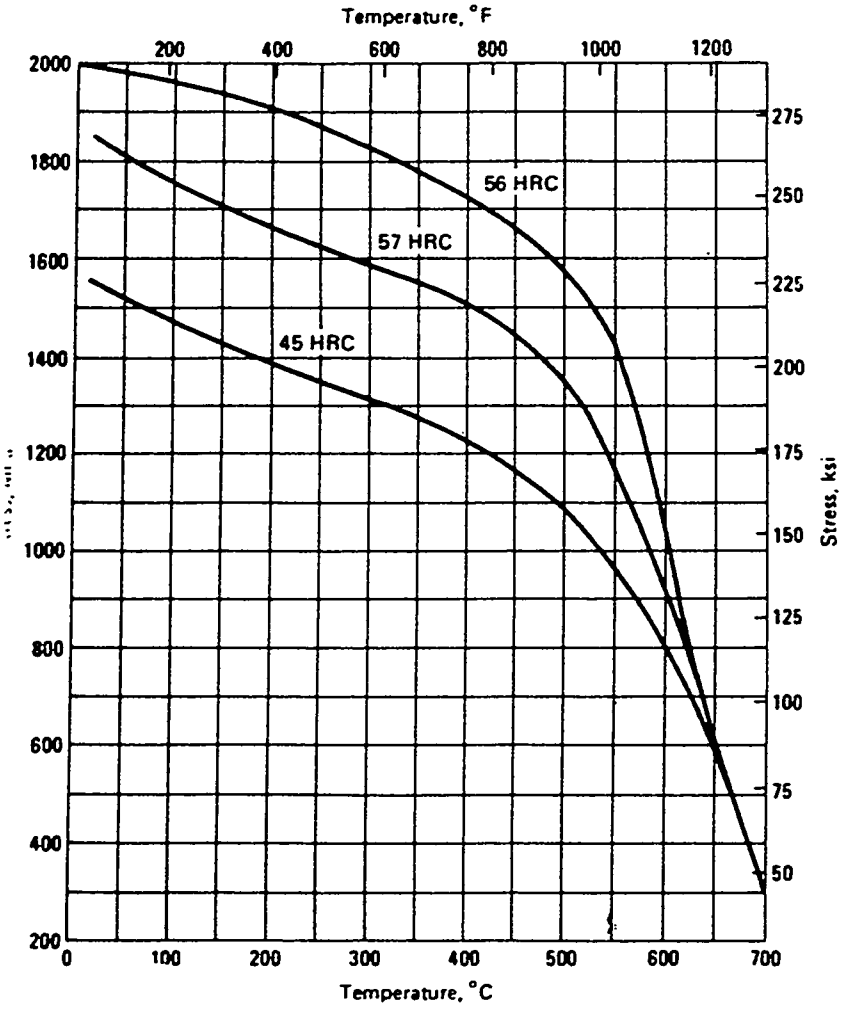

H13: Hardness Versus Tempering Temperature. (a) H13: Austenitized at 1850 °F (1010 °C), oil quenched, and tempered for 2 hr. (b) H13: Austenitized at the indicated temperatures, air quenched, and tempered for 2 hr. (Source: *Metals Handbook*, 8th ed., Vol 2, American Society for Metals, 1964)

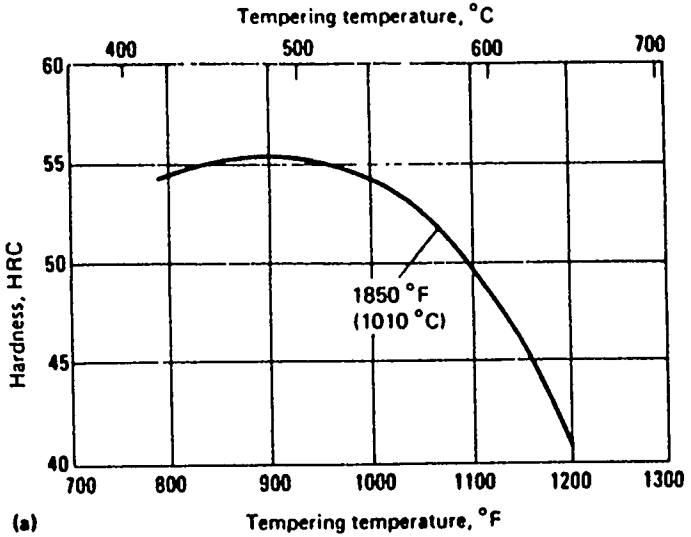

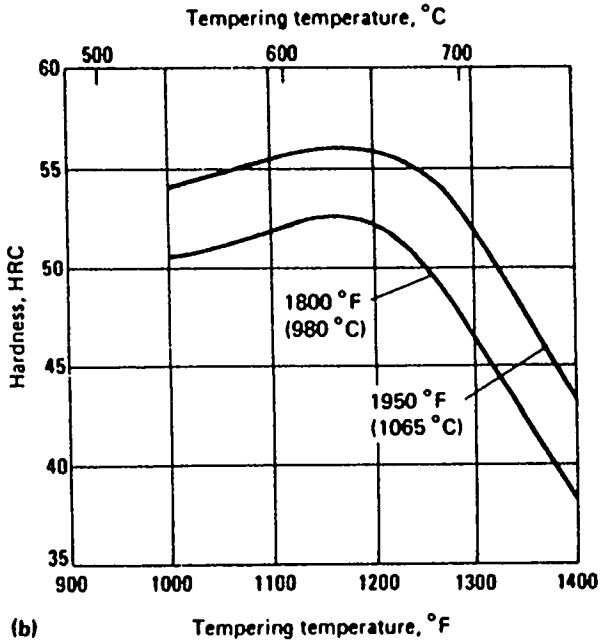

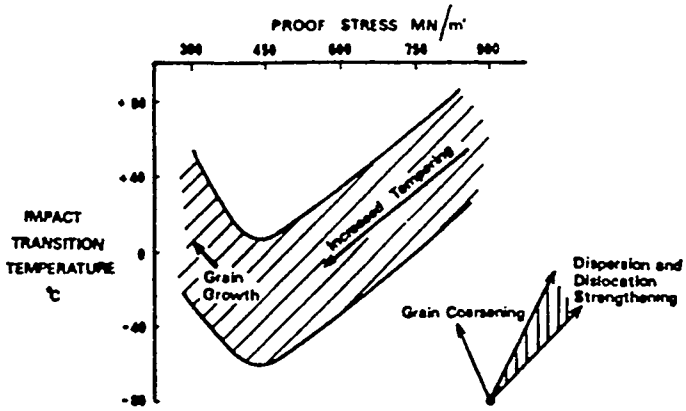

Effect of tempering on the toughness of bainite.

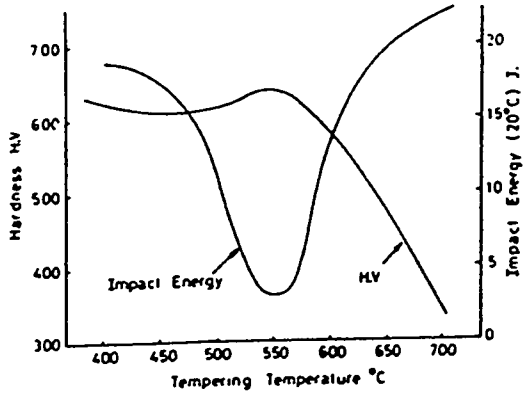

Loss of toughness due to secondary hardening in H13 steel.

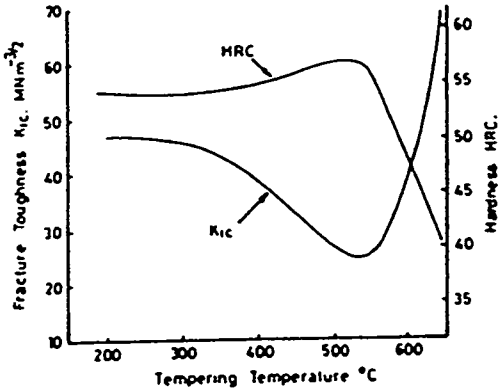

Minimum K_{IC} value associated with secondary hardening in H13 steel (Pickering)

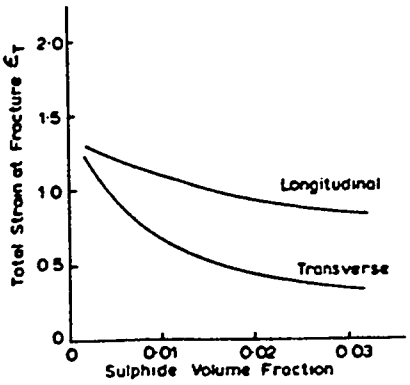

Effect of MnS volume fraction on strain at fracture, showing anisotropy.

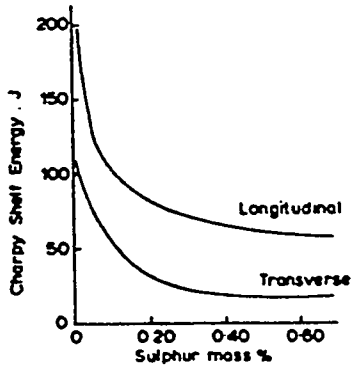

Effect of sulphur content on Charpy shelf energy showing anisotropy.

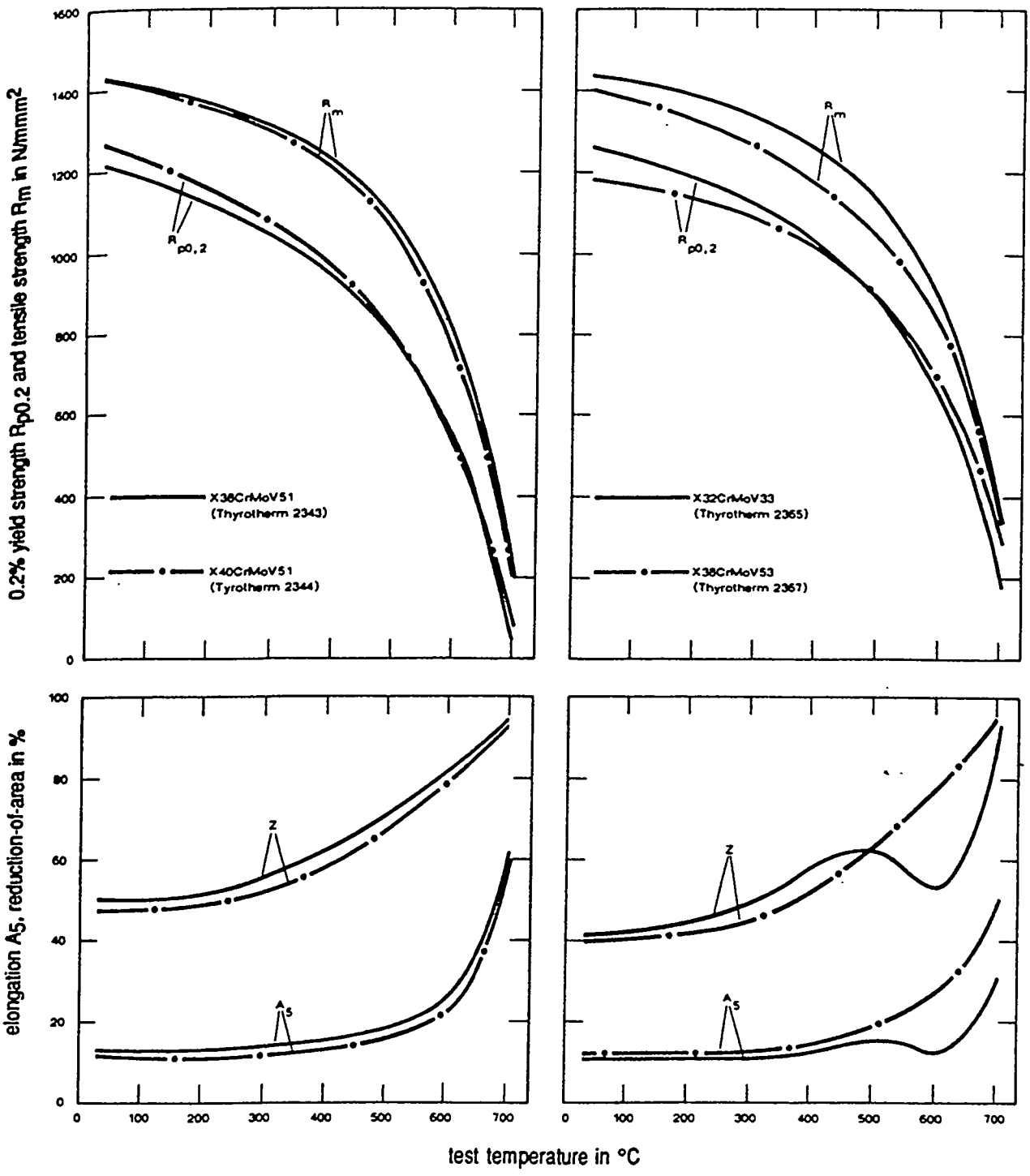

Hot-tensile strength and toughness of hot-work tool steels X 38 CrMoV 5 1 (Thyrotherm 2343), X 40 CrMoV 5 1 (Thyrotherm 2344), X 32 CrMoV 3 3 (Thyrotherm 2365) and X 38 CrMoV 5 3 (Thyrotherm 2367)

(Berns 1990).

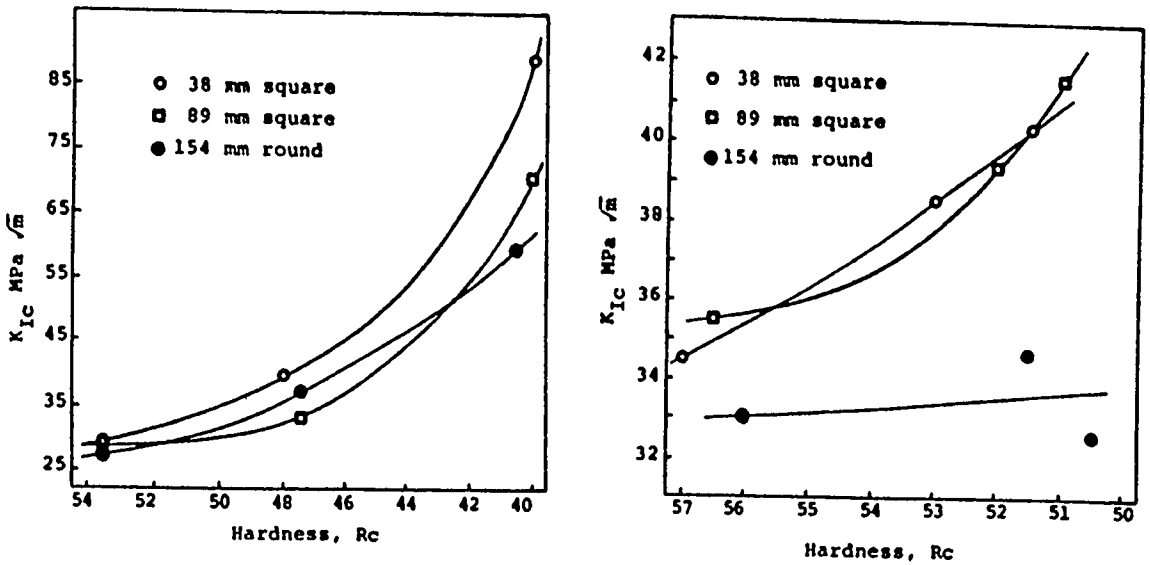

a) AISI Type H13

b) AISI Type S7

Effect of section size and tempered hardness on fracture toughness of AISI Types H13 **(Berns)**

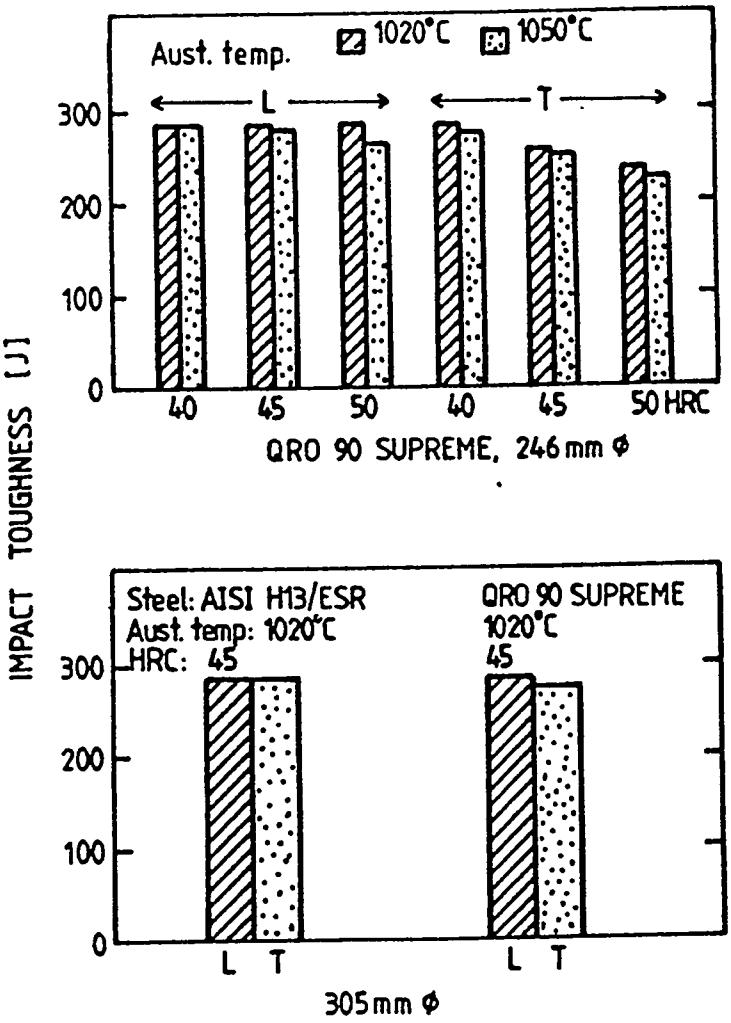

Unnotched impact toughness (specimen: 7 x 10 x 55 mm) as a function of hardness and austenitizing temperature for two hot-work tool steels (Sandberg et al.)

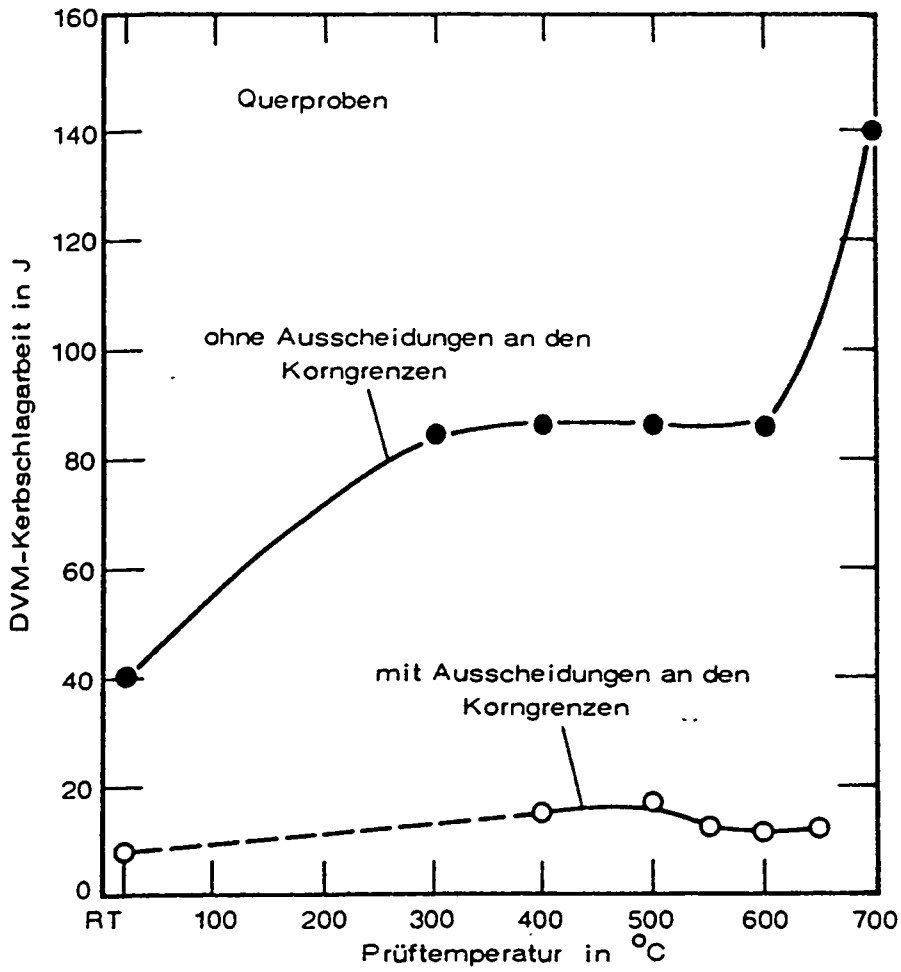

Influence of the coarse carbide precipitations at the grain boundaries on the DVM absorbed impact energy of the hot-work tool steel X40CrMoV51 (Thyortherm 2344) (Schruff).

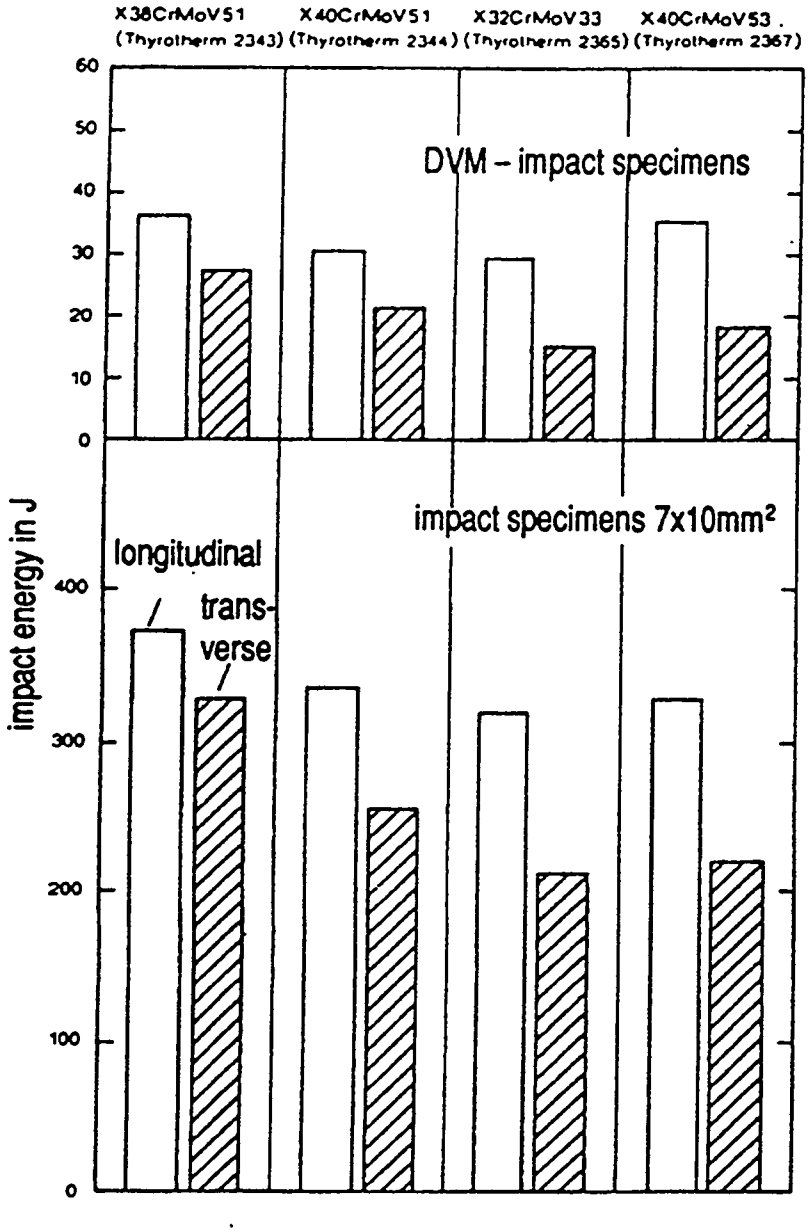

Specimen position: transition of 130 mm dia.
hardened and tempered: 40 to 42 HRC

Impact toughness of hot-work tool steels X38CrMoV51 (Thyrotherm 2343), X40CrMoV51 (Thyrotherm 2344), X32CrMoV33 (Thyrotherm 2365) and X38CrMoV53 (Thyrotherm 2367) at room temperature (Schruff).

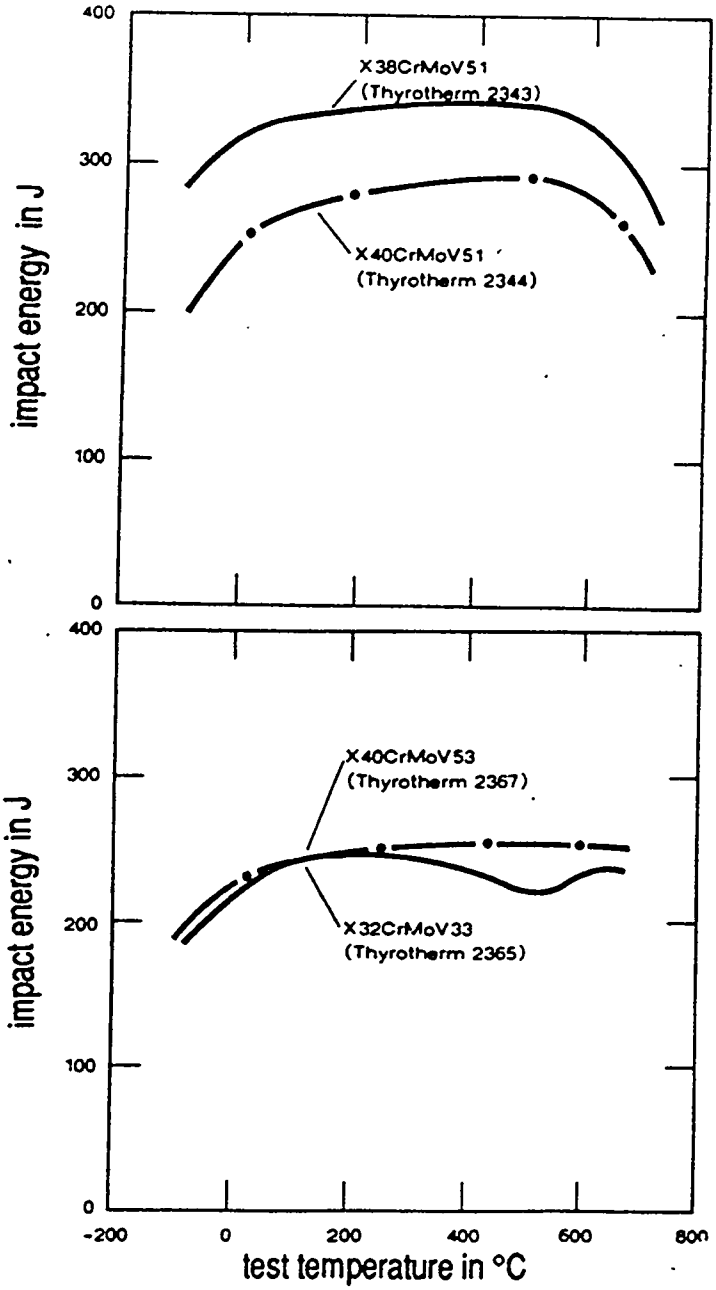

Dependence of impact toughness of the hot-work tool steels examined on test temperature. Impact test specimens (7x10 mm²) taken from transverse position, heat-treated to 42 to 44 HRC (Schruff).

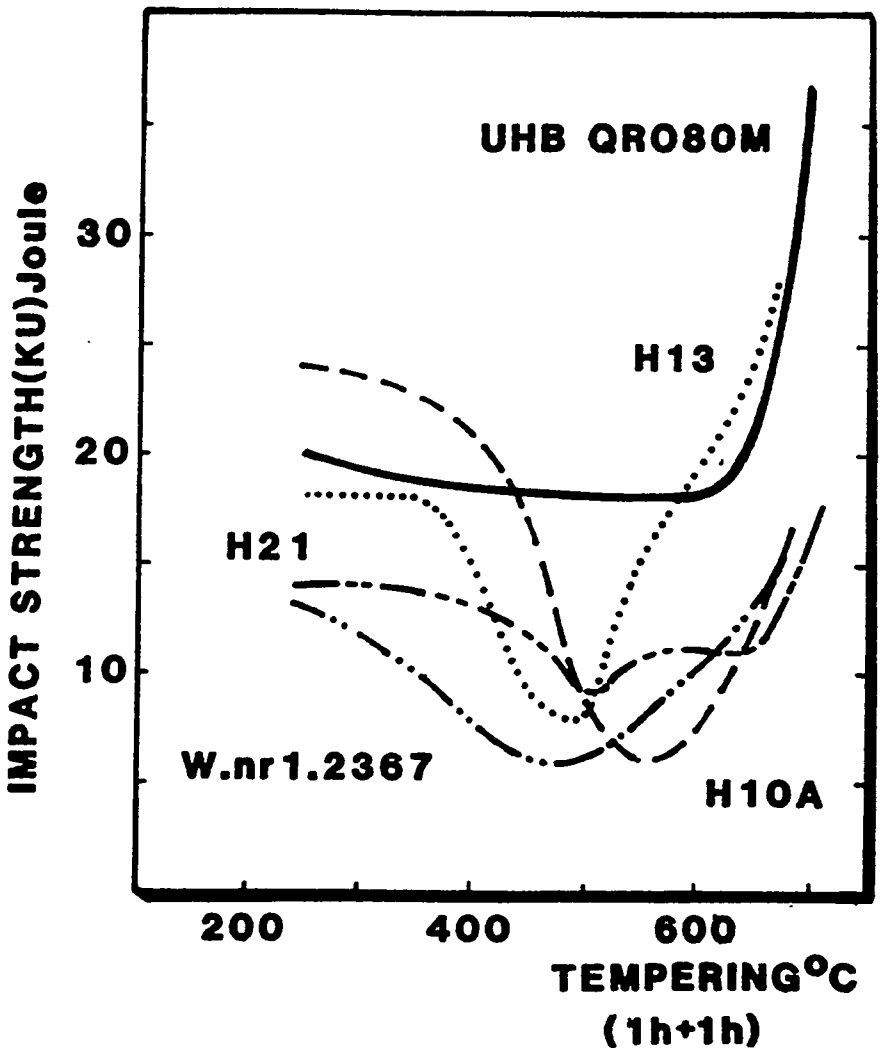

Impact toughness (Ku) of H13 at room temperature after quenching and double tempering between 200 and 700°C (Norstrom).

4.3.4 Creep and Creep Rupture Properties

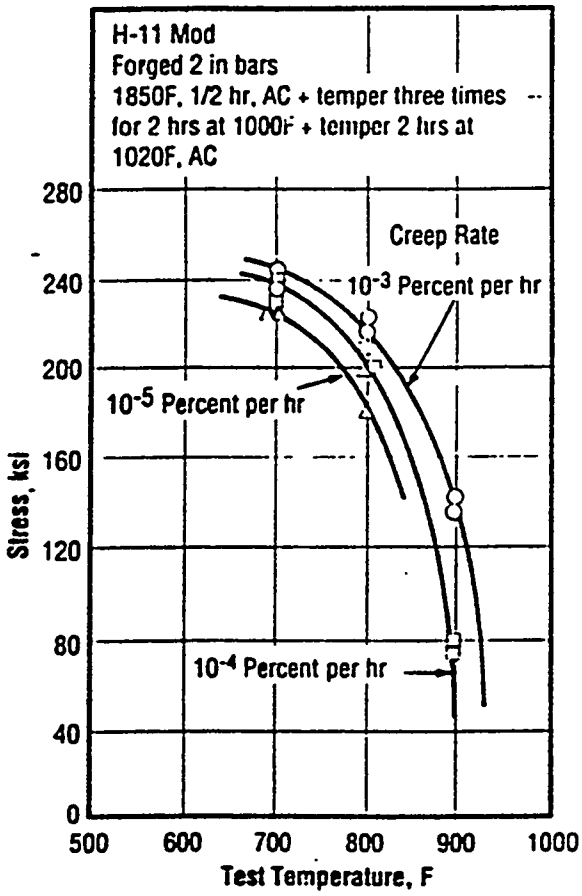

Stress to produce creep rates 0f 10^{-3} to 10^{-5} percent per hour at 700 to 900°F in H11 (VanEcho).

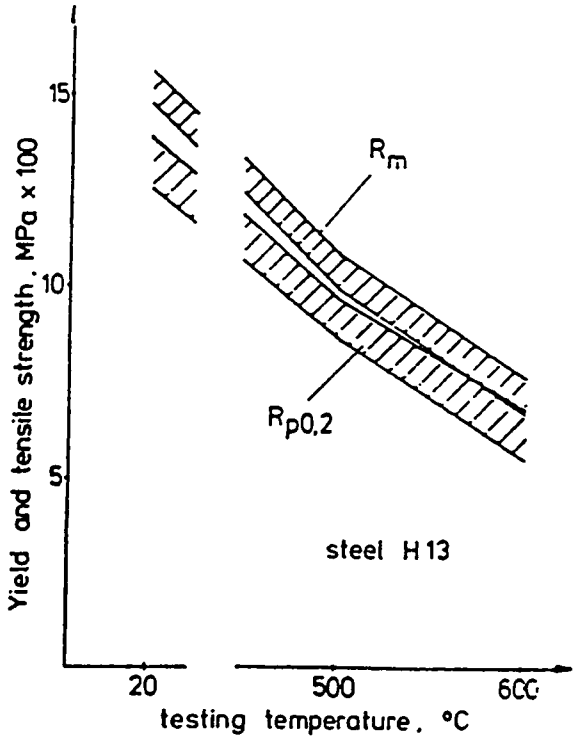

Strength of differently manufactured stock (N, D, ESR, CaT, HIPW in longitudinal and transvers direction and HIP)(Berns)

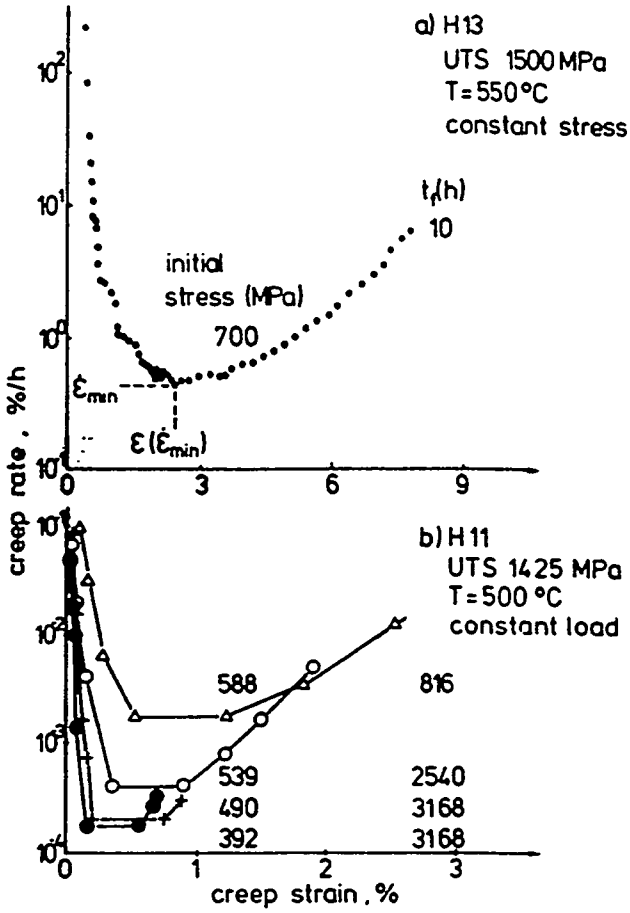

Creep rate depending on creep strain for short and longtime creep tests (Berns)

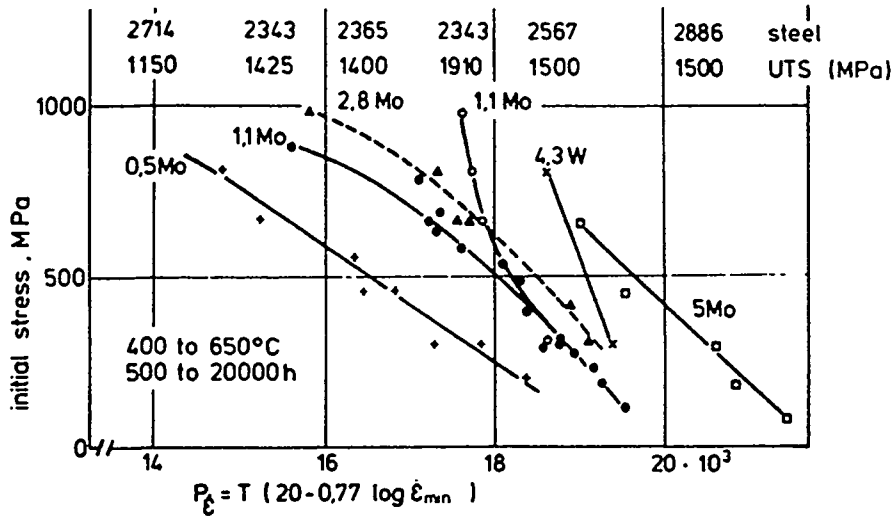

Influence of alloy content on the creep resistance (1)

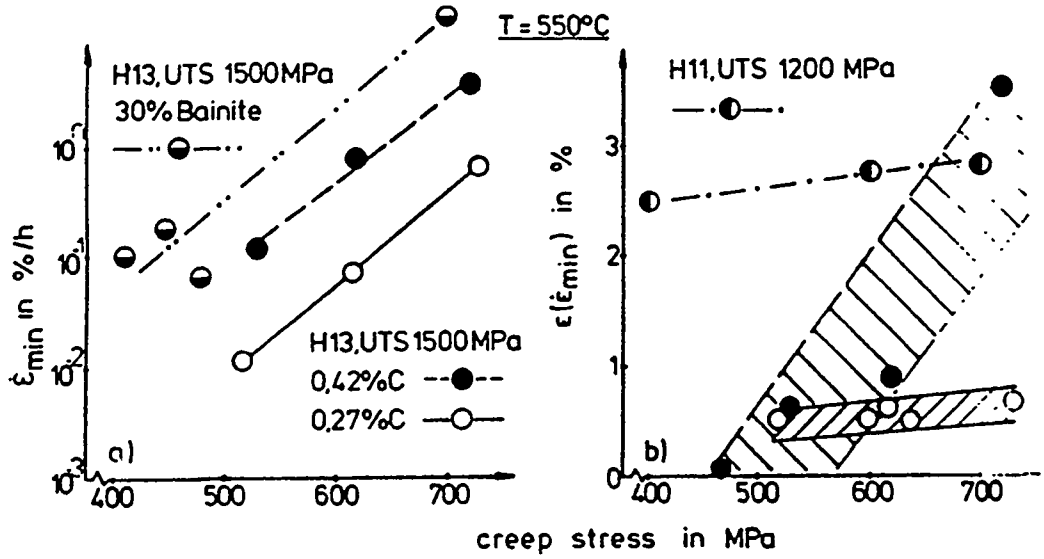

Minimum creep rate and the plastic creep deformation to reach it (Berns)

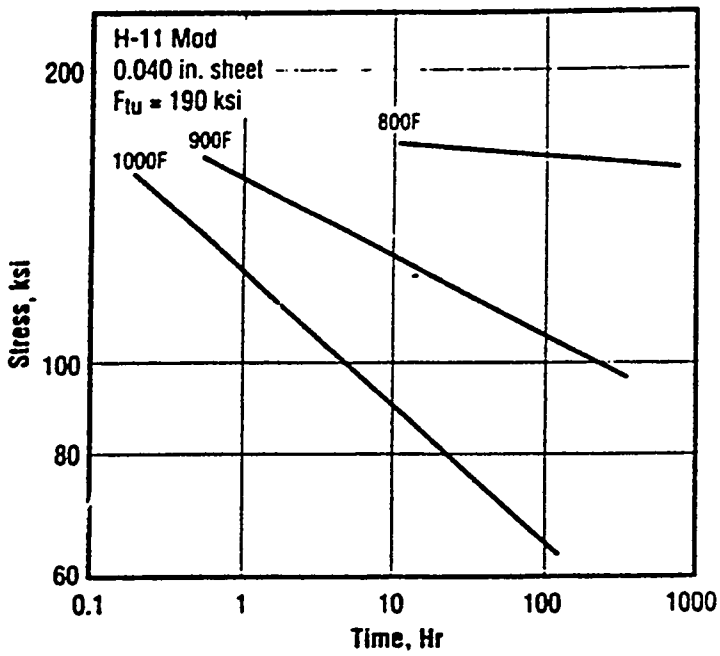

Creep rupture curves at 700 to 1000°F
for H11 sheet heat treated to F_{tu}=190ksi (Crucible).

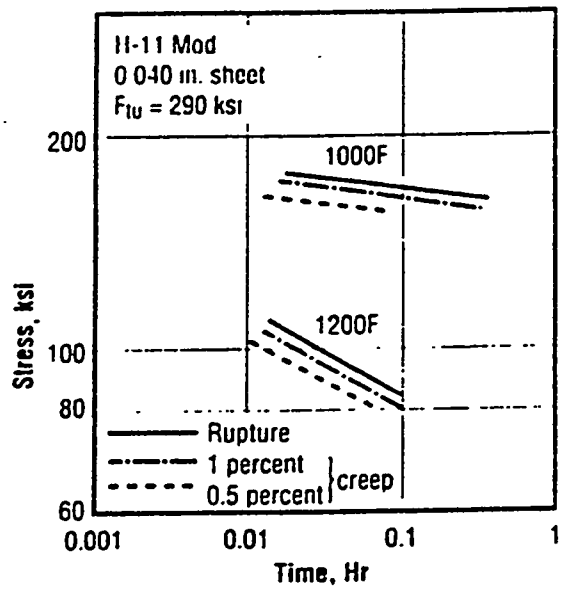

Short time and creep rupture curves at 1000°F and 1200°F
for H11 sheet heat treated to F_{tu}=290ksi (INCO).

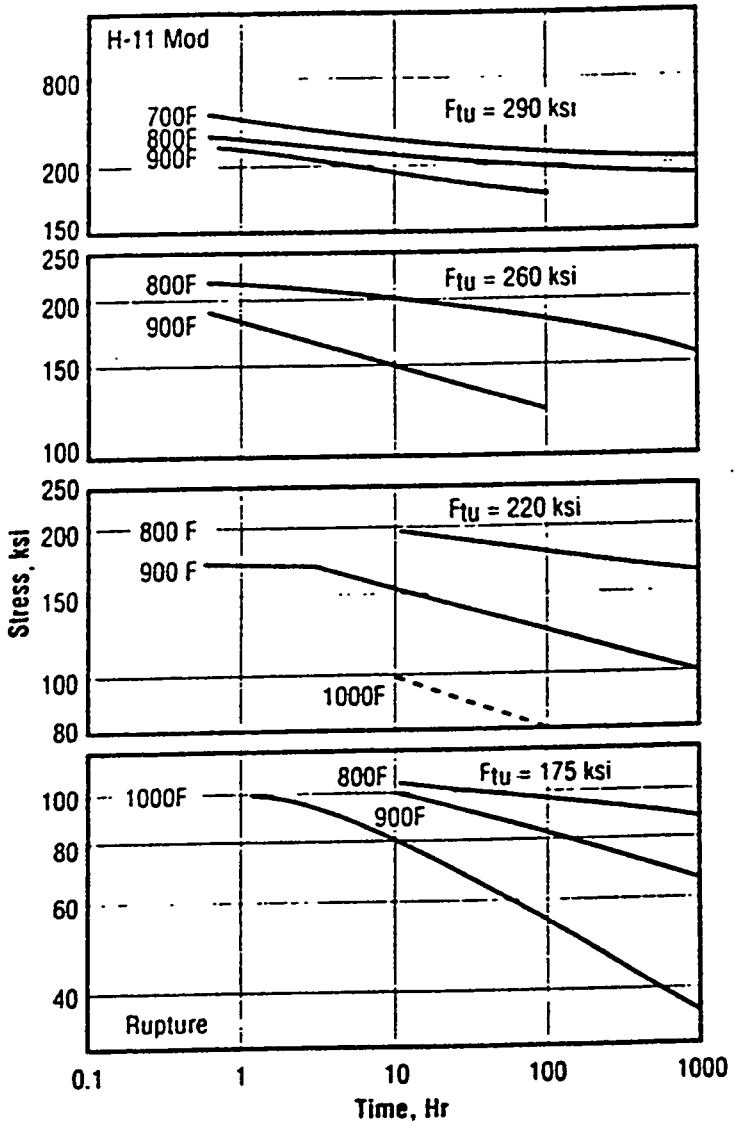

Creep rupture curves for H11 at various strength levels at 700 to 1000°F (Crucible).

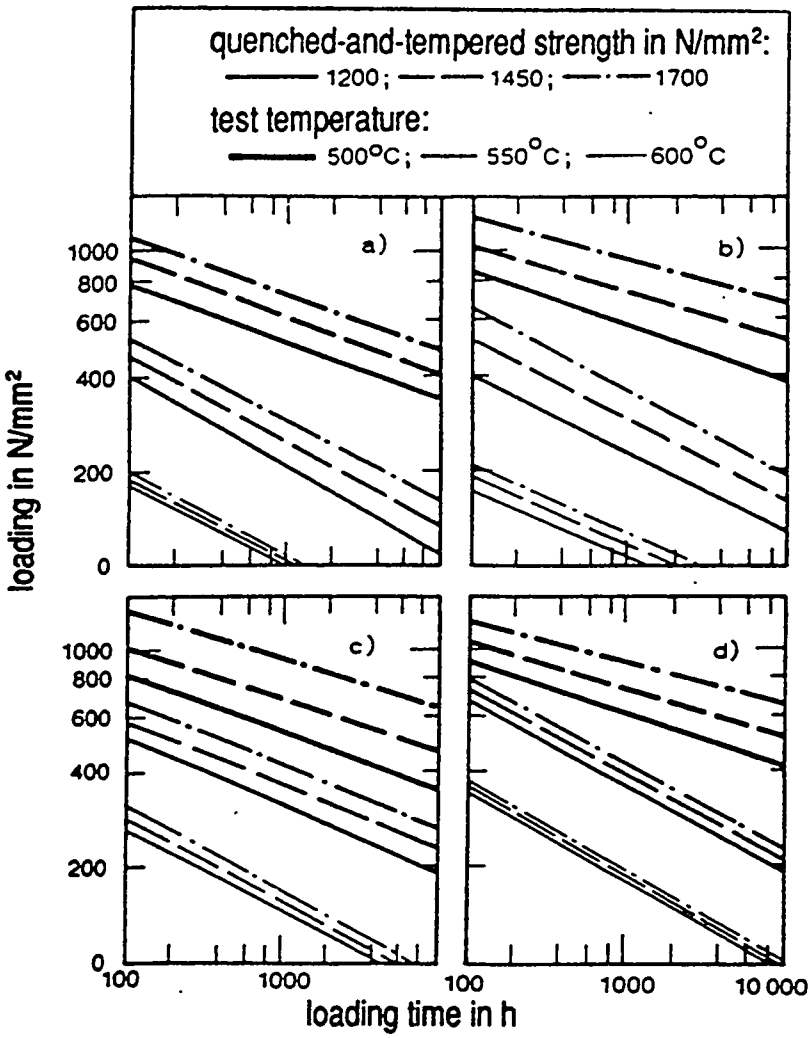

Creep rupture strenght of hot-work tool steels a) X 38 CrMoV 5 1 (Thyrotherm 2343), b) X 40 CrMoV 5 1 (Thyrotherm 2344), c) X 32 CrMoV 3 3 (Thyrotherm 2365) and d) X 38 CrMoV 5 3 (Thyrotherm 2367) with dependence on as-heat treated tensile strength and test temperature (Schruff).

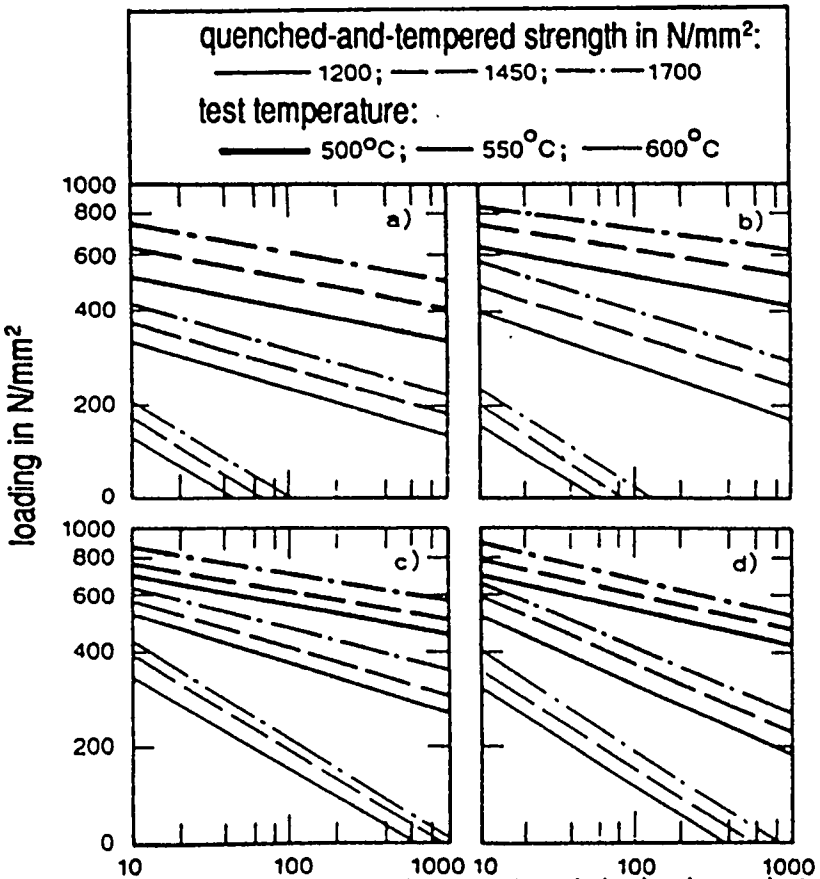

1% creep stresses of hot-work tool steels, depending on quenched-and-tempered strength and test temperature (Schruff).

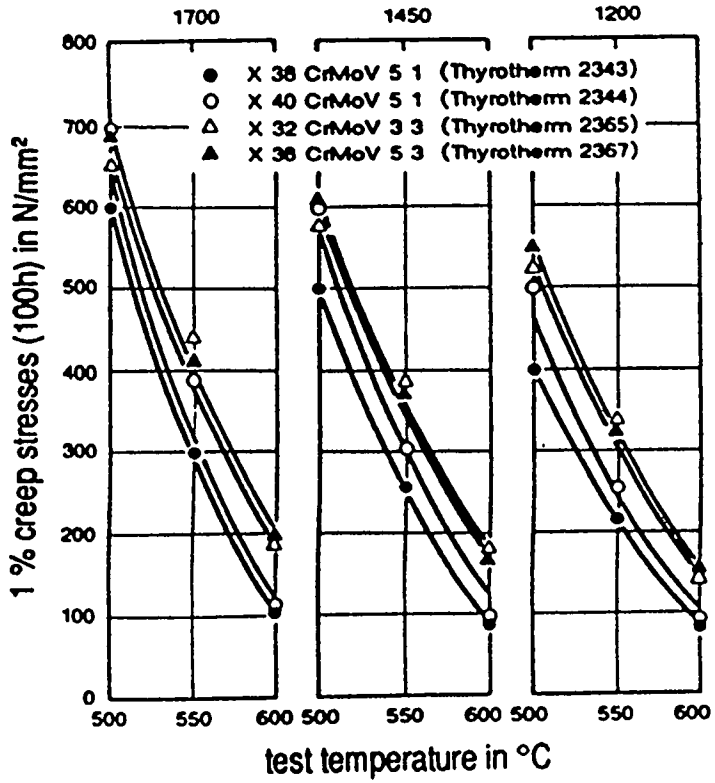

Comparison of 1 %-creep stresses between various hot-work tool steels (Schruff).

4.3.5 Fatigue Properties

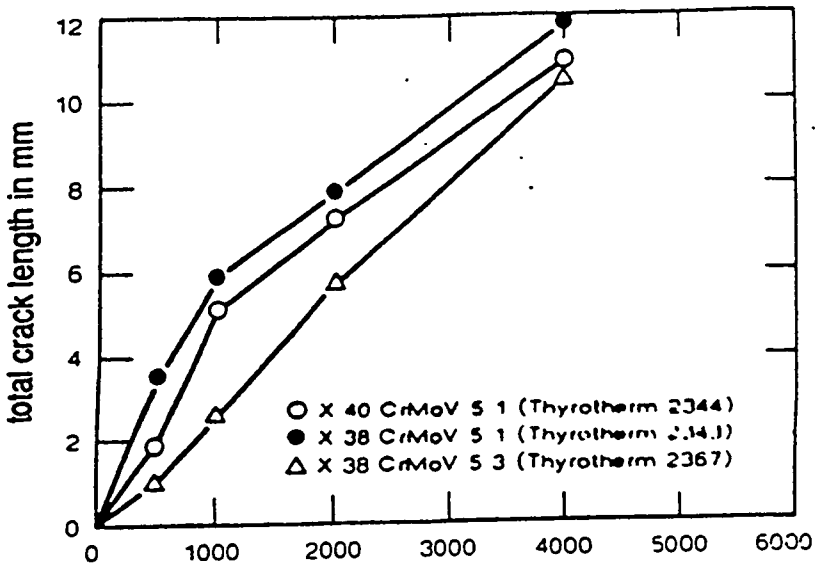

Comparison of thermal fatigue restistance between hot-work steels of varying compositions (Schruff).

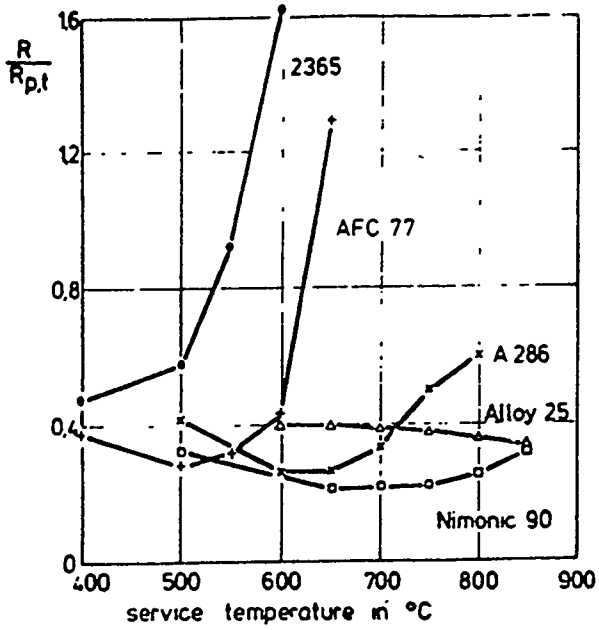

R = true flow stress of brass 65

$R_{p,t}$ = 1% - 1000h creep strength of tool

Materials selection for tooling in brass extrusion (2)

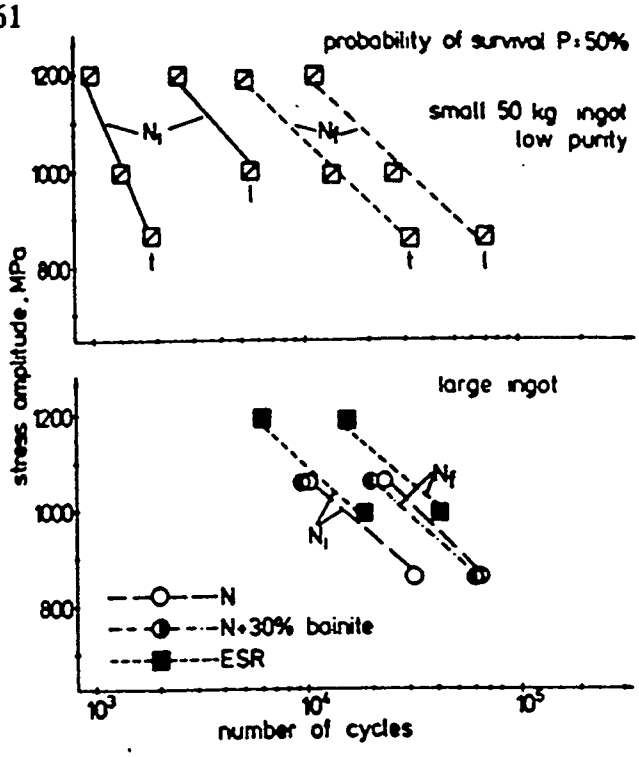

Fatigue life in rotating bending of steel H13 (Berns)

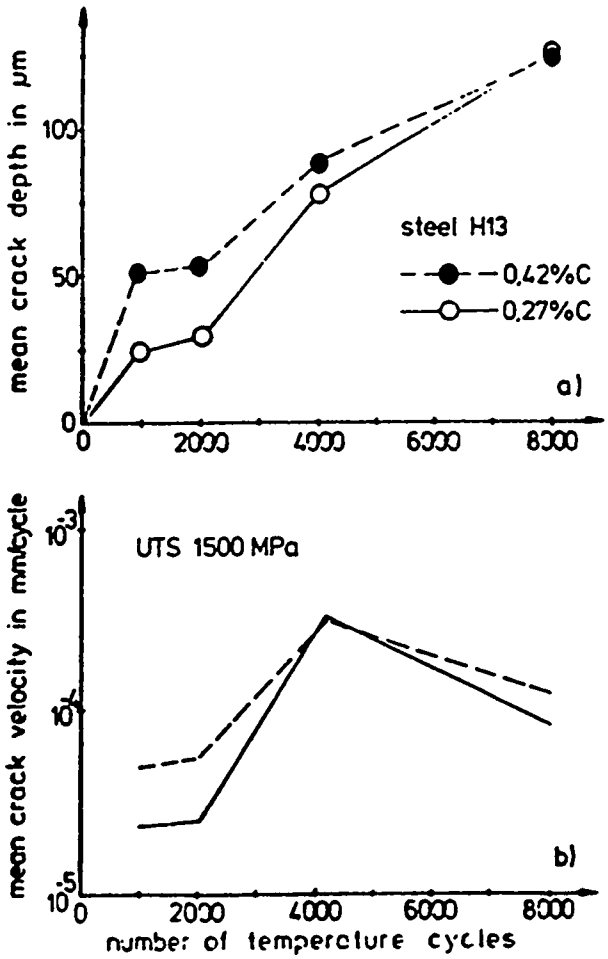

Crack velocity in thermal fatigue testing (7)

Wedge-like penetration of Al into fatigue crack of an extrusion tool forming a hard compound as shown by the hardness indentations

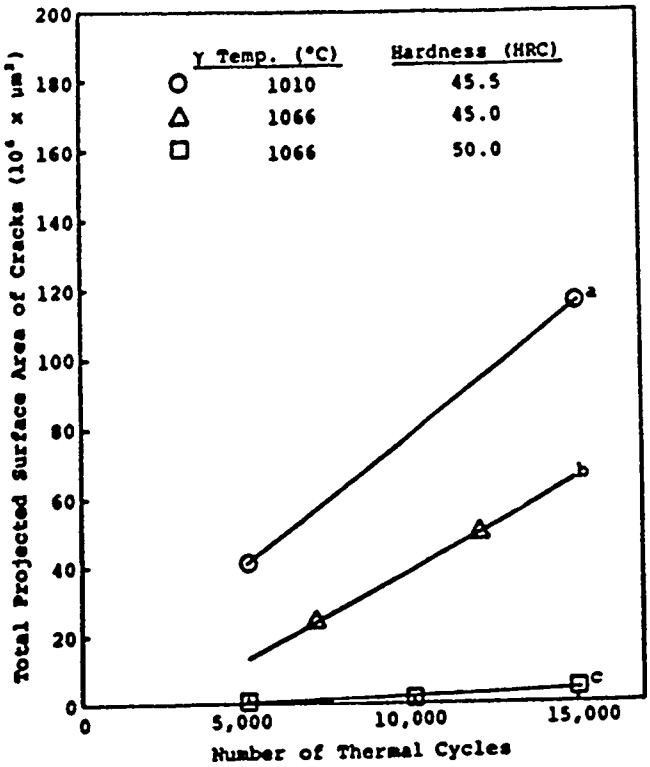

Thermal fatigue resistance of H-13 tool steel (data obtained from work by Wallace).

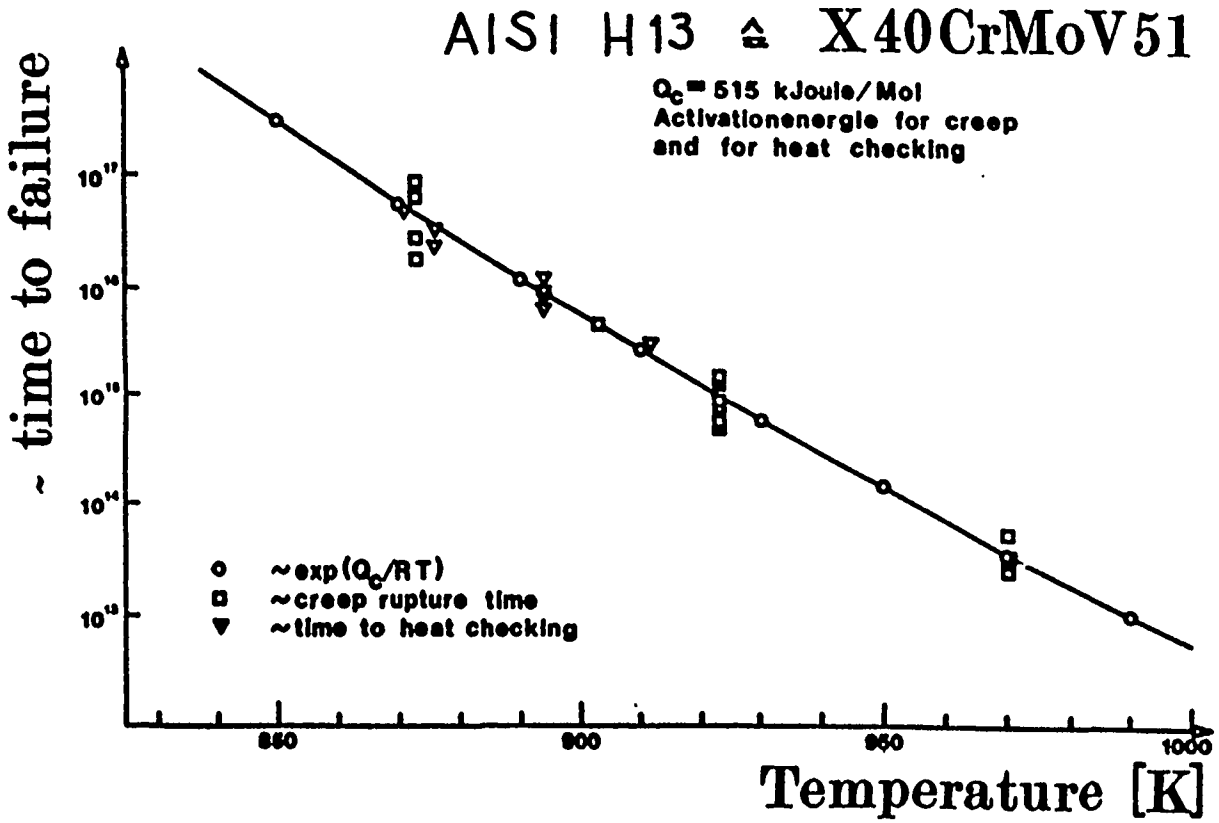

H-13 - life time versus temperature. (Zleppnig et al.)

5. FEM Models of an H-13 Block

5.1 Cup Model

Following are thermal and stress predictions for a cup shaped object made of H13 steel. The dimensions of the cup are shown on the cross-section view in figure 5.1. The cross-section is symetrical with respect to the center-line. Only the right half is shown.

The 2-D model assumes a pinned node at location (0,0) - i.e. this point is fixed and cannot move in any direction as shown in figure 5.2. Also that the center line side is on rollers - i.e. it can move up and down, but not sideways. The temperature at t=0 is 1900°F. The model has 2000 elements and 2021 nodes. The location of the nodes used in the graphs is shown on the schematic.

The color plots show the temperature distribution in the cup as a function of time. The enclosed sequence includes four plots at 1, 5, 10 and 90 seconds shown in figure 5.3-5.6. The legend identifies the temperature range. Notice the faster cooling at the corners. The isotherms follow the shape of the cup, leaving a "heat spot" at the thickest cross section.

The graph in figure 5.7 shows the temperature change as a function of time for the surface(430) and center(440) nodes. As expected, initially the temperature of the center lags behind the surface, catching up with it after longer times. The cooling rates are fast enough to generate a martensitic structure troughout the cup.

The radial displacement curves, shown in figure 5.8, predict some warpage of the cup: Nodes 2112 and 1991 originally on the top and bottom of the side wall, show a slight radial difference early on during the cooling. The axial dispacement curves shown in figure 5.9 predict dimensional changes in the 0.005 range for node 1912 and 661. The model was generated with the Topaz and Nike PC finite element codes. No adequate die was available to validate the prediction of this model. At this point it was decided to only generate finite element models for simple shapes or dies that would also be available for experimental validation.

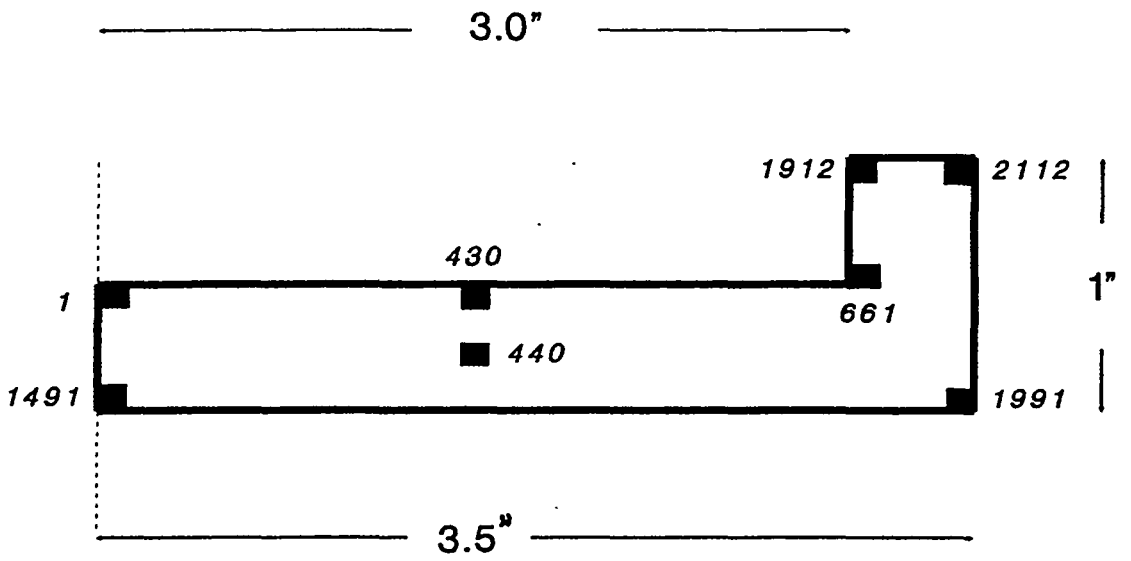
3.0"
1912
2112
430
1
661
1"
440
1491
1991
3.5"

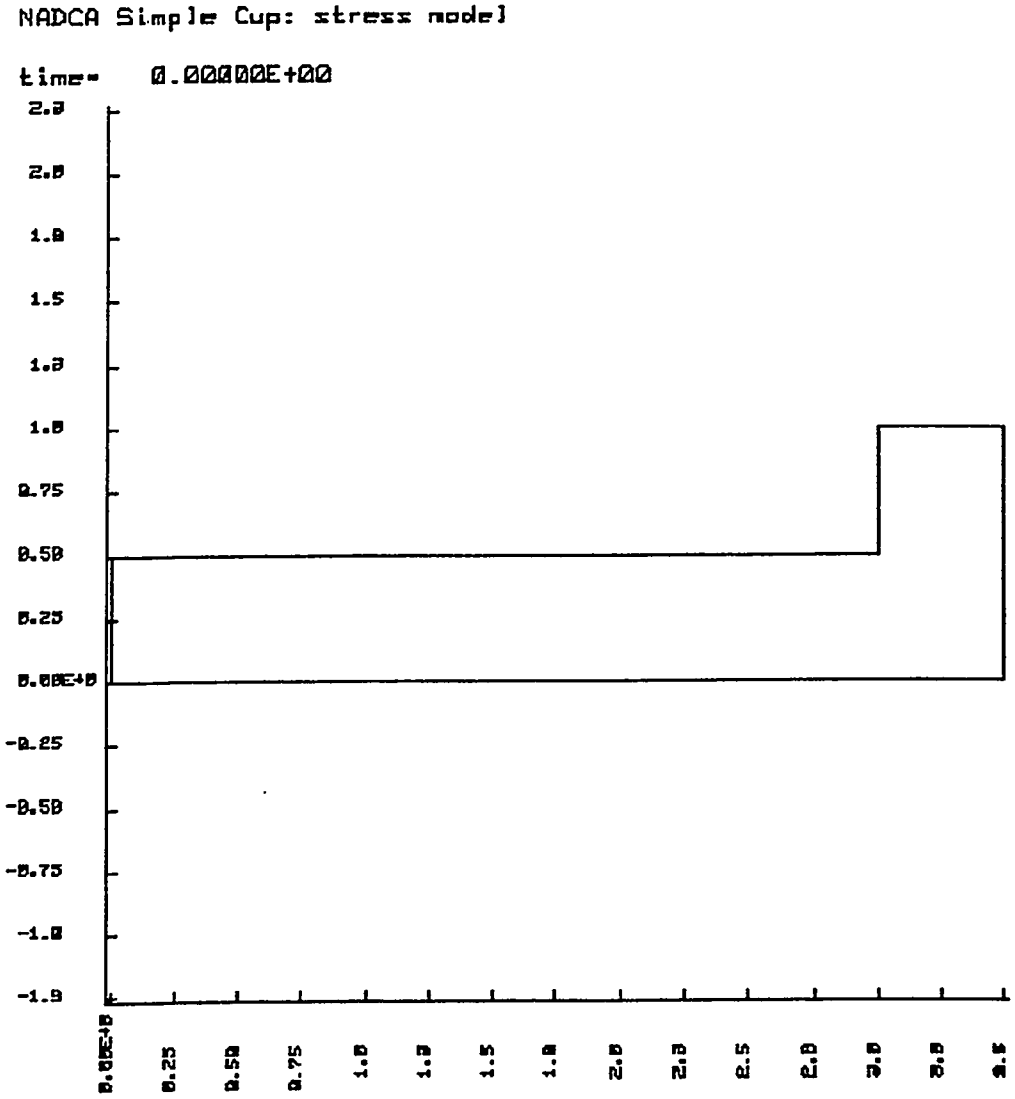
NADCA Simple Cup: stress model
time= 0.000000E+00
2.2
2.0
1.8
1.5
1.2
1.0
0.75
0.50
0.25
0.00E+0
-0.25
-0.50
-0.75
-1.0
-1.2
0.00E+0
0.25
0.50
0.75
1.0
1.2
1.5
1.8
2.0
2.2
2.5
2.8
3.0
3.2
3.5

Temperature Distribution - Cup 3
t= 1 sec (t=0, T=1900F)

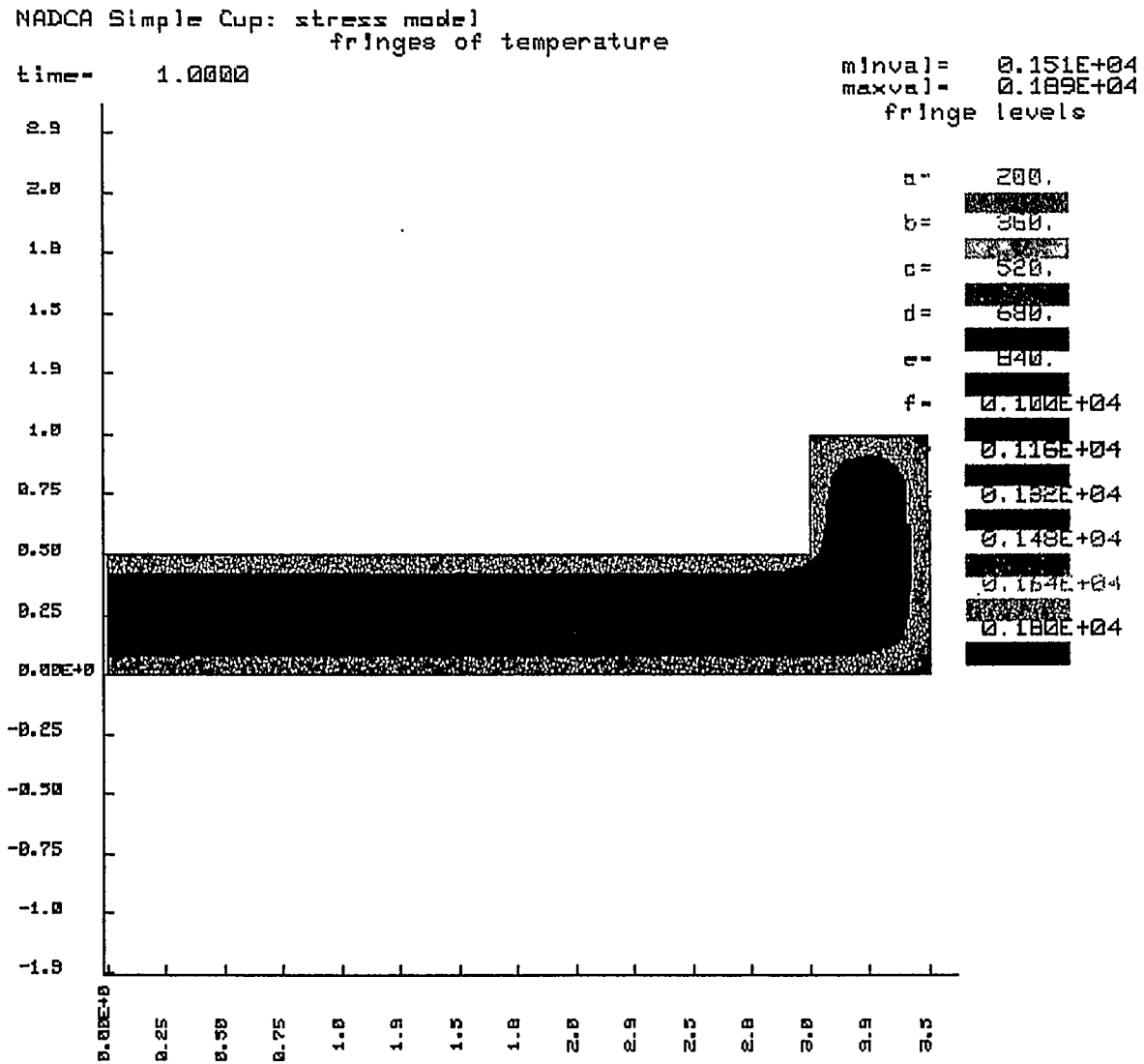

Temperature Distribution - Cup 3
t= 5 sec (t=0, T=1900F)

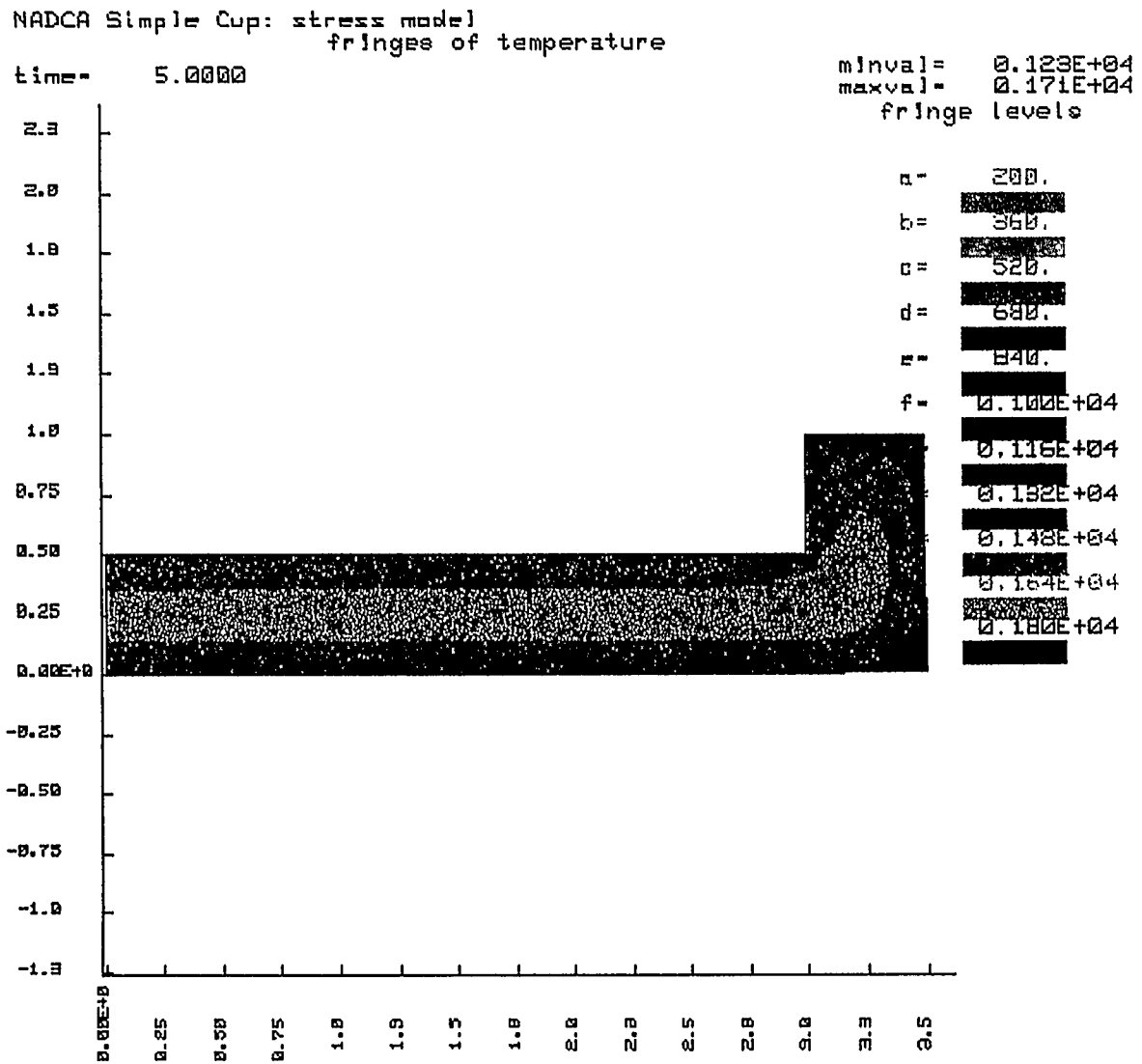

Temperature Distribution - Cup 3
t= 10 sec (t=0, T=1900F)

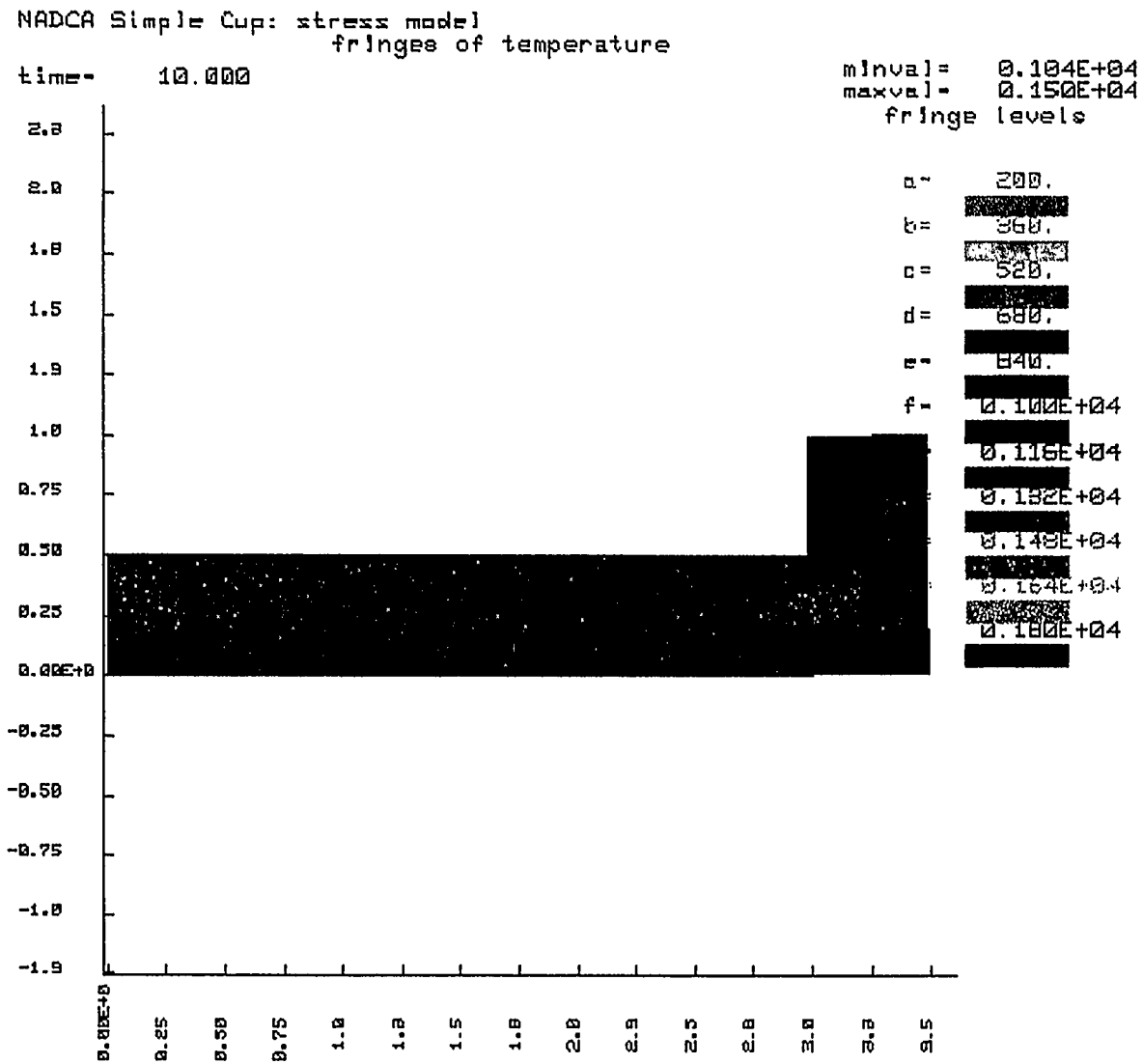

Temperature Distribution - Cup 3
t= 90 sec (t=0, T=1900F)

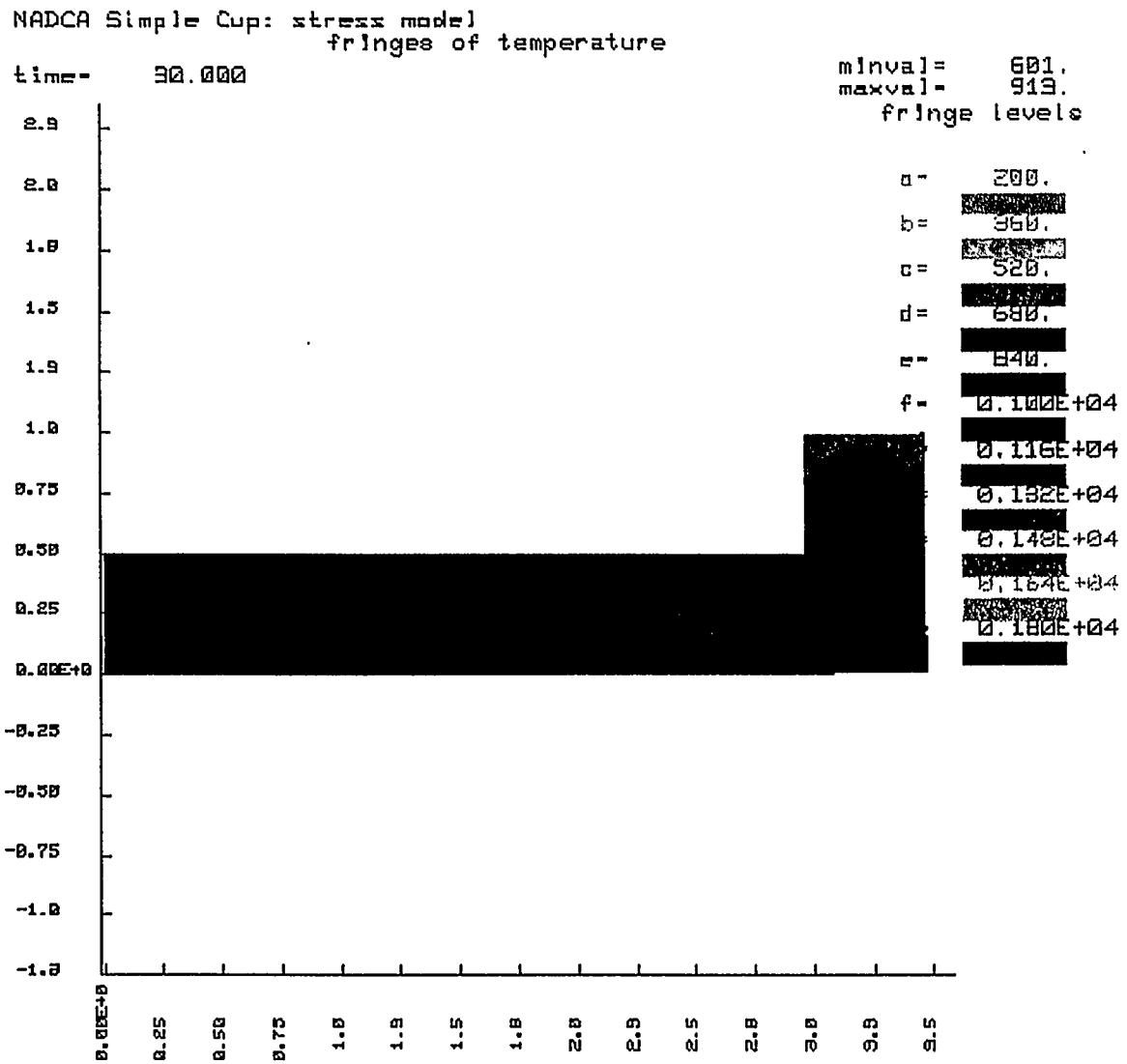

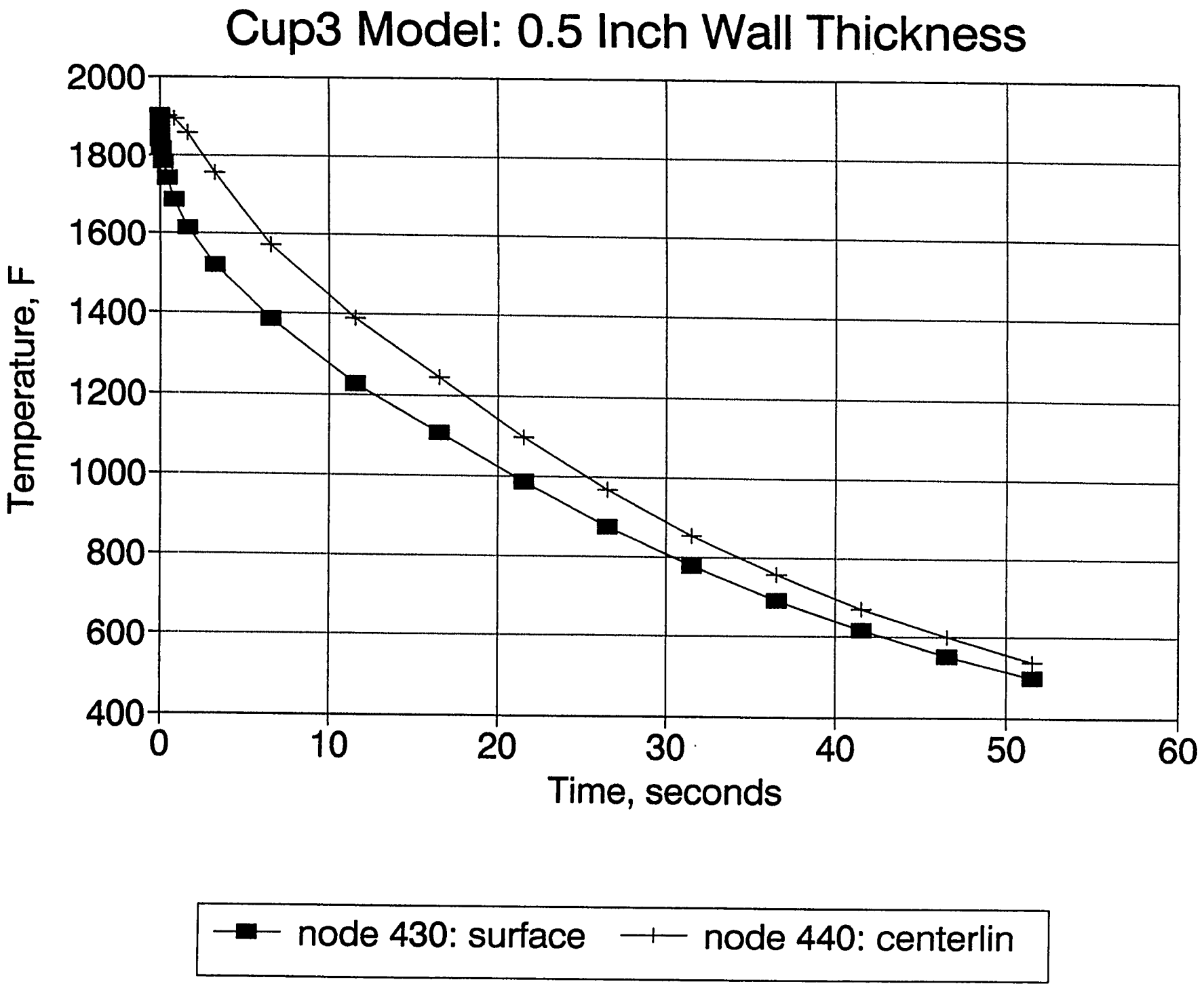
Cup3 Model: 0.5 Inch Wall Thickness
Temperature, F
2000
1800
1600
1400
1200
1000
800
600
400
0
10
20
30
40
50
60
Time, seconds
node 430: surface
node 440: centerlin

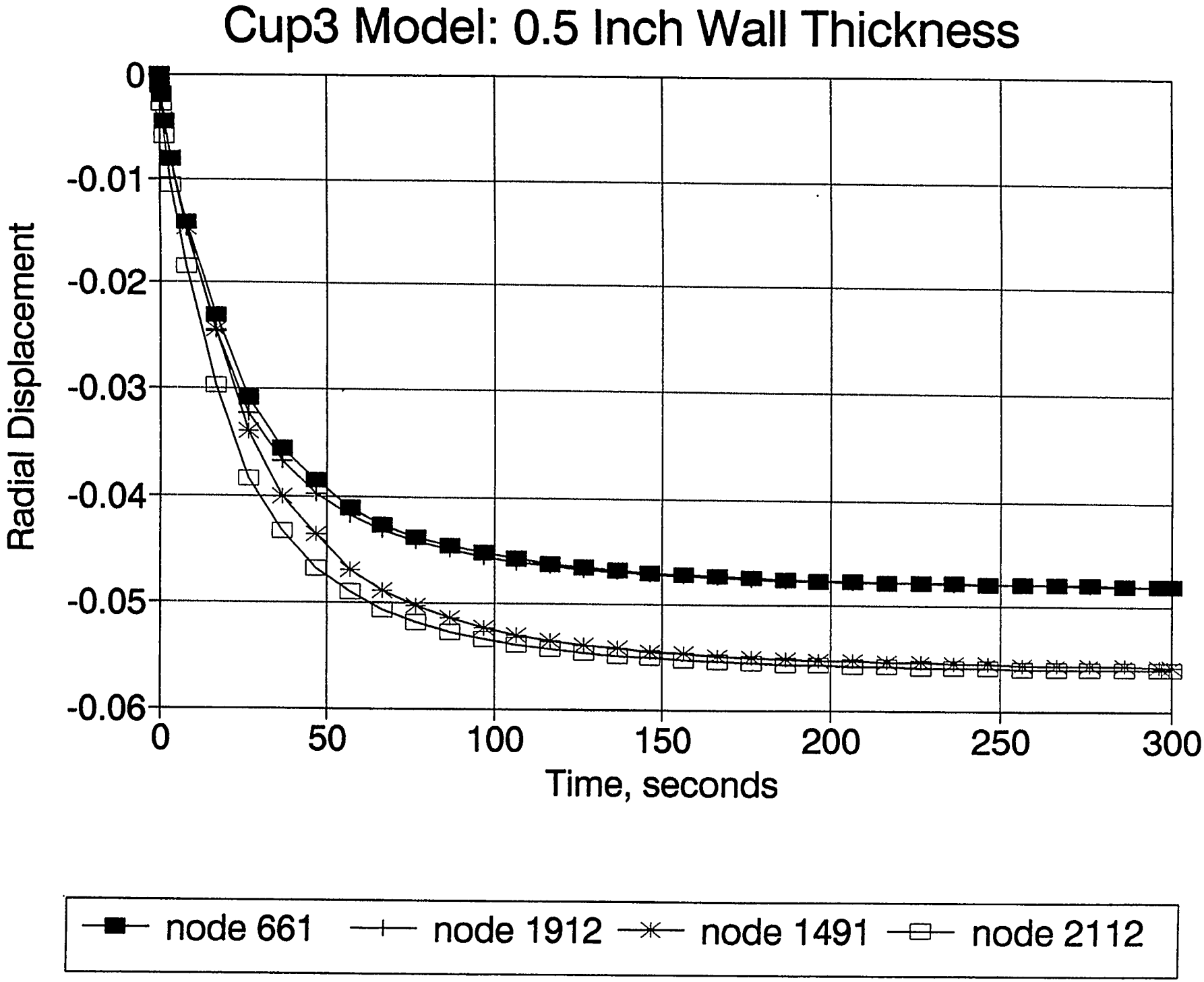
Cup3 Model: 0.5 Inch Wall Thickness
Radial Displacement
0
-0.01
-0.02
-0.03
-0.04
-0.05
-0.06
0
50
100
150
200
250
300
Time, seconds
node 661
node 1912
node 1491
node 2112

5.2 Block Model

A large 20"x8.5"x6.75 block of H-13 was contributed to the project by the industrial sponsors. This block was subjected to detailed pre and post quenching dimensional measurements. The experimentally measured distortion and residual stresses induced by the quenching are described in section 6.

2-D and 3-D modeling of the block was conducted:

5.2.1 2-D Thermal Model

The relatively large length to cross-section ratio allows 2-D modeling of the heat transfer. The results are only valid for the center cross section. The Algor PC code was used to model the transient heat transfer during quenching of the block from 1875°F. A snapshot of the temperature distribution in the cross section of the block, 30 minutes into the quench is shown in figure 5.10. Further results of this 2-D FEA model are described in section 6.

While less demanding in terms of hardware requirements, this model is limited to predicting cooling curves in the center cross section. To determine temperatures at other cross sections of the block, a 3-D model is required.

TEMPERATURE DISTRIBUTION IN A QUADRANT OF THE BLOCK

2-D MODEL PREDICTION, 30 MINUTES INTO QUENCH

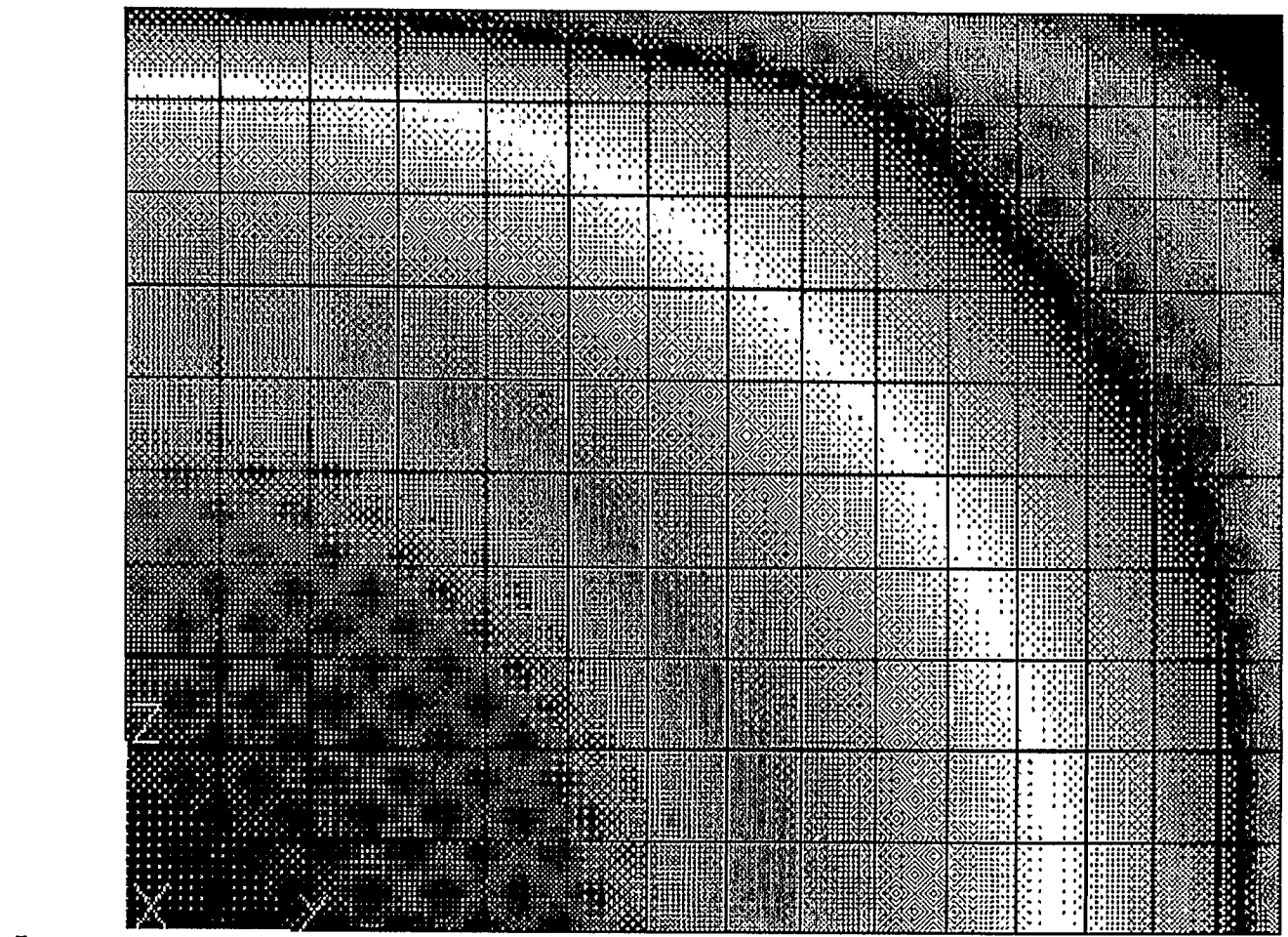

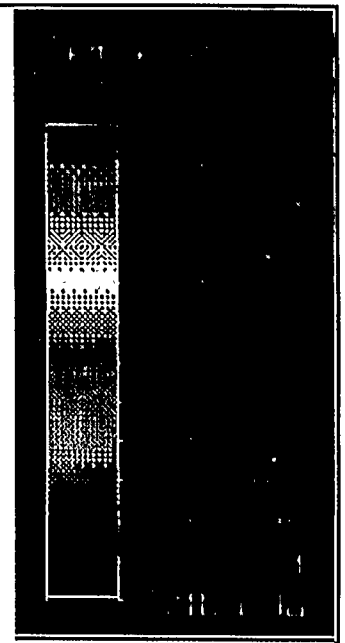

5.2.1 3-D Thermal Model

A number of codes were used to model the block. Among them Topaz and Nike 3-D, as well as the Algor heat transfer code. All these models provided reasonable predictions for the cooling rates of the block. However, none was capable at the time of this writing to also predict distortion and residual stress.

The 3-D model of the block was run by Deformation Control Technology using ABAQUS on a SUN workstation. In addition, to incorporate the phase transformation during quenching of the H-13 steel, the TRAST subroutine was added. This subroutine provides a complete model of the thermomechanical steel behavior during heat treating.

The ABAQUS calculations are performed in two parts: a thermal run and a stress run. In the thermal run, the temperature and phase composition are calculated using the heat diffusion elements of ABAQUS. During the stress run, an interface program uses the thermal and phase composition history calculated in the thermal run. The TRAST materials model accounts for elastic, thermal and transformation strains as well as conventional and transformation plasticity.

Due to symetry consideration, only one eight (1/8) of the block needs to be modeled. The other parts of the block are a mirror image of this part. The model assumes no distortion during the heating to 1875°F. In the stress maps, positive values indicate a tensile stress, while negative ones indicate compressive stresses.

The following plots show results of this model, in the following sequence:

Figure 5.11. Meshed finite element model of Block #1.

TEMPERATURES

Figure 5.12: FEA temperature distribution in Block #1 (5000 seconds into the quench).

Figuer 5.13: FEA cooling curves for Block #1. Note: the red curve shows temperature of the center; the green curve shows temperature of the corner.

PHASE TRANSFORMATION

Figure 5.14: H-13 TTT curves used by the TRAST subroutine.

Figure 5.15: Martensite evolution curve based on the Koistinen-Marburger equation.

Figure 5.16: FEA austenite distribution in Block #1.

Figure 5.17: FEA pearlite distribution in Block #1.

Figure 5.18: FEA austenite distribution in Block #1.

Figure 5.19: FEA bainite distribution in Block #1.

Figure 5.20: FEA martensite distribution in Block #1.

Figure 5.21: Temperature dependency of austenite decomposition and martensite formation in the center of Block #1. Note: the red curve shows formation of martensite in the center; the green curve shows decomposition of austenite in the center.

Figure 5.22: Austenite decomposition and martensite evolution in two elements of Block #1, as a function of time. Note: the red curve shows formation of martensite in the center; the green curve shows decomposition of austenite in the center; the blue curve shows formation of martensite in the corner; the yellow curve shows decomposition of austenite in the corner.

RESIDUAL STRESS

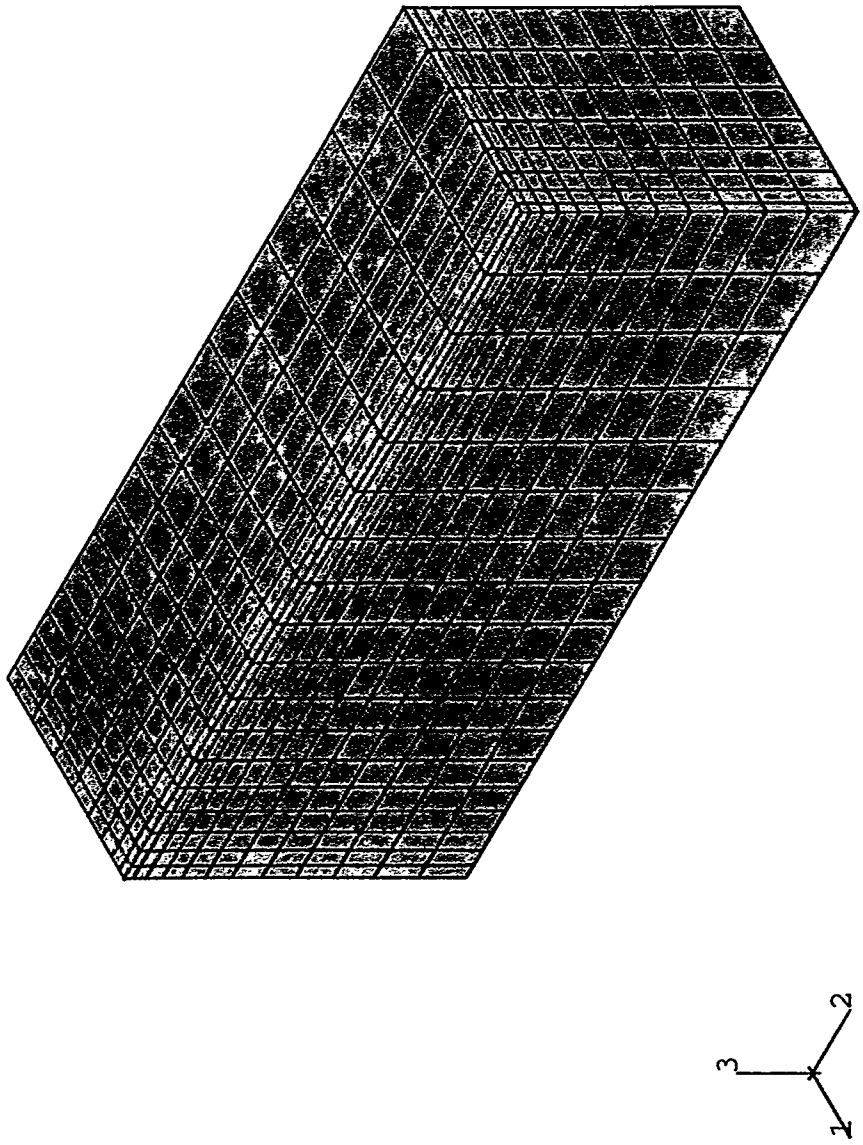

Figure 5.11: Meshed finite element model of Block #1.

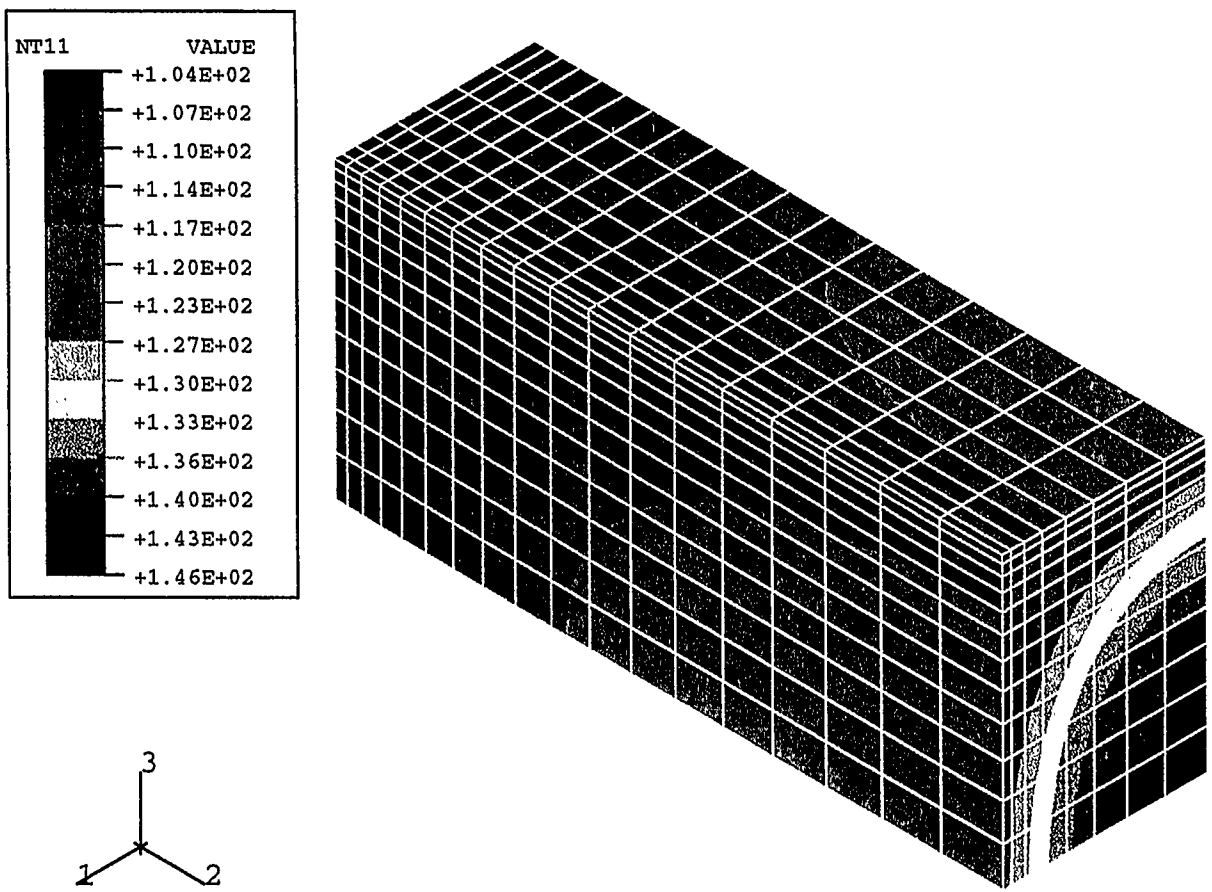

Figure 5.12: FEA temperature distribution in Block #1 (5000 seconds into the quench).

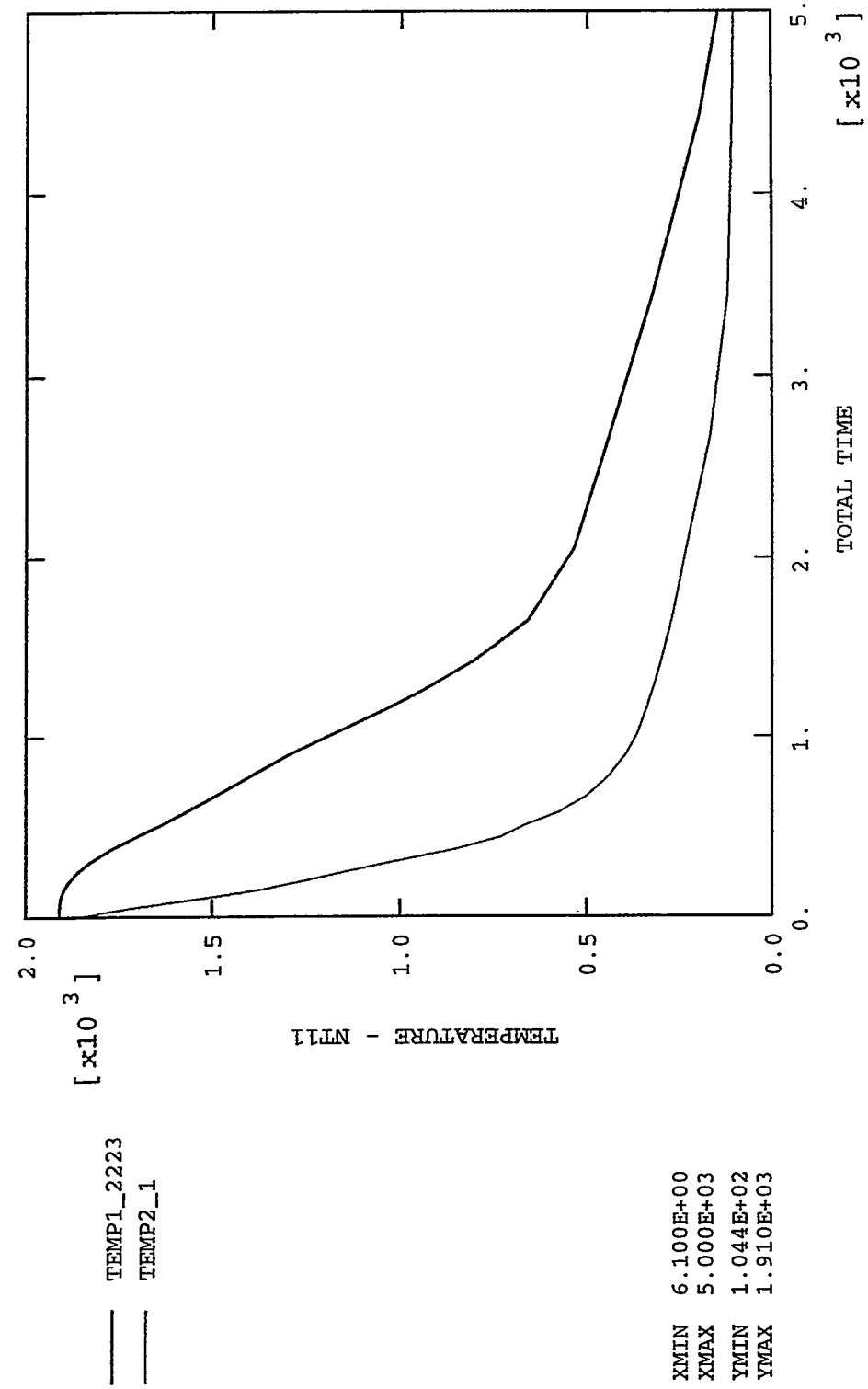

Figure 5.13: FEA cooling curves for Block #1. Note: the red curve shows temperature of the center; the green curve shows temperature of the corner.

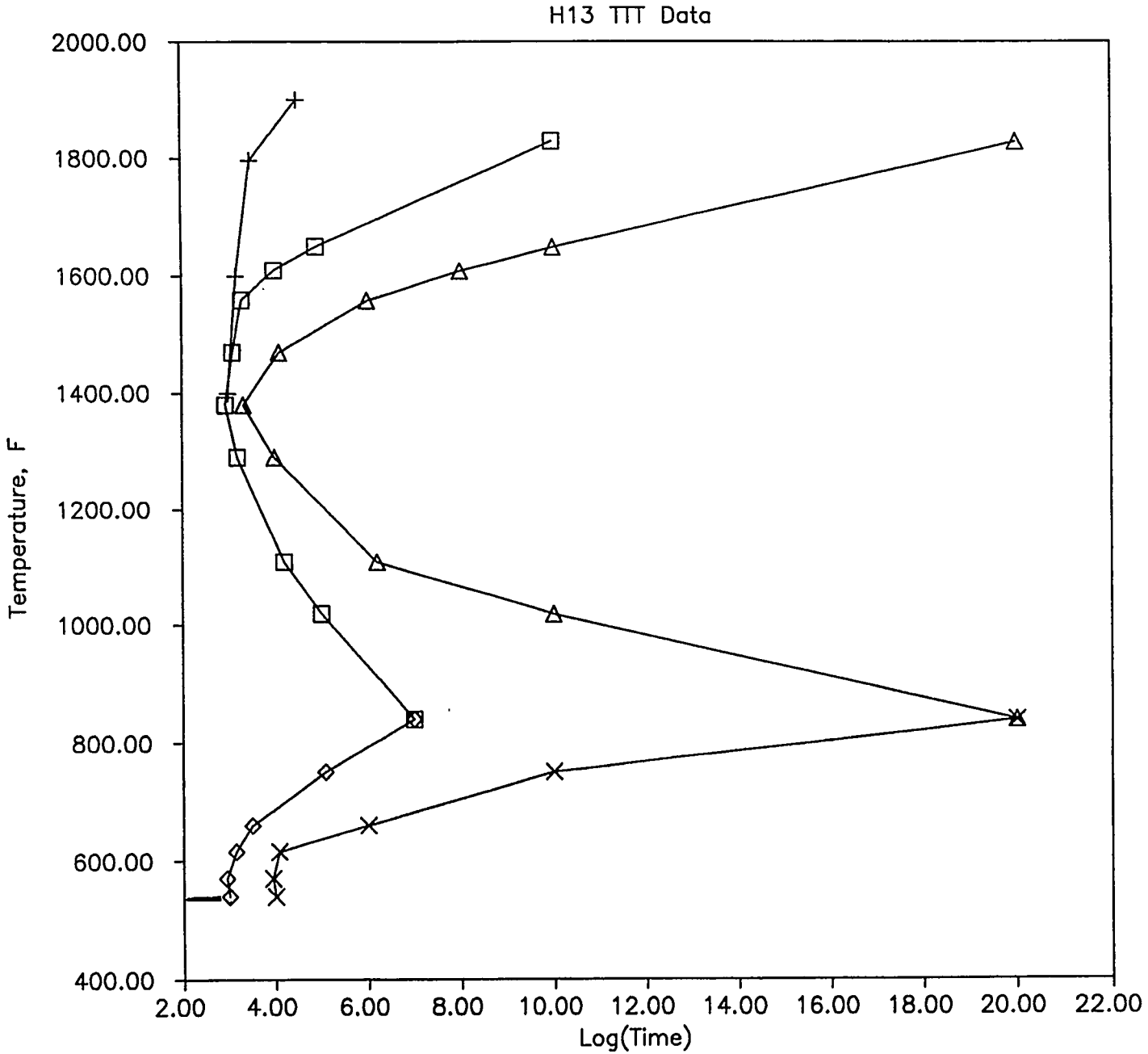

Figure 5.14: H-13 TTT curves used by the TRAST subroutine.

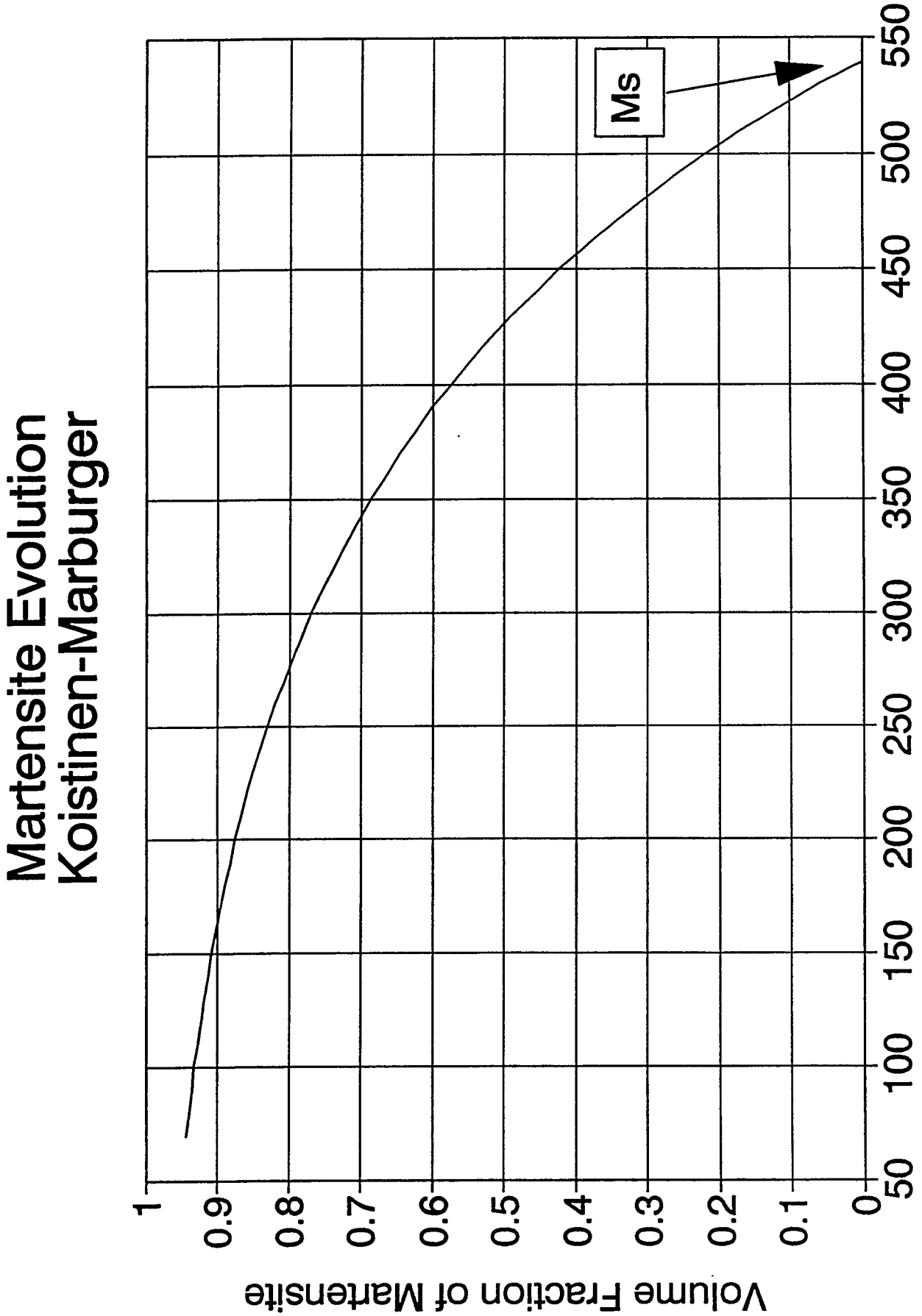

Figure 5.15: Martensite evolution curve based on the Koistinen-Marburger equation.

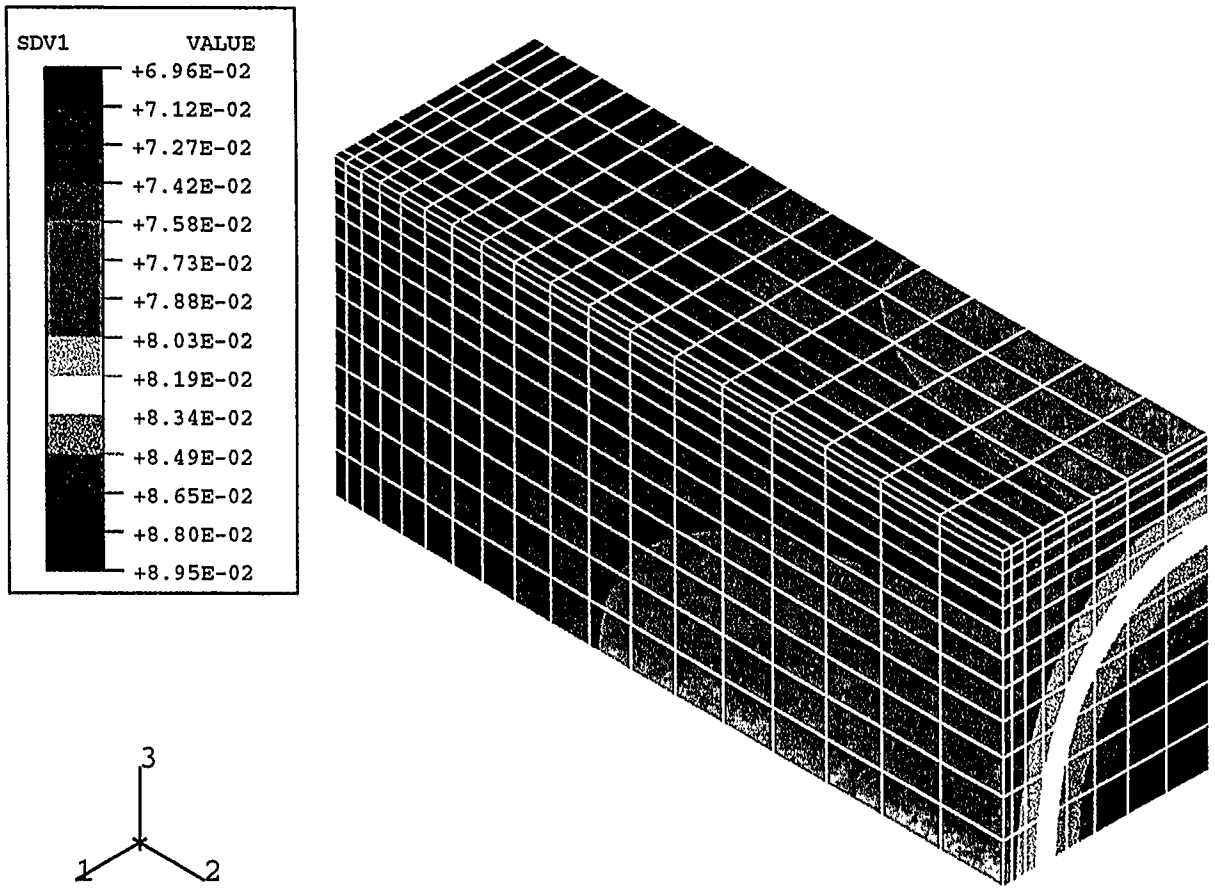

Figure 5.16: FEA austenite distribution in Block #1.

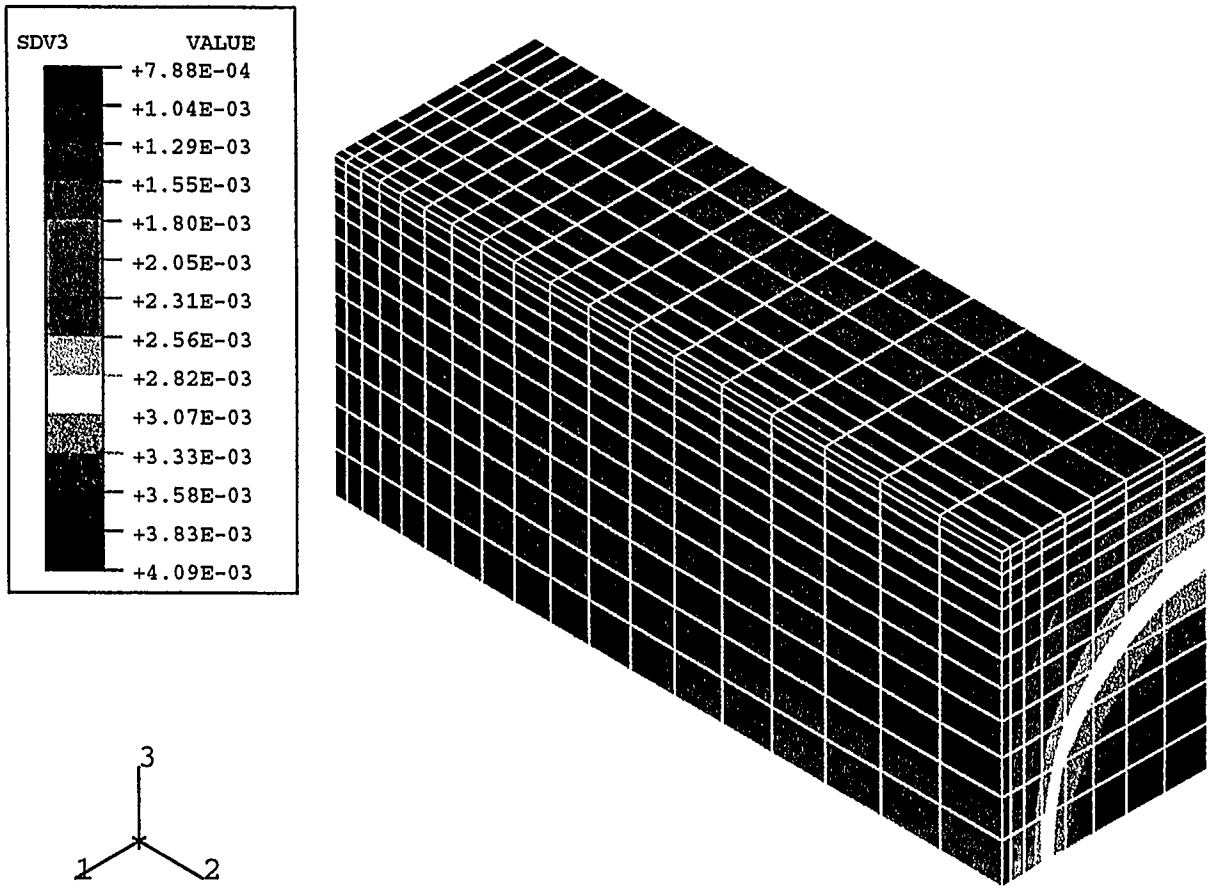

Figure 5.17: FEA pearlite distribution in Block #1.

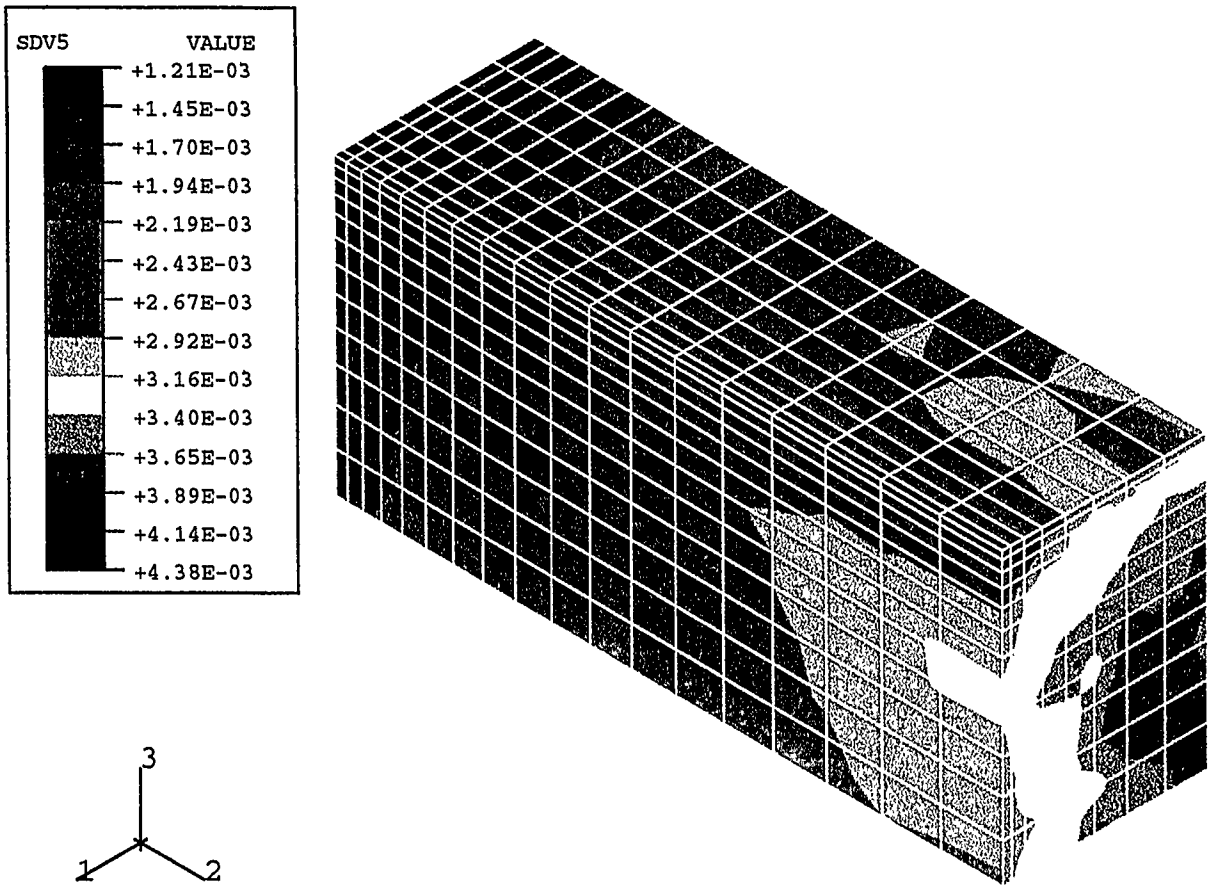

Figure 5.19: FEA bainite distribution in Block #1.

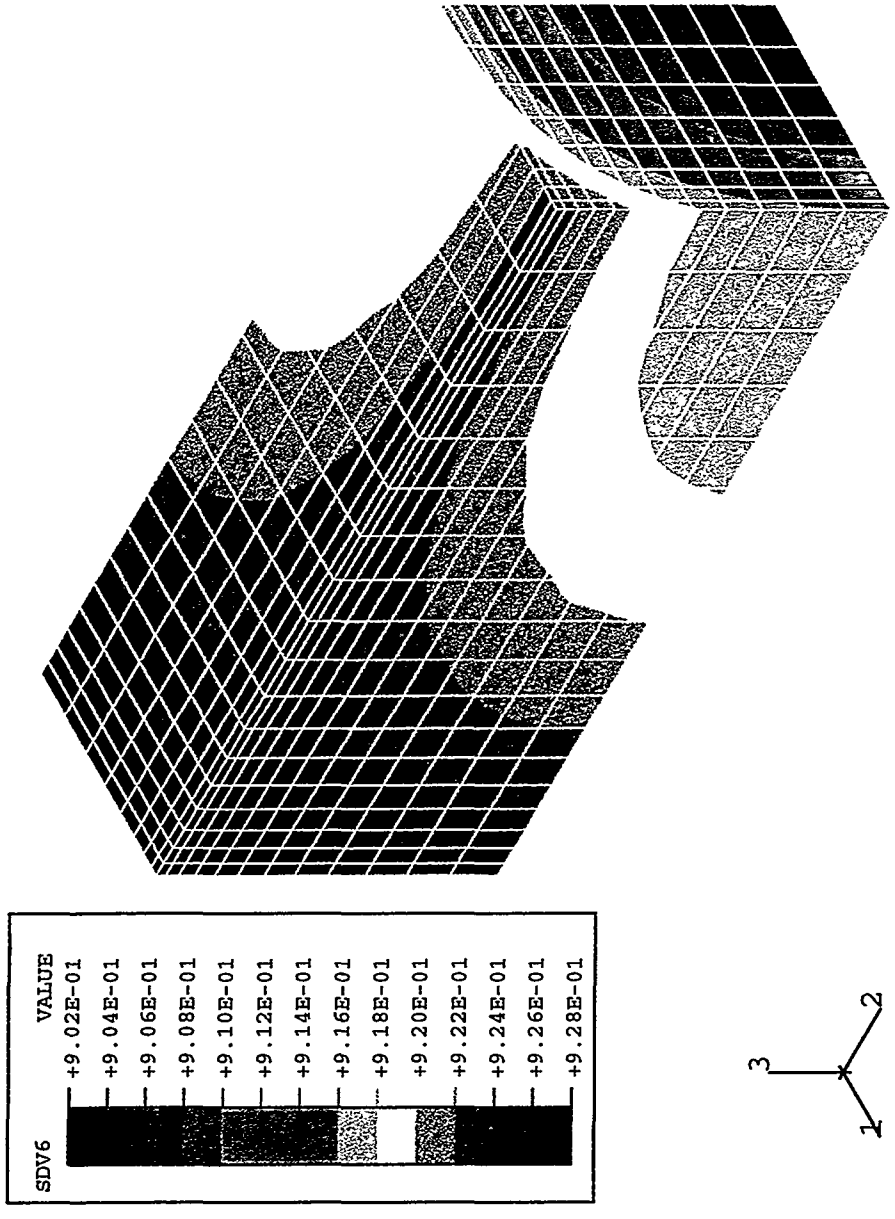

Figure 5.20: FEA martensite distribution in Block #1.

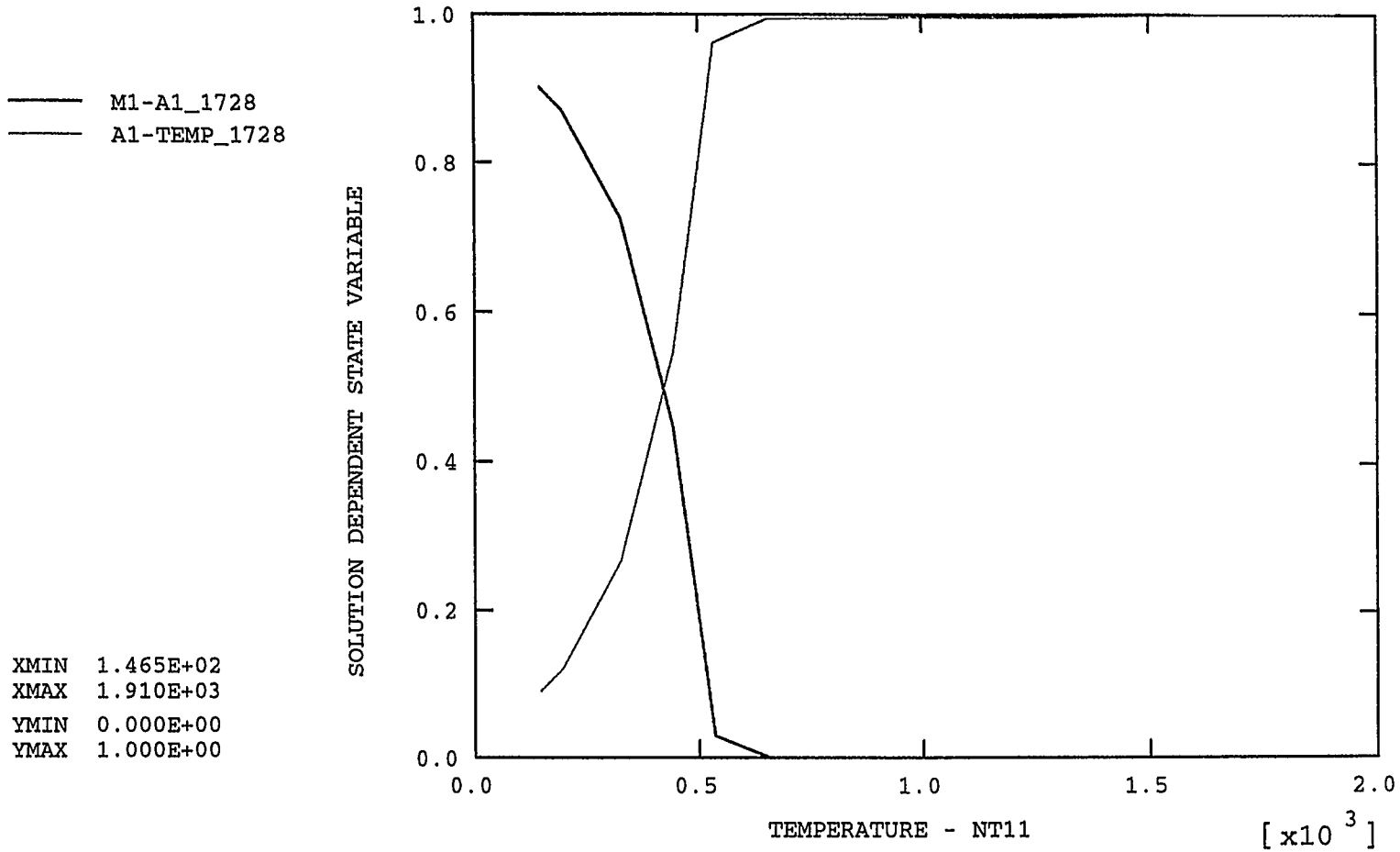

Figure 5.21: Temperature dependency of austenite decomposition and martensite formation in the center of Block #1. Note: the red curve shows formation of martensite in the center; the green curve shows decomposition of austenite in the center.

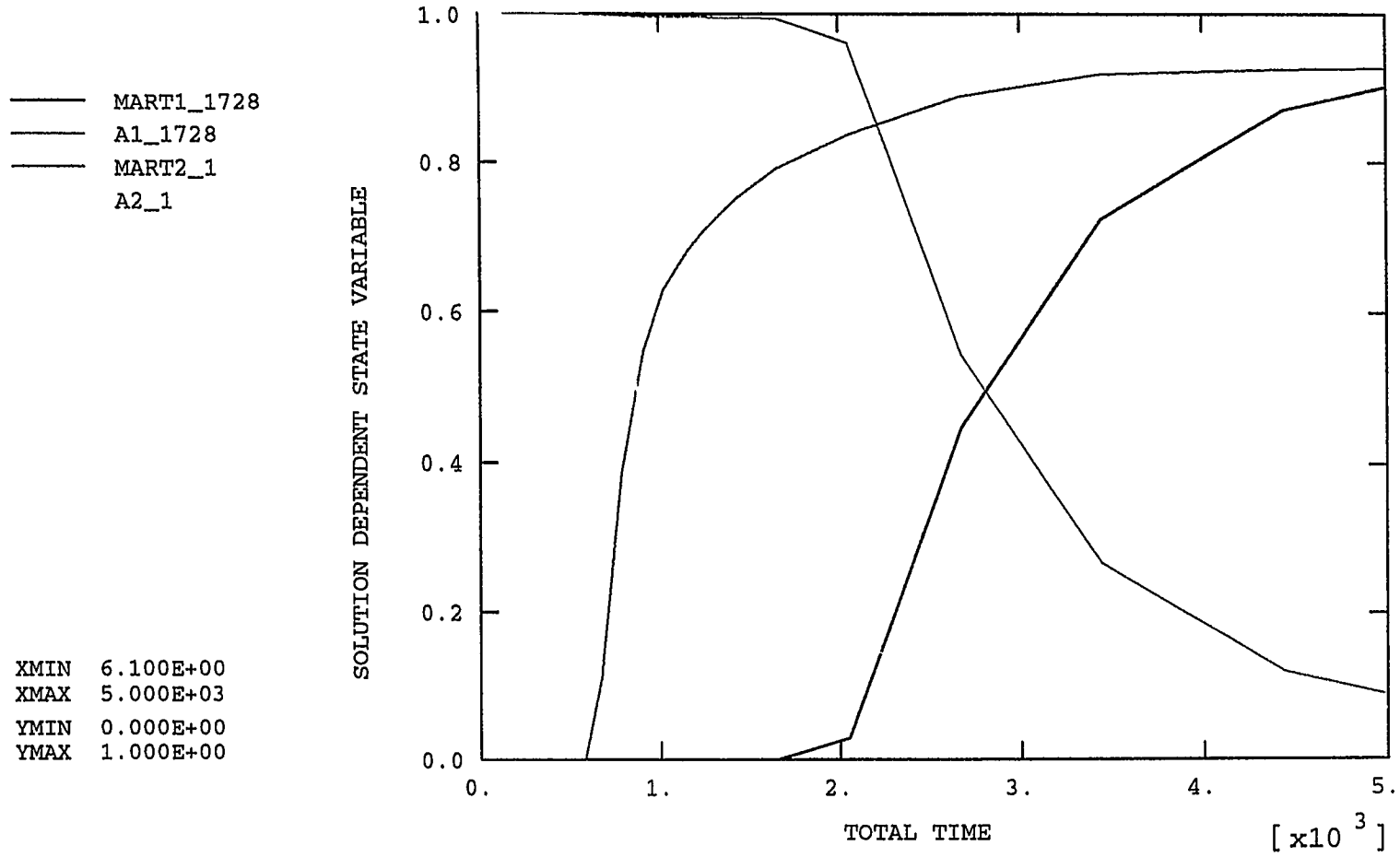

Figure 5.22: Austenite decomposition and martensite evolution in two elements of Block #1, as a function of time. Note: the red curve shows formation of martensite in the center; the green curve shows decomposition of austenite in the center; the blue curve shows formation of martensite in the corner;

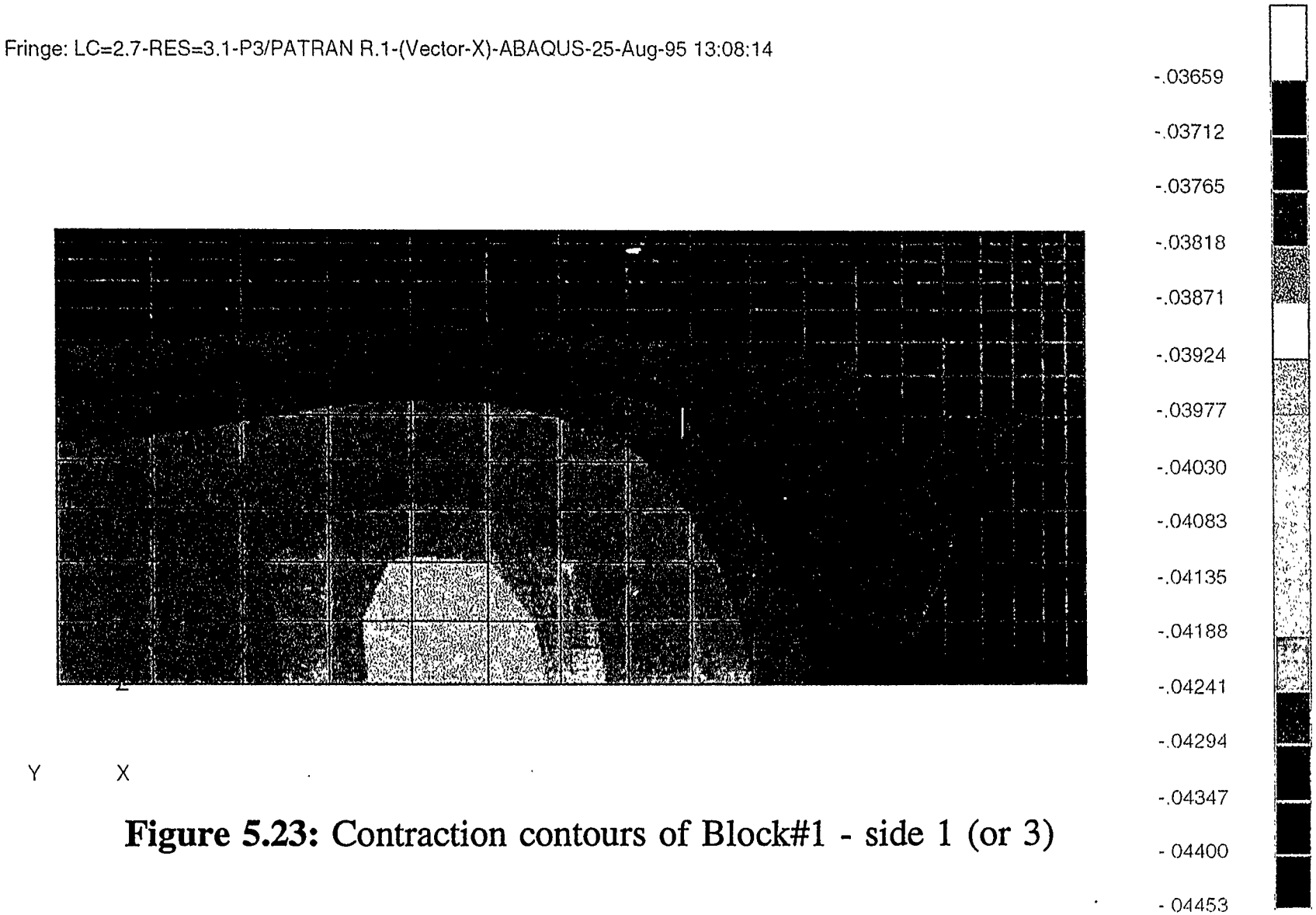

Figure 5.23: Contraction contours of Block#1 - side 1 (or 3)

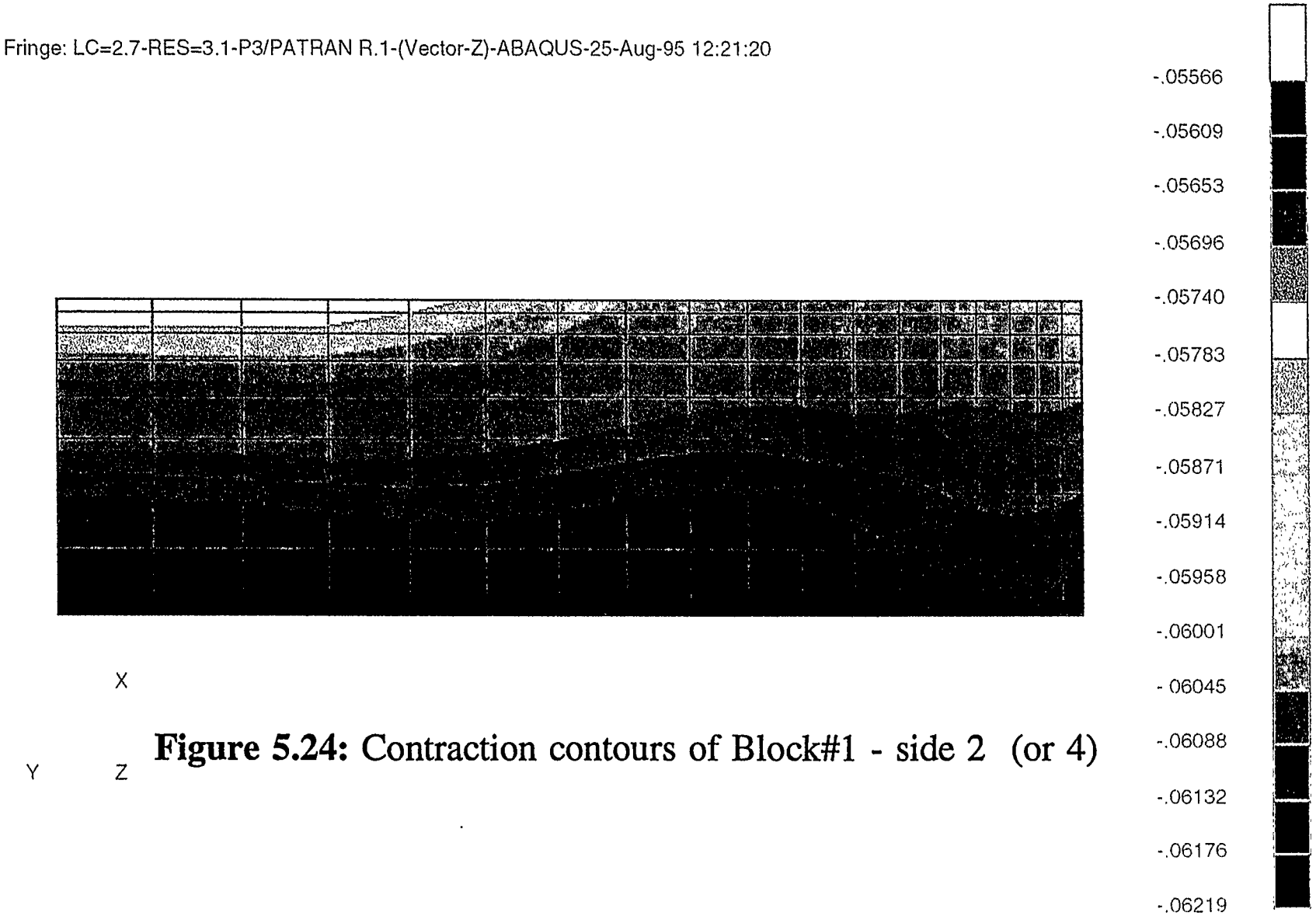

Figure 5.24: Contraction contours of Block#1 - side 2 (or 4)

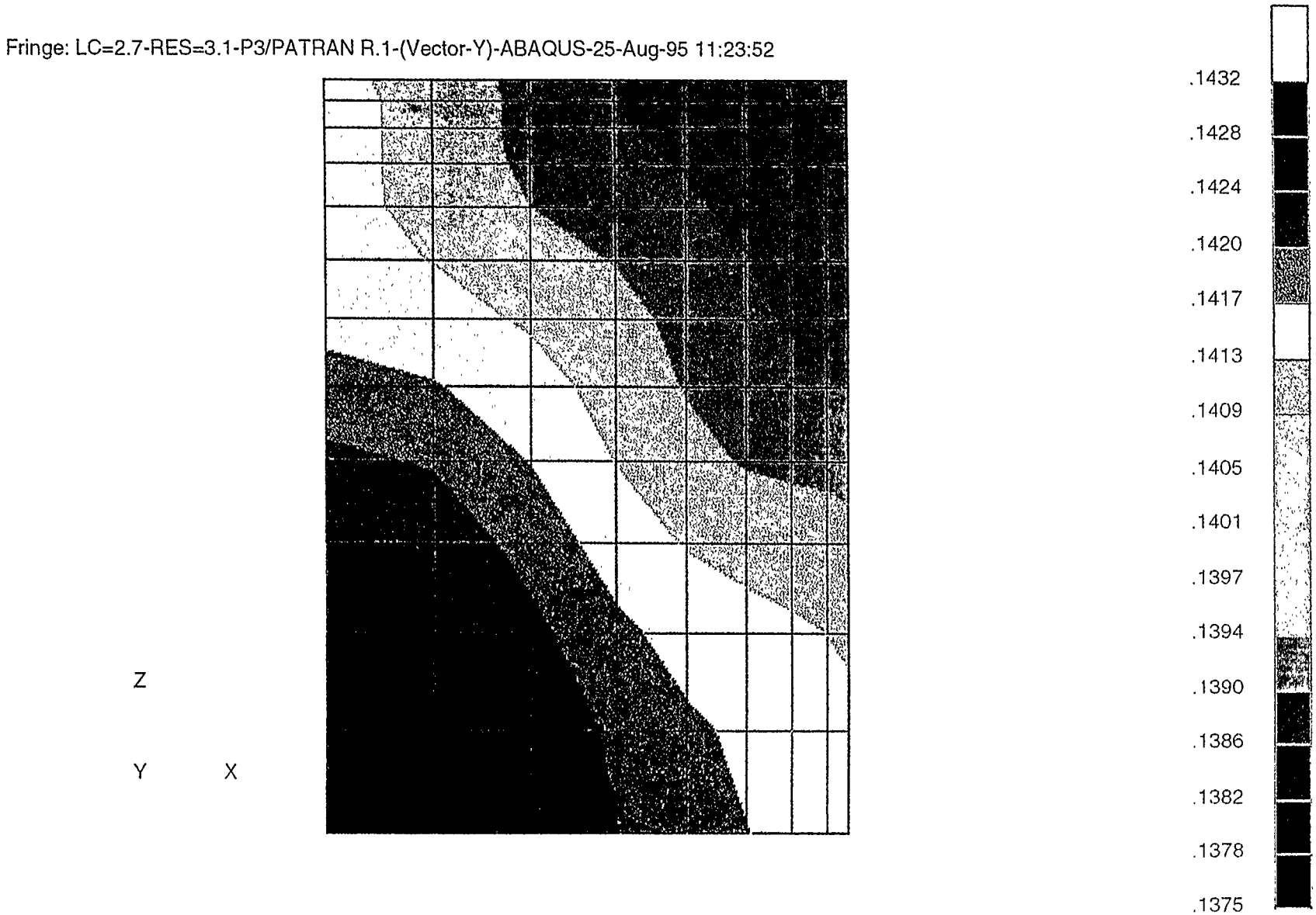

Figure 5.25: Contraction contours of Block#1 - top (or bottom)

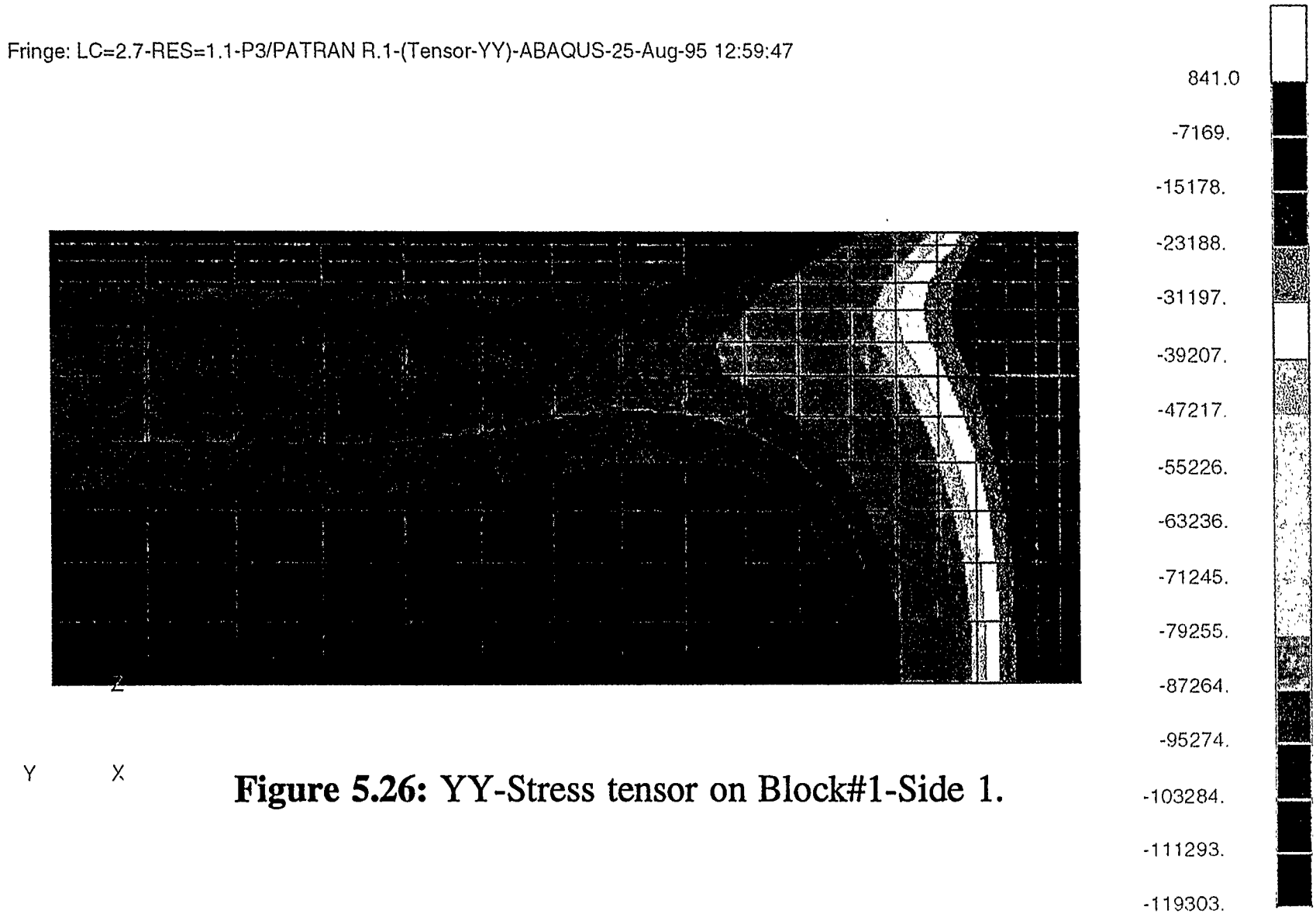

Figure 5.26: YY-Stress tensor on Block#1-Side 1.

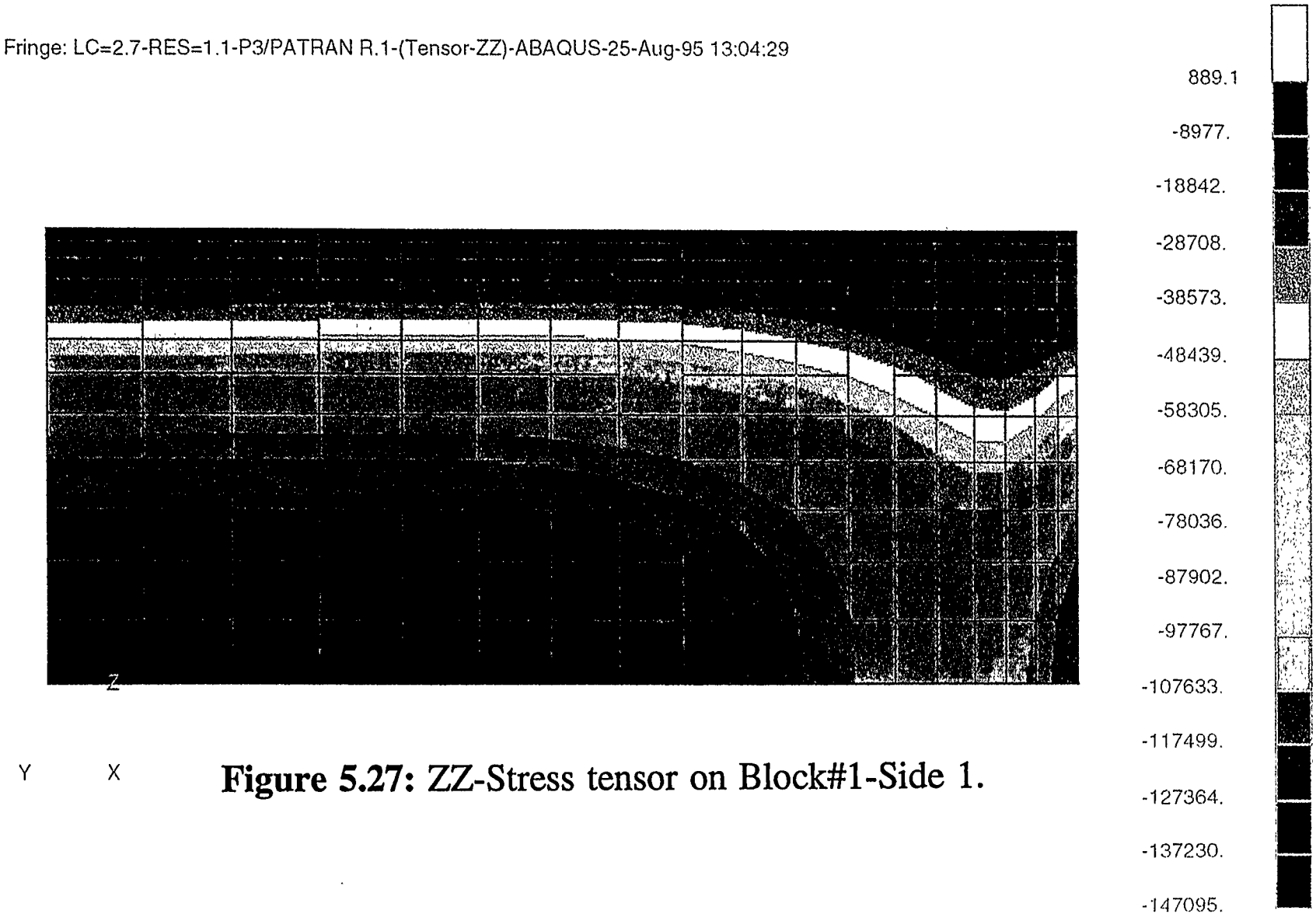

Figure 5.27: ZZ-Stress tensor on Block#1-Side 1.

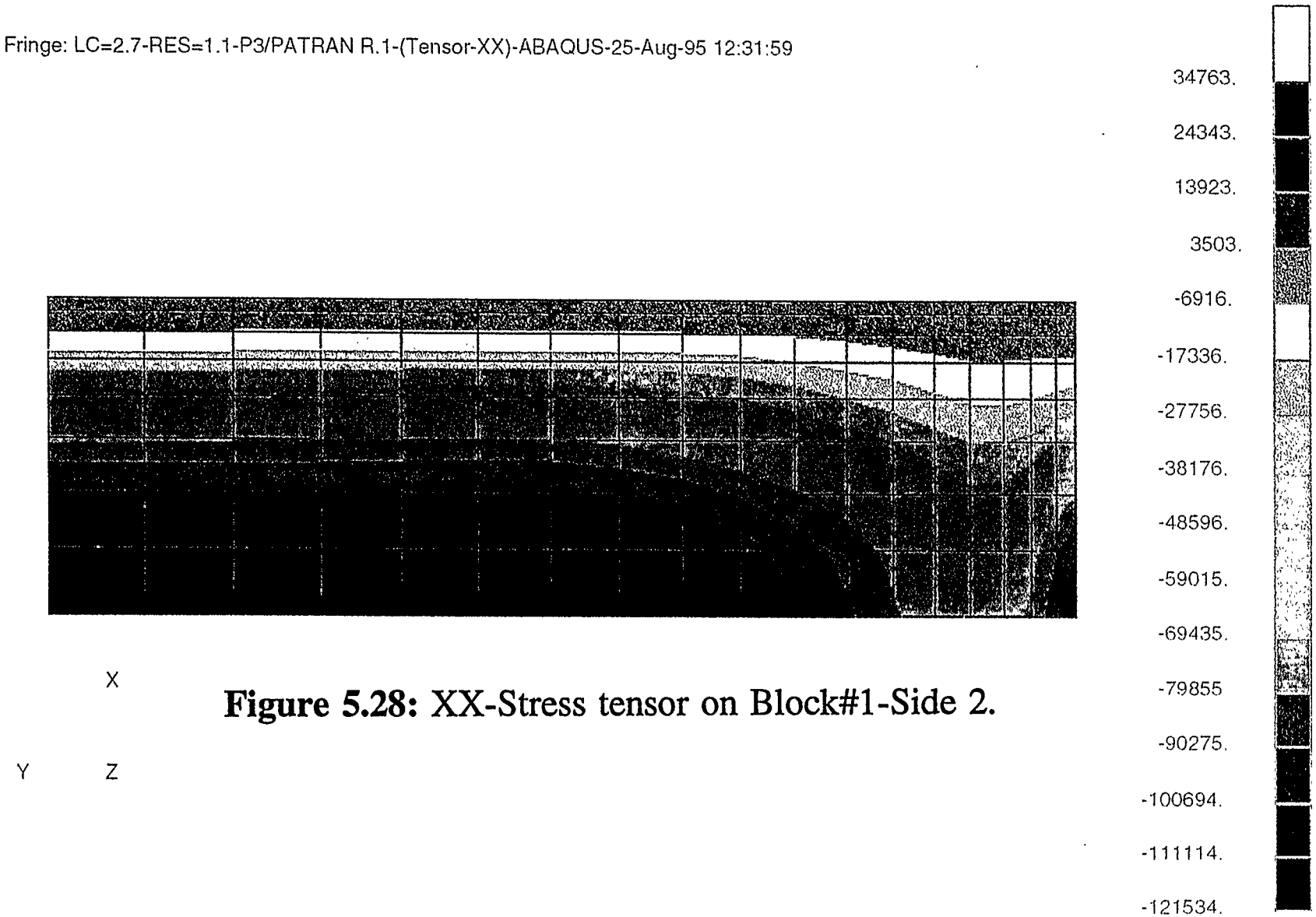

Figure 5.28: XX-Stress tensor on Block#1-Side 2.

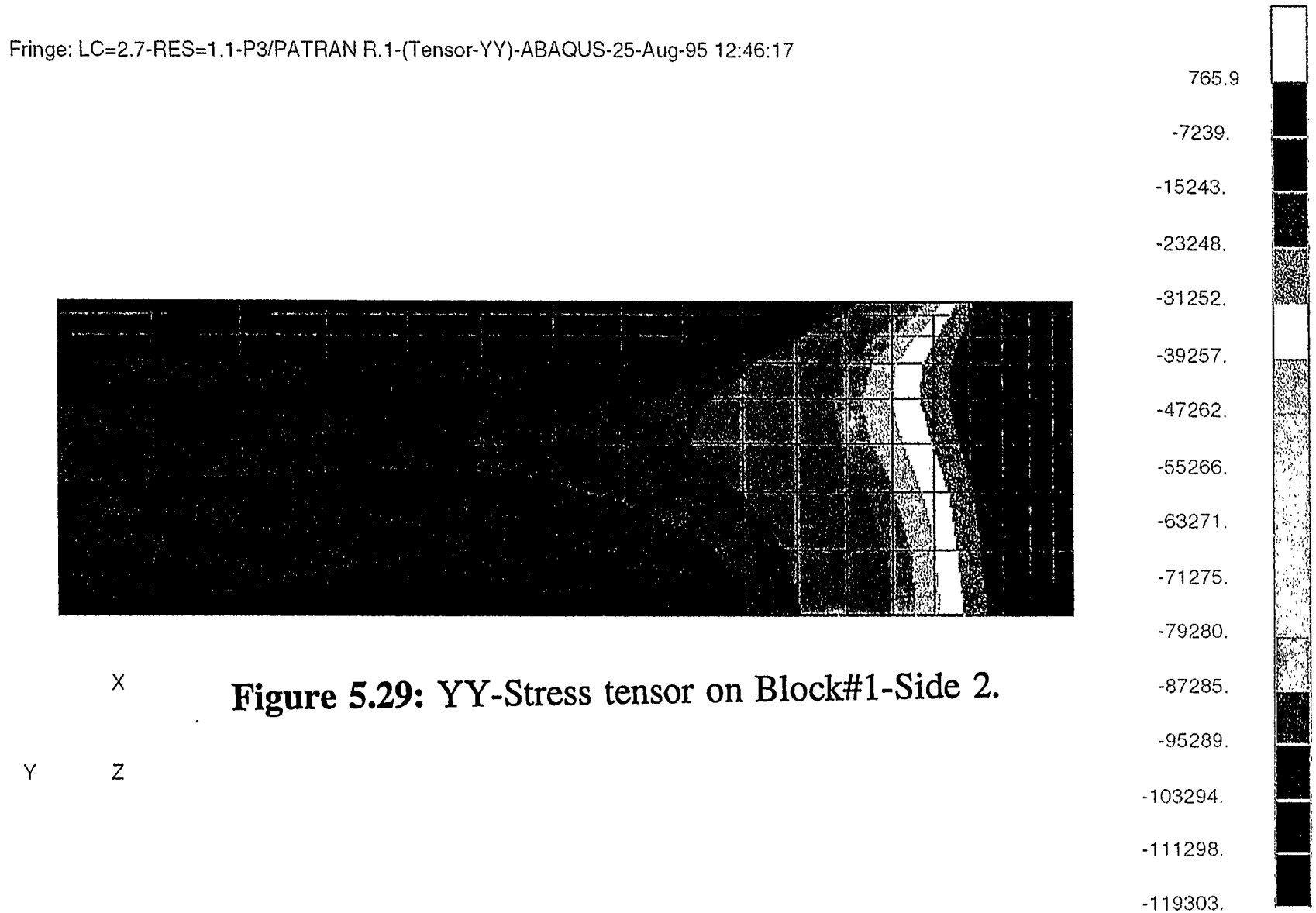

Figure 5.29: YY-Stress tensor on Block#1-Side 2.

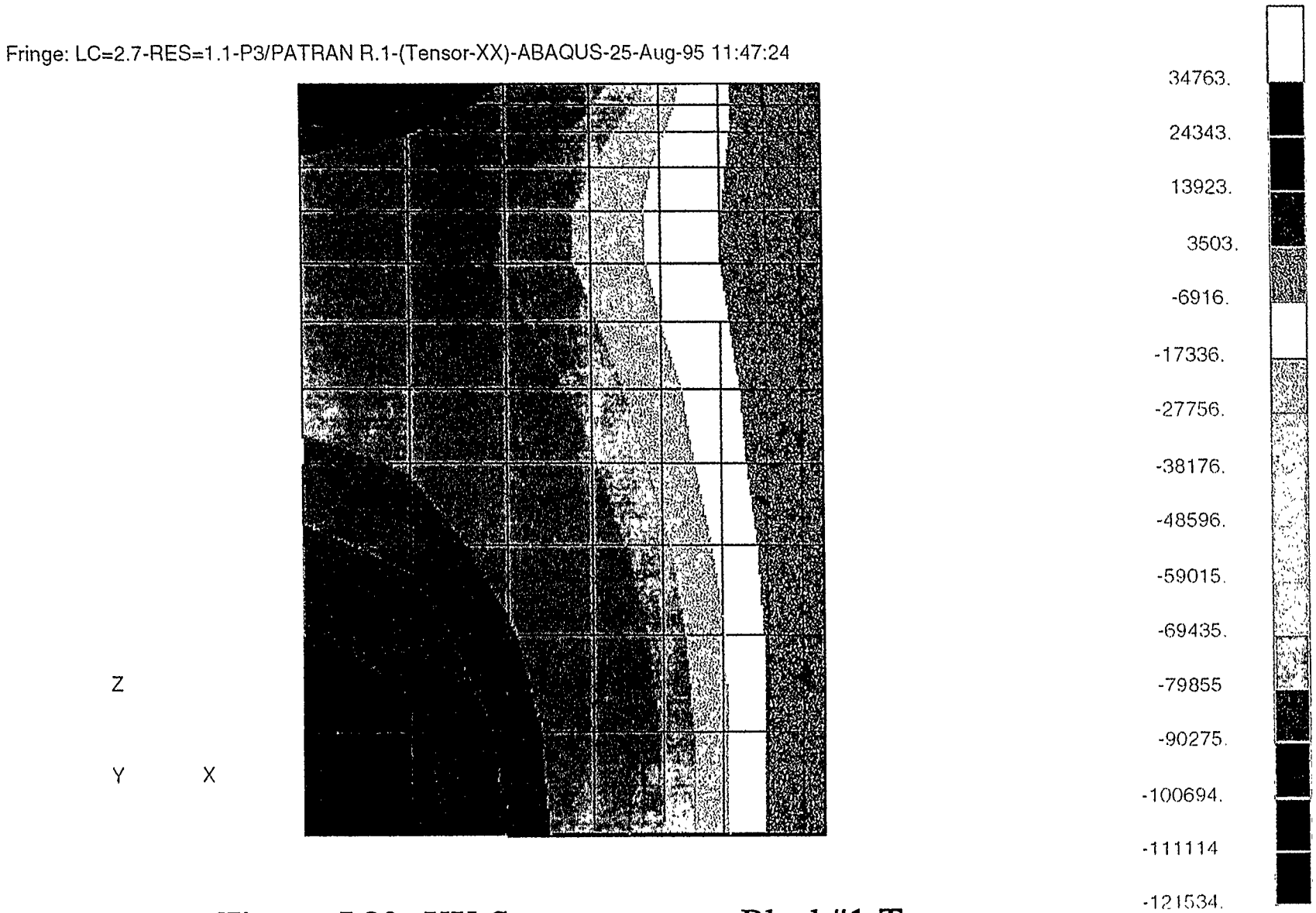

Figure 5.30: XX-Stress tensor on Block#1-Top.

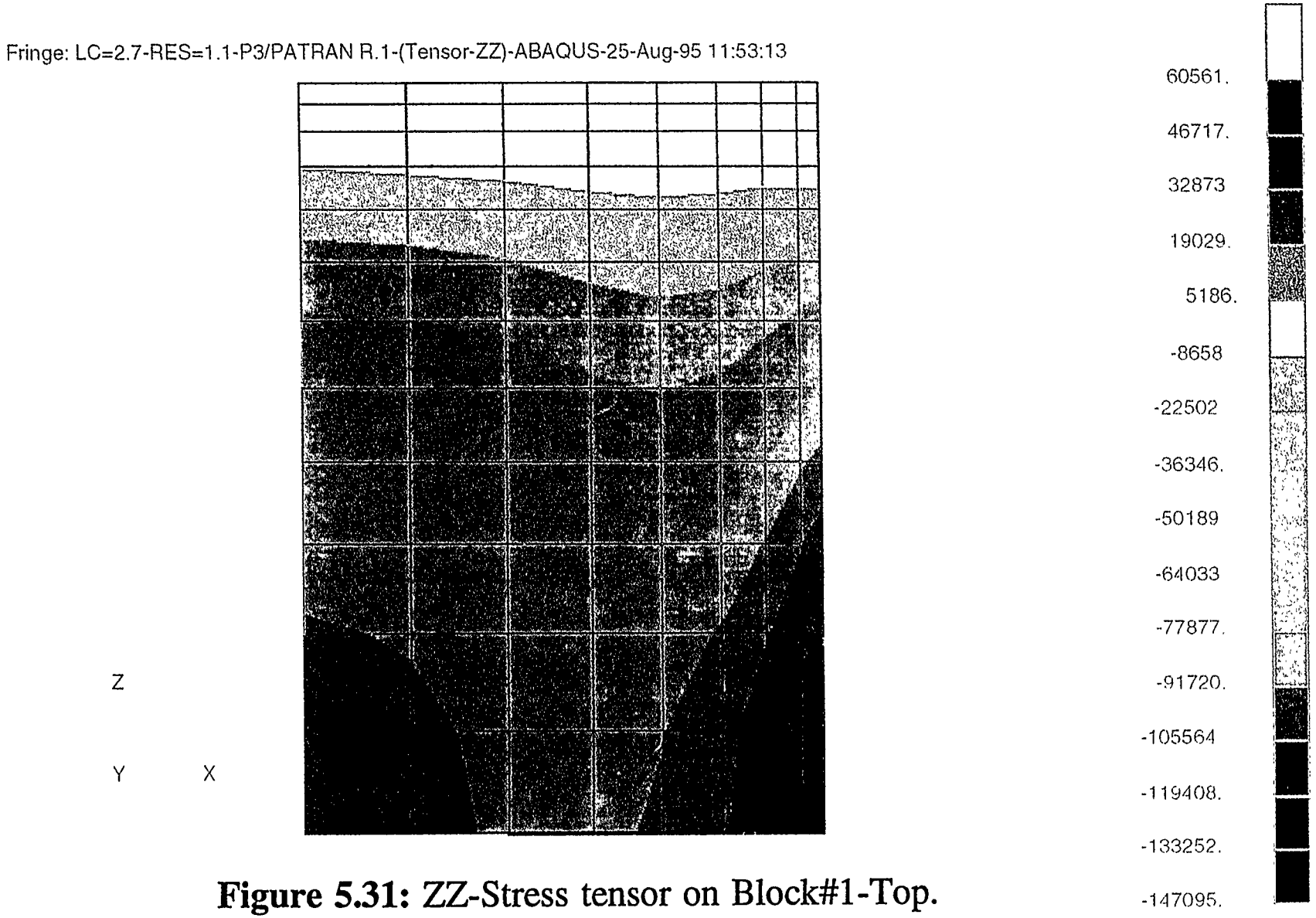

Figure 5.31: ZZ-Stress tensor on Block#1-Top.

6. Experimental Verification of Thermal, Residual Stress and Distortion Models of the Block

A common method for processing H13 steel dies for aluminum die castings is to machine the die close to final dimensions in the annealed condition and then to heat treat the die in a vacuum furnace. The heat treatment is comprised of austenitizing in the vacuum furnace, followed by quenching with nitrogen gas. High cooling rates are necessary to obtain good mechanical properties, but also result in die distortion, residual stresses, and in extreme cases die fracture. The objective of this experimental verification was to determine the quenching conditions required to attain good thermal fatigue resistance and toughness in at least the first one half inch of the die face. This objective is pursued by controlling the cooling rate of that face from the austenitizing temperature so that it is at least 50°F/minute over the 1750 - 550°F temperature range. The project has studied the rates of cooling obtained for various depths within H13 steel dies during gas cooling in vacuum furnaces. The die distortion that occurs is also considered, as well as the properties and residual stress that result from the gas quench.

The studies conducted utilize computer programs based on finite element analyses that consider the rates of surface heat transfer and the properties of the H13 steel at various temperatures. The programs developed are corrected for die temperature observations based on the experimentally measured cooling rates in selected dies.

Dies for use in aluminum die casting are frequently produced from H13 steel by machining the steel close to final dimensions in the annealed condition. The dies are then heat treated by austenitizing in a vacuum furnace and cooling at a controlled rate by the introduction of an inert gas into the vacuum chamber. The gas jets are arranged so that they impinge on the furnace load to provide reasonably rapid cooling through the transformation temperatures of H13 steel. The pressure, velocity and volume of this inert gas affect the rate of cooling through this critical temperature zone. Prior work has shown that the rate of cooling through the transformation temperature affects the toughness of the H13 steel as measured by the Charpy V-notch impact test and the thermal fatigue resistance as determined by the cracking pattern obtained on a specially designed thermal fatigue test. Improved toughness and thermal fatigue resistance are obtained at relatively rapid rates of cooling through the transformation temperature range. Inferior die properties result when the cooling rate is slow with the transformation of H13 steel resulting in pearlite and precipitation of grain boundary carbides.

The vacuum heat treatment offers advantages in processing dies. The surface of the dies is critical to their proper performance since any decarburization will reduce the surface strength and can lead to premature thermal fatigue cracking. Vacuum treatment avoids damage from this source. However, it is also necessary to cool the die through the transformation regions fast enough to avoid the formation of undesirable phases. It has been shown (1-5) that this fairly rapid cooling rate is even more important to good die life than the use of the premium grade H13 steel required by the NADCA specification. Very rapid cooling rates from the austenizing temperature can, however, produce serious distortion and even cracking of the dies. Accordingly, the cooling rate has to be controlled so that satisfactory transformation structures are attained without serious distortion or cracking of the dies. Minor die distortion can be tolerated because the die can brought to final dimensions by grinding after tempering. The inert gas method of cooling offers the possibility of obtaining the needed cooling rates without die damage if the gas jets have sufficient cooling capability and can be directed to the proper surfaces. The configuration and size of the die are significant factors in determining the pressure, quantity of flow and direction of the cooling gas.

This section discusses these interrelated factors as they apply to the cooling of H13 dies from vacuum austenitizing furnaces with inert gas jets at pressures in excess of one atmosphere. Measurements of the cooling rate were made at different locations in H13 die blocks. Since the first half inch of die surface has the greatest impact on the die behavior, that portion of the die is considered to be the most important area for attaining the desired rates of cooling and types of transformations. The effect of the position of the inert gas jets on the cooling rate of a die block at different locations is evaluated. Since the distortion of the die during this cooling is also important in practice, the change in dimensions of the die as a result of cooling from the austenitizing temperature with inert gas in the vacuum furnace is determined. The resulting residual stresses obtained at these different die locations are measured.

The initial experimental work has been performed with a simple rectangular die block. The data on rates of cooling and distortion from this simple shape will provide a stepping stone to more complex die shapes.

With the varied, and at times complex dimensions of dies, a means of calculating the cooling rate and dimensional changes in dies under different cooling conditions is needed. This complex computation requires computer programs for the thermal behavior and the dimensional variations. Toward this goal computer programs are being developed using established properties of H13 steel over the temperature ranges experienced. At present, the program can predict temperature variations during cooling of the steel.

The prediction of dimensional changes is considerably more difficult. All programs developed have to be validated by the experimental results obtained.

6.1 Materials and Procedure

A majority of the experimental work accomplished to date has been on a 20" long x 8.75" wide by 6" thick block of premium grade H13 die steel donated to the program by Latrobe Steel Company. The block surface has been drilled and reamed to place 3/16" diameter x 3/16" deep reamed holes in a regular pattern on all die surfaces as shown in Figure 6.1. These holes serve as measuring locations for dimensional changes and locations for the thermocouple placed in holes drilled to various depths, as indicated in Figure 6.2. The die block with these holes and thermocouples indicated in Figure 6.2 was placed in a new vacuum heat treating furnace of the Abar Ipsen TurboTreater™ H4848TT type at the Universal Heat Treating Company as illustrated in Figure 3. This work was performed without charge by Universal. The location of the nitrogen gas inlets on the far wall of this furnace is shown in this figure. The identification of the sides of the block by number as positioned in this furnace is also indicated in this figure. This identification is used subsequently in reporting dimensional changes.

The 20" x 8.75" x 6" block with thermocouples was placed in the vacuum furnace, heated to 1450°F at an average rate of 5°F/min, then to 1900°F, where it was held for 8 hours. The vacuum level in the furnace was 400 micron nitrogen partial pressure. During the cooling cycle, nitrogen gas at a pressure of two bars and flow rate of 19,000 cu ft/min was injected into the hot chamber from the vents shown in Figure 6.3. The thermocouples junctions at the tip of each were held firmly against the block at the bottom of each hole by compression fittings threaded into the block. Chromel-alumel thermocouples (type K) with a 0.01" diameter wire were used for all measurements. The thermocouple readout was recorded on a Honeywell DP 3000 instrument at a chart speed of 24 inches/hour, with an acquisition rate of 14 scans per minute per channel. The output of the instruments was plotted as temperature - time curves to show the rate of cooling at different locations within the block. The electric heating elements of the furnace were turned off prior to the nitrogen gas quench.

The amount of distortion that occurred as a result of this quenching was measured utilizing the regularly spaced holes illustrated in Figure 6.1. The exact location of these various holes was determined in a coordinate measuring machine at Modern Tool and Die Company. This work was performed pro bono

as a contribution to the research. The measurements of hole locations were established before and after the quenching treatment with 2 bars of nitrogen gas. The data obtained from these measurements was plotted on graphs that show the changes in dimensions at various locations throughout the block.

In addition to the 20" x 8.75" x 6" block, detailed information on the cooling rates of dies during gas quenching was provided by FMP Heat Treating, Elk Grove, Illinois. Six die inserts used previously to produce an antenna housing were donated to the project by Crown Equipment Company of London, Ohio. Two of these die inserts, about 12" x 12" x 7" in dimension produced from H13 steel, are shown in Figure 6.4. They were not worn out, but their use was discontinued because of a design change in the product. These dies are being employed to check the residual stress patterns and distortion in an actual die shape. Plans have been made to heat treat these dies in vacuum furnaces with nitrogen gas cooling and to measure the distortion in a coordinate measurement machine and the residual stress pattern after quenching with nitrogen gas from 1900°F. A portable Rockwell C hardness device was employed to check the hardness of these smaller dies and the 20" x 8.75" x 6" block.

The technique for checking the residual stresses in the die steels employs a special rosette strain gage of the EA-06-125RE-12/Option SE type. A special drilling rig produced by Measurements Group is used to drill a 0.125" diameter hole in the center of the gage after the gage has been affixed by adhesive to the die surface. The elements of the rosette are zeroed out by the P-3500 Strain Indicator instrument that measures their resistance in microohms. Then, a hole is drilled in the center of the rosette to depths of 0.010", 0.020", 0.030" and 0.040" with resistance readings taken after each depth is drilled (6). This provides readings that can be converted into stresses by means of well established formulae available in mechanical engineering texts. The results of the calculations show the residual stress pattern at these four depths from the die surface.

The thermal data obtained was utilized to prepare a computer program based on a finite element analysis of the block. The program was based on the thermal readouts of the various thermocouples shown in Figure 6.2 and the pertinent thermal conductivity and heat capacity data for H13 steel at temperatures throughout the range of interest. This thermal conductivity and heat capacity data is shown in Table 6.1. It is necessary to include the heat of transformation obtained when the austenite transforms to lower temperature transformation products during cooling. This computer program will be rechecked for other shapes during the course of the work.

A similar type of computer program to predict the dimensional changes during quenching and other heat treatment is also under development, but has not as yet, proved to be viable. Work is continuing on this program.

6.2 Results and Discussion

The actual measurements of temperature changes with time when quenching the 20" x 8.75" x 6" die block from 1900°F are shown in Figure 6.5. This plot shows the actual temperature as function of time after the start of the 2 bar nitrogen quench. The curve marked nitrogen is from the control thermocouple. This couple was directly exposed to the nitrogen gas flowing through the furnace chamber and shows the temperature of the gas. Thermocouples in the H13 steel block provide the variation in temperature with time at the die surface, at mid-depth or 1½" from the surface and at the center of the block or 3" from the surface. It is noted that the cooling rate of the mid-depth and center are very close to one another. The significant temperature range during cooling that determines the structure of the H13 is from 1750° to 550°F. The cooling rate for the center and midwall of this block is about 30°F/min in this range. This is at the slower limit of the rates considered necessary to provide good die properties. The cooling rate on the surface is about 50°F/min over this temperature range. While this is better , it still will provide a bainitic structure and some grain boundary carbides in the quenched H13 die. These cooling curves have been plotted on a continuous cooling transformation (CCT) plot for H13 in Figure 6.6 to show the entire central part of the block is transformed to bainite. Cooling curves that are fast enough to avoid this bainitic area and form martensite will provide somewhat better properties, but will be more susceptible to distortion.

Distortion in dies can result from a number of sources. The distortion occurs when temperature and transformation vary from one portion of the die to another. A list of these sources is presented in Table 6.2. The distortion measured on the 20" x 8.75" x 6" has been plotted for each side of the four long sides of the block as identified in Figure 3. Before quenching, the sides were flat and at right angles to each other. After quenching, the block tried to assume a rounded configuration. Figures 6.7a,b demonstrate how the originally flat surface of Side 1 (20" x 8.75") changed after quenching. In these plots, the dimensional variations are plotted in tenths of thousands of an inch or 0.0001" units. Figures 6.8 and 6.9 show how the two 8.75" x 20" sides of the block changed and also indicate the position of the nitrogen gas cooling vents in the furnace. The negative numbers indicate the dimension is moving out of plane towards the observer; the positive numbers indicate that the dimensions are moving away from the observer. The plots show the

rounding effect and indicate that it is affected by the location of the gas vents. The rounding is more severe at the end closest to the entering nitrogen gas. The same dimensional changes are illustrated in Figures 6.10 and 6.11 for the 6" x 20" sides of the block. The rounding effect is evident, but now the bulge out at the center is less than for the wider sides. The dimensional changes are less, however, over these reduced distances. The distortion at the end directly facing the entering nitrogen gas is more severe. A similar type of rounding or bulging out of the center of the block is exhibited at the 8" x 6" end facing the vents as shown in Figure 6.12. The overall shrinkage of the block is illustrated by the change in the 20" length or long side across the 8" face in Figure 6.13. Hardness readings taken on the 20"x8.75"x6"block after quenching showed a uniform hardness of 52 Rockwell C. The H13 die inserts of the antenna housing were about 47 Rockwell C.

The development of the computer programs to predict the temperatures, transformation phases and distortion in these H13 steel dies is proceeding more slowly. This technique considers volumes of symmetry in the block which can be only one eighth of this sample shaped right parallepiped. A two dimensional plot of this area is illustrated in Figure 14. A two dimensional temperature prediction for this area during the gas cooling of the 20"x8.75"x6" block in the vacuum furnace with 2 bar nitrogen gas is shown in Figure 6.15. This two dimensional computer analysis utilizes the interfacial heat transfer at the die surface obtained from the quenching experiment described above for the 20" x 8".75" x 6" block and the thermal data for H13 shown in Table 6.1. This computer program closely predicts the cooling rate at the mid depth and center of the block, but reports a somewhat slow cooling rate at the surface. It is intended to make this program more accurate and three dimensional to allow its adoption to actual die configurations.

The computer program to predict the dimensional changes or distortion is proving to be difficult to develop and is not available. Residual stress measurements from the drilling technique discussed are shown in Figures 6.16 and 6.17.

6.4 Summary of the 2 bar gas/vacuum quenching experiments

This project is a work in progress and this is a progress report of work conducted to date. The cooling rates attainable for a premium grade H13 steel block of 20" x 8.75" x 6" dimensions, cooled from 1900°F in a vacuum heat treating furnace with a 2 bar nitrogen quench are shown. The surface of the block was cooled through the significant transformation temperature range (1750 - 550°F) at a rate of 50°F/min at the surface and 30°F/min at mid depth (1.5") and center (3") from the surface. The distortion resulting

from this cooling is demonstrated. The side near the location of the entering nitrogen gas distorts somewhat more than the opposite side.

The computer program based on 2-dimensional symmetry has been developed to predict the temperature profiles in the die with the 2 bar nitrogen quench. This program has subsequently been expanded to three dimensions. The model that predicts the dimensional changes has also been developed. The model predicts well the patterns (contours) of the distortion. However, the magnitudes of the distortion and residual stresses predicted by the model, as presented in section 5, do not match well with the experimental values. Further fine tuning of the model is required to improve this fit.

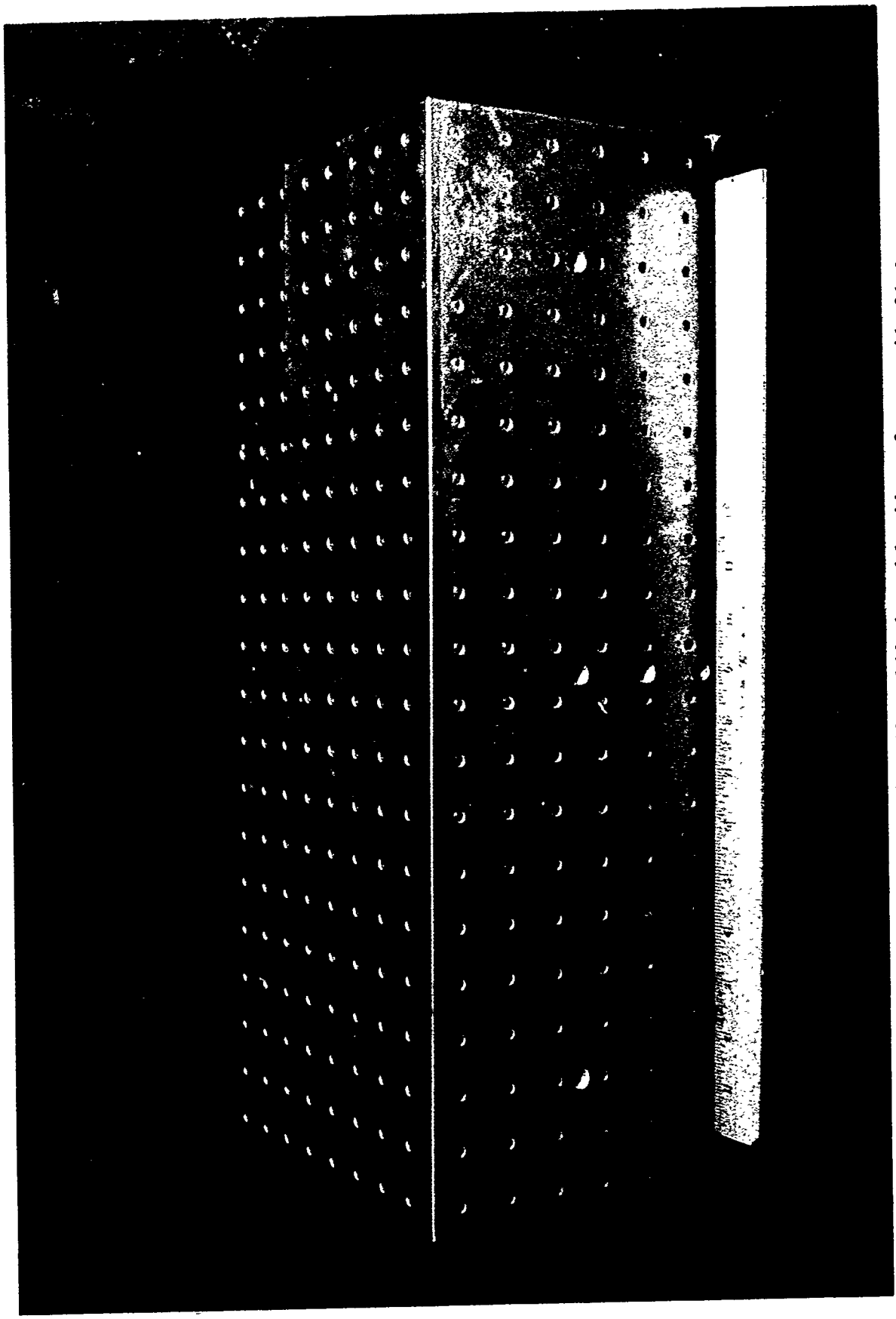

Figure 6-1: The 20"x8.75"x6" H-13 steel block model, with a reference grid of holes.

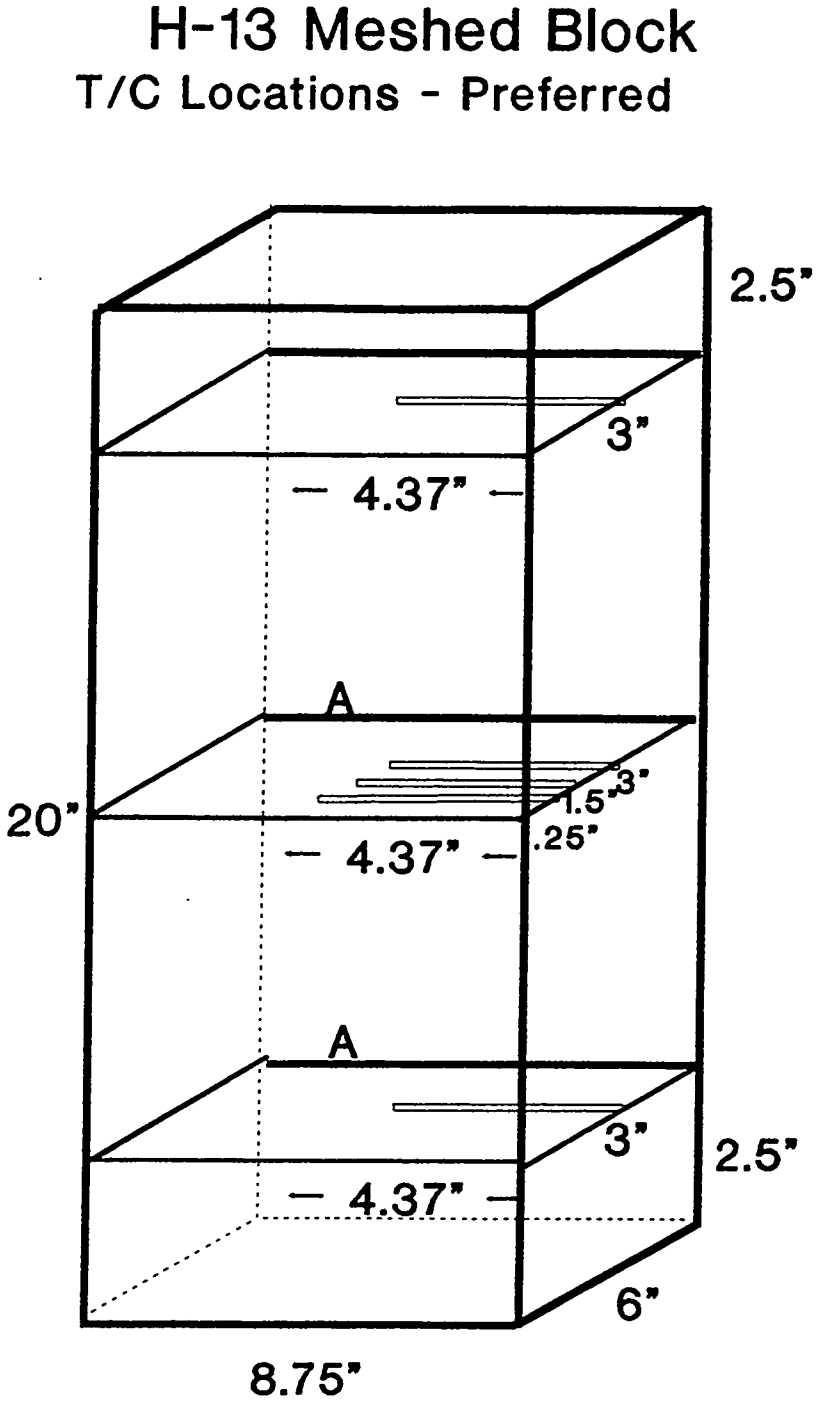

Figure 6-2: Location of the thermocouples in the steel block.

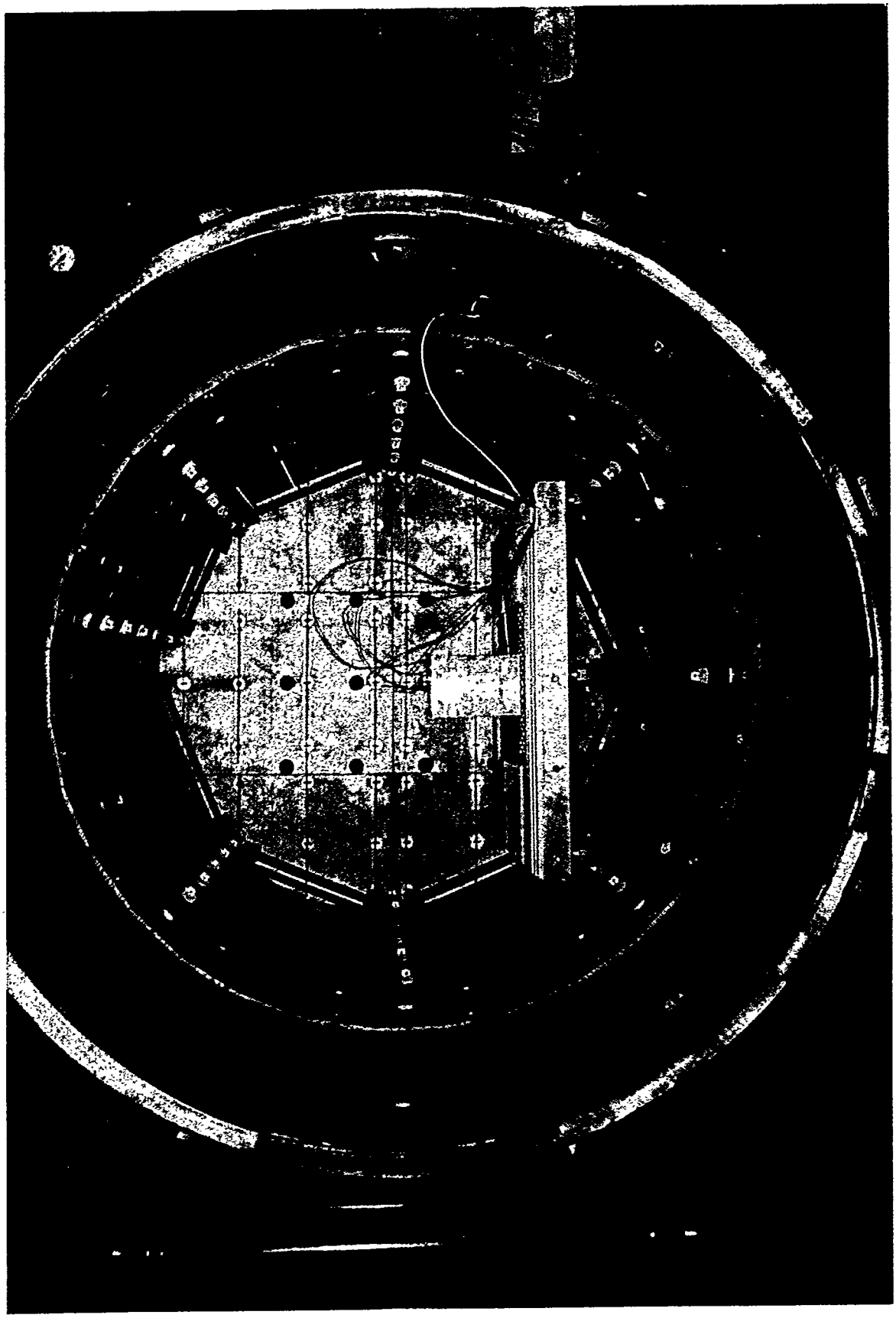

Figure 6-3: Position of the steel block inside the vacuum furnace.

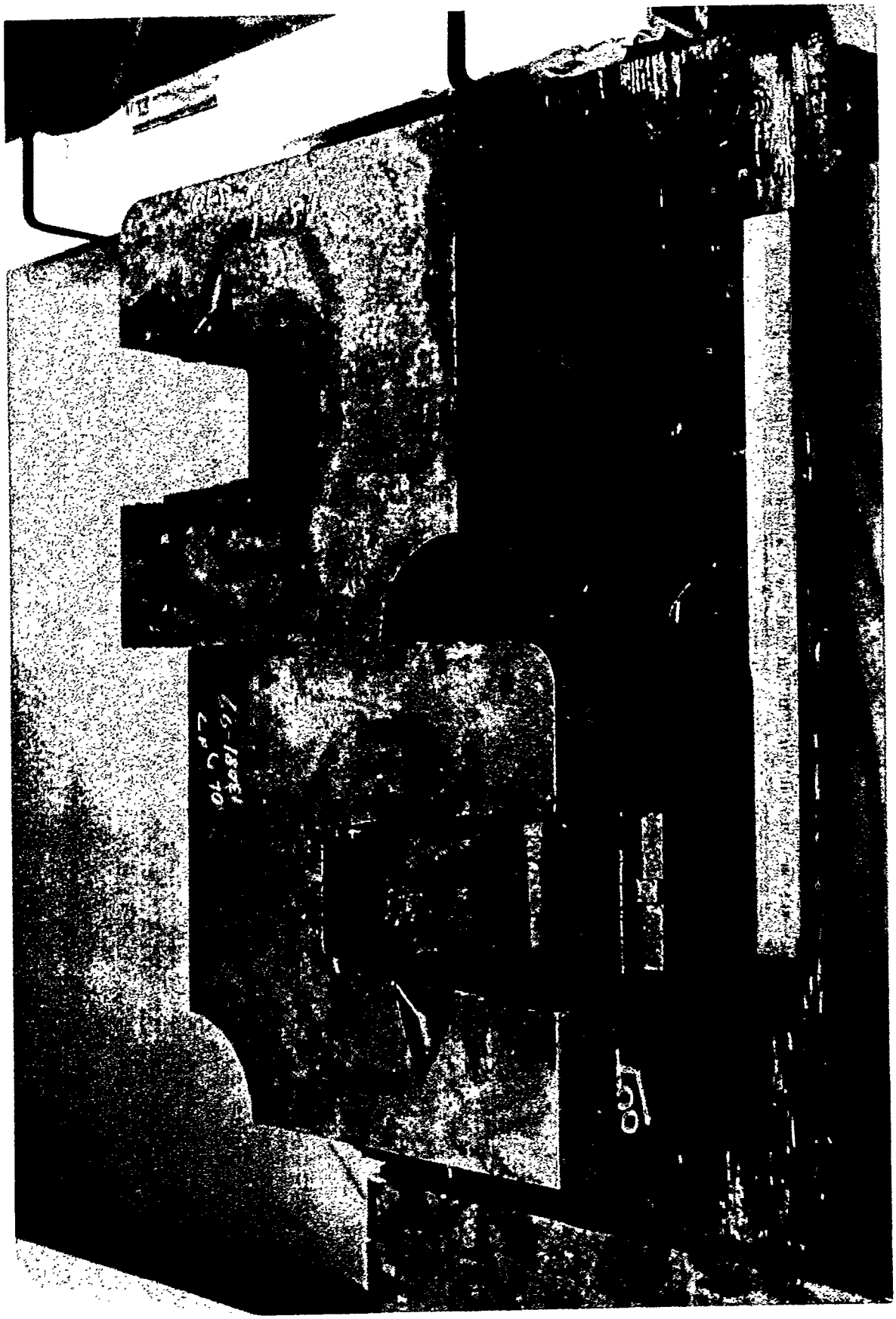

Figure 6-4: H-13 die inserts used in the distortion study.

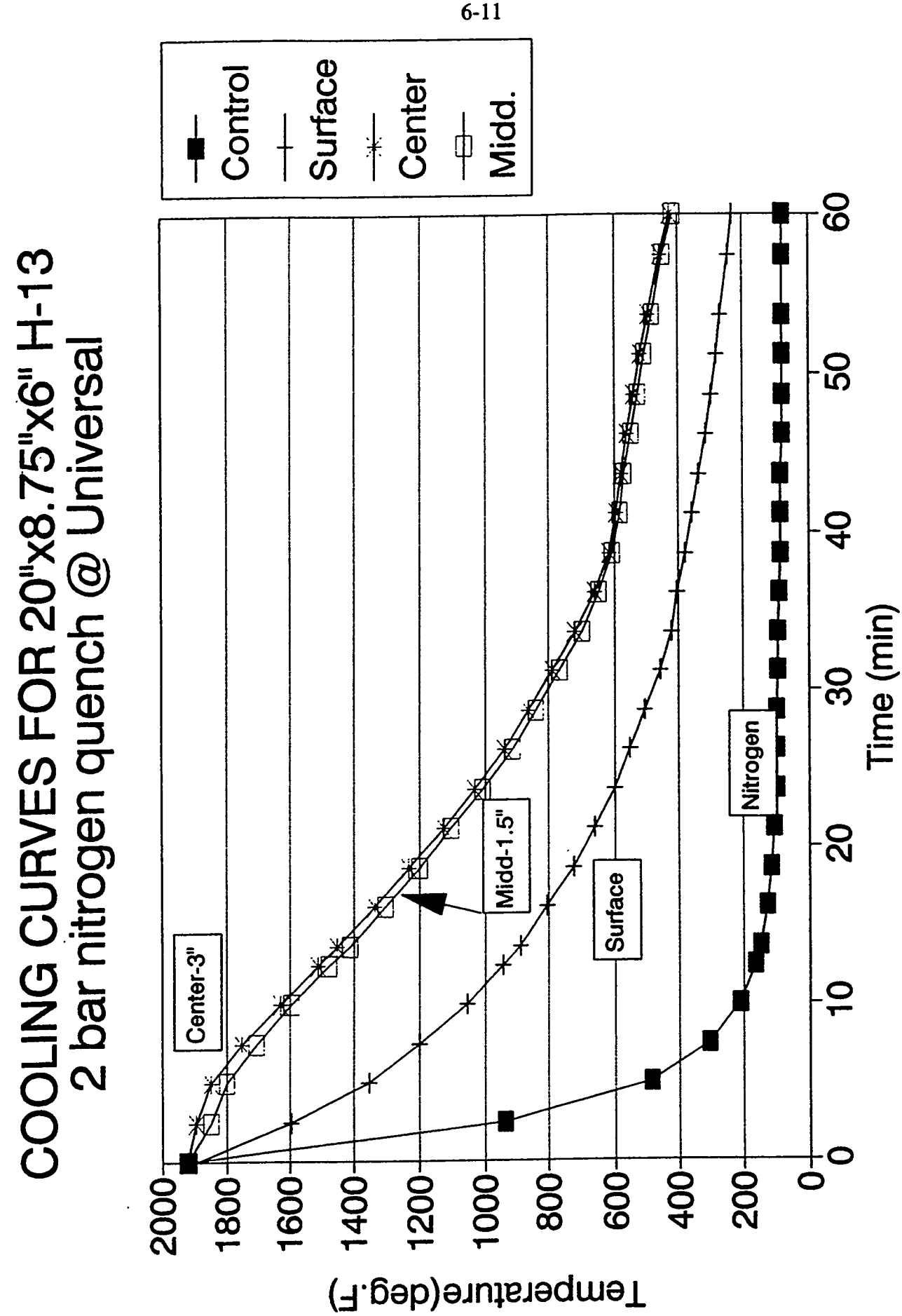

Figure 6-5: Experimental time-temperature plots.

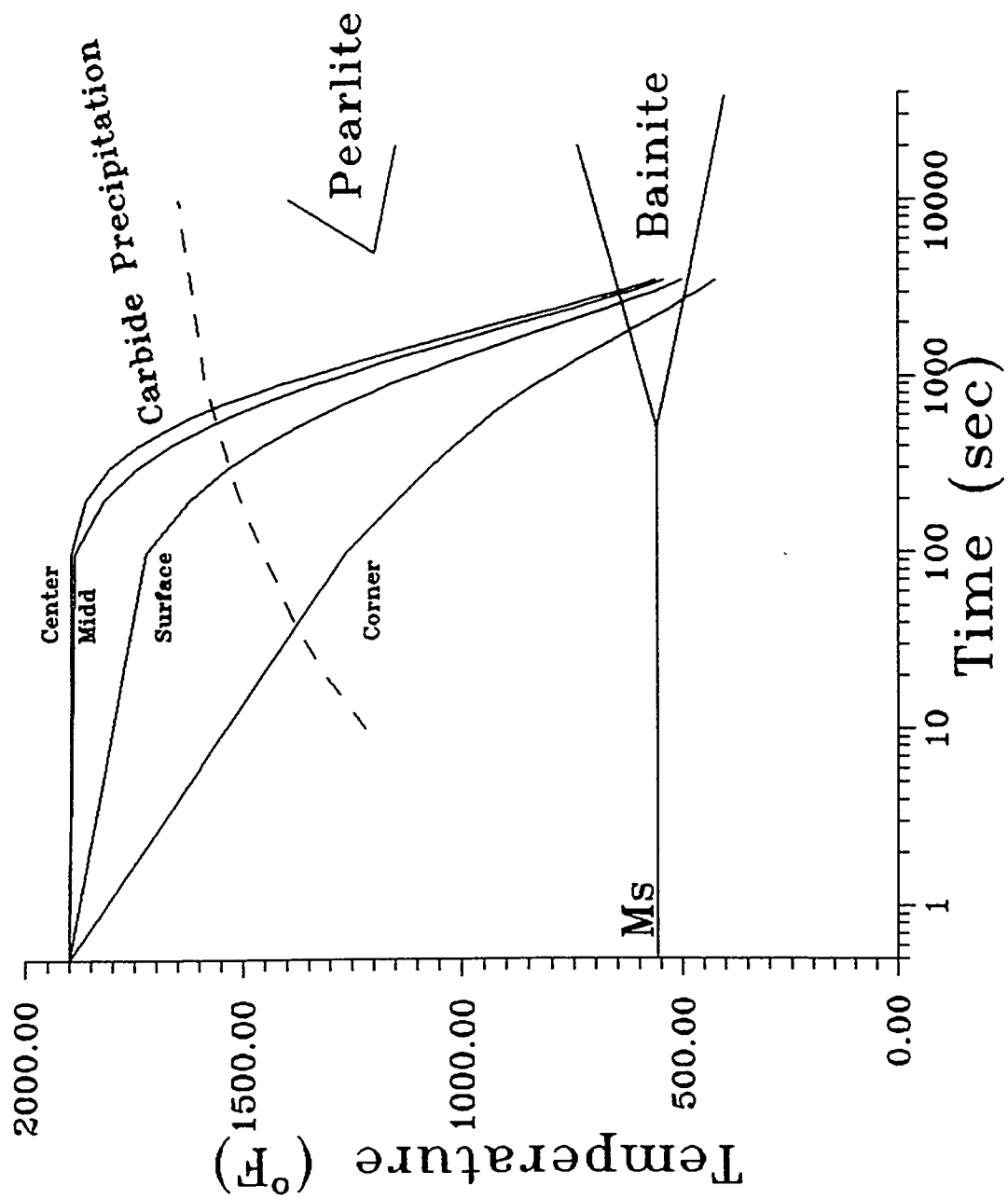

Figure 6-6: CCT diagram of H-13 with the experimental cooling curves.

Figure 6-7a: 3-D distortion map of the 20"x8.75"side (side 1) before quenching.

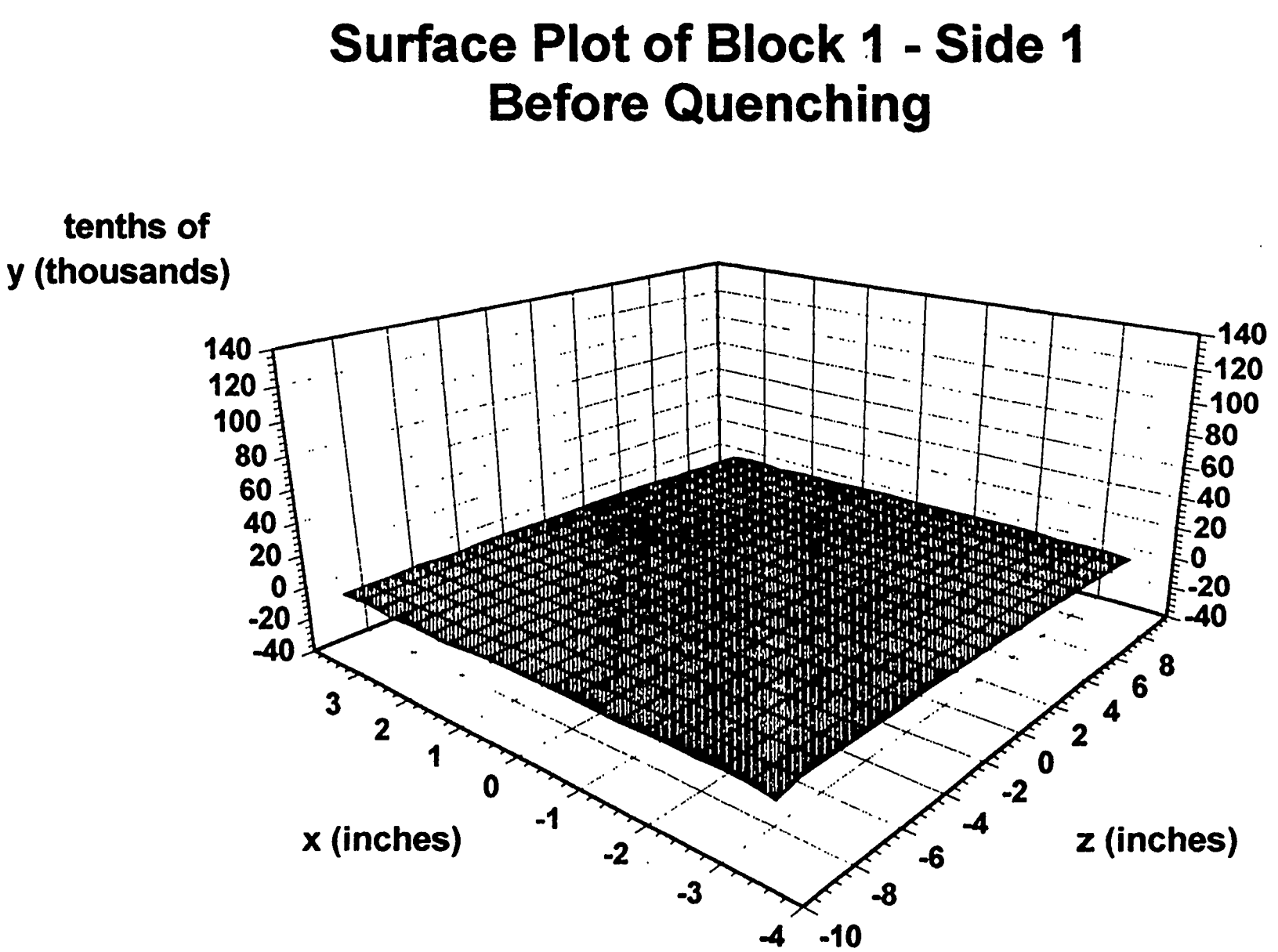

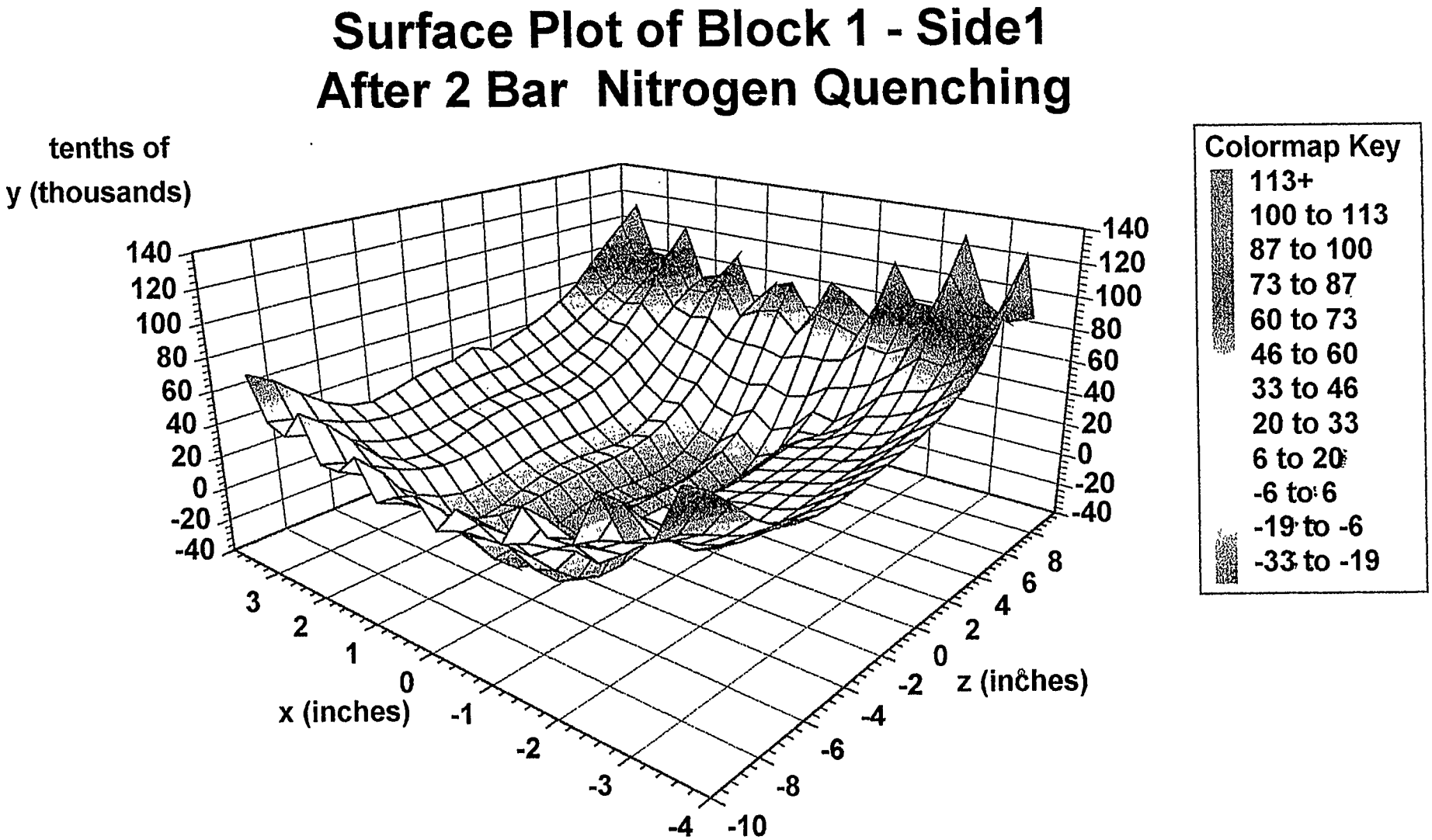

Figure 6-7b: 3-D distortion map of the 20"x8.75"side (side 1) after quenching.

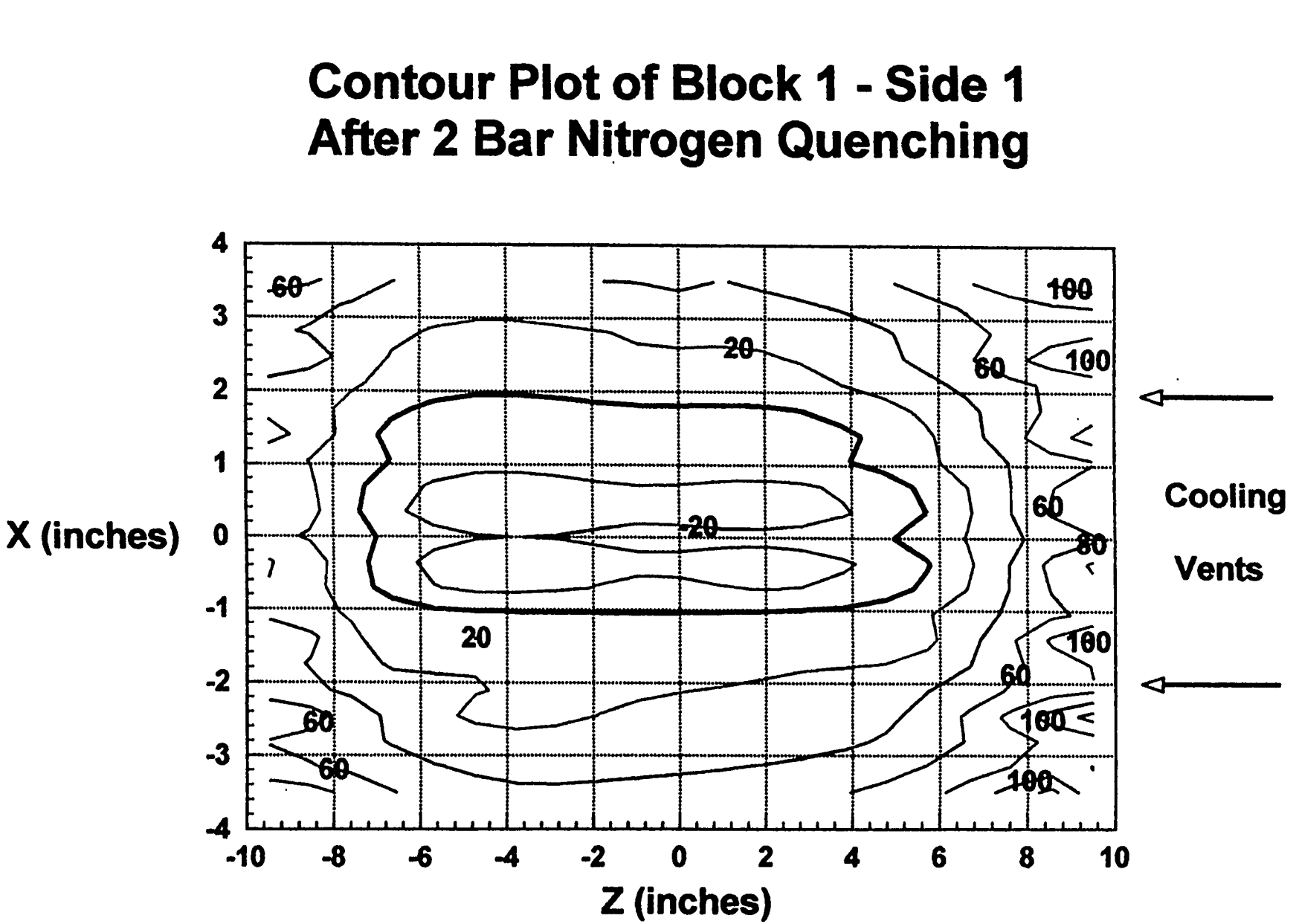

Figure 6-8: Contour distortion map of the 20"x8.75" side (side 1) after quenching.

Contour Plot of Block 1 - Side 3
After 2 Bar Nitrogen Quenching

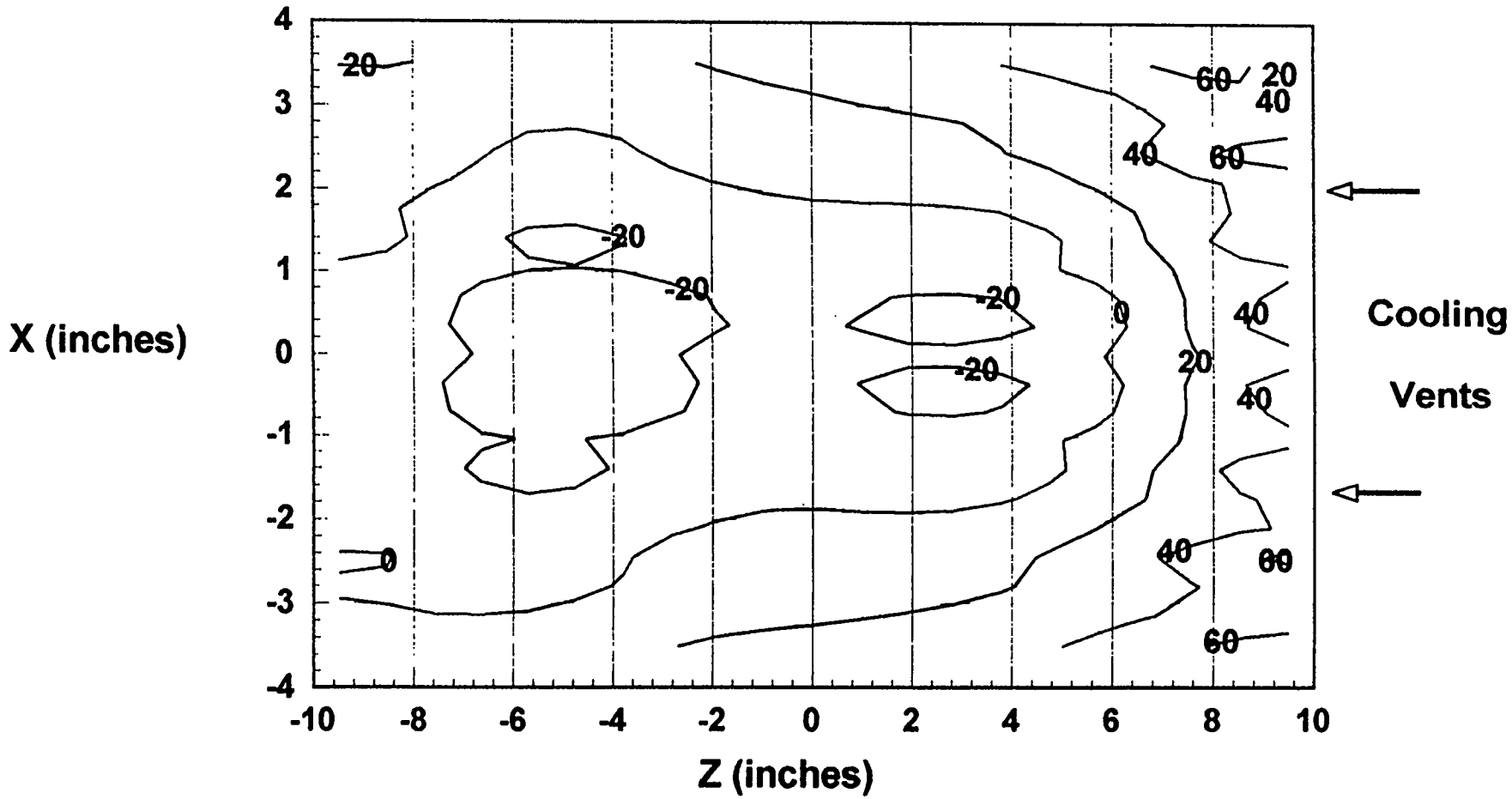

Figure 6-9: Contour distortion map of the 20"x8.75" side (side 3) after quenching.

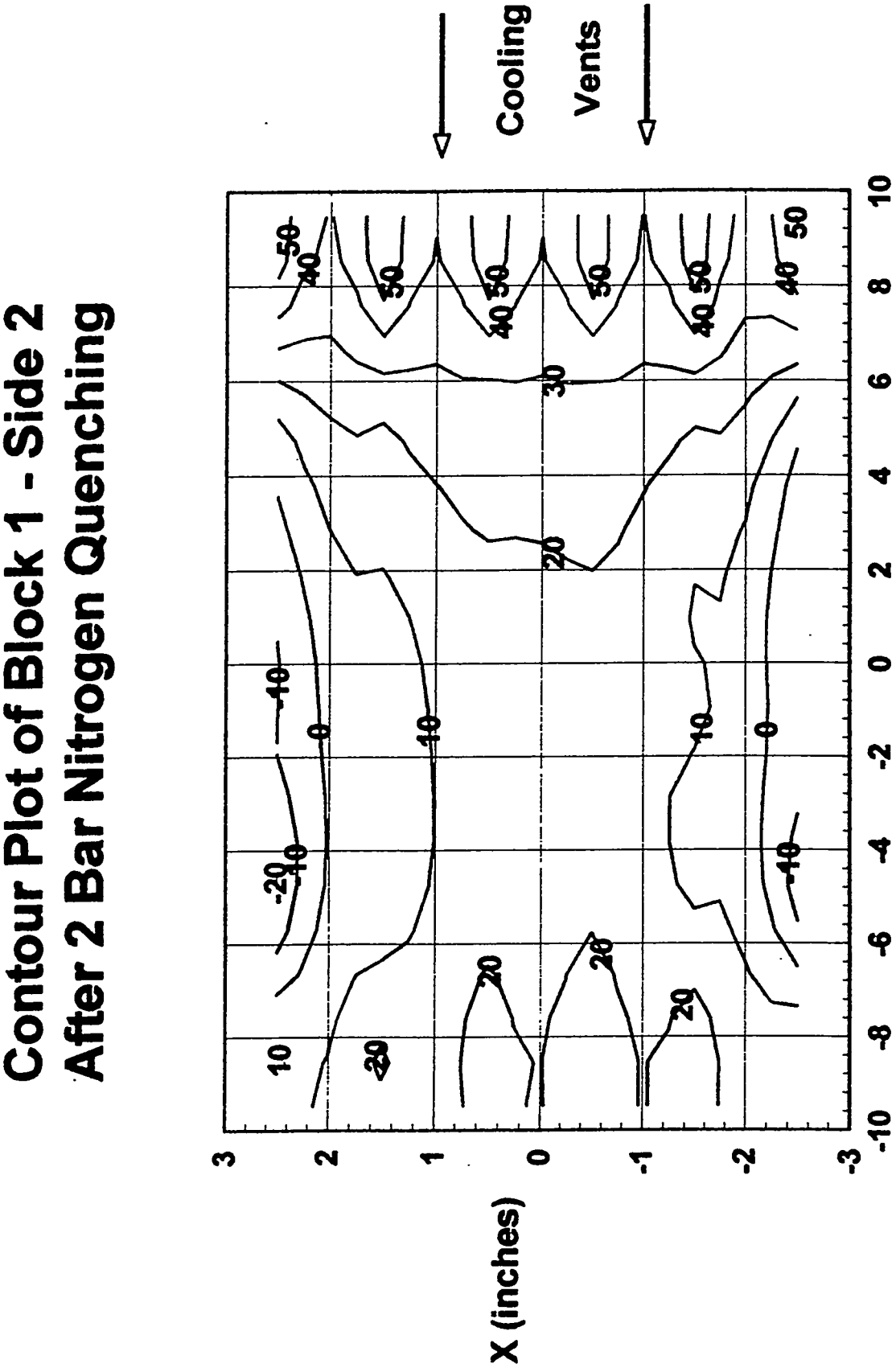

Figure 6-10: Contour distortion map of the 20"x6" side (side 2) after quenching.

Contour Plot of Block 1 - Side 4
After 2 Bar Nitrogen Quenching

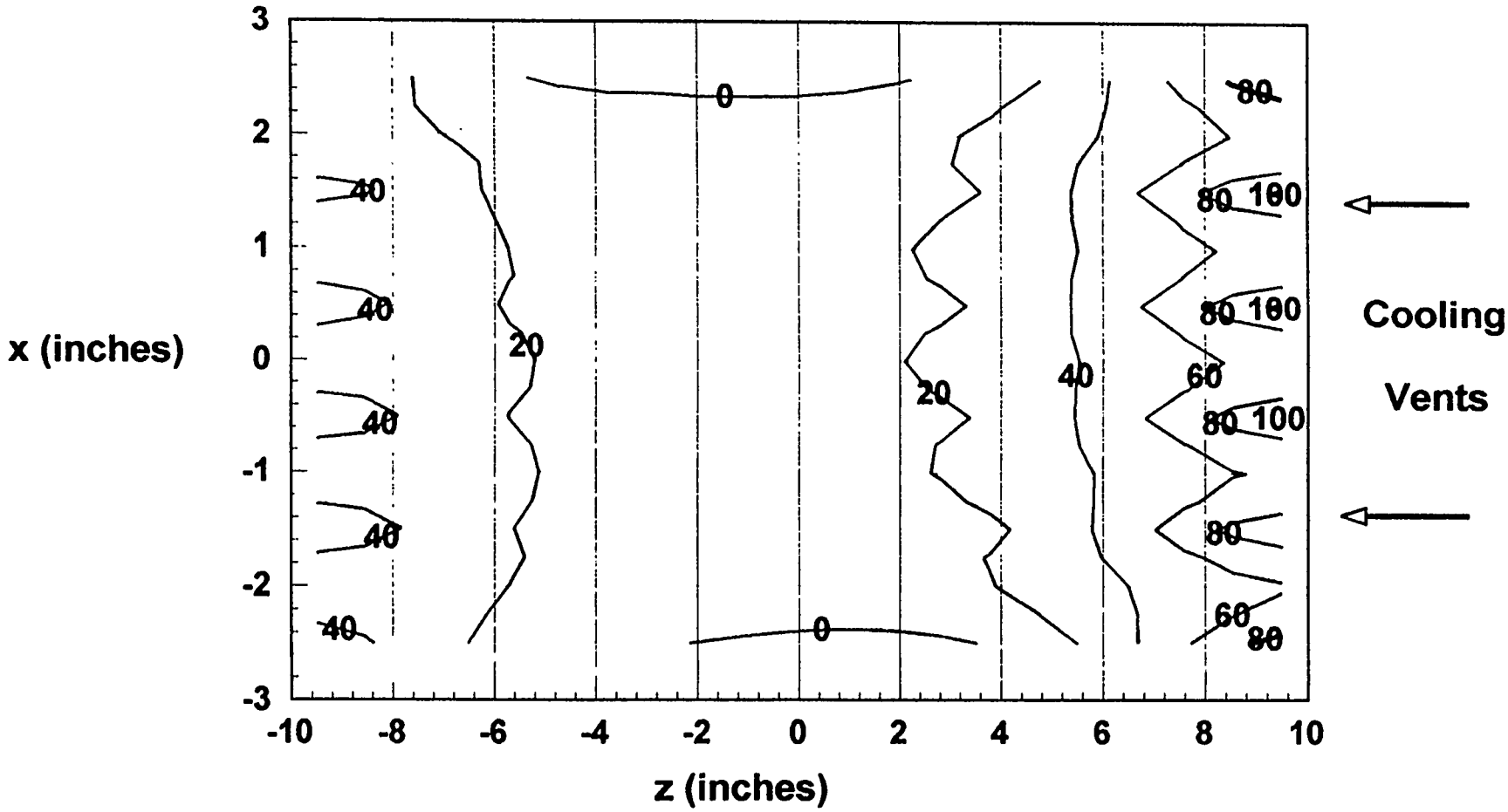

Figure 6-11: Contour distortion map of the 20"x6" side (side 4) after quenching.

Contour Plot of Block 1 - Top Side After 2 Bar Nitrogen Quenching

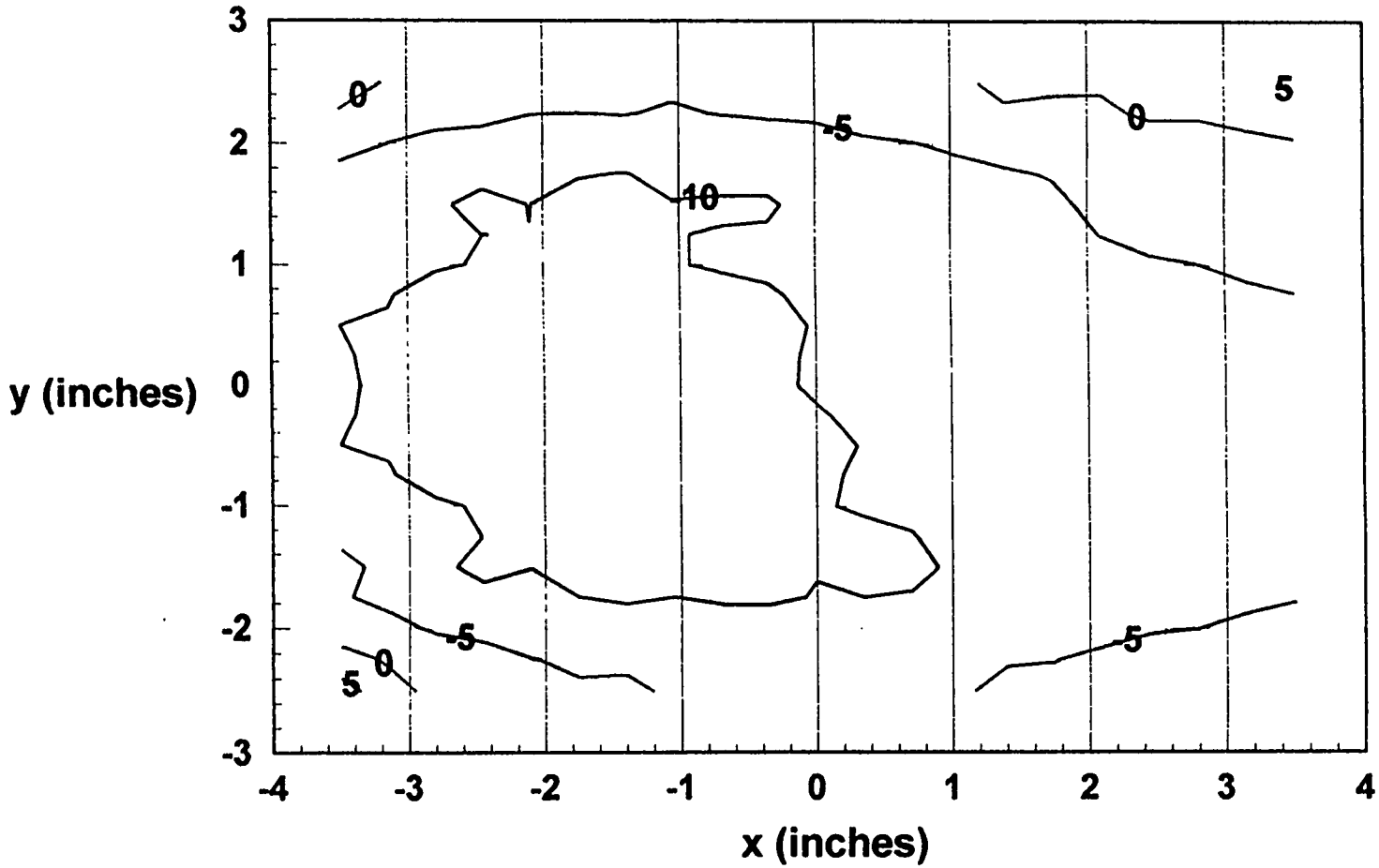

Figure 6-12: Contour distortion map of the 8.75"x6" side (top) after quenching.

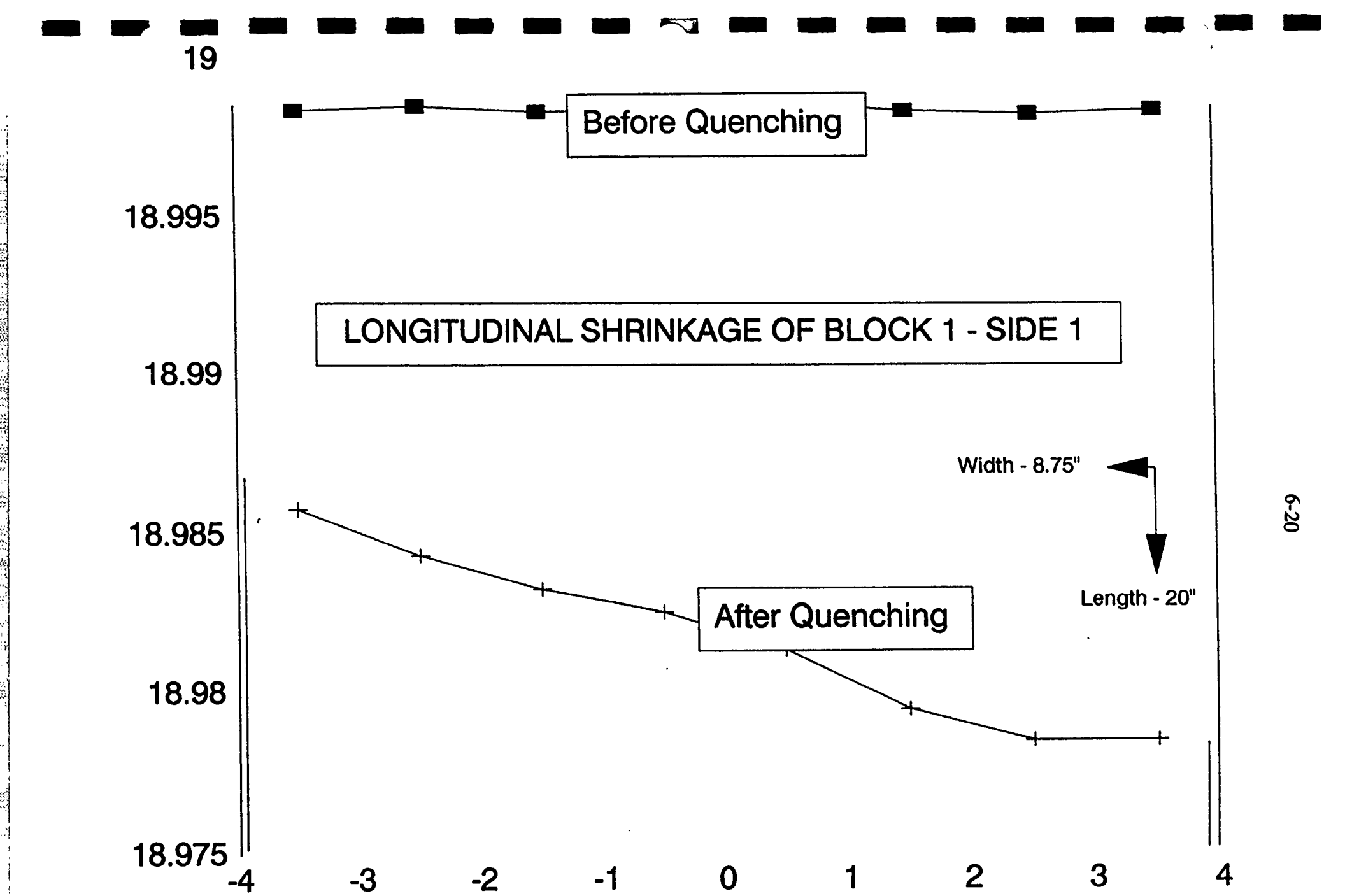

Figure 6-13: Dimensional change of the block during quenching.

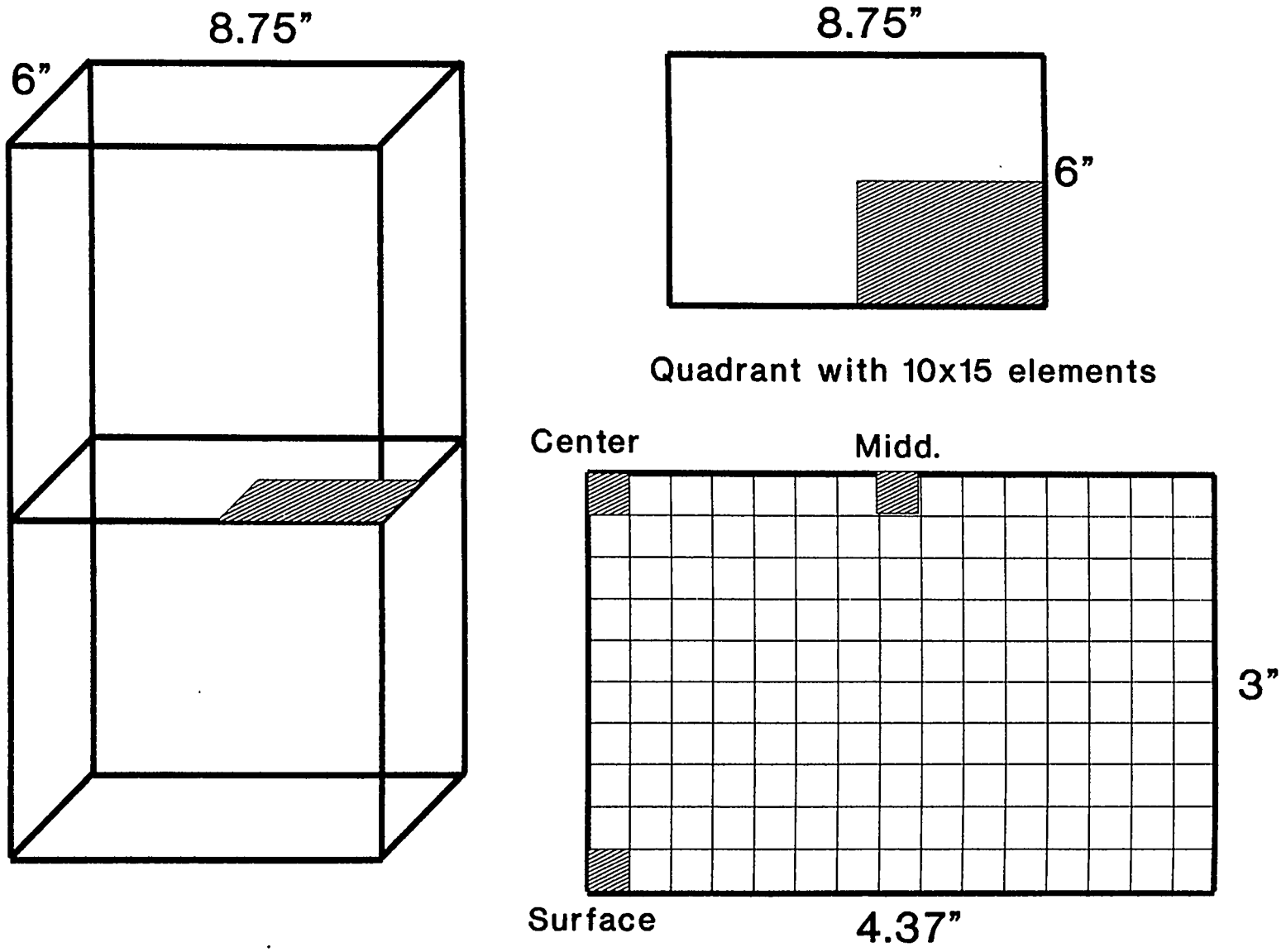

Figure 6-14: Quadrant of the block used in the 2-D finite element model

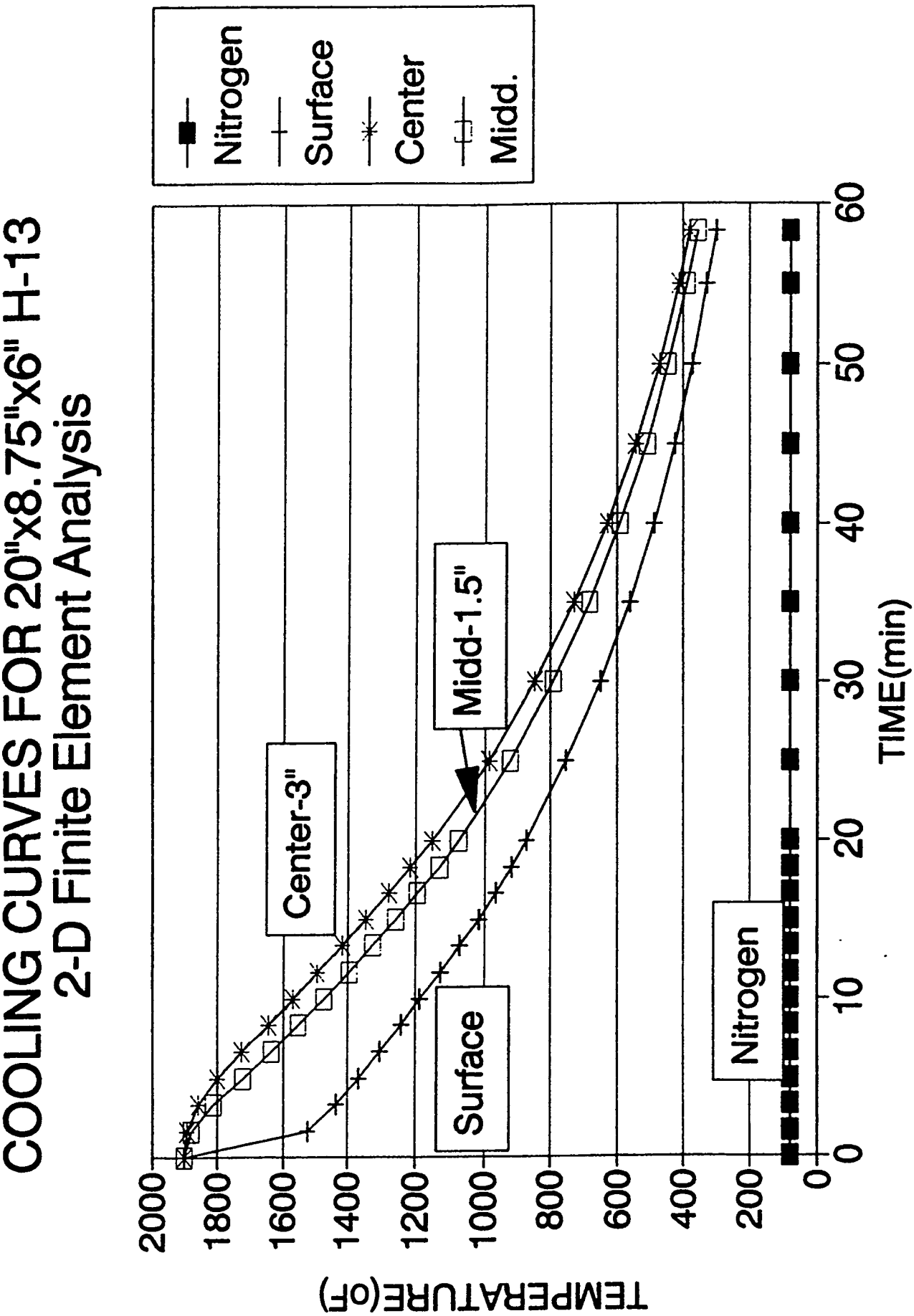

Figure 6-15: Time-temperature prediction of the 2-D model shown in figure 6-14.

Table 6-1: Thermal properties of H-13.

Temperature(°F)	Specific Heat (BTU/lb*°F)	Thermal Conductivity (BTU/ft*hr*°F)
73.4	0.1104	11.984
212	0.1174	12.977
392	0.1260	14.162
572	0.1341	14.676
752	0.1458	15.335
932	0.1618	16.022
1112	0.1829	16.369
1292	0.2331	16.277
1472	0.2032	16.329
1652	0.1649	16.485
1832	0.1690	17.334
2012	0.1733	18.322
2192	0.1759	19.091

Table 6-2: Sources of heat treating distortion in steel.

Operation	Size Distortion	Shape Distortion
Austenitizing	● Formation of austenite ● Solution of carbides	● Relief of residual stresses ● Irregular expansion stresses ● Thermal stress sagging
Quenching	● Formation of martensite bainite and pearlite	● Thermal stresses ● Transformation stresses ● Introduction of residual stresses

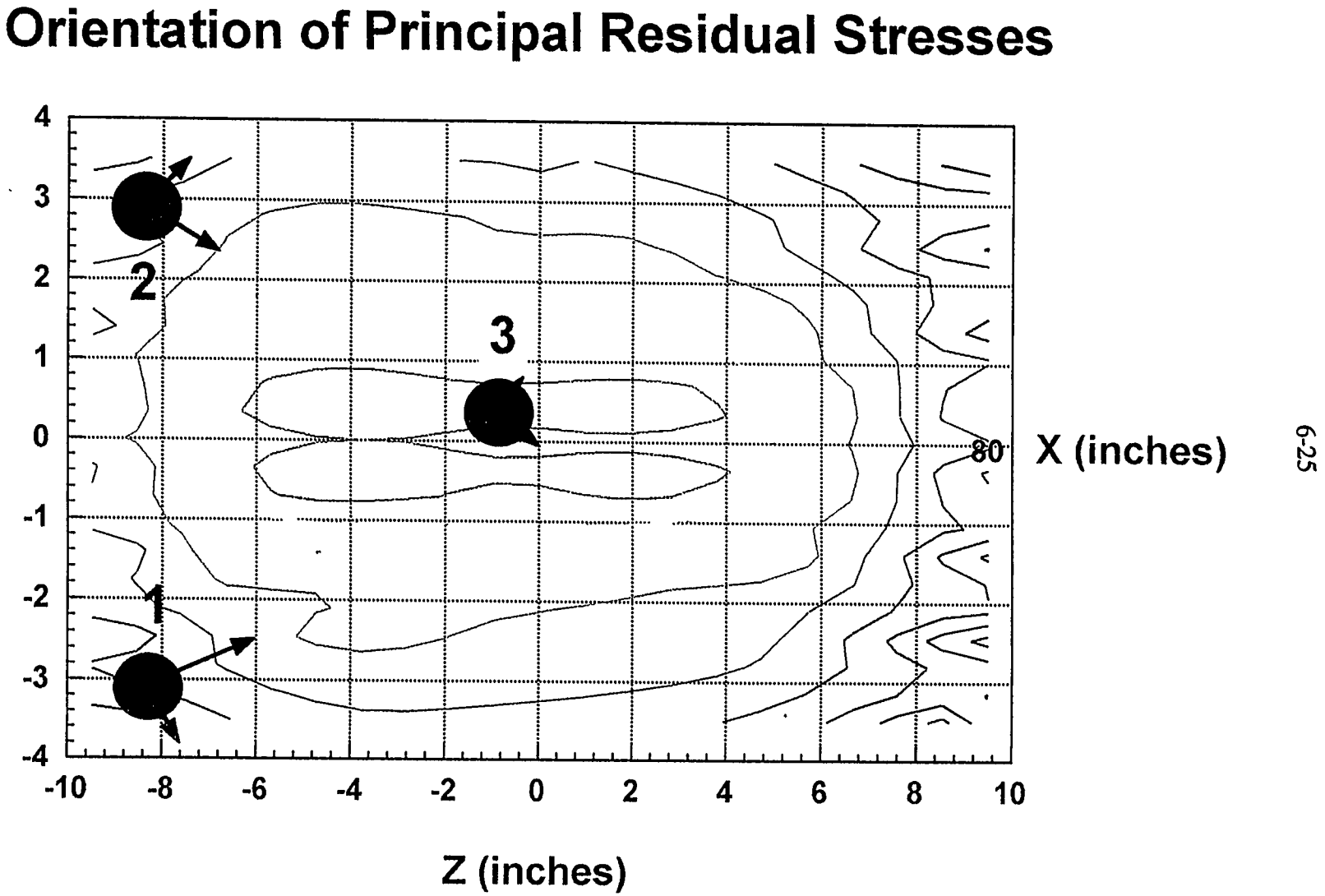

Figure 6.16: Location of residual stress measurement taken on Block #1

THE HOLE-DRILLING RESIDUAL STRESS METHOD

PRINCIPAL STRESSES

RESULTS

#	ε_1	ε_2	ε_3	$\varepsilon_1+\varepsilon_3$	$\varepsilon_3-\varepsilon_1$	$\varepsilon_3+\varepsilon_1-2\varepsilon_2$	σ max	σ min	α
1	-222	-220	-500	-722	-278	-282	71.9	40.5	-22.5°
2	-115	-70	-120	-235	-5	-100	22.3	14.4	43.5°
3	-110	-140	-80	-190	30	90	18.5	11.1	35.8°

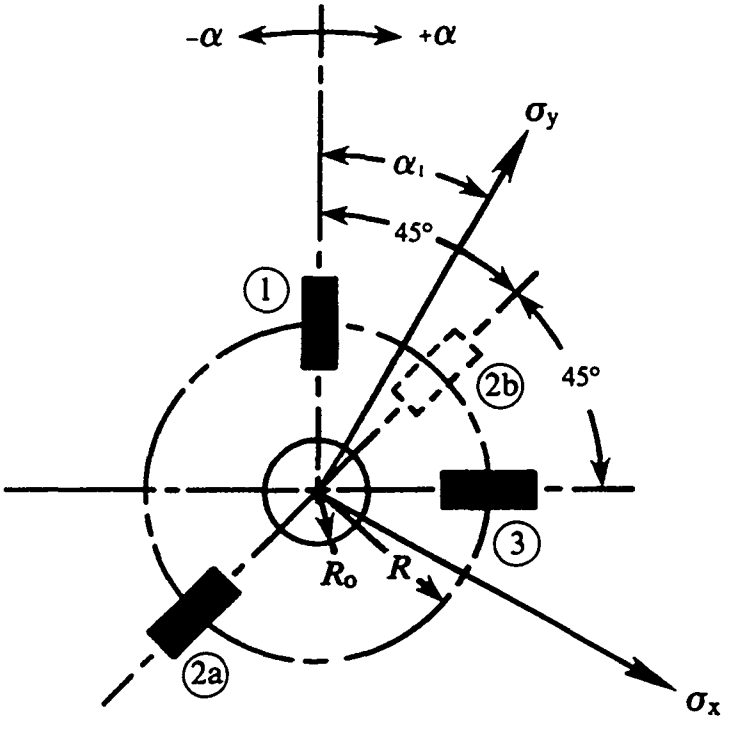

Figure 6.17: Magnitude of principal residual stress measurements taken on Block #1

7. Experimental Results of the Vacuum/Gas Quenching of H-13 Dies

A set of used H-13 die inserts donated to the project by Crown Equipment in London, Ohio. The set comprises six separate pieces, and weighs over 1,100 pounds. It was used to die cast an antenna housing, and had to be replaced due to a change in design. The largest two of the die inserts are about 12"x12"x7". The initial hardness of the as-supplied inserts was measured by Euclid Heat Treating, and yielded values of 48-49 Rc. The inserts were first annealed at General Metal Heat Treating in Cleveland, Ohio. The annealing was provided by General Metal Heat Treating as an in-kind contribution to the project. Subsequently, the two die inserts were taken to a machine shop where they were machined: six 3/16"x2.5" holes with NPT threads were drilled for the thermocouples. About 500 3/16" x 3/16" holes for distortion mapping were also drilled in each die insert.
The largest two of the die inserts are about 12"x12"x7". These were transported to General Metal Heat Treating in Cleveland, Ohio, where they received an annealing treatment to soften the steel.

Subsequently, the two die inserts were taken to a machine shop in Mentor, Ohio where they were machined. Six 3/16"x2.5" holes with NPT threads were drilled for the thermocouples. About 500 3/16" x 3/16" holes for distortion mapping were also drilled in each die insert.

7.1 Die #2

One of the die inserts - Die 2 was taken to the Inspection Branch of NASA Lewis. Mr. William Waters who is a member of the NADCA Die Materials Committee, assisted us in accessing this facility. The die was mapped by the measurement experts at NASA, using a high precision Coordinate Measurement Machine. Accurate x,y,z coordinates of each hole were determined in the pre-quenched condition.

Die #2 was subsequently taken to Universal Heat Treatment. There, it was quenched under

identical conditions with the previously heat treated H-13 Block#1. The die was located in the center of the furnace, with no other parts. The quenching was done with nitrogen at a pressure of 2 bars, while acquiring time-temperature data at different locations. Universal Heat Treatment conducted this experiment as an in-kind contribution to the project.

The objective of this identical heat treatment was to provide a common baseline for the Finite Element Modeling. Experimental data obtained from the previous quenching of Block #1 will be utilized to model the thermal profile and distortion of the die. The prediction will then be compared with the actual data from the die.

After the quenching was completed, Die #2 was returned to NASA Lewis for another round of accurate mapping. By measuring the x, y, z coordinates of the 500 holes, the dimensional changes induced by the quenching was determined.

The 2 bar Vacuum Furnace at Universal

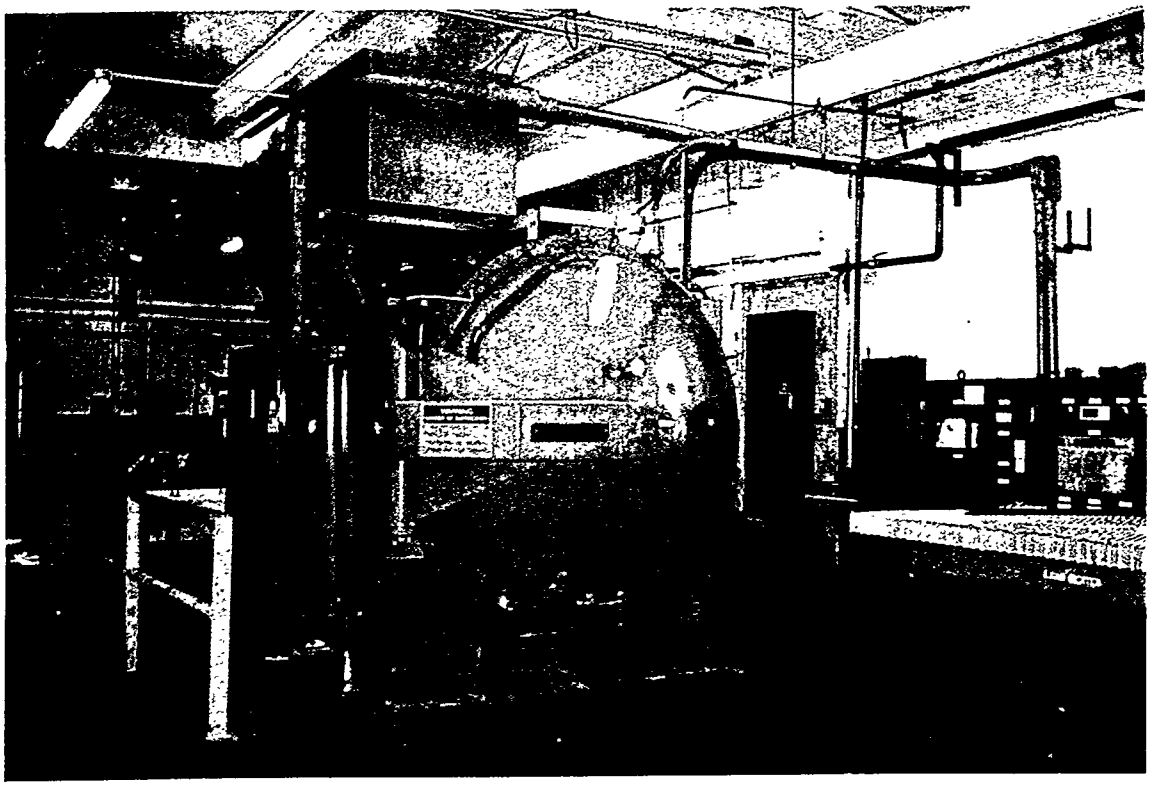

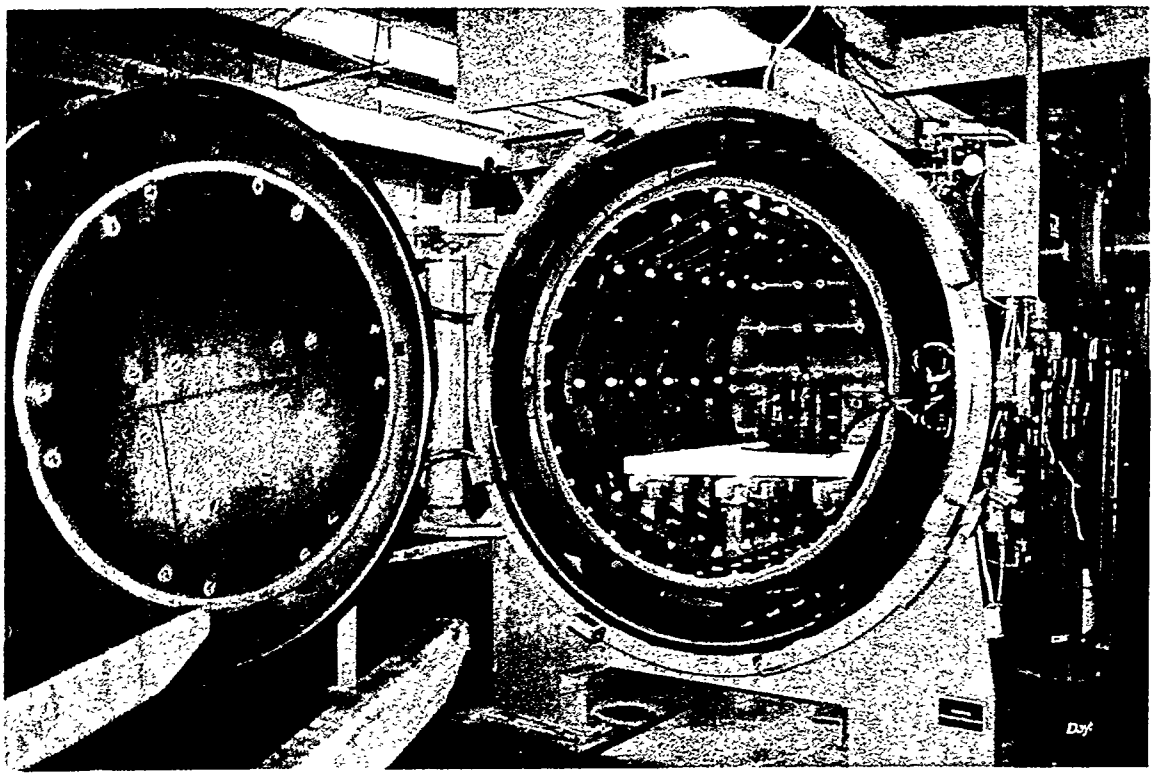

Die #2 in the Universal Vacuum Furnace

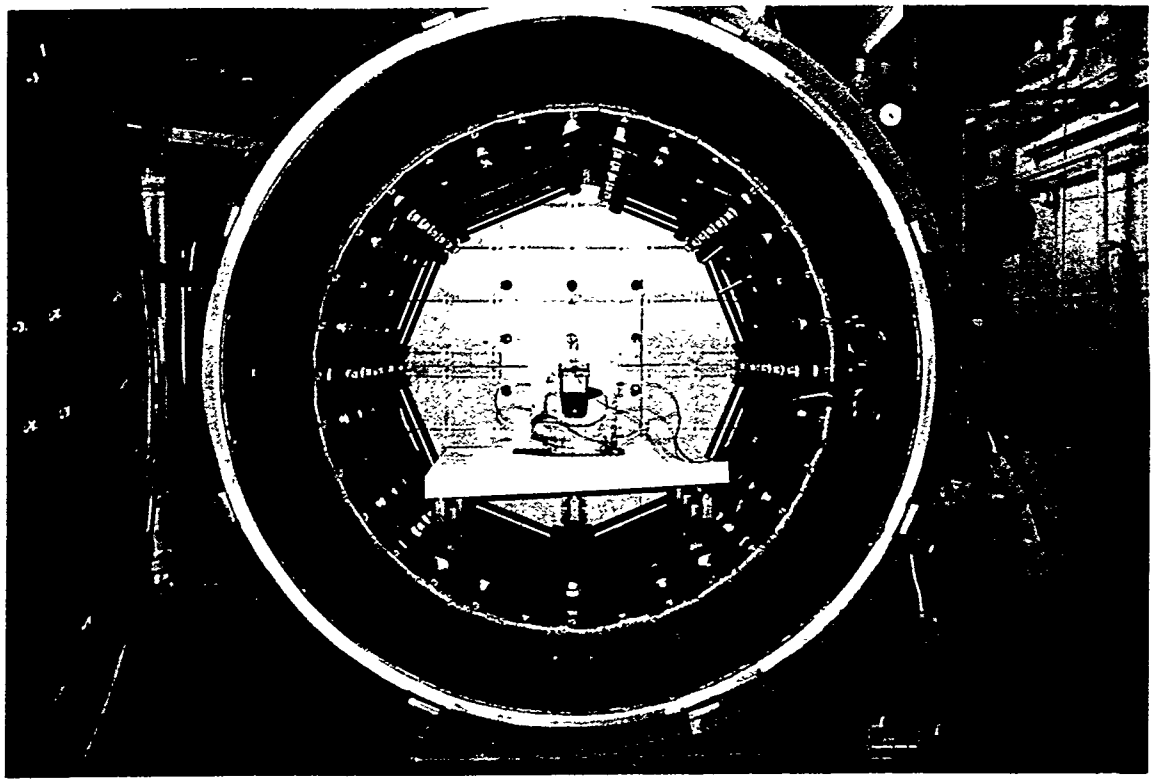

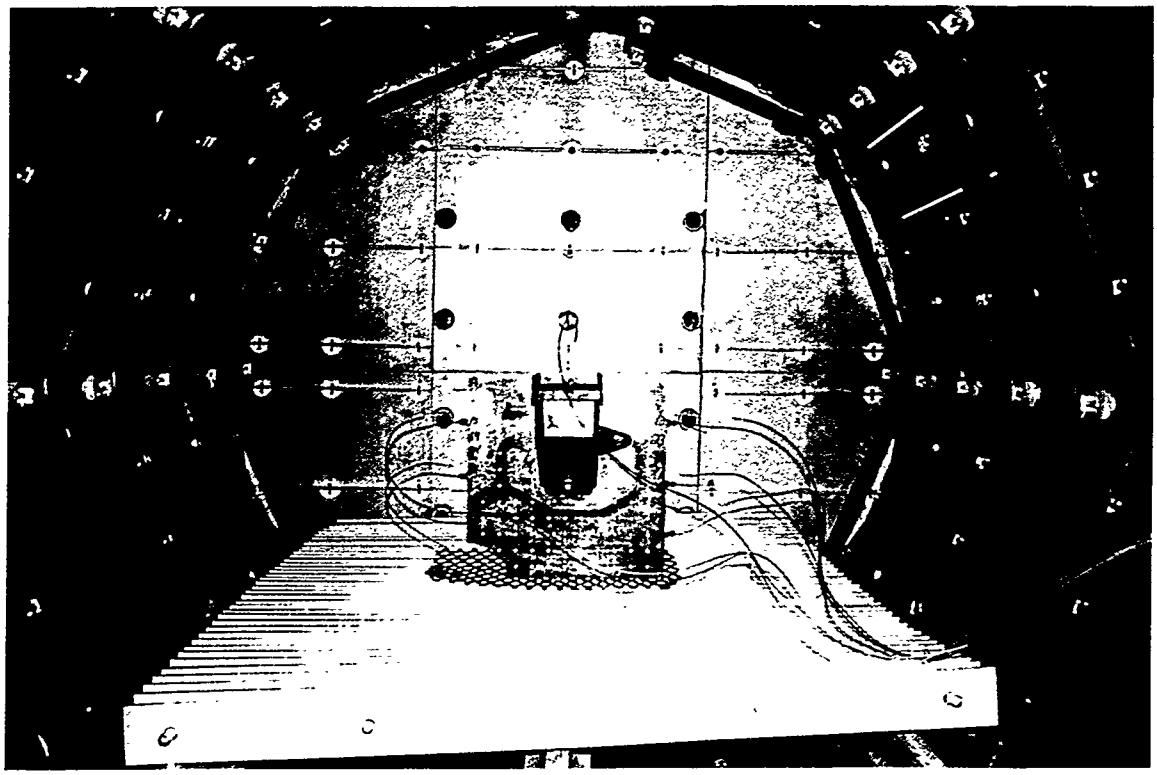

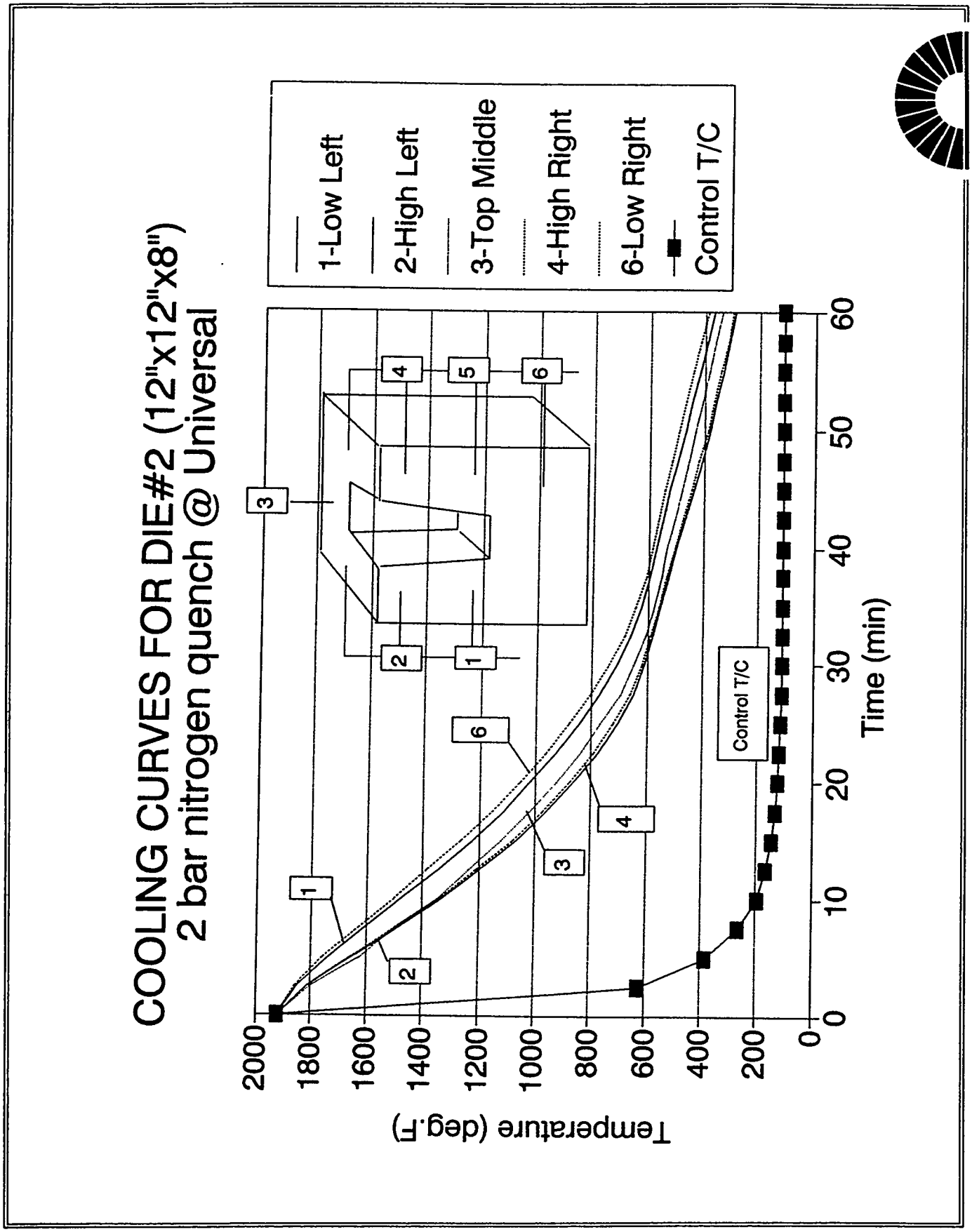
COOLING CURVES FOR DIE#2 (12"x12"x8")
2 bar nitrogen quench @ Universal
1-Low Left
2-High Left
3-Top Middle
4-High Right
6-Low Right
Control T/C
Temperature (deg.F)
Time (min)
2000
1800
1600
1400
1200
1000
800
600
400
200
0
0
10
20
30
40
50
60
1
2
3
4
5
6
Control T/C

7.2 Die #3

Die #3 was taken to the Inspection Department of the American Steel Foundries in Alliance, Ohio, where it was mapped using a Coordinate Measurement Machine. Accurate x,y,z coordinates of each hole were determined in the pre-quenched condition.

Die #3 was subsequently taken to Industrial Materials Technology (IMT) in London, Ohio. There, it was quenched in a 6 Bar Abar Ipsen TurboTreater Vacuum furnace. The die was located in the center of the furnace, with no other parts. The quenching was done with argon at a pressure of 4 bars, while acquiring time-temperature data at different locations. IMT conducted this experiment as an in-kind contribution to the project.

Die #3 was then taken back to the Inspection Department of the American Steel Foundries in Alliance, Ohio, where it was mapped using the same Coordinate Measurement Machine. Accurate x,y,z coordinates of each hole were determined in the post-quenched condition.

The 6 bar Vacuum Furnaces at IMT

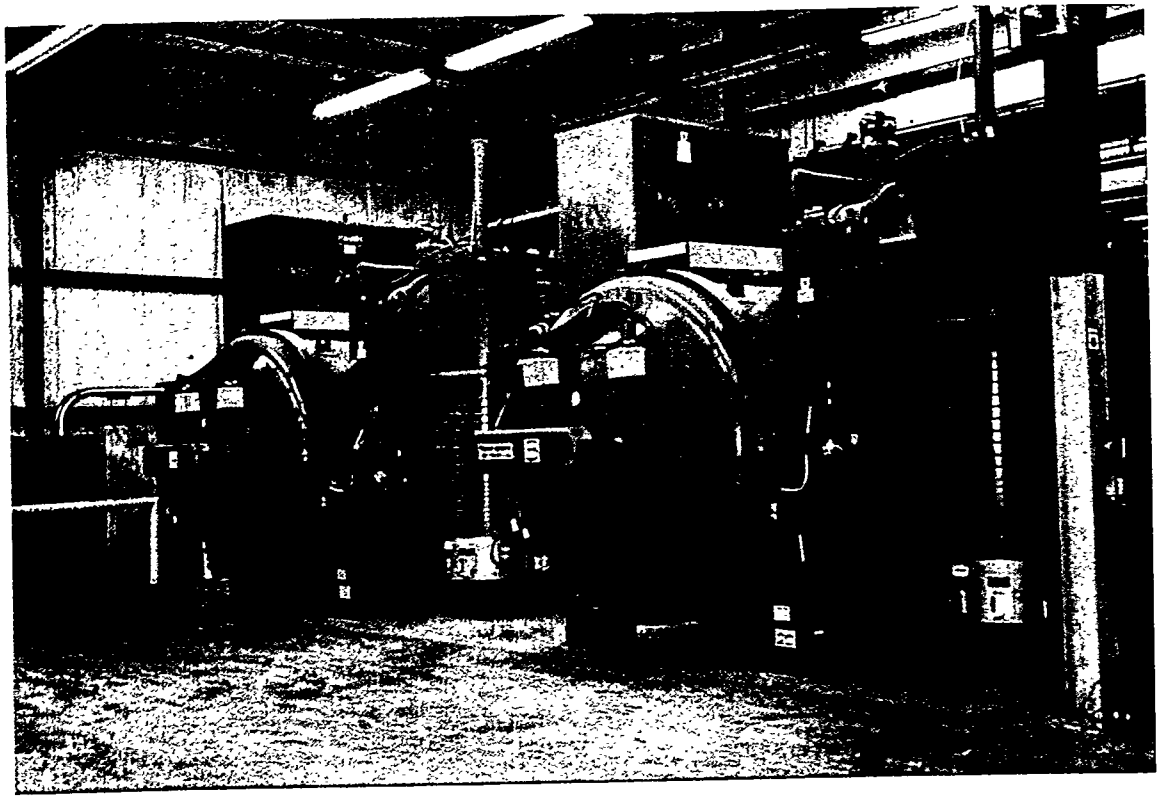

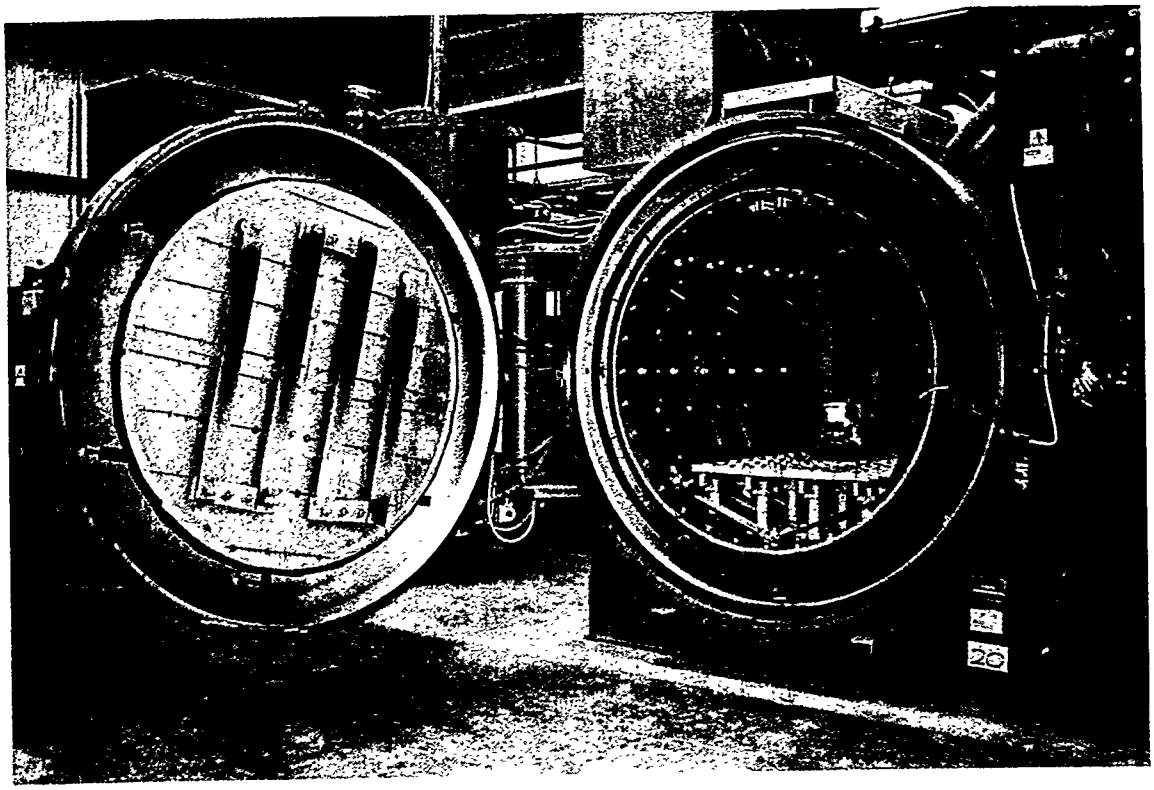

Die #3 in the IMT Vacuum Furnace

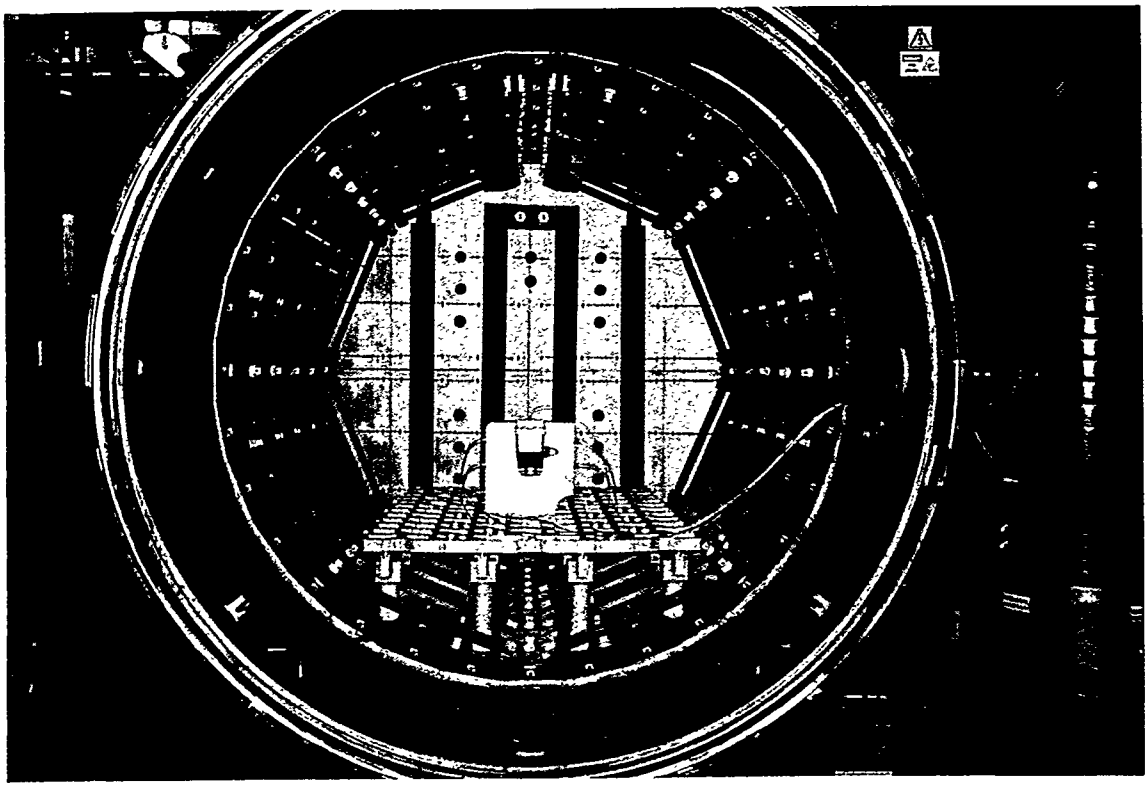

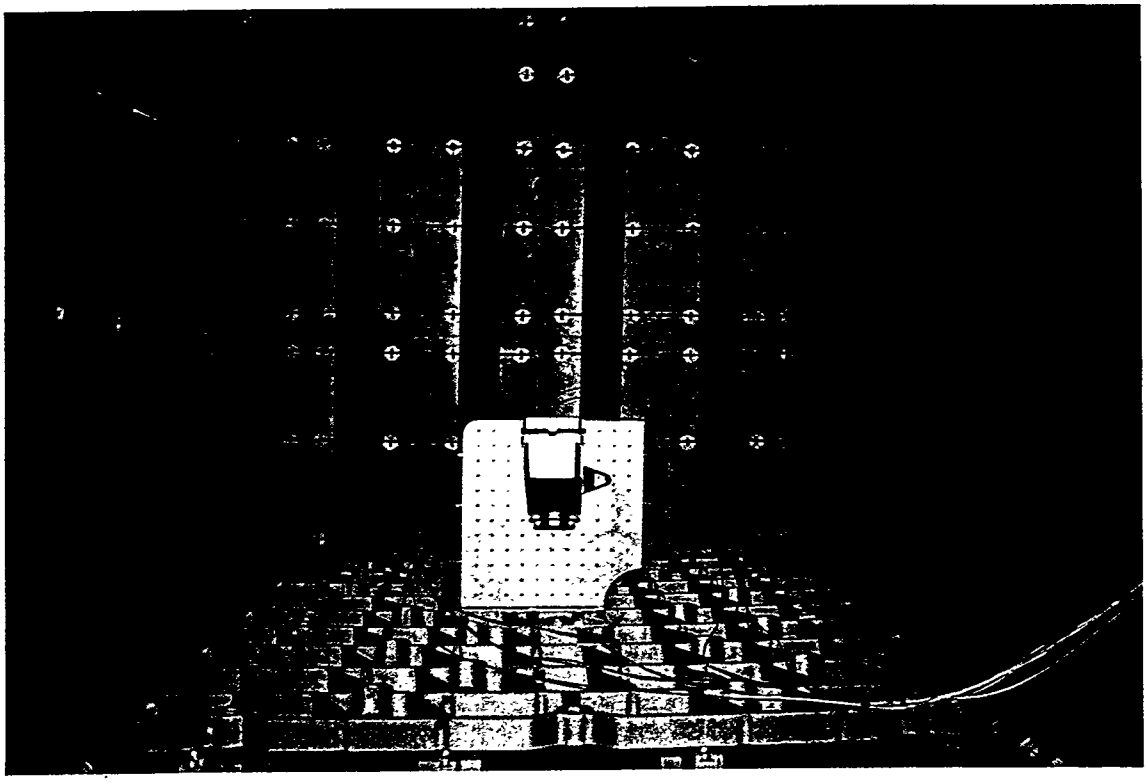

COOLING CURVES FOR DIE#3 (12"x12"x8")
4 bar argon quench @ IMP

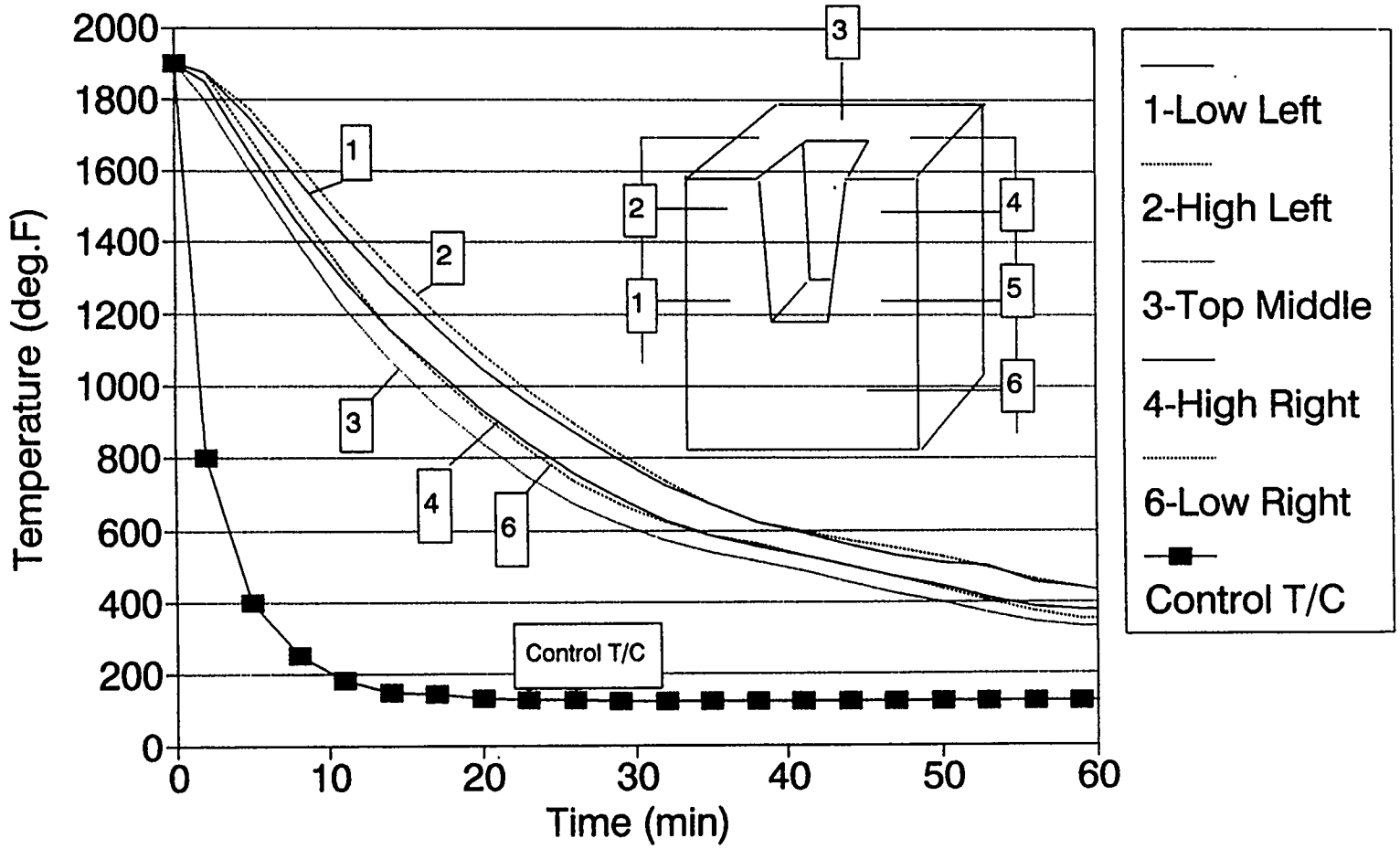

7.3 Die #4 and Die #5

The two identical dies were shipped to FPM Heat Treating in Chicago, Illinois. At FPM, the dies were quenched separately in two vacuum, gas quenching furnaces:

(a) The first die was austenitized at 1875°F and quenched in a VFS Model #HIQ 5750-10 furnace with 8000 cfm 10 bar Nitrogen gas quenching capabilities. The quenching was performed at a 7 bar pressure.

(b) The second die was austenitized at 1875°F and quenched in a Abar Ipsen Model H48x48 at 5 bar Nitrogen.

Cooling curves were obtained for each die, at six different locations. Hardness values of 53.5 Rc were measured on the dies.

In addition to the die, each load comprised two thermal cycling ("Dunk") samples, 12 Charpy bars and two control coupons. One of the control coupons was removed after the quenching; the samples were subsequently tempered twice. Another coupon was removed after the first temper, to be used as a witness sample. After the second temper, the hardness was in the 47-49 Rc range.

John Fitzgerald of FPM facilitated the heat treatments, that were provided by the company at no charge. Mr. Fiztgerald is chairman of the Heat Treating Subcommittee of the NADCA Die Material Committee. FPM is one of the largest heat treatment companies in the US with a workforce approaching 200 and customers in over 35 states.

The 5 bar Vacuum Furnace at FPM Heat Treating

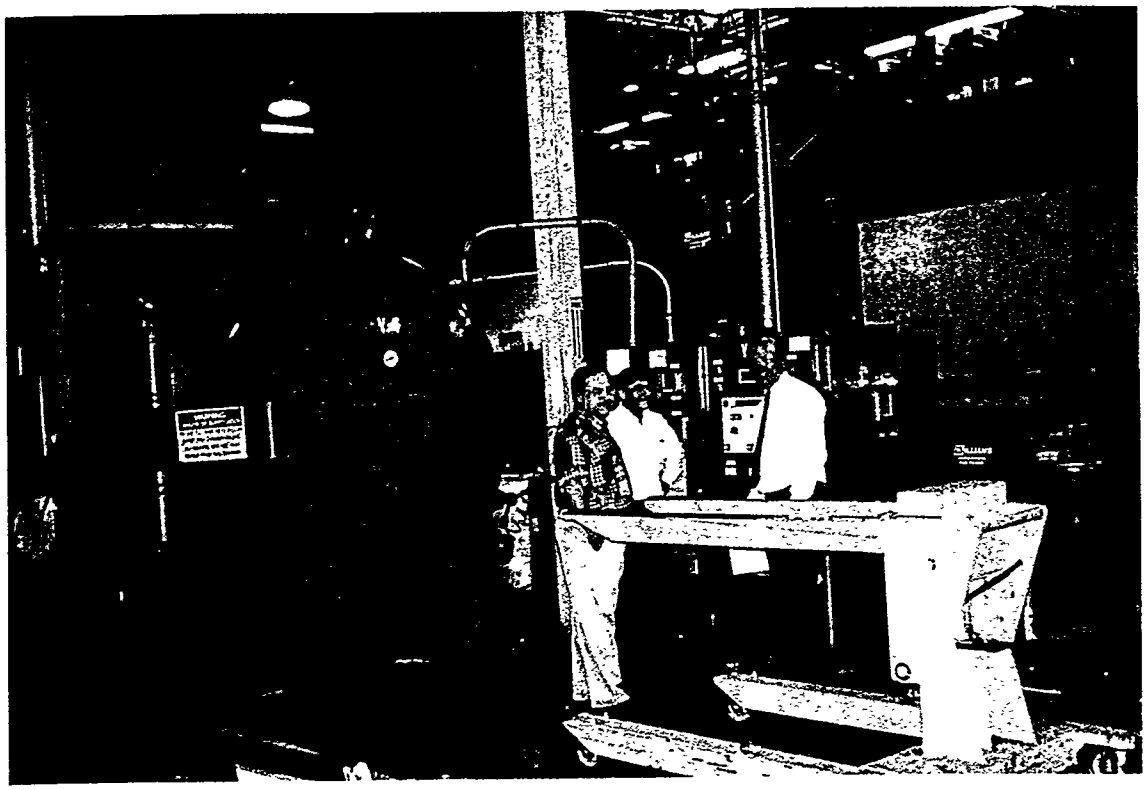

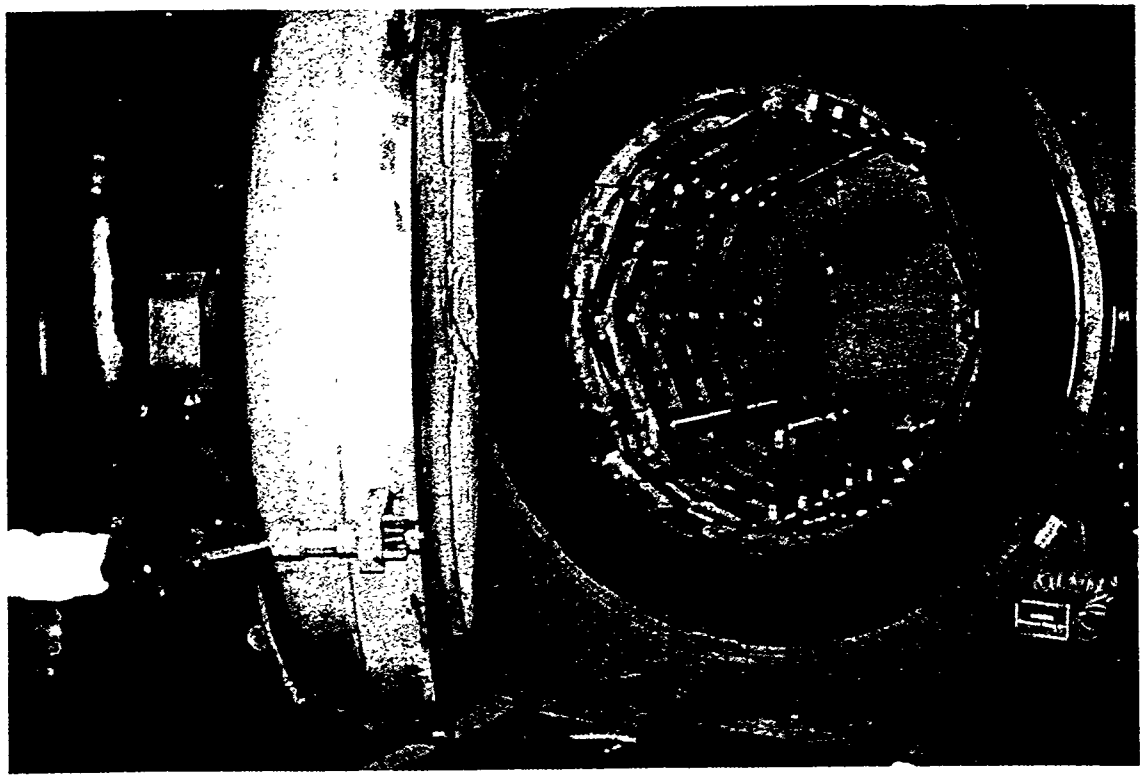

Die #4 Ready for the 5 bar Furnace at FPM

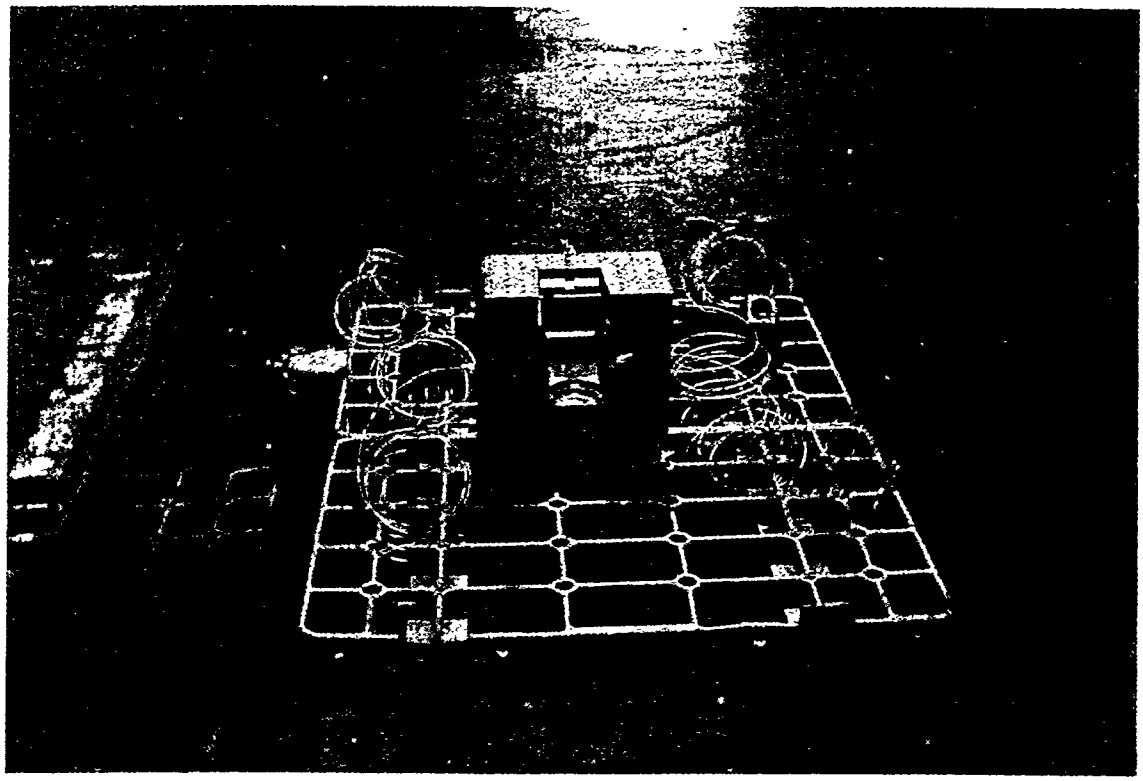

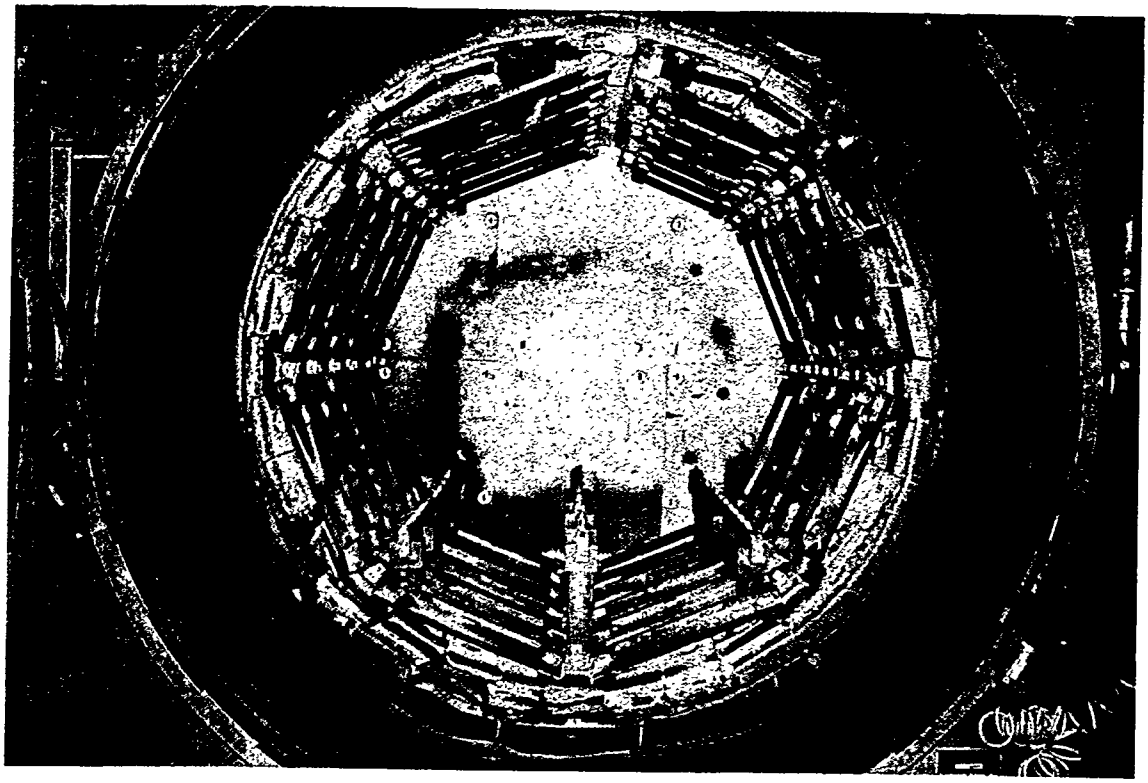

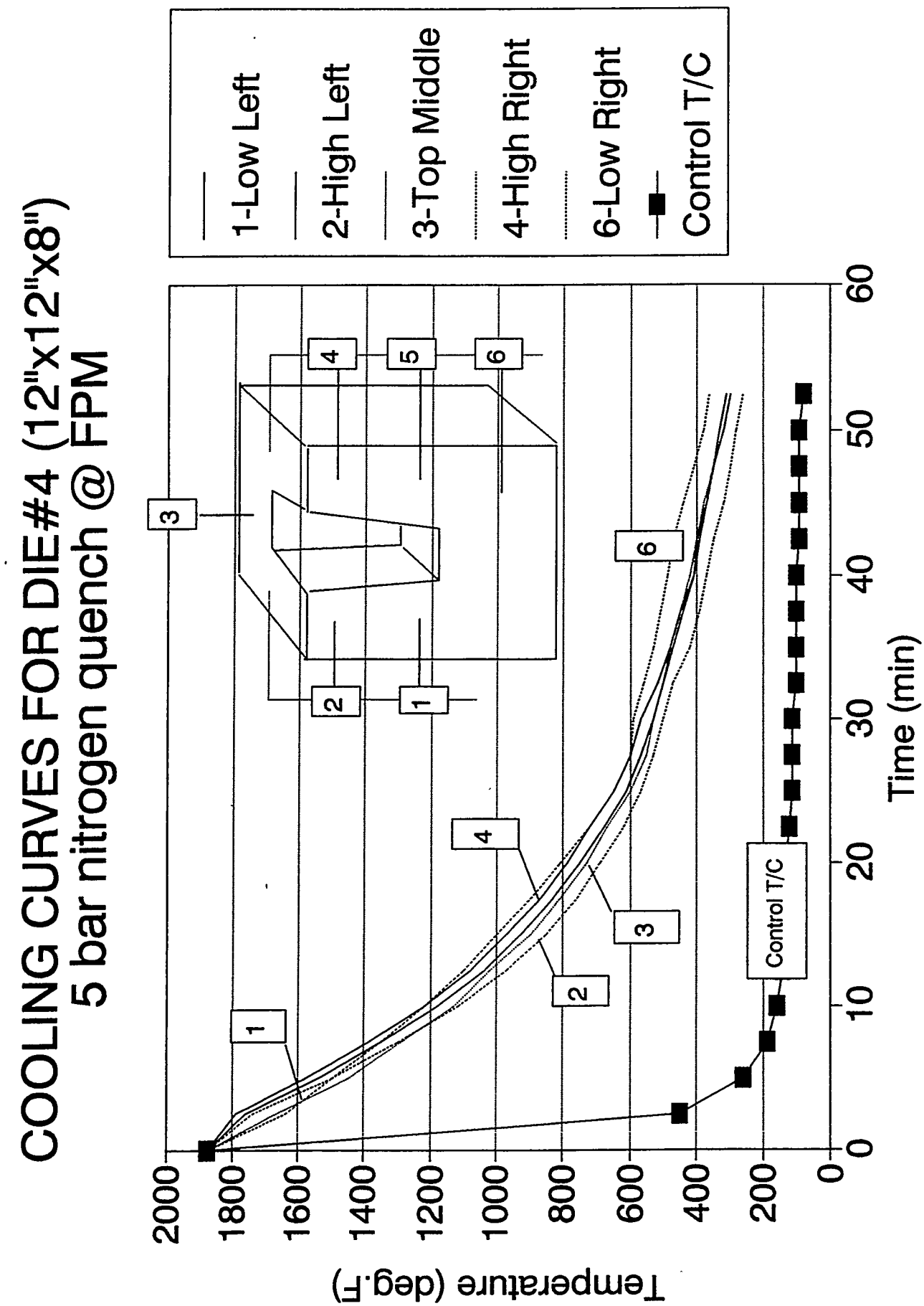
COOLING CURVES FOR DIE#4 (12"x12"x8")
5 bar nitrogen quench @ FPM
1-Low Left
2-High Left
3-Top Middle
4-High Right
6-Low Right
Control T/C
Temperature (deg.F)
Time (min)
2000
1800
1600
1400
1200
1000
800
600
400
200
0
0
10
20
30
40
50
60
1
2
3
4
5
6
Control T/C

The 10 bar Furnace at FPM Heat Treating

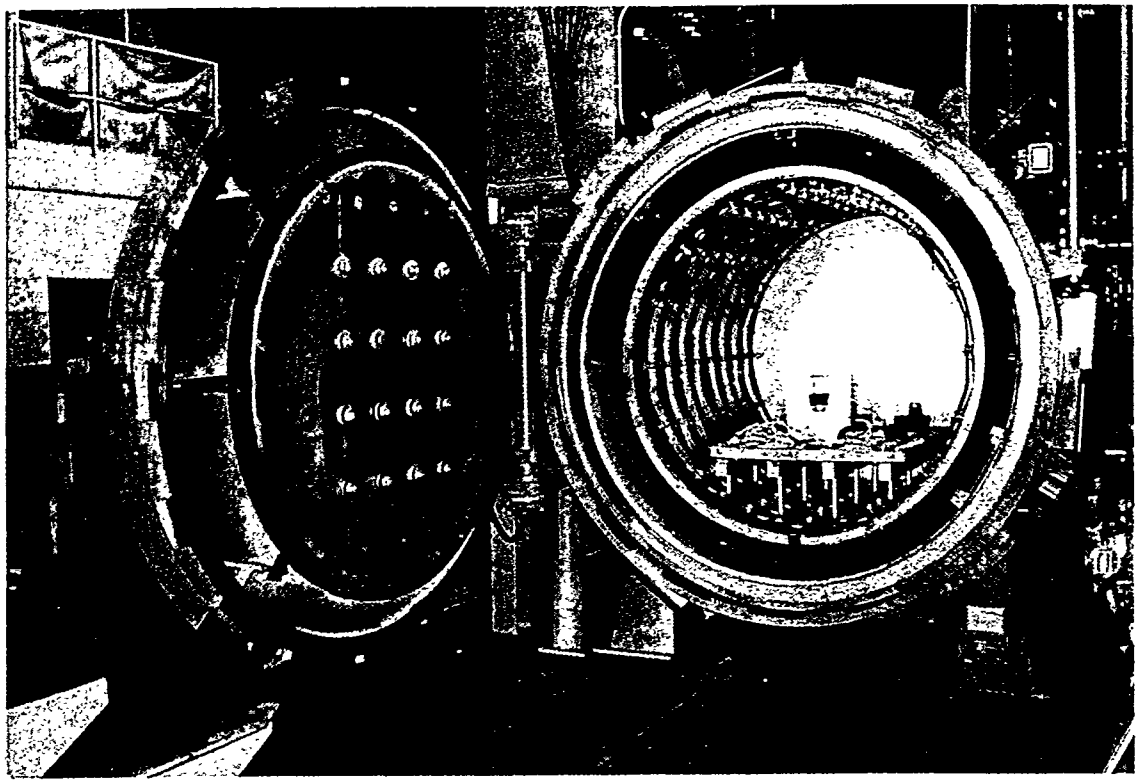

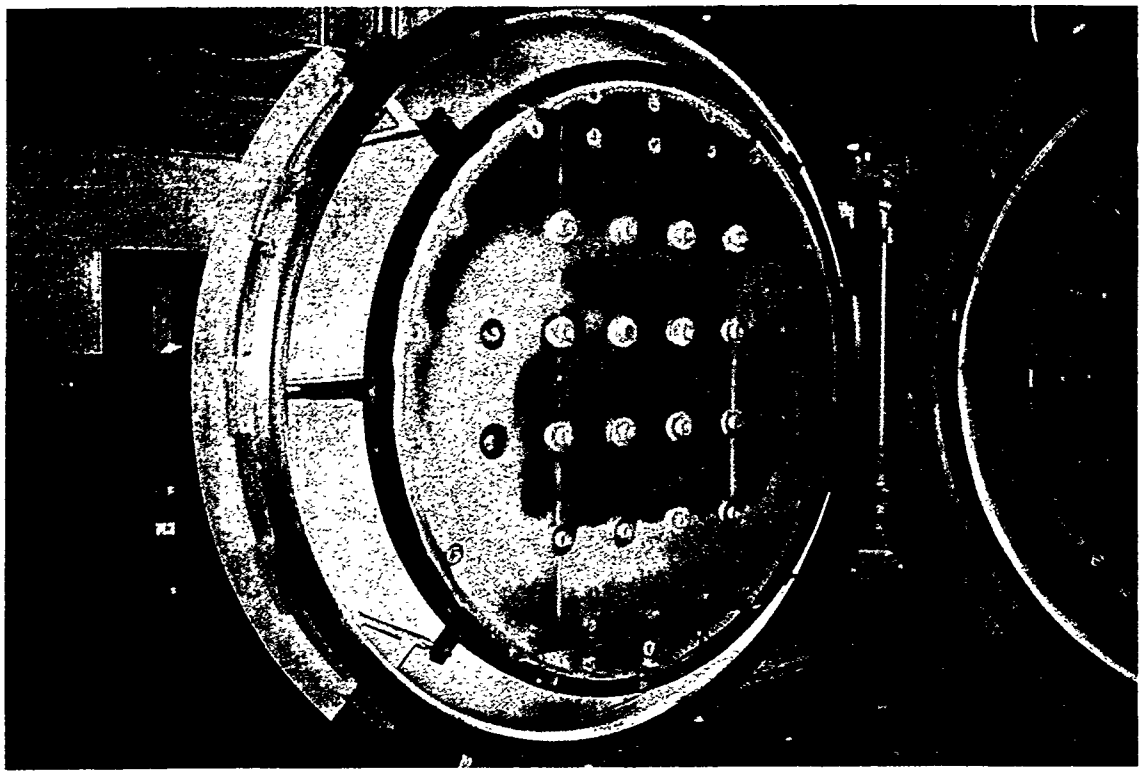

Die #5 in the 10 bar Furnace at FPM

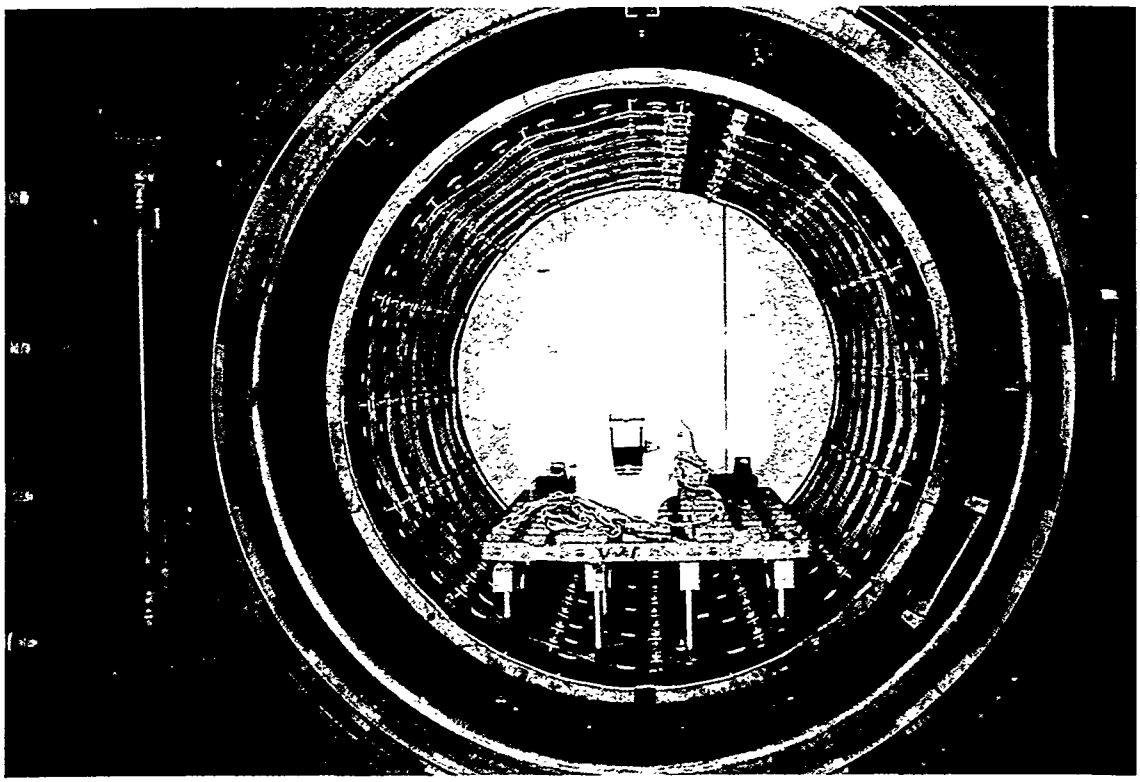

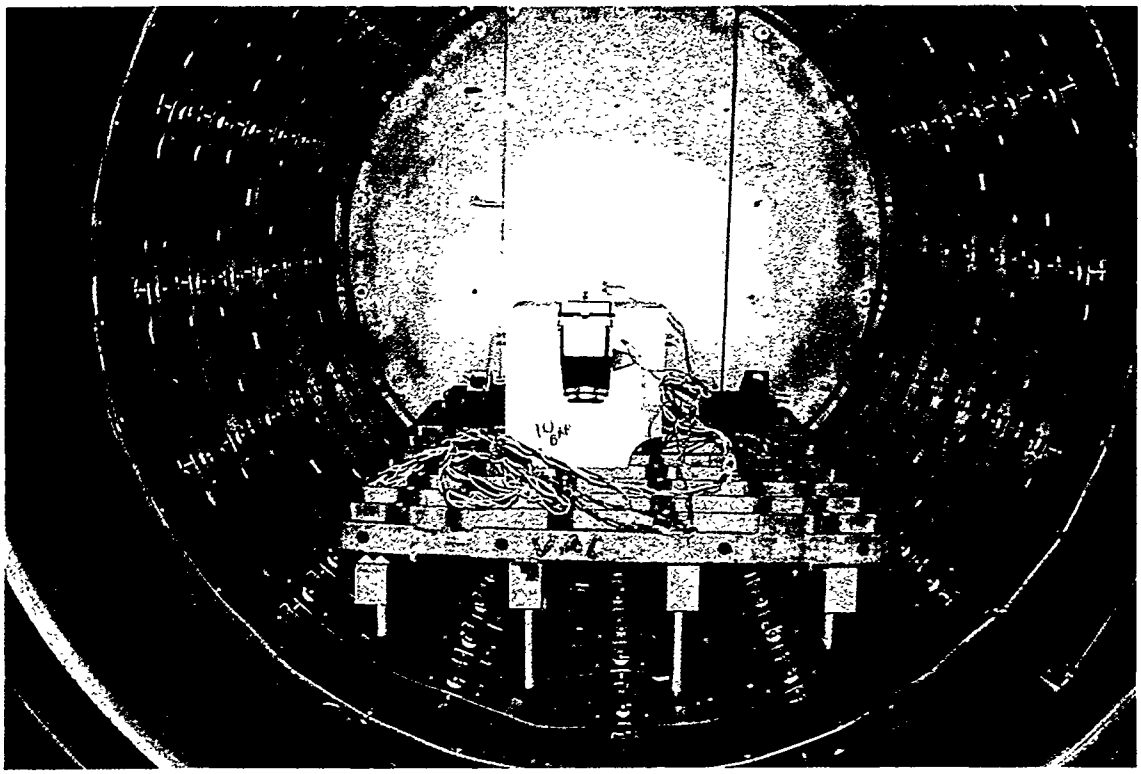

COOLING CURVES FOR DIE#5 (12"x12"x8")
7.5 bar nitrogen quench @ FPM

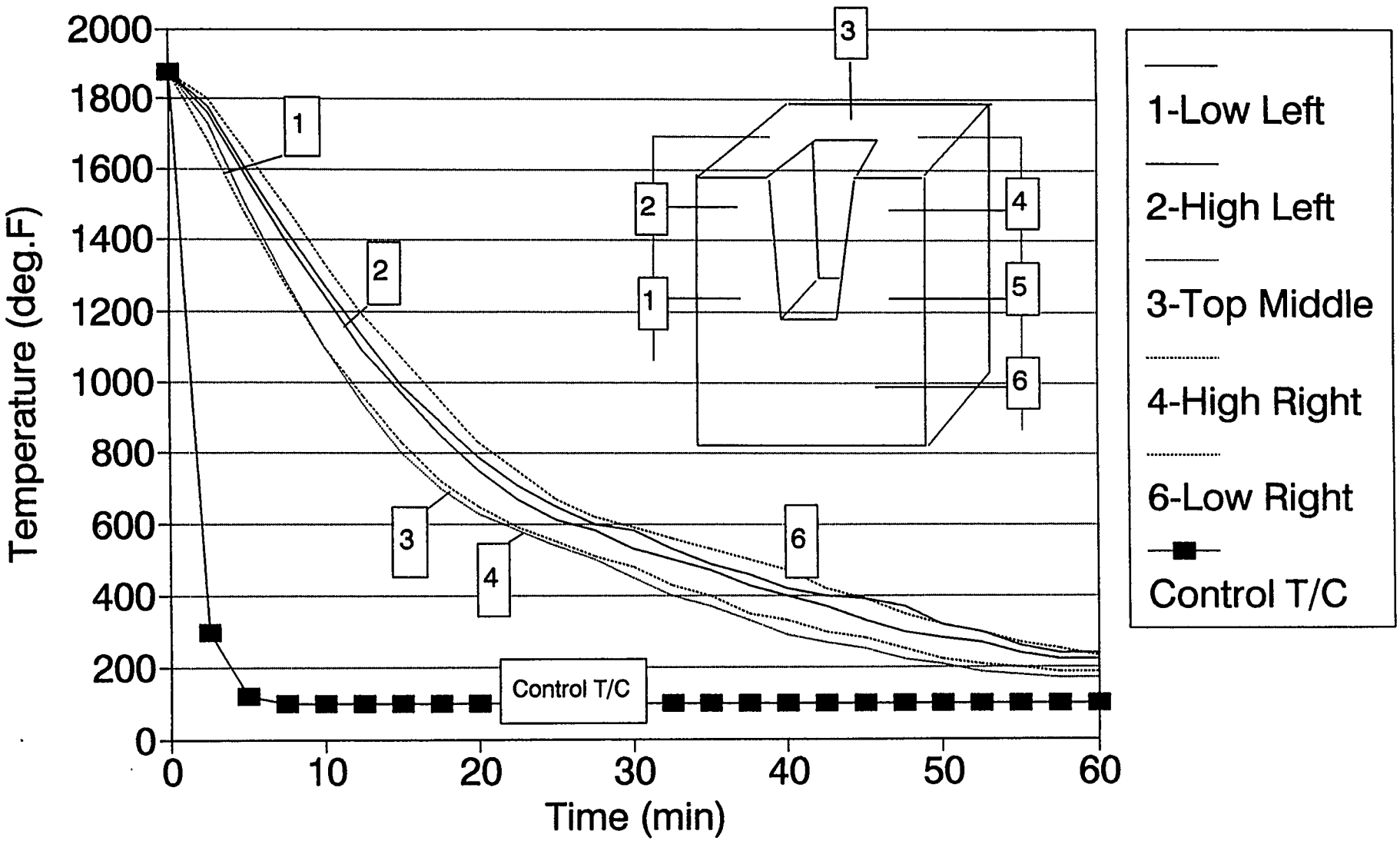

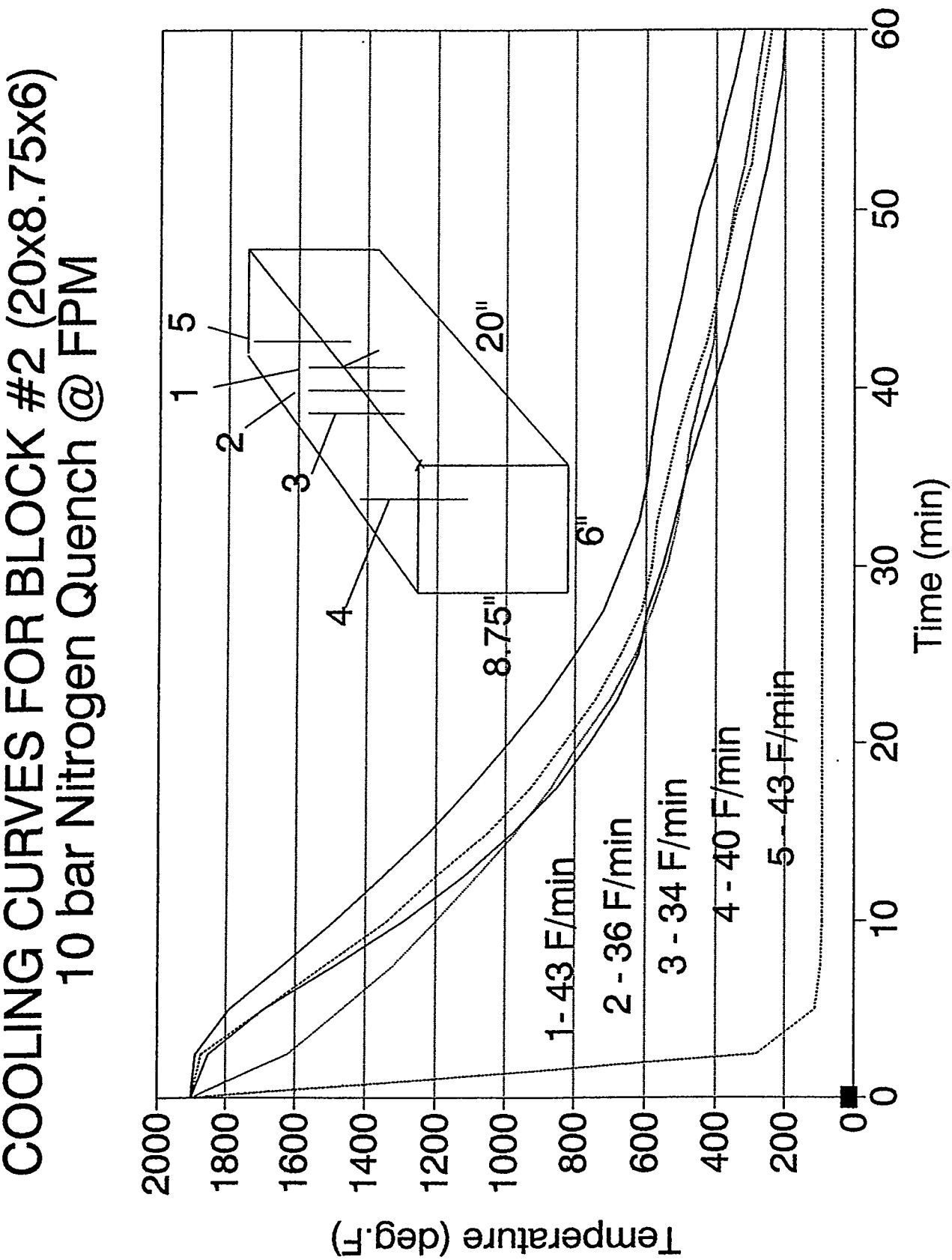
COOLING CURVES FOR BLOCK #2 (20x8.75x6)
10 bar Nitrogen Quench @ FPM
Temperature (deg.F)
Time (min)
2000
1800
1600
1400
1200
1000
800
600
400
200
0
0
10
20
30
40
50
60
1
2
3
4
5
20"
8.75"
6"
1- 43 F/min
2 - 36 F/min
3 - 34 F/min
4 - 40 F/min
5 - 43 F/min

Surface Plot of Block 2 - Side1
After 10 Bar Nitrogen Quench

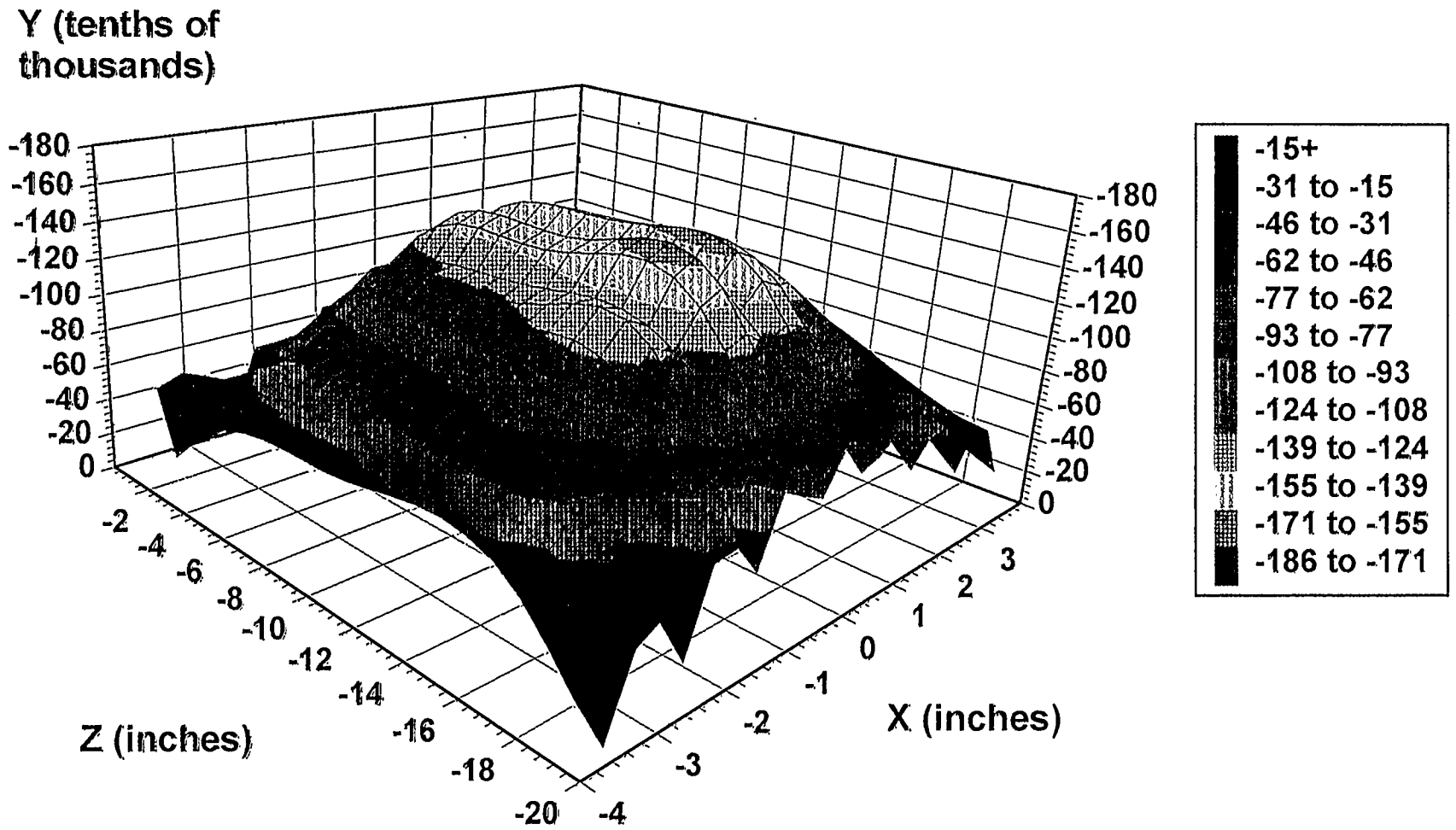

Contour Plot of Block 2 - Side 1
After 10 Bar Nitrogen Quench

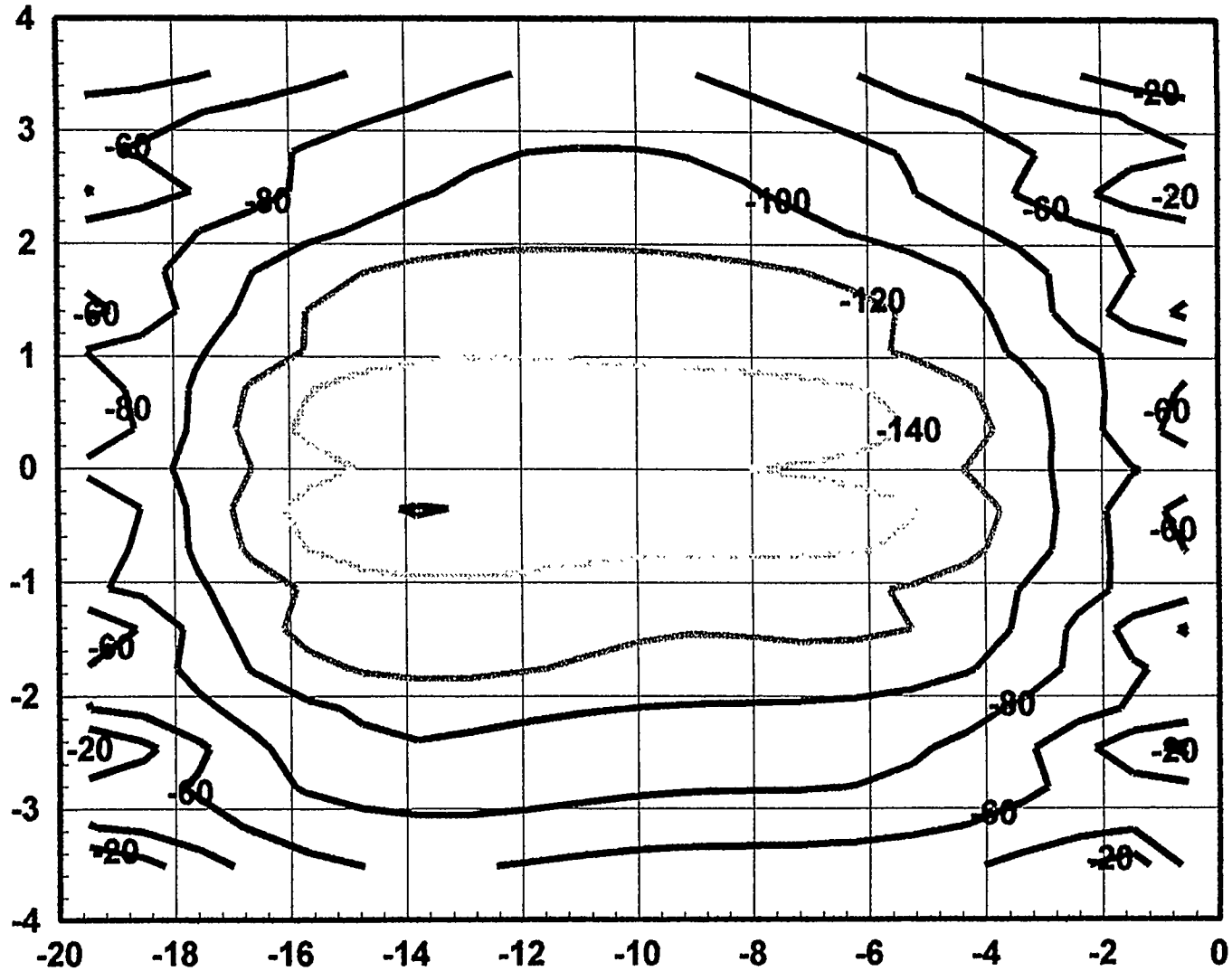

Surface Plot of Block 2 - Side 2
After 10 Bar Nitrogen Quench

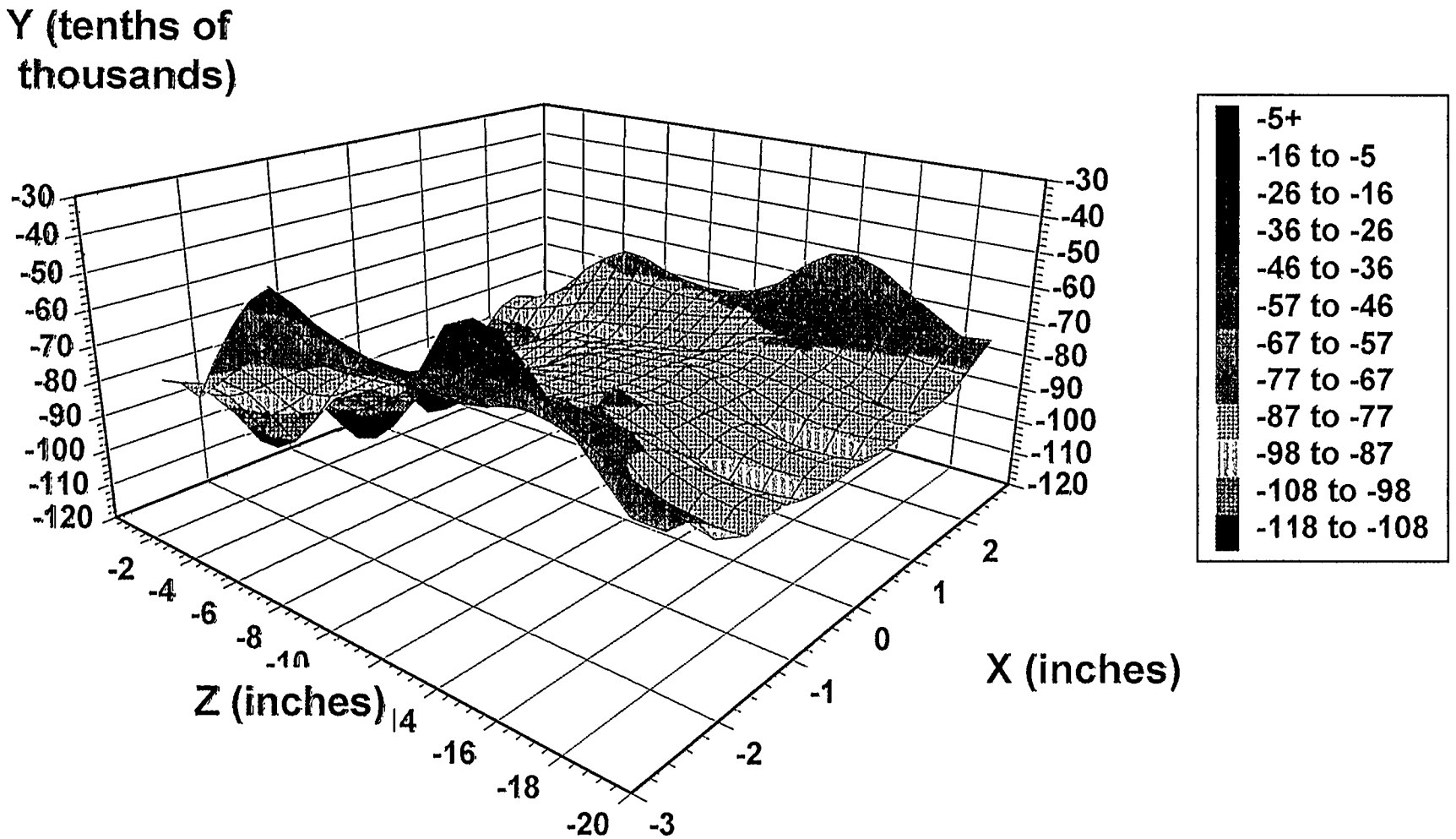

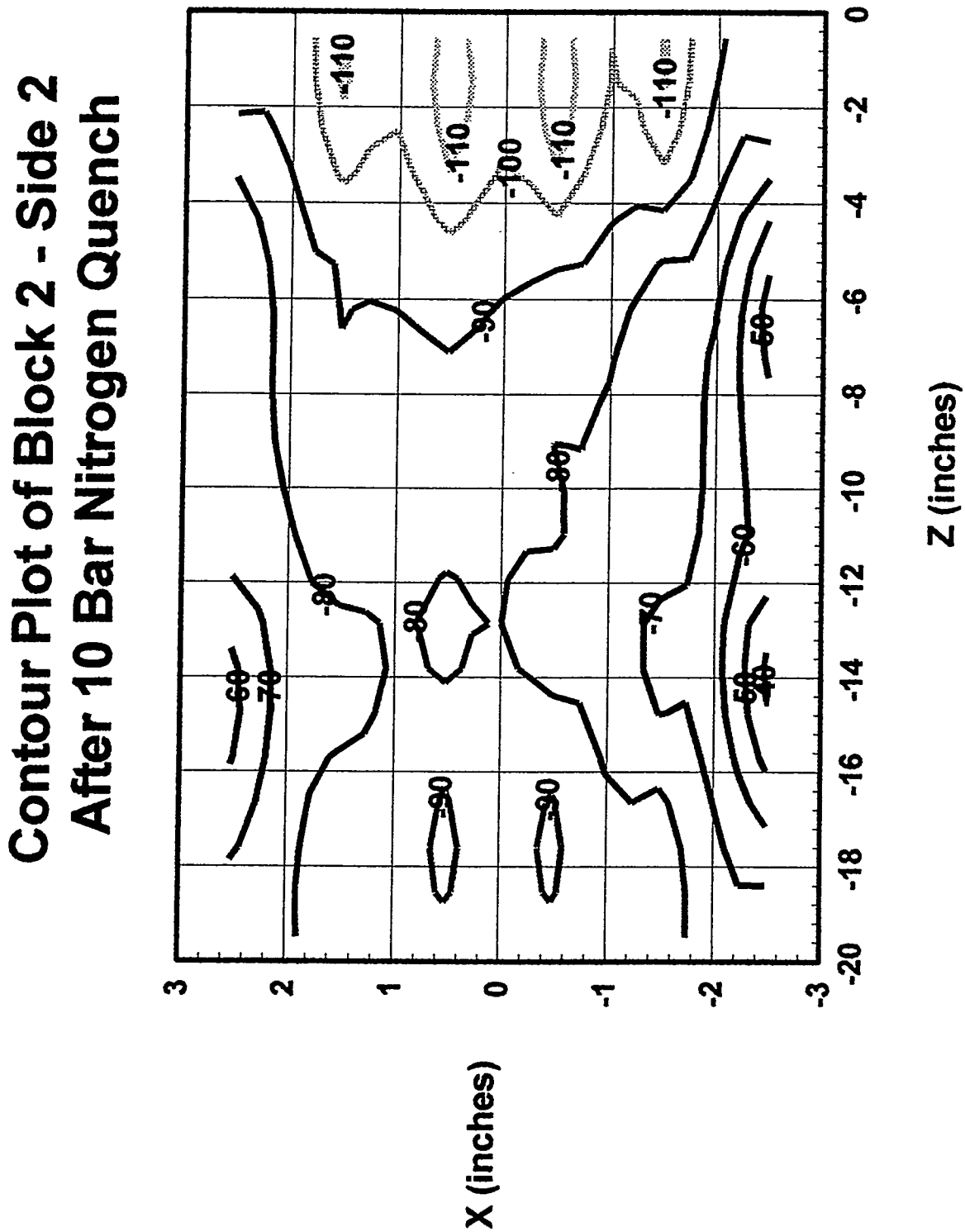
Contour Plot of Block 2 - Side 2
After 10 Bar Nitrogen Quench
X (inches)
Z (inches)
3
2
1
0
-1
-2
-3
0
-2
-4
-6
-8
-10
-12
-14
-16
-18
-20
-60
-70
-80
-90
-100
-110

Vector Plot of Side 1 - Block 2(20"x8"x6.75")
10 bar nitrogen quench @FPM

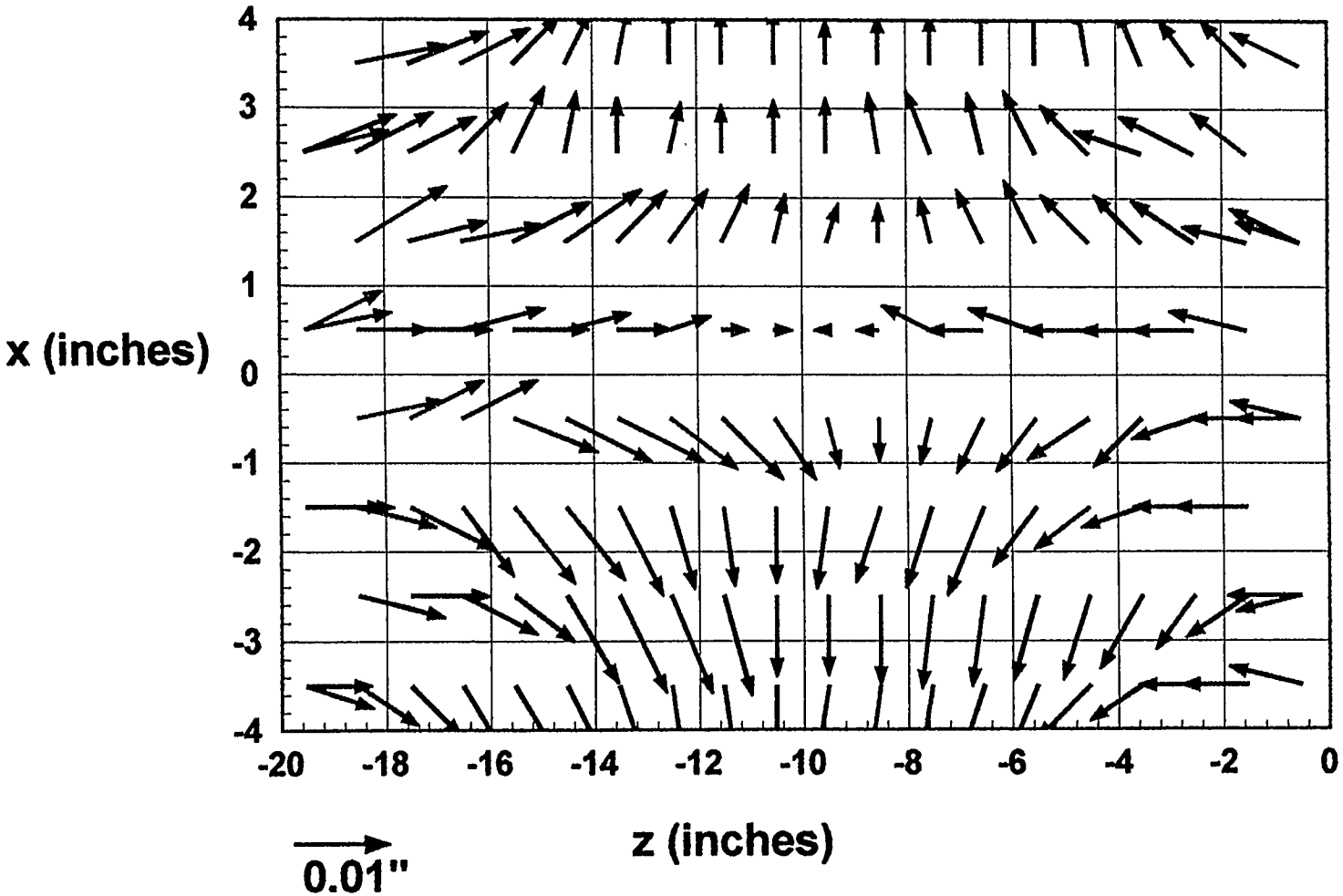

Shows the direction and magnitude of x-z move for every point on Side 1 as a result of the quench

COOLING CURVES FOR BLOCK #3 (20x8x6.75)
10 bar interrupted quench @ FPM

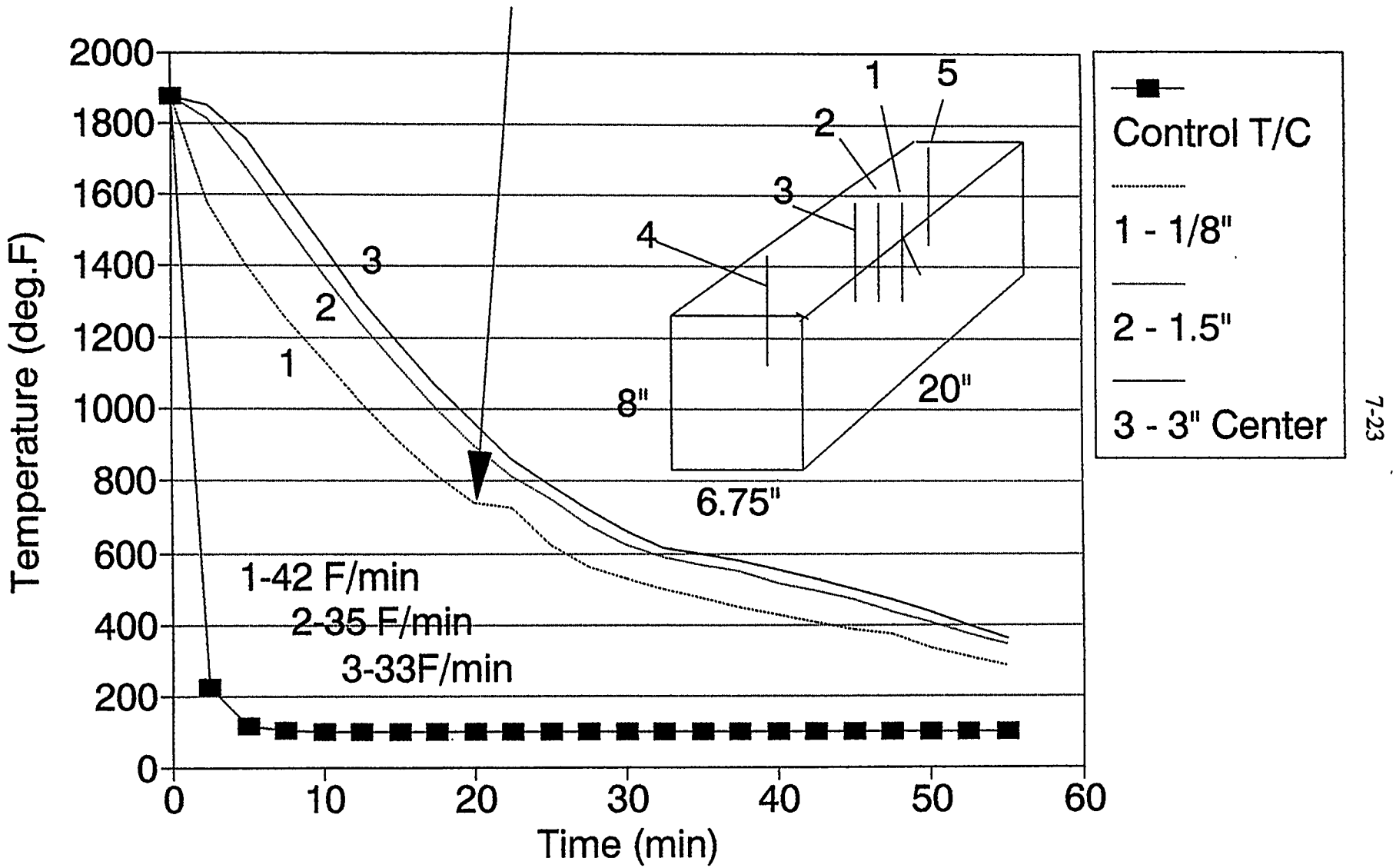

Surface Plot of Block 3 - Side 1
After 10 Bar Interrupted Quench at FPM

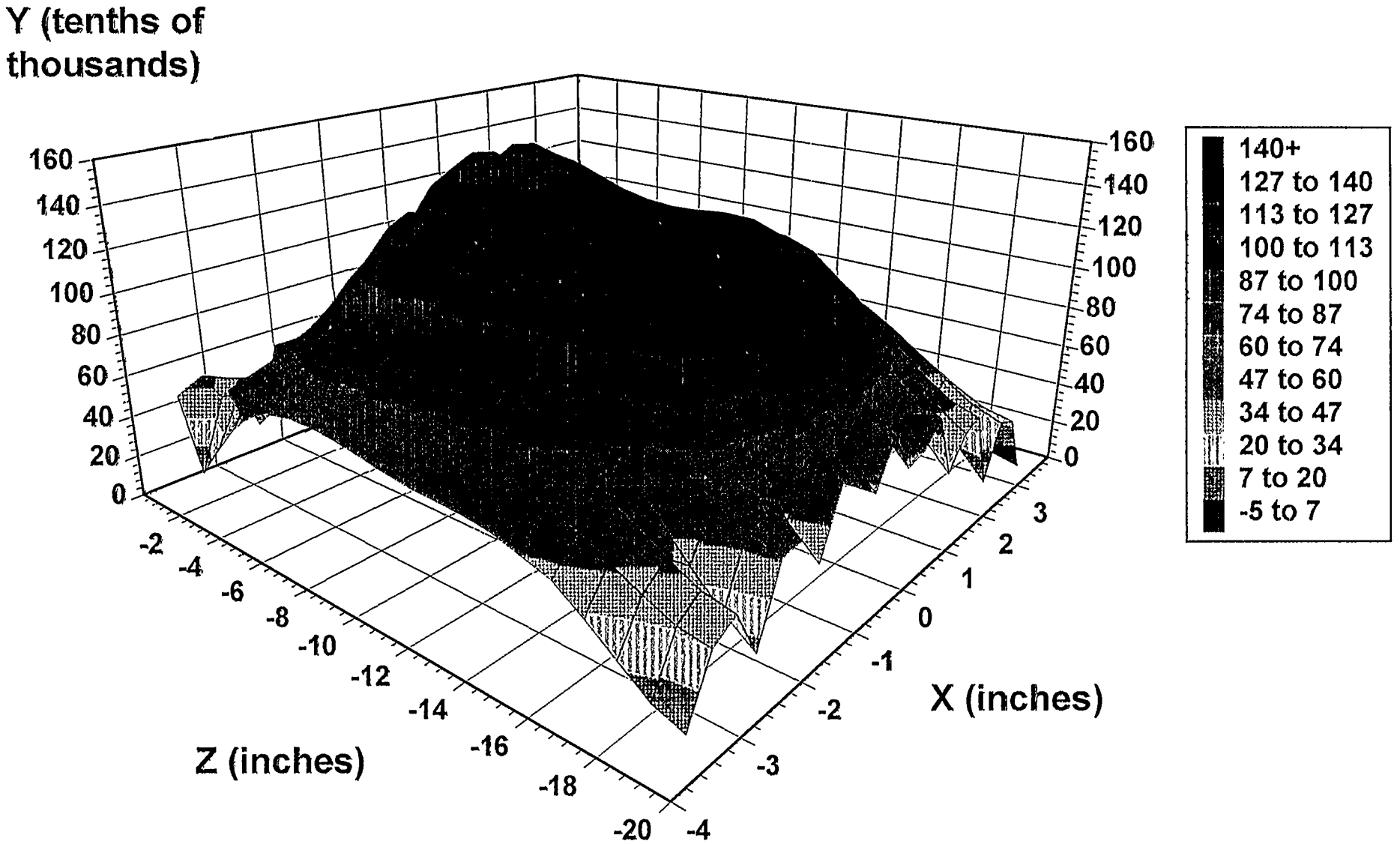

Contour Plot of Block 3 - Side 1
After 10 Bar Interrupted Quench at FPM

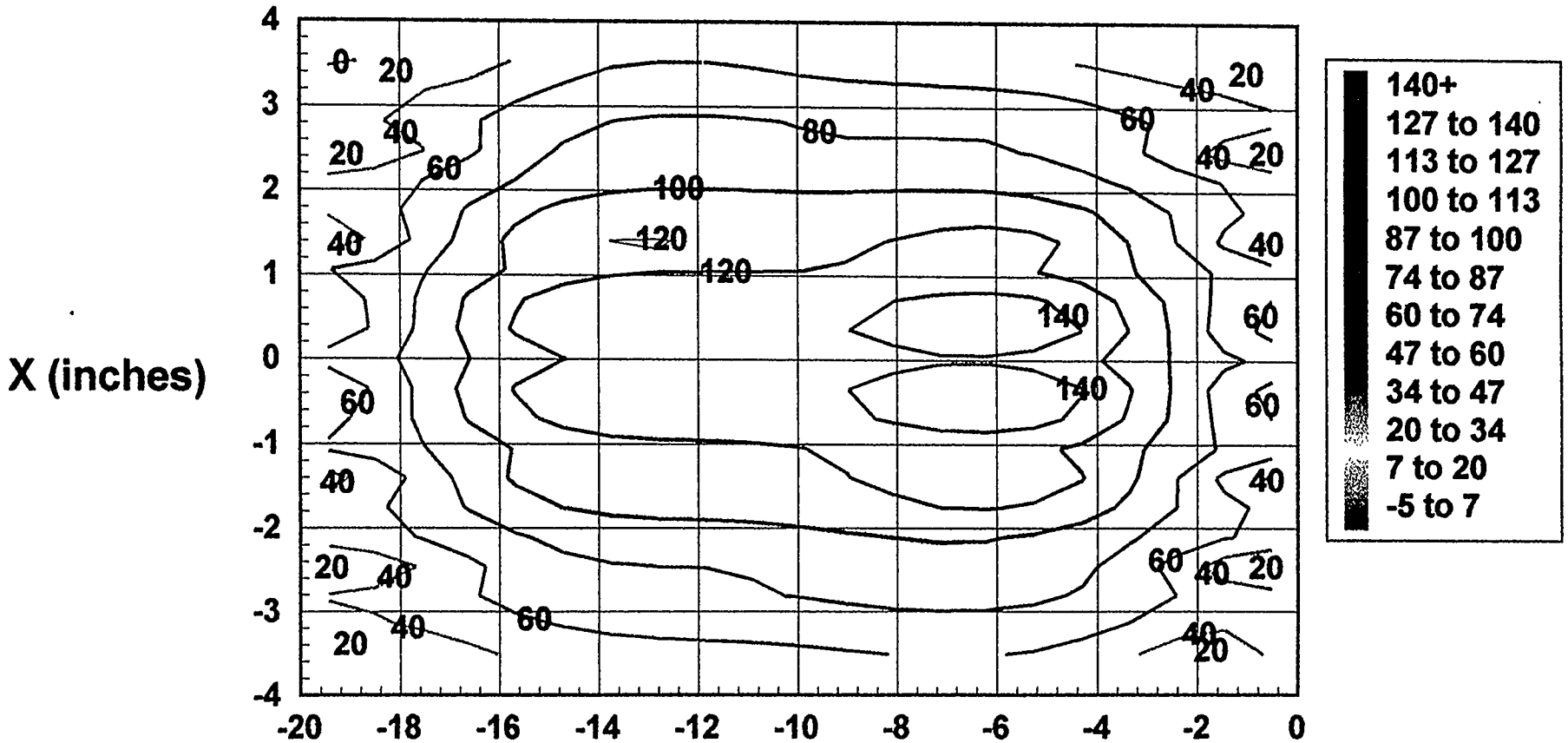

Vector Plot of Side 1 - Block 3(20"x8"x6.75")
10 Bar Nitrogen Interrupted Quench @FPM

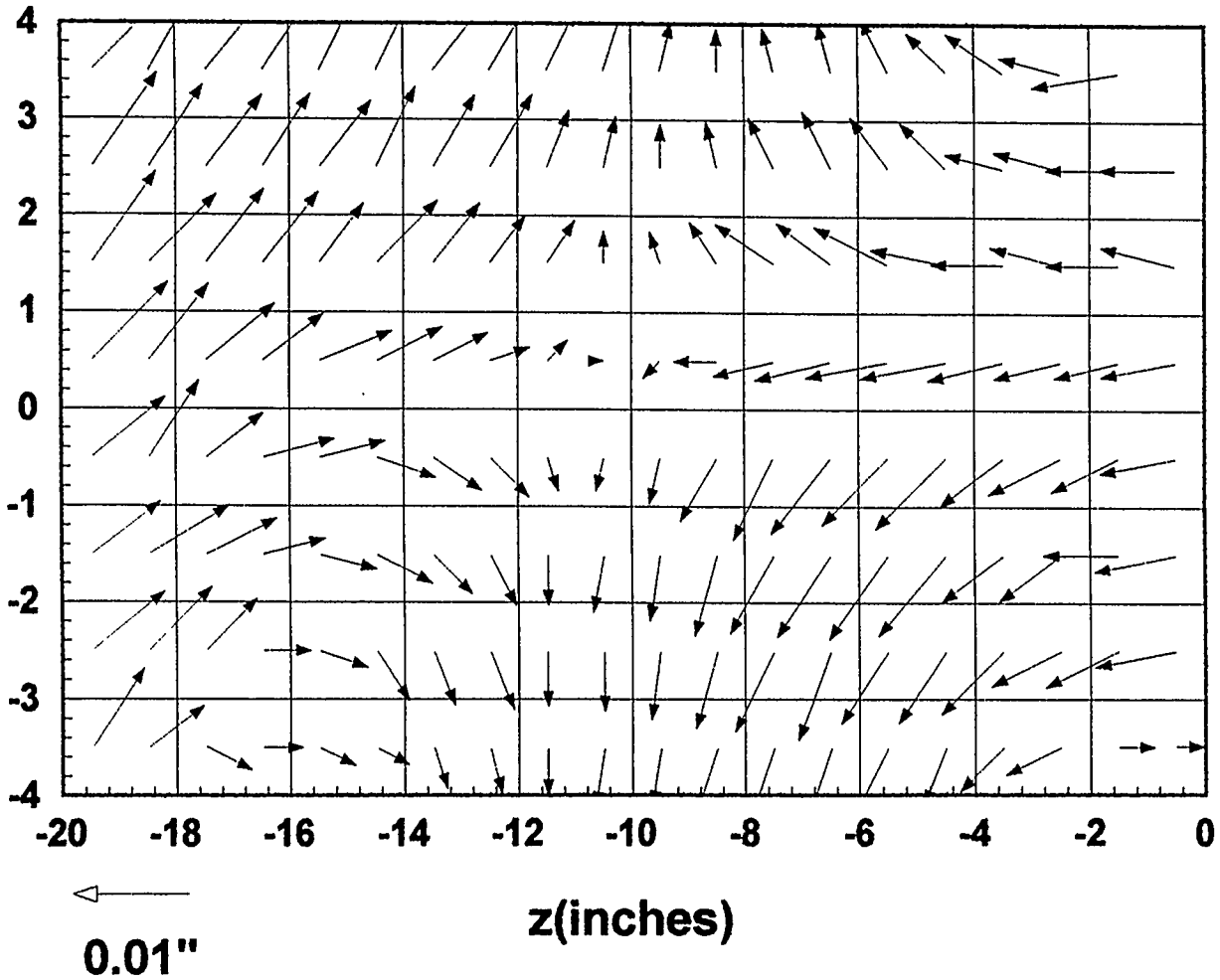

Shows the direction and magnitude of the x-z move for every point on Side 1 as a result of the quench

HEAT TREATING CYCLE FOR BLOCK #5 (20"x8.75"x6")

20 bar Nitrogen + Helium quench @ Kowalski

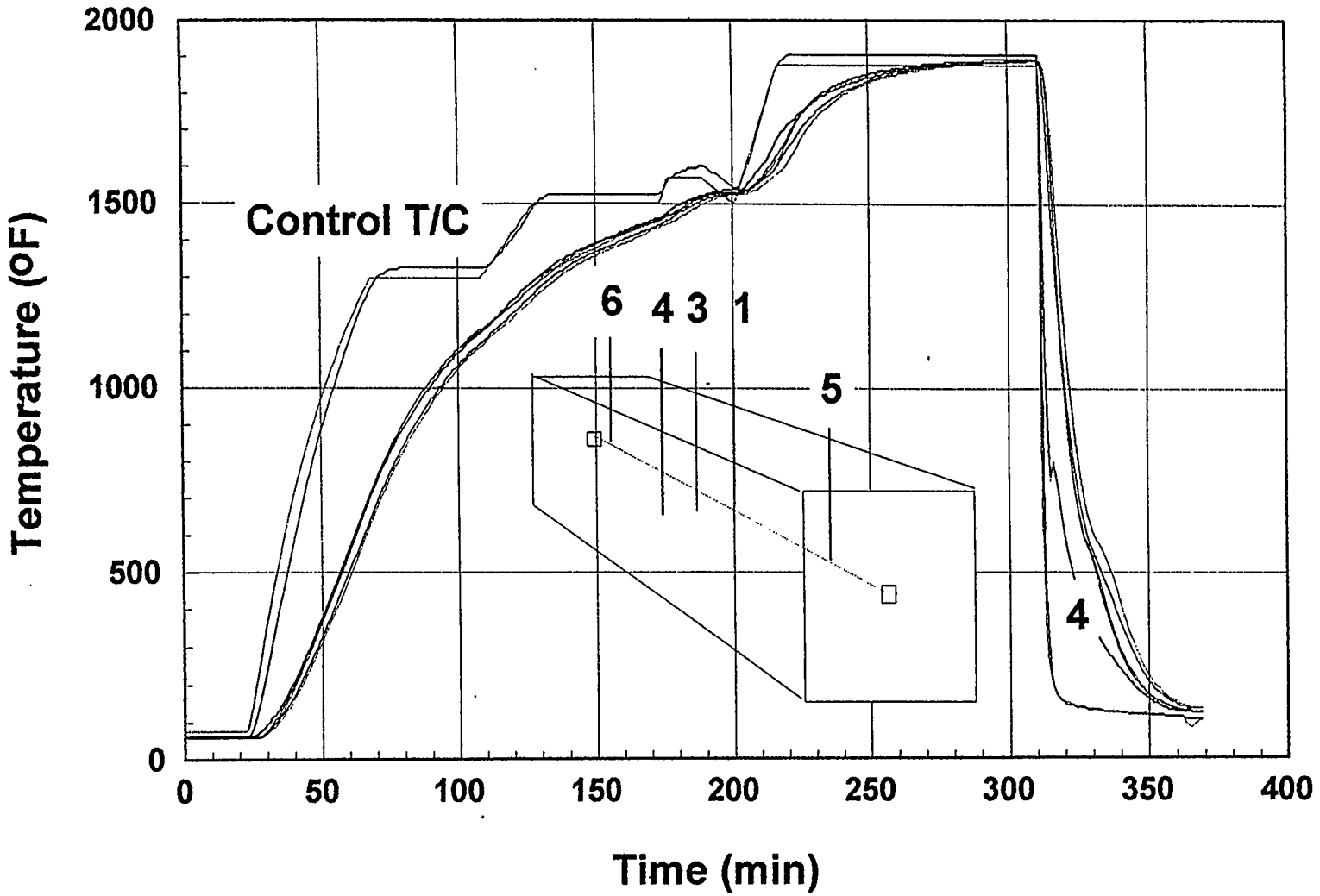

1 - center (3"), 3 - mid (1.5"), 4 - surface (1/8"), 5,6 - ends (3")

1 - center = 62°F/min 4 - surface (1/8") = 126°F/min

COOLING CURVES FOR BLOCK #5 (20"x8.75"x6")

20 bar Nitrogen + Helium quench @ Kowalski

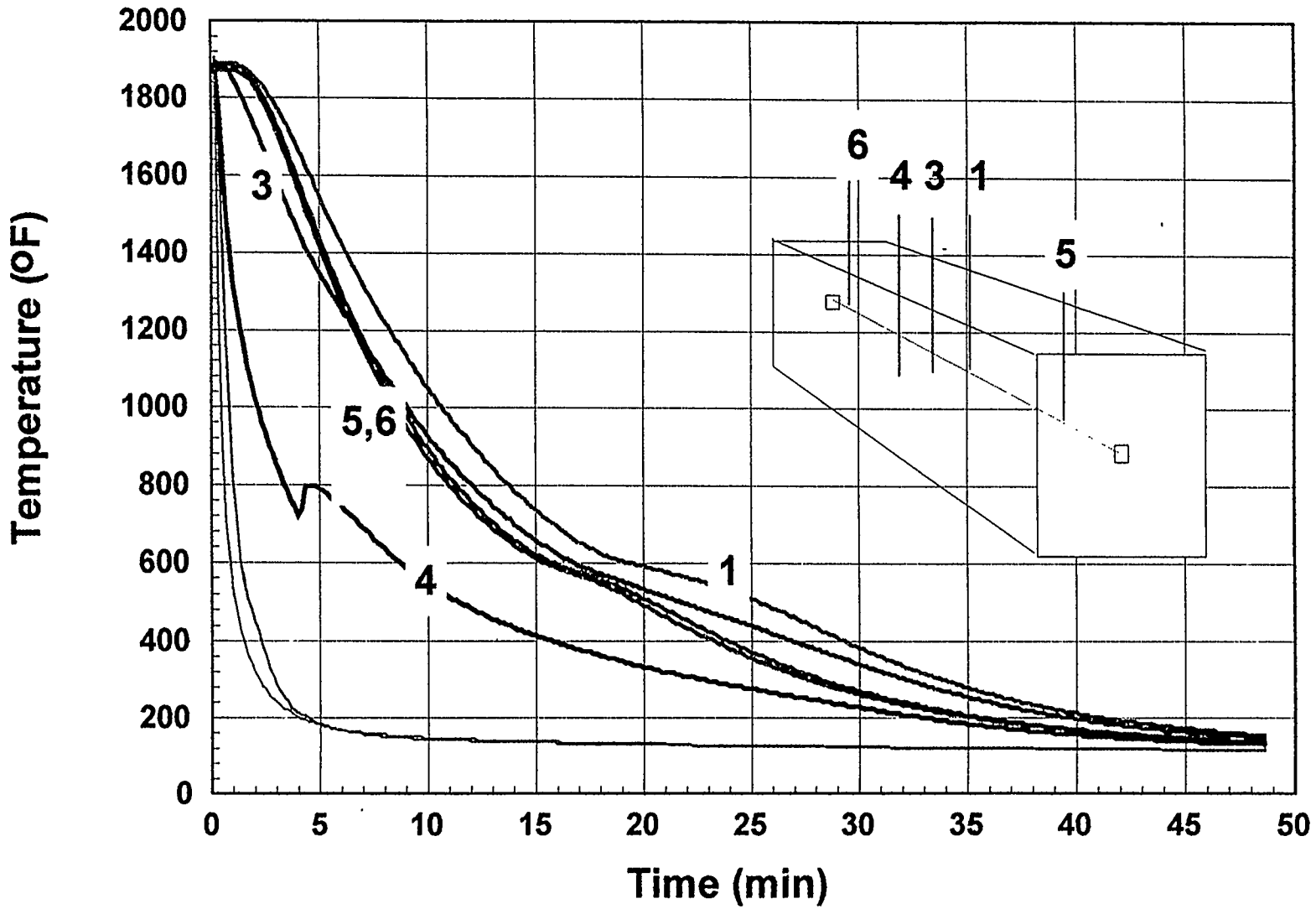

1 - center (3"), 3 - mid (1.5"), 4 - surface (1/8"), 5,6 - ends (3")

1 - center = 62°F/min 4 - surface (1/8") = 126°F/min

Surface Plot of Block 5 Side 1
20 bar Nitrogen+Helium @ Kowalski

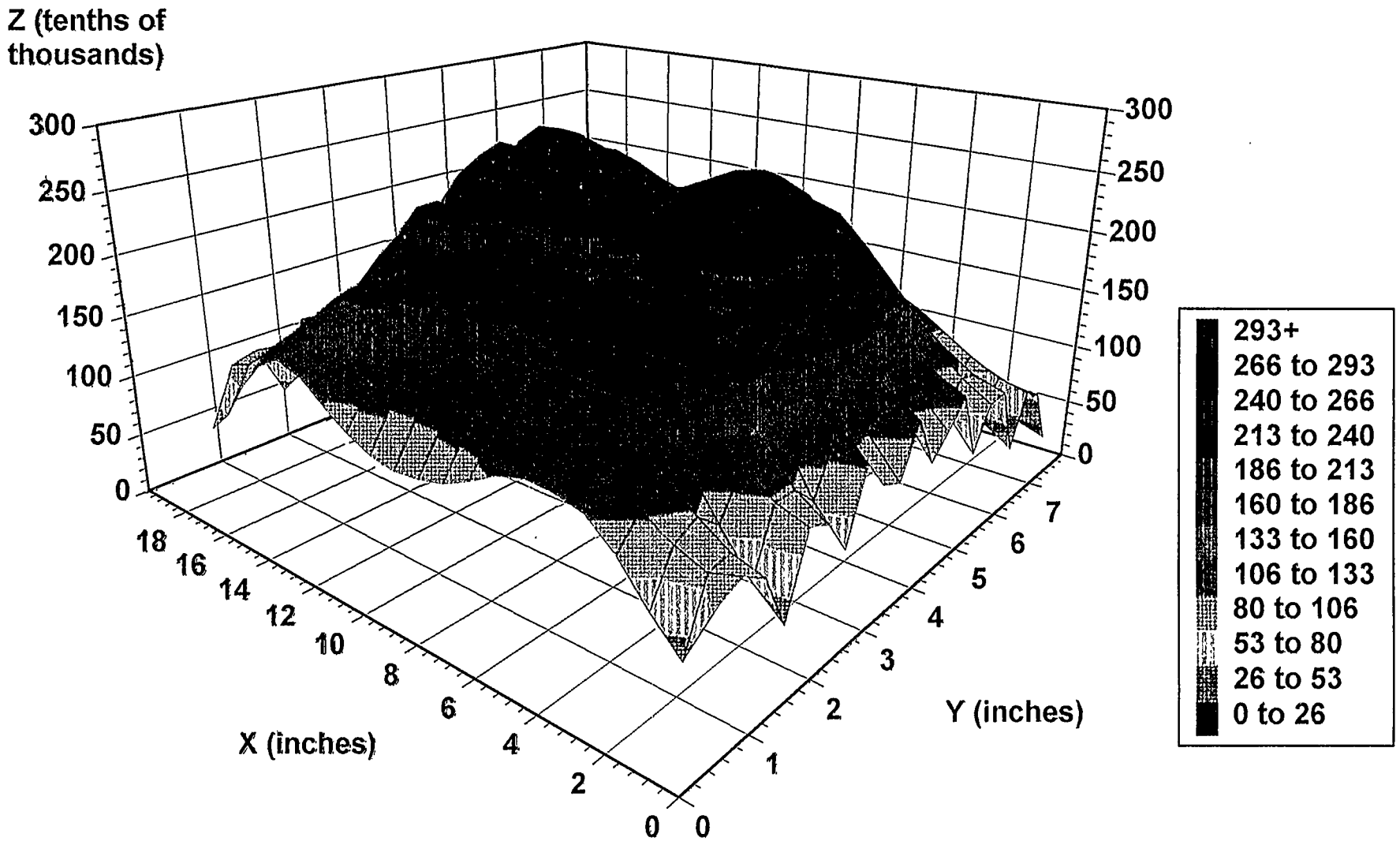

Surface Plot of Block 5 Side 2
20 bar Nitrogen+Helium @ Kowalski

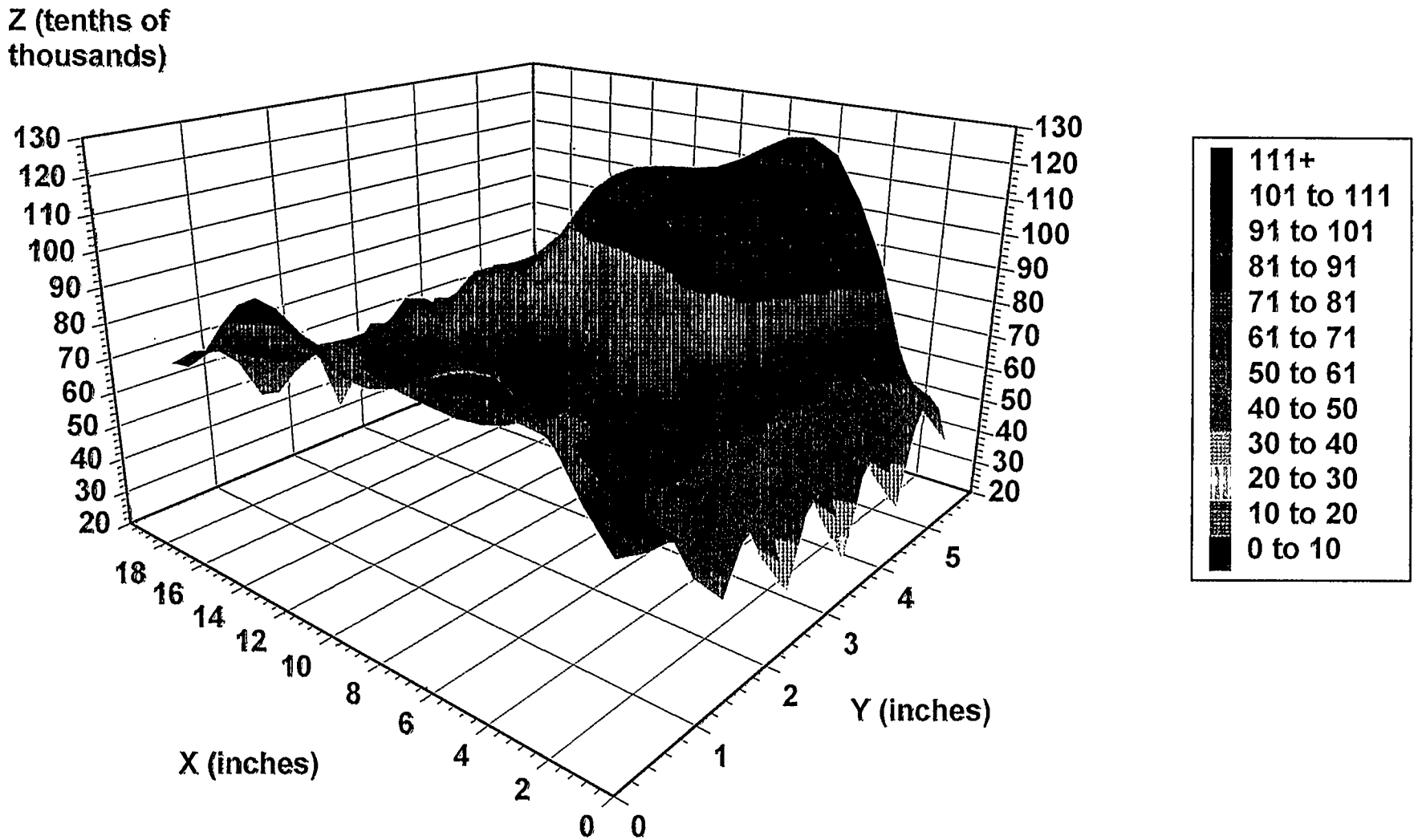

Surface Plot of Block 5 Side 3
20 bar Nitrogen+Helium @ Kowalski

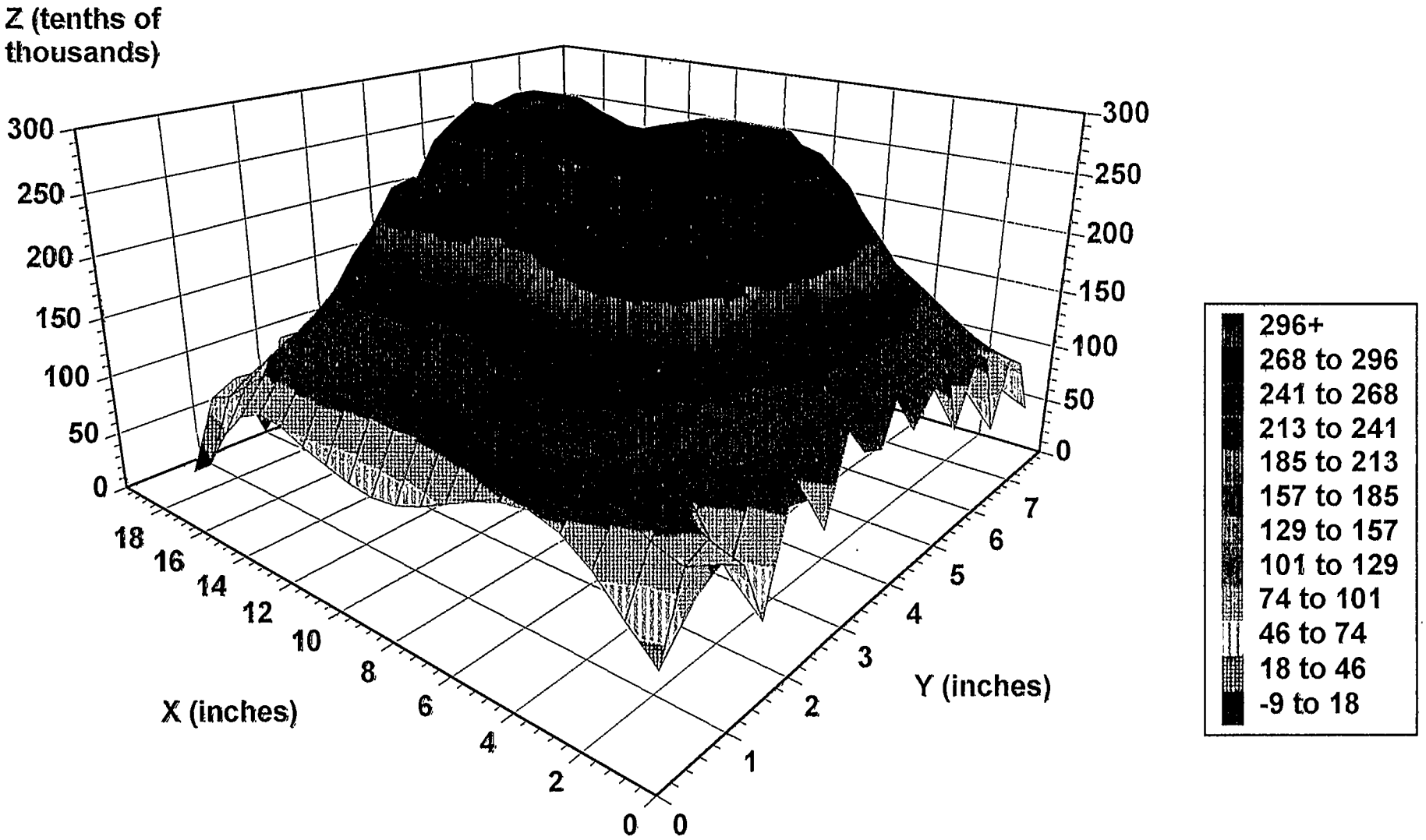

Surface Plot of Block 5 Side 4
20 bar Nitrogen+Helium @ Kowalski

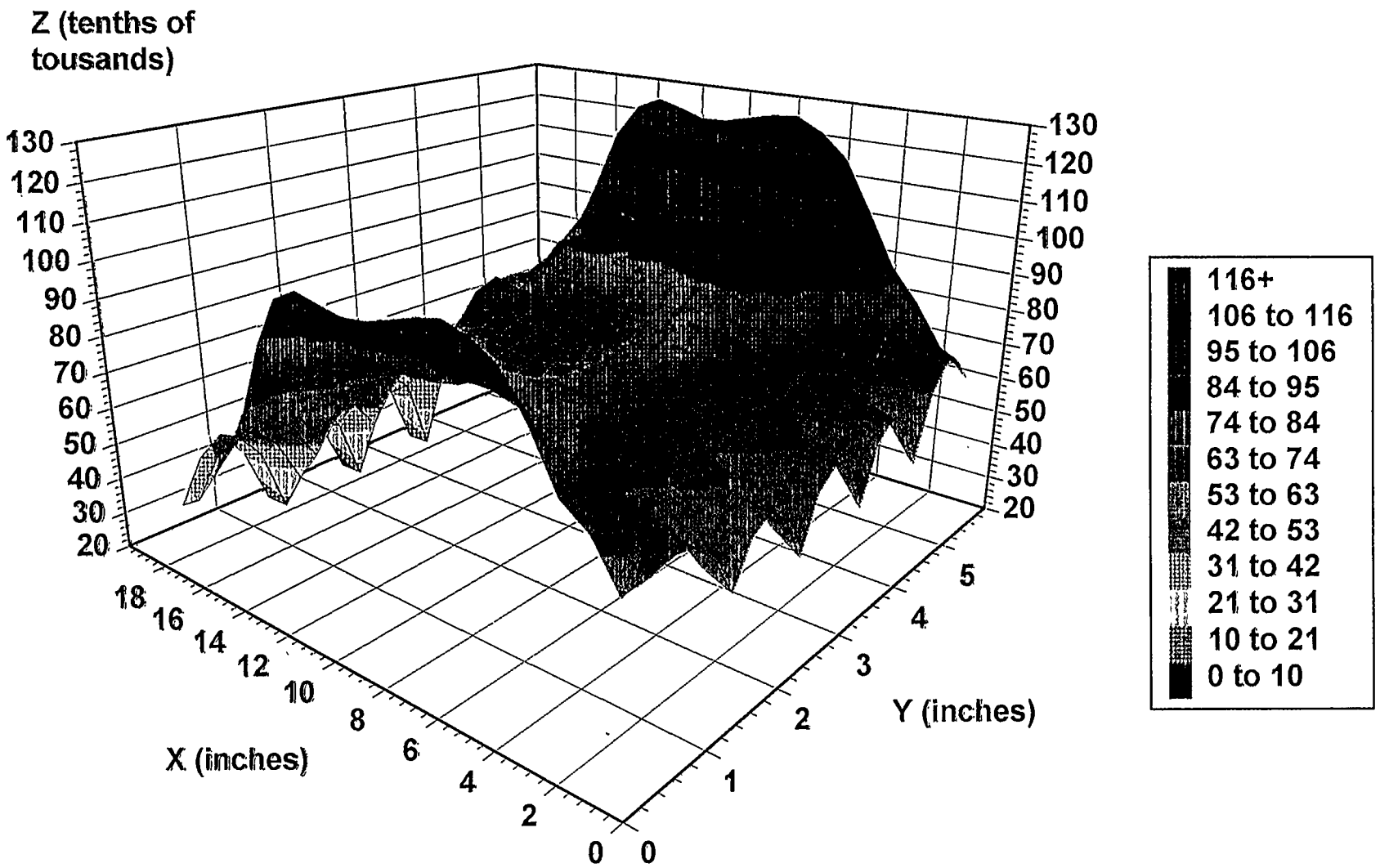

BLOCK 6 (20.25"x9.25"x7.12") - INTERRUPTED OIL QUENCH @EHT

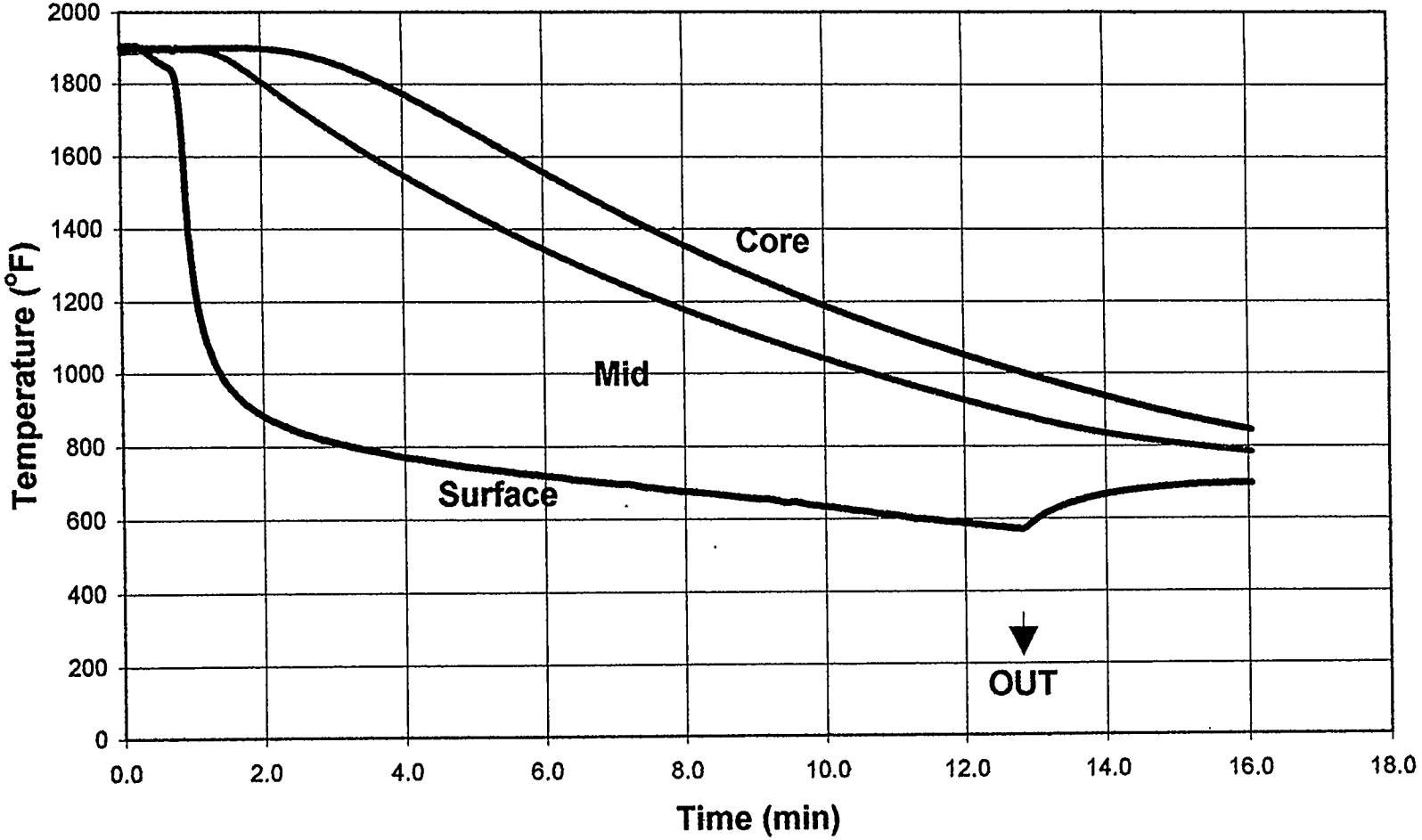

Surface (1/8") cooling rate in the 1750° F- 550° F range = 120° F/min

BLOCK #6 (20.25"x9.25"x7.12") - INTERRUPTED OIL QUENCH @EHT

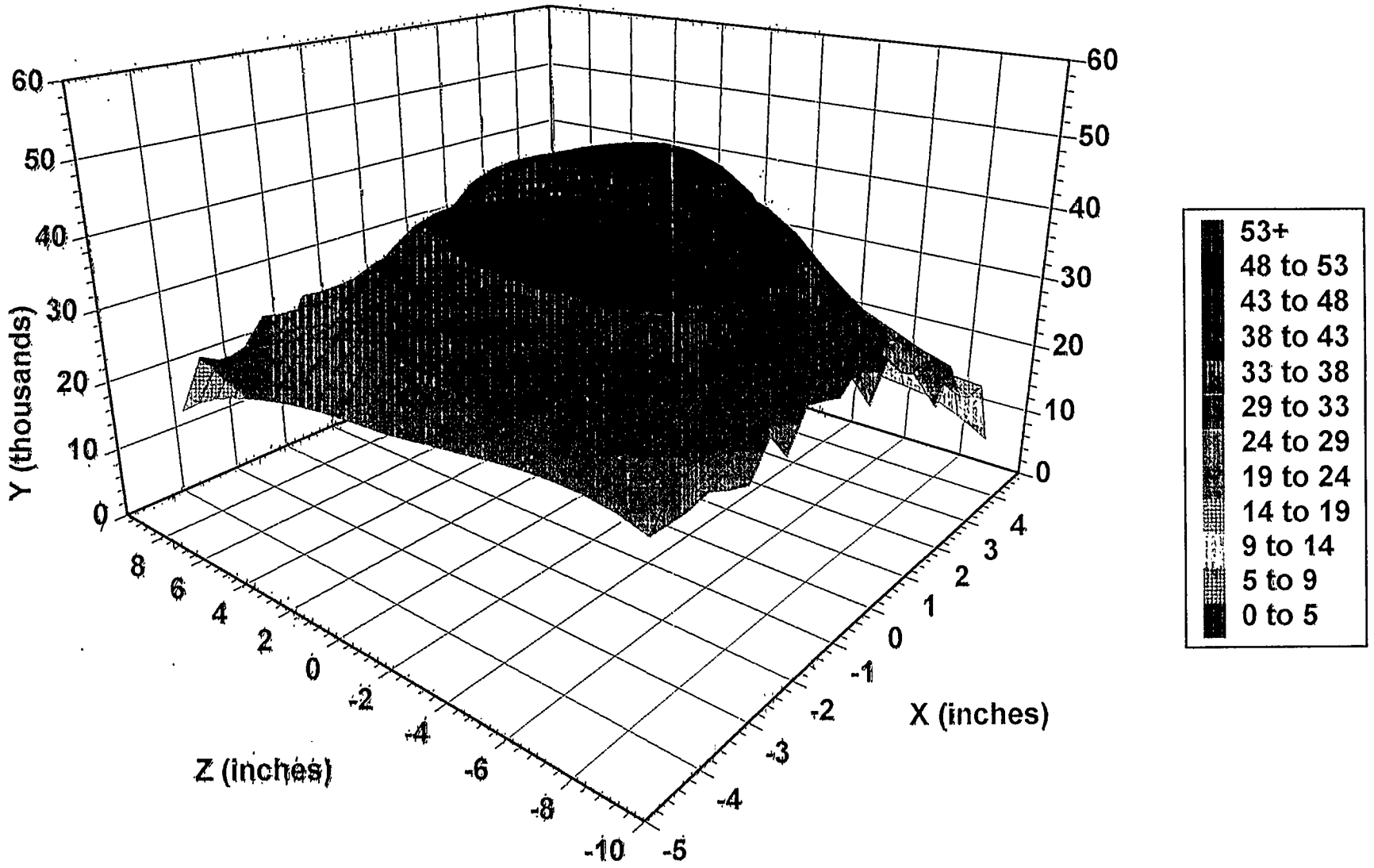

The large face of the block bulges 0.048" above the corners.
The block is 0.030" shorter than before the quench.

7.4 Summary of Cooling Rates Measurements

The cooling rates measured in the vacuum/gas quenching experiments of the block and the dies are summarized in Table 7.1. The purpose of the measuring cooling rates at different locations in the dies is to validate the prediction of the FEA models. Also, to evaluate the cooling rates attainable with state of the art gas quenching methods.

The gas pressure employed during the quench is only one factor that determines the cooling rate. Other factors include the size and distribution of the gas nozzles, the power of the fan and the size of the furnace. The Abar Ipsen furnaces utilized in this project is the largest. The VFS furnace is a medium size furnace. The Seco Worwick furnace is the smallest. As such, it brings the gas nozzles closer to the part. In conjunction with the higher pressure, it achieves the fastest quench rate. The oil quench was conducted to provide a baseline both for quenching rates and for distortion.

It should be noticed that the surface cooling rates are more responsive to the pressure of the gas quenching than the core cooling rates. The reason for this slow internal cooling rate is the finite conductivity of the steel. While for small parts, the "bottleneck" of the heat transfer is the convection, in larger parts the conductivity becomes dominating, limiting the cooling rate. Figure 3.10 highlights this aspect of heat transfer: for 1" diameter part a minor increase in convection results in a very large increase in cooling rate; there is a very small increase for the same increase in convection, if the part is 10" in diameter.

Table 7.1: SUMMARY OF QUENCHING EXPERIMENTS

Part	Heat Treater	Furnace	Pressure	Surface Cooling Rate (°F/min)	Core Cooling Rate(°F/min)	Quenchant
Block #1	Universal HT	Abar-Ipsen	2 bar	39	30	Nitrogen
Die #2	Universal HT	Abar-Ipsen	2 bar	37	26.2	Nitrogen
Die #3	IMP, London	Abar-Ipsen	4 bar	37.5	28.6	Argon
Die #4	FPM, Chicago	Abar-Ipsen	5 bar	48	36	Nitrogen
Die #5	FPM, Chicago	VFS	7.5 bar	52	40	Nitrogen
Block #2	FPM, Chicago	VFS	10 bar	43	34	Nitrogen
Block #3	FPM, Chicago	VFS	10 bar	42	33	Nitrogen
Block #5	Kowalski HT	Seco-Warwick	20 bar	126	62	N_2 +He
Block #6	Euclid HT	Oil	oil	120	N/A	Oil

8. Bibliography

1. A. J. Fletcher. Thermal Stress and Strain Generation in Heat Treatment. New York: Elsevier; 1989.

2. Adams J.G. The Determination of Spectra; Emissivities, Reflectivities and Absorptivities of Materials and Coatings . : Northrop Corporation Report; 1961 Aug 3; Nor. 61-189.

3. Allegheny Lundum Steel Corp. Potomac, A Hot Work and Structural Steel AISI Type H-11. . 1972.

4. Andersen, W. T. Die Cost/Die Life = Market (Success or Failure). Proceedings of the Symposium on Tools for Die Casting; Sunne, Sweeden. ; 1983.

5. Aspinwall, D. K.; Radford, M.; Wise, M. L. H. (University of Birmingham (England)). Machining of Hardened AISI H13 Hot Work Die Steel Using Advanced Ceramic Tool Materials. Eurotech Direct '91: Materials and Processes. ; 1991.
A range of carbide, oxide and nitride cutting tool materials have been evaluated in the turning of AISI H13 hot work die steel, heat treated to its typical service hardness of 50/52 HRC. While considerable wear was observed with cemented carbide, sialon and CBN tools, mixed ceramic tools outperformed alumina tools reinforced with 25 vol.% SiC whiskers and pure oxide alumina tools. Whisker reinforced alumina tools were the best under chatter conditions and had greater resistance to fracture than the other oxide tools used.

6. B. Liscic, H. M. Tensi and W. Luty (eds). Theory and Technology of Quenching. Heidelberg: Springer-Verlag; 1992.

7. Barrow B.J. Effect of Selected Surface Treatment, Welding Procedures and Stress Relieving on the Thermal Fatigue Behavior of H13 Steel for Aluminum Die Casting Dies. Cleveland, Ohio: Case Western Reserve University; 1982.
Note: M.Sc. Thesis.

8. Becker H.J. and Fuchs K.D. Microstructure and Technological Properties of Hot Work Tool Steel for Pressure Die Casting Dies. Transactions, NADCA 16th International Die Casting Congress and Exposition; 1991; Detroit, Michigan. ; Paper No. G-T89-053.

9. Becker H. J., Bach J. ,. Gerlach, G. and Wupper, K. D. Modern Heat Treatment of Tools and Dies. Proceedings of an International Conference on Tool Materials for Molds and Dies. : Colorado School of Mines; 1987 Oct.

10. Benedyk J.C. Thermal Fatigue Behaviour of H13 Die Steels. Cleveland, Ohio: Case Western Reserve University; 1969.
Note: Ph.D. Thesis.

11. Berger C. M. Effect of Specimen Notching on Impact Toughness of Premium H-13 Tool Steel. Transactions, NADCA 16th International Die Casting Congress and Exposition; 1991; Detroit, Michigan. ; Paper No. G-T91-084.

12. Berger C.M. Effects of Percentage Primary Carbide on Charpy V-Notch Impact Strength of Premium H-13 Die Steel. Transactions, NADCA 15th International Die Casting Congress and Exposition; 1989; St. Louis, MO. ; Paper G-T-89-012.

13. Berns, H. Haberling E. and Wendl, F. Influence of the Annealed Microstructure on the Toughness of Hot-Work Tool Steel. Thyssen Edelstahl Technische Berichte. 1990 May: p. 45.

14. Berns, H. Strength and Toughness of Hot Working Tool Steels. Proceedings of an International Conference on Tool Materials for Molds and Dies. : Colorado School of Mines; 1987 Oct.

15. Berns H., Haberling E. and Wendl F. Influence of the Annealed Microstructure on the Toughness of Hot-worked Steels. Thyssen Edelstahl. 1990 May(Special Issue): 45-52.

16. Bertolo R.R. Fracture Toughness of Aluminum Die Casting Die Steels and Related Thermal Fatigue Behavior. Cleveland, Ohio: Case Western Reserve University; 1976.
Note: Ph.D. Thesis.

17. Bertolo R.R. Fracture Toughness of Aluminum Die Casting Die Steels and Related Thermal Fatigue Behavior. Cleveland, Ohio: Case Western Reserve University; 1976.
Note: Ph.D. Thesis.

18. Birch, J. Prevention of Soldering with Surface Coating of Dies. Transactions, NADCA 16th International Die Casting Congress and Exposition; 1991; Detroit, Michigan. ; Paper No. G-T91-023.

19. Bostrom. L. Heat Treatment of Molds for Aluminum Die Casting. Proceedings of the Symposium on Tools for Die Casting; Sunne, Sweeden. ; 1983.

20. Boyer, Howard E. Practical Heat Treating. Metals Park, Ohio: American society for Metals.

21. Branco, J. R. T. and Kraus, G. Heat Treatment and Microstructure of Tool Steels for Molds and Dies. Proceedings of an International Conference on Tool Materials for Molds and Dies. : Colorado School of Mines; 1987 Oct.

22. Branco, J. R. T.; Krauss, G. Alloy Partitioning and Grain Growth Control of H13 Steel. Heat Treatment and Surface Engineering: New Technology and Practical Applications. ; 1988.
Colorado School of Mines. Carbide particle dispersions retained during austenitizing of H13 steel control austenite grain size and remove alloying elements important for secondary hardening from solid solution. Carbide types and amounts were determined by X-ray diffraction, transmission electron microscopy (TEM), and scanning electron microscope (SEM) X-ray microanalysis of particle electrolytically extracted from annealed specimens and specimens austenitized at 1020 and 1070 deg C. Atomic absorption of filtrate gave the matrix composition. The dominant retained carbide in annealed specimens is M sub 7 C sub 3 and in austenitized specimens is MC containing primarily vanadium as the metal component. Analysis of the MC particle dispersions with the Gladman equation shows an excess of MC particles for grain growth control. Possible additions of Nb to H13 for grain size control as a means to more economically utilize V for secondary hardening is discussed. 24 ref.--AA.

23. Brandis, H. and Heberling, E. New Materials for Plastic Molds and Die Casting Dies. Proceedings of an International Conference on Tool Materials for Molds and Dies. : Colorado School of Mines; 1987 Oct.

24. Breitler, R. Recent Development in Die Steels for Pressure Die Casting. Transactions, NADCA 16th International Die Casting Congress and Exposition; 1991; Detroit, Michigan. ; Paper No. G-T91-083.

25. Breitler R., Schindler Alfred M. The Importance of Heat Treatment of H-13 for Die Casting Dies. SDCE 13th International Die Casting Congress and Exposition ; 1985 Jun 3; Milwaukee, Wisconsin. ; Paper No. G-T85-044.

26. Carpenter 883 Plus (Die-Casting Die Steel; AISI Type H13). Alloy Dig. ; 1987 Jan. 0002-614X. Carpenter 883 Plus is a premium quality die-casting die steel. It is electroslag remelted and this, together with processing adaptations, give it metallurgical consistency and improved isotropic properties.--AA.

27. Centa L.L. and Wallace J.F. Effect of Electro-Discharge Machining on the Surface and Sub-Surface Micro Structure of H-13 Steel. Transactions, NADCA 15th International Die Casting Congress and Exposition; 1989; St. Louis, MO. ; Paper No. G-T89-032.

28. Clegg, A. J.; Das, A. A. The Production of Precision Cast H13 Die Steel Tooling by the Shaw Process. Br. Foundryman. 1987 Apr; : 80, (3) 137-144; ISSN: 0007-0718.
The Shaw Process is a precision casting process capable of the production of accurate castings, with excellent surface finish and metallurgical integrity, from permanent precision patterns . Moulds are produced using highly refractory aggregates bonded with silica. A high temperature firing treatment is part of the production sequence and this produces an inert mould into which the majority of commercial ferrous and non-ferrous alloys can be cast with confidence. The paper reviews the factors of importance in the production of precision castings by the Shaw Process. Particular attention is given to the pratical aspects of mould production using a composite technique with a sodium silicate bonded backing and ethyl silicate bonded facing material. The application of the process in the production of cast H13 steel tools and dies is considered from the viewpoints of surface finish and dimensional accuracy attainable. 27 ref.--AA.

29. Cocks, D. L. Longer Die Life From H13 Die Casting Dies by the Practical Application of Recent Research Results. Tool Materials for Molds and Dies: Application and Performance. ; 1987.

A synopsis is given of the first two phases of a three-phase project, aimed at producing accurate information on quench rates, structure and properties of H13 hot work die steels used for die castig dies. By using the techniques developed and the information generated, the heat treater will be able to predict the structure and impact values achieved when cooling a die block of known dimensions by various quenching systems. This will enable the heat treater to choose the optimum quenching technique to be used to get the best properties, at the minimum risk of distortion and cracking of the die. The practical application of this work is being encouraged by the Die Casting Research Foundation, who are continuing the project. A computer program is planned to make it easier for the heat treater to choose optimum quench conditions for any die block. It is anticipated that a significant increase in die casting die lives will result. 4 ref.--AA.

30. Cocks, D. L. Longer Die Life from H13 Die Casting Dies by the Practical Application of Recent Research Results. Proceedings of an International Conference on Tool Materials for Molds and Dies. : Colorado School of Mines; 1987 Oct.

31. Cole, B. Die-casting Die Performance. Proceedings of the Symposium on Tools for Die Casting; Sunne, Sweeden. ; 1983.

32. Cromo-High V (Hot-Work Tool Steel; AISI Type H13). Alloy Dig May 1973, (TS-254), 2 p.

33. Crucible Steel Co. of America. Crucible 218, Martensitic Type High Temperature Steel. ; 1958 May.

34. Danzer R., Krainer E. and Schindler F. M. Creep Behaviour of AISI H10 and H13 Materials with Regard to Die Life in Die Casting of Brass and Aluminum. Transactions of the 12th International Die Casting Congress and Exposition; 1903 Oct 31; Minneapolis, Minessota . ; Paper No. G-T83-012.

35. Danzer, R.; Krainer, E.; Schindler, F. M. Creep Behavior of AISI H10 and H13 Materials With Regard to Die Life in Die Casting of Brass and Aluminum. Die Casting Technology--Yesterday's Art, Today's Science. ; 1983.

Heat checking is one of the primary reasons for the failure of die-casting dies. The die surface may fail for a number of reasons but, by far, the most prevalent reason is the formation of surface cracks due to high-temp. low-cycle fatigue. To improve tool materials and their heat treatment, the relevant material properties have to be identified. For Al and brass die casting, it appears that creep rather than fatigue causes the heat checking on tool surfaces. The die life has been predicted by "Linear Accumulation of Creep Damage" and has been plotted as a function of max. surface temp. and preheating temp. of the die. It is shown that bainitic rather than martensitic heat treated steels (H10, H13) have better high-temp. strength and better creep properties. Therefore, the service life of die-casting dies can be improved using tool steels heat treated to a bainitic structure. 14 ref.--AA.

36. Das, S. K. (Case Western Reserve University). Effect of Heat Treatment on the Thermal Fatigue Behavior and Fracture Toughness of H13 Steel for Aluminum Die Casting Dies. Diss. Abstr. Int. 1981 May; : 41, (11) Pp 190.

The effect of different rates of cooling from the austenitizing temp. on the thermal fatigue resistance and fracture toughness of H13 steel designed for use on dies for Al die casting was studied. The rates of cooling included: oil quenching to martensite; two different rates of air cooling that produced mixed martensitic and upper bainitic structures; and quenching into molten salts for isothermal transformation to lower bainite. All steels were subsequently tempered to approx 46 Rockwell C. A high-temp. homogenizing treatment was employed on some of the steels to produce grain boundary carbides in the annealed microstructure. The faster cooling rates from the austenitizing temp. that produced completely martensitic structures exhibited superior thermal fatigue behavior and fracture toughness compared to more slowly cooled steels with mixed bainitic--martensitic structures. The isothermal treatments to produce lower bainite provided better thermal fatigue and toughness than slowly cooled specimens. The high-temp. homogenizing treatment used to influence the annealed microstructure reduced the macrosegregation of the alloying elements and resulted in better toughness and thermal fatigue resistance compared to the unhomogenized steels. The high-temp. homogenizing reduced the tendency for obtaining both different matrix structures and severe carbide networks in the steel because of the increased uniformity of the

chemical composition resulting from this treatment. Higher fracture toughness values resulted in lower rates of thermal fatigue crack propagation. (8109578).--AA.

37. Das S.K. Effect of Heat Treatment on the Thermal Fatigue Behavior and Fracture Toughness of H13 Steel for Aluminum Die Casting Dies. Cleveland, Ohio: Case Western Reserve University; 1980.
Note: Ph.D. Thesis.

38. Dittrich, A. Haberling ,. E. ,. Rache, K. and Schruff, I. Alloy Optimization of Hot-Work Tool Steel X40CrMoV51 Thyrotherm 2344) for Large Tools Subject to High Toughness Load. Thyssen Edelstahl Technische Berichte. 1990 May: p. 25.

39. Dittrich A., Haberling H. ,. Rasche K. and Schruff I. Alloy Optimization of Hot-worked Tool Steel X40CrMoV51 (Thyrotherm 2344) for Large Tools Subject to High Toughness Load. Thyssen Edelstahl. 1990 May(Special Issue): 25-31.

40. Dorsch, C. J. and Nichols, H. P. The Effects of EDM on the Surface of Hardened H-13 Die Components. Transactions, NADCA 15th International Die Casting Congress and Exposition; 1989; St. Louis, MO. ; G-T89-031.

41. Dorsh, C. and Ried P. P. Evaluating the Heat Treatment of Premium Quality H-13 Die Casting Components. Transactions, NADCA 16th International Die Casting Congress and Exposition; 1991; Detroit, Michigan. ; Paper No. G-T91-081.

42. Engberg, G.; Larsson, L. (Svenskt Stal, Swedish Institute for Metals Research). Elevated-Temperature Low Cycle and Thermomechanical Fatigue Properties of AISI H13 Hot-Work Tool Steel. Low Cycle Fatigue. ; 1988.
Thermal fatigue of the martensitic hot work tool steel AISI H13 is complicated by structural degradation which, in turn, is influenced by plastic deformation. These properties are dependent upon plastic deformation, temperature, and time, and thus it is of vital importance to find a description which allows inter- or extrapolation to the thermal load experienced in various practical applications. Isothermal, low cycle fatigue testing was performed mainly at 500 and 600 deg C and also to a limited amount at 80, 300, and 750 deg C. The material was tempered to three different hardness levels (43, 47, and 51 HRC) prior to testing. The main

bulk of tests were performed on the 47 HRC variant. At 600 deg C, no difference in life was observed between the different hardness variants. The cyclic stress--strain curves, evaluated at half lives, were also almost identical. Thermomechanical fatigue testing (simultaneous cycling of both strain and temperature, half a period out of phase with one another) was performed with a maximum temperature of 600 deg C in the cycle. The minimum temperature, T-min, was varied from 80-400 deg C. In comparison to the isothermal 600 deg C data, life was reduced when T-min was <= 200 deg C, but remained fairly unaffected when a T-min of 400 deg C was used. As expected, softening increased with increasing minimum temperature. The same hardness variants as described above were also tested with the 200-600 deg C cycle. No significant differences in life were obtained, although the cyclic stress--strain curves (maximum tensile stress at half life) differed. The Ostergren method for life prediction fit the data reasonably well, if the plastic work is normalized with the cube of the shear-modulus. 6 ref.--AA.

43. Firedie 13 (Hot-Work Tool Steel; AISI Type H13). Alloy Dig. ; 1986 Sep.
0002-614X. Firedie 13 is the standard 5% Cr hot-work tool steel with increased vanadium for improved wear resistance and toughness. In addition, this steel possesses excellent hot-hardness properties. Its many applications include die-casting tools (for Al, magnesium and Zn), extrusion tools (for Al and Mg), hot-heading dies, forging dies, hot punches and heavy shear blades.--AA.

44. Fuchs, K. D. Haberling, E. and Rasce, K. Microstructure and Technological Properties of Hot-Work Tool Steels for Pressure Die Casting Dies. Thyssen Edelstahl Technische Berichte. 1990 May: p. 16.

45. Fuchs K.D., Haberling H. and Rasche K. Microstructure and Technological Properties of Hot-work Tool Steels for Pressure Die Casting. Thyssen Edelstahl. 1990 May(Special Issue): 16-24.

46. Gao, Y.; Sun, G.; Zhang, T.; Ji, C.; Shen, J.; Chen, J.; Yang, J. (General Research Institute for Nonferrous Metals (China), Beijing Normal University). Electron-Microscopic Study of Titanium Ion-Implanted H13 Steel. Rare Metals (China). 1991; : 10, (2) 93-97.
Transmission electron microscope was used to study the influence of Ti ion implantation on the quenched and tempered structure of H13 steel. After implantation, the surface microhardness

of H13 steel was one to three times higher than that of unimplanted specimen, while the wear coefficient was two to three times lower than that of the unimplanted. In the implanted layer, the tempered martensite structure disappeared, and remarkable grain refinement occurred. During further annealed > 500 deg C, dispersed precipitates of Fe sub 2 Ti were formed in the implanted layer. Graphs, Photomicrographs, Diffraction patterns, Spectra. 2 ref.--AA.

47. Gao, Y.; Sun, G.; Zhang, T.; Ji, C.; Shen, J.; Chen, J.; Yang, J. (General Research Institute for Nonferrous Metals (China), Beijing Normal University). Electron-Microscopic Study of Titanium Ion-Implanted H13 Steel. Rare Metals (English Edition). 1991; : 10, (2) 93-97; ISSN: 1001-0521.

Transmission electron microscope was used to study the influence of Ti ion implantation on the quenched and tempered structure of H13 steel. After implantation, the surface microhardness of H13 steel was one to three times higher than that of unimplanted specimen, while the wear coefficient was two to three times lower than that of the unimplanted. In the implanted layer, the tempered martensite structure disappeared, and remarkable grain refinement occurred. During further annealing > 500 deg C, dispersed precipitates of Fe sub 2 Ti were formed in the implanted layer. Graphs, Photomicrographs, Diffraction patterns, Spectra. 2 ref.--AA.

48. Gao, Yuzun Sun ,. Guiru (General Research Inst for Non-ferrous Metals, Beijing, China). Electron-microscopic study of Ti Ion-implanted H13 steel. 1991; . CODEN: XIJID9; ISSN: 1001-0521.

Transmission electron microscope was used to study the influence of Ti ion implantation on the quenched and tempered structure of H13 steel.^After implantation, the surface microhardness was 1-3 times higher than that of an unimplanted specimen. The wear coefficient was 2-3 times lower than that of the unimplanted steel. In the implanted layer, the tempered martensite structure disappeared and grain refinement occurred. During further annealing above 500 degree C, dispersed precipitates of Fe//2Ti were formed in the implanted layer. (Edited author abstract) 2 Refs.

49. Gaven, J. A. Tool Performance of Aluminum Die Casting Dies. Proceedings of the Symposium on Tools for Die Casting; Sunne, Sweeden. ; 1983.

50. Gaven Jan-Ake, Norstrom Lars -Ake and Worbye John. Performance of Newly-Developed Hot Work Tool Steel for Die Castings. Transactions of the 12th International Die Casting Congress and Exposition; 1903 Oct 31; Minneapolis, Minessota . : Paper No. G-T83-011.

51. Gehricke B., Wendl F. and Wupper K. Influence of Surface Conditions on Toughness of Hot Work Steels. Transactions, NADCA 16th International Die Casting Congress and Exposition; 1991; Detroit, Michigan. ; Paper No. G-T91-082.

52. George A. Roberts and Robert A. Cary. Tool Steels. Metals Park, Ohio: American Society for Metals; 1980.

53. GIVEN, NO AUTHOR. AISI TYPE H13 --HOT WORK TOOL STEEL--. ALLOY DIG TS-193, MAY 1967, 2 P.

54. GIVEN, NO AUTHOR. THERMOLD H13 --HOT WORK TOOL STEEL -AISI H13--. ALLOY DIG MAR. 1972, --TS-241--, 2P.

55. Goodrich, G.; Divinsky, I. Failure of an ASTM A681-89 H13 Die Segment for Die Casting of Aluminum. Handbook of Case Histories in Failure Analysis. Vol. 1. ; 1992.
Taussig Associates. A segment from a premium-quality H13 tool steel die for die casting of aluminum failed after only 700 shots. The segment was subjected to visual, macroscopic, hardness, and metallographic testing. The investigation revealed that failure occurred as a result of fatigue at an electrical-discharge-machined surface where the resulting rehardened layer had not been removed. This rehardened layer had cracked, providing a source for fatigue initiation.

56. Graham R.R. Thermal Processing Structure and Thermal Fatigue Relations in Die Steel. Cleveland, Ohio: Case Western Reserve University; 1974.
Note: M.Sc. Thesis.

57. Graham R.R. Thermal Fatigue Mechanisms in Aluminum Die Casting Die Steels. Cleveland, Ohio: Case Western Reserve University; 1974.
Note: Ph.D. Thesis.

58. Guterl H-13 (Hot Work Tool Steel; AISI Type H13). Alloy Dig. 1982 Oct; : (TS-405) Pp 2; ISSN: 0002-614X.
Guterl H-13 is an air-hardening Cr--Mo--V tool steel that finds wide use as a die in the forging, extrusion and die-casting industries. It has good hot hardness and wear resistance, extreme toughness and high resistance to heat checking and erosive action. Also, it has excellent machinability in the annealed condition and relatively good freedom from distortion and scaling during heat treatment. Among its many uses are dies to cast Al- and Zn-base alloys, forging-die inserts, hot gripper and header dies and Al and Mg extrusion dies, inserts and support tubing.--AA.

59. Hamaker J. and Vater E.J. Carbon Strength Relationships on 5 Percent Chromium Ultra High Strength Steels. Proceedings of the ASTM. 1960; 60.

60. Hanna G.L. and Steigerwalt E.A. Fracture Characteristics of Structural Metals. : TAPCO Division Thompson Ramo Wooldridge; 1963 Jun 30; Final Summary Technical report ER-5426.

61. Hemphill, R. M. and Wert D. E. Impact and Fracture Toughness Testing of Common Grades of Tool Steels. Proceedings of an International Conference on Tool Materials for Molds and Dies. : Colorado School of Mines; 1987 Oct.

62. Henning R.G. and Brisbane A.W. Mechanical Properties of AM 350, Potomac M, and Vaso Jet-1000 Steel Alloys in the Annealed Condition. ; 1963 May; ASD TDR-63-116.

63. Hindle, R. W. Getting the Best Out of H13 Die Steel. Metallurgia Feb. 1978, 45, (2), 103.

64. Hong, Xiao (Shandong Univ of Technology, Shandong, China). Wear behaviour and wear mechanism of ceramic tools in machining hardened alloy steel. 1990; . CODEN: WEARAH; ISSN: 0043-1648.

Machining tests were carried out on hardened AISI H13 hot-work steel (HRC 43-48) using a series of different ceramic tools, i.e. SiC whisker- reinforced alumina, Si-Al-O-N, alumina, mixed alumina and cubic boron nitride (CBN). The wear behaviour and wear mechanisms of the tools are discussed. Significant differences in tool life were noticed between the different ceramic tools under the same cutting conditions. It was found that the tool life was limited mainly by

crater wear when using Si-Al-O-N, whisker-reinforced alumina and CBN. Alumina-based ceramic tools showed superior crater wear resistance. Whisker-reinforced alumina tools showed microfracture during cratering. CBN tools revealed evidence of diffusion wear. (Author abstract) 13 Refs.

65. Hutchings, R. Collins ,. G. A. Tendys, J. (Australian Nuclear Science and Technology Organisation, Menai, Aust). Plasma immersion ion implantation. Duplex layers from a single process. 1992; . CODEN: SCTEEJ; ISSN: 0257-8972.
Plasma immersion ion implantation (PI**3) is an alternative non-line-of- sight technique for implanting ions directly from a plasma which surrounds the component to be treated. In contrast to plasma source ion implantation, the PI**3 system uses an inductively coupled r.f. plasma. It is shown that nitrogen can be retained during implantation at elevated temperatures, even for unalloyed steels. This allows controlled diffusion of nitrogen to greater depths, thereby improving the load bearing capacity of the implanted layer. Components can be heated directly, using the energy deposited by the incident ions during the pulsed implantation. The necessary temperature control can be accomplished simply by regulating the frequency and length of the high voltage pulses applied to the component. Chemical depth profiles and microstructural data obtained from H13 tool steel are used to show that PI**3 can, in a single process, effectively produce a duplex subsurface structure. This structure consists of an outer non-equilibrium layer typical of nitrogen implantation (containing in excess of 20 at.% nitrogen) backed by a substantial diffusion zone of much lower nitrogen content. The relationship between implantation temperature and the resultant subsurface microstructure is explored. (Author abstract) 14 Refs.

66. International Nickel Co.(INCO). ; 1958.

67. Jessop Dica B Vanadium (Hot Work Tool Steel; AISI Type H13). Alloy Dig. 1983 Dec; : (TS-419) Pp 2; ISSN: 0002-614X.
Jessop Dica B Vanadium is an excellent hot work steel. It has an outstanding combination of shock resistance, red hardness and abrasion-resisting properties. It is especially well adapted as a die steel for Al and Mg die casting. This tool steel is capable of withstanding rapid cooling without premature checking.--AA.

68. Johansson B., Jonsson L. and Worbye J. Some Aspects on the Properties of QRO 80M and Die Casting Die Performance. SDCE 13th International Die Casting Congress and Exposition ; 1985 Jun 3; Milwaukee, Wisconsin. ; Paper No. G-T85-042.

69. Justusson W.M. and Zackay V.M. Engineering Properties of Ausformed Steel. Metal Progress. 1962 Dec; 82(6).

70. K. Heindlhofer. Evaluation of Residual Stress. New York: McGraw-Hill; 1948.

71. Kajoch, W. and Fajkiel A. Testing the Soldering Tendency in Aluminum Die Casting Alloys. Transactions, NADCA 16th International Die Casting Congress and Exposition; 1991; Detroit, Michigan. ; Paper No. G-T91-034.

72. Karamis, M. B. (Erciyes Univ, Kayseri, Turk). Investigation of the properties and wear behaviour of plasma-nitrided hot- working steel (H13). 1991; . CODEN: WEARAH; ISSN: 0043-1648.
The microstructural properties and wear behavior of AISI H13 steel which had been plasma-nitrided at 530 and 550 degree C for times between 4 and 100 h have been investigated. The effects of treatment temperature and time on the microstructure have been examined. The wear behavior of material treated for 4 and 100 h has also been observed. It was seen that a total case depth of 0.55 mm with a hardness of 1000 HV can be achieved in 100 h. However, the white layer thickness is increased to 17 mu m, while the core hardness is reduced to 480 HV at 550 degree C. The wear rate of the sample treated at 550 degree C for 100 h is higher than that of the sample treated at 550 degree C for 4 h. (Author abstract) 12 Refs.

73. Karamis, M. B. (Erciyes Universitesi). An Investigation of the Properties and Wear Behaviour of Plasma-Nitrided Hot-Working Steel (H13). Wear. 1991 Oct 21; : 150, (1-2) 331-342; ISSN: 0043-1648.

The microstructural properties and wear behaviour of AISI H13 steel which had been plasma nitrided at 530 and 550 deg C for times between 4-100 h have been investigated. The effect of treatment temperature and time on the microstructure have been examined. The wear behaviour of material treated for 4 and 100 h has also been observed. It was seen that a total case depth of 0.55 mm with a hardness of 1000 HV can be achieved in 100 h. However, the white

layer thickness is increased to 17 mu m while the core hardness is reduced to 480 HV at 550 deg C. The wear rate of the sample treated at 550 deg C for 100 h is higher than that of the sample treated at 550 deg C for 4 h.

74. Karamis, M. B. (Univ of Erciyes, Kayseri, Turk). Some effects of the plasma nitriding process on layer properties. 1992; . CODEN: THSFAP; ISSN: 0040-6090.
The layer properties of AISI 722M24, AMS 6472 and AISI H13 materials plasma nitrided under various conditions were defined. The materials were plasma nitrided at temperatures between 510 and 590 degree C for times ranging between 4 and 100 h in a dissociated ammonia atmosphere. The effects of duration, temperature, chemical composition and the shape of sample on the layer properties were determined. It was determined that the total case increased with treatment time and temperature increases the white layer thickness and the effective case depth. The increase in the white layer thickness is very sharp up to a total case depth of 0.3 mm, but it is very slow between 0.3 and 0.75 mm total case. The chemical composition of the material also effects the depth and hardness of the case. High alloy steels have higher hardness but thinner case than low alloy steels. Although the gamma prime -Fe//4N single-phase compound layer was formed on 722M24 steel, a thick and mixed epsilon - gamma prime (Fe//2// minus //3N plus Fe//4N) phase was produced on H13 steel. The hardness distributions from curved and flat surfaces to the core of the test material exhibit different profiles. (Author abstract) 16 Refs.

75. Kendall D.P. and Davidson T.E. The Effect of Strain Rate on Yielding of High Strength Steels" . : Watervliet Arsenal; 1966 May; WVT 6618.

76. Kendall D.P. The Effect of Strain Rate and Temperature on Yielding of Steels" . : Watervliet Arsenal; 1970 Nov; WVT 7061.

77. Kim H.J. Analysis of Mitigation of the Influence of EDM on the Thermal Fatigue Behavior of H13 Die Steel . Cleveland, Ohio: Case Western Reserve University; 1982.
Note: M.Sc. Thesis.

78. Kogler, E. Breitler ,. R. and Schindler A. Die Steel Quality and Die Life Requirements for Aluminum Die Casting Dies. Transactions, NADCA 15th International Die Casting Congress and Exposition; 1989; St. Louis, MO. ; Paper No. G-T89-052.

79. Korach, M. Low-Cycle Fatigue and Thermal Fatigue of Hot-Work Tool Steels. Proceedings of the Symposium on Tools for Die Casting; Sunne, Sweeden. ; 1983.

80. Lehtinen, B. and Roberts, W. Microstructural Changes During Tempering of Hot-Work Tool Steels - a Comparison of AISI H13 and UHB QRO 80. Proceedings of the Symposium on Tools for Die Casting; Sunne, Sweeden. ; 1983.

81. Lehtinen, E.; Roberts, W. Microstructural Changes During Tempering of Hot Work Tool Steels--a Comparison of AISI H13 and UHB QRO 80. Tools for Die Casting. ; 1983.
The microstructure in the vicinity of the secondary-hardening max. was compared for two hot work tool steels, UHB Orvar 2M (equivalent to AISI H13; 0.35C--5Cr--1.5Mo--1V) and UHB QRO 80 (0.4C--2.5Cr--2Mo--1.2V). The latter is a recently-developed grade with better temper resistance than H13. HVEM transmission studies on thin foils and analysis of extracted secondary carbides in an analytical TEM enabled a correlation to be made between the temper resistance, precipitation sequence and chemistry for the grades studied. Secondary MC precipitates are greater in number and grow faster in Orvar as compared with QRO 80. Furthermore, a transition from MC -> M sub 23 C sub 6 proceeds in Orvar during tempering at > 550 deg C; this Cr-rich carbide coarsens rapidly because of the relatively high Cr content (approx 5%). In QRO 80, M sub 23 C sub 6 is not formed before 690 deg C and only then in relatively small amounts; the Cr level in this steel is relatively low (approx 2.5%). The fact that the MC -> M sub 23 C sub 6 transition is delayed in QRO 80 means that the secondary particles present at a given temp. are smaller, and thus the hardness greater, than in H13 (better temper resistance); the rapid coarsening of M sub 23 C sub 6 in Orvar is also conducive to recovery of the martensite substructure, which contributes further to a rapid loss of hardness following the secondary-hardening peak.--AA.

82. Lin, W. L. Ding, X. J. Sang, J. M. Xu, J. Wang, Z. Y. Zhou, S. Y. Li, Y. L. (Beijing Normal Univ, Beijing, China). Effects of C on tribological properties and microstructure of Ti-implanted H-13 steel. 1993; . CODEN: SCTEEJ; ISSN: 0257-8972.
Ti ion implantation into steels under controlled conditions has been demonstrated to be very effective for decreasing both the friction and wear rate of various steels. In the present work, the effects of C incorporated into Ti-ion-implanted H-13 steel (both with and without additional C ion implantation) on the tribological properties and microstructure of implanted layers have

been investigated. Metallurgically polished H-13 steel specimens were prepared for C, Ti and (Ti plus C) ion implantations which were performed using the MEVVA source ion implantation system at room temperature. Ball-on-disk sliding tests, scanning electron microscopy and profilometry of the wear track have been used to examine the tribological behaviour of implanted H-13 steel. Auger electron spectroscopy, energy- dispersive spectroscopy, X-ray diffraction and transmission electron microscopy were also employed to characterize the composition and microstructure of the ion-implanted layers of H-13 steel. From the results, we conclude that sufficient concentrations of both Ti and C are essential to produce the amorphous ternary surface alloy and significant reductions in both the friction coefficient and wear rate of implanted H-13 steel. (Author abstract) 6 Refs.

83. Liu, Y.; Fu, R. (Shanghai University of Technology). Effects of Pretreatment on the Impact Toughness of H13 Cast Steel. Foundry Technology (China). 1992 Sep; : (5) 3-5.
The effect of microstructure on the impact toughness of H13 cast steel (Ch13) used as casting dies of Al alleys is studied. The test results showed that the homogenization annealing improved the impact toughness. By means of the SEM analysis, methods of improving the impact toughness have been discussed.

84. Lu, Jinsheng Chen ,. Xiuyu Gu, Min (Zhengzhou Mechanical Research Inst, MMI, Zhengzhou, China). Study on ion oxy-sulpho-nitriding of die steel. 1994; . CODEN: JRECDB; ISSN: 0254-6051.
In this paper the processes of ion oxy-sulpho-nitriding on die steels H13, Cr12MoV, LD1 and 3Cr2W8V by medium SO//2 plus N//2 plus //2 were studied. The optimum process parameter for 4 kinds of material are obtained. The wear and seizing teat were taken place and compared with those of ion nitriding, hardening and tempering. Finally, the process is examined on die products. (Edited author abstract).

85. Moracz D.J. Thermal Fatigue Behaviour of Die Materials for Die Casting Dies. Cleveland, Ohio: Case Western Reserve University; 1969.
Note: M.Sc. Thesis.

86. NADCA. Transactions of the 15th International Die Casting Congress and Exposition; 1989 Oct 16; St. Louis, MO.

87. Nieh C.Y. Thermal Fatigue Behavior of H13 Steel for Aluminum Die Casting Dies [with Various Ion Sputtered Coatings]. Cleveland, Ohio: Case Western Reserve University; 1981. Note: M.Sc. Thesis.

88. Nihols, H. P. Preparation of Standard H-13 Charpy Blanks and Heat Treat Acceptance Criteria. Transactions, NADCA 16th International Die Casting Congress and Exposition; 1991; Detroit, Michigan. ; G-T91-085.

89. Nilsson, H. Roberts ,. W. and Sandberg, O. Estimation of Thermal-Shock Resistance of Hot-Work Tool Steels - A Fracture Toughness Approach. Proceedings of the Symposium on Tools for Die Casting; Sunne, Sweeden. ; 1983.

90. Nilsson, H. Sandberg ,. O. and Roberts, W. The Influence of Austenitization Temperature and Cooling Rate after Austenitization on the Mechanical Properties of the Hot-Work Tool Steels H11 and H13. Proceedings of the Symposium on Tools for Die Casting; Sunne, Sweeden. ; 1983.

91. Nilsson, H.; Sandberg, O.; Roberts, W. The Influence of Austenitization Temperature and the Cooling Rate After Austenitization on the Mechanical Properties of the Hot Work Tool Steels H11 and H13. Tools for Die Casting. ; 1983.
The hot work tool steels AISI H11 and H13 have been studied with regard to the influence of austenitization temp. and the cooling procedure after austenitization on the hot strength, hot ductility and impact toughness in the hardened and tempered condition. Five different cooling procedures were examined and the deterioration in ductility and impact toughness, engendered by increasing amounts of grain-boundary carbide precipitation and the presence of different forms of bainite as the cooling rate is reduced, was monitored. The ductility during tensile testing at elevated temp. and the impact toughness at room temp. and 600 deg C depend strongly on the amount of grain boundary carbides precipitated during cooling from the austenitization temp. In particular, the precipitation of carbides in a matrix of high-temp. (upper) bainite resulted in poor ductility and impact toughness.--AA.

92. Nordberg, H. Review on Fracture Toughness of Tool Steel. Proceedings of the Symposium on Tools for Die Casting; 1983; Sunne, Sweeden.

93. Norstrom, L. A. The Importance of Ductility and Toughness in Hot Work Die Steels: Proper Testing Procedures. Transactions, NADCA 15th International Die Casting Congress and Exposition; 1989; St. Louis, MO. ; Paper No. G-T89-014.

94. Norstrom, L. A. ,. Johansson, B. and Klarenfjord, B. Thermal Fatigue and Thermal Shock Behaviour of Some Hot-Work Tool Steels. Proceedings of the Symposium on Tools for Die Casting; Sunne, Sweeden. ; 1983.

95. Norstrom, Lars Ake Jonson, Lennart Johnson, Brian (Uddeholms AB, Hagfors, Swed). New premium steel for the 1990s. 1988; . CODEN: FUTJAD; ISSN: 0015-9042.
Diecasters are acutely aware of the need to increase die life and decrease die maintenance costs, as well as to increase process productivity by shortening shot cycle times for example. Technically complex, these matters include subjects like die design, die manufacturing and working conditions for the dies and so on. The strong influence of crucial die material properties on these factors is discussed in this article and the importance of premium die steel is demonstrated. Also discussed is the role of the die material regarding short cycle times and a new die steel which offers beneficial effects on all these factors. Die casting of aluminum and brass is discussed with respect to evaluation of the die material.

96. North American Aviation, Inc Columbus Div. Thermold A, Thermold J. and Vascojet 1000 Steel Sheet Evaluation. ; 1958 Jul 22; NA 58H-302.

97. North American Aviation, Inc Columbus Div. Thermold J. and Vascojet 1000 Bar and Billet Evaluation. ; 1958 Oct 9; NA 58H-416.

98. Nu-Die XL (Premium-Quality Die Steel; AISI Type H13). Alloy Dig. ; 1986 Dec.
0002-614X. Nu-Die XL is manufactured to meet the demanding specifications for long-run die-casting dies for Al. Sound centers are produced in both large and smaller sizes. Its many applications include die-casting dies, die inserts, cores and extrusion dies for Al and magnesium.--AA.

99. Okorafor, O. E. Fracture Toughness of M2 and H13 Alloy Tool Steels. Mater. Sci. Technol. 1987 Feb; : 3, (2) 118-124; ISSN: 0267-0836.
The influence of microstructural variations on the fracture toughness of two tool steels having

compositions (wt.%) 1C--4Cr--5Mo--2V--6W (AISI M2 high-speed steel) and 0.35C--5Cr--1.5Mo--1V (AISI H13 hot-work steel) was investigated. In the as-hardened condition, the H13 steel has a higher fracture toughness than M2 steel, and the latter steel is harder. In the tempered condition, the H13 steel is again softer and has a higher fracture toughness than M2. There is a decrease in fracture toughness and an increase in hardness when the austenitizing temperature is above 1050 deg C for M2 steel and above 1100 deg C for H13 steel, in both the as hardened and hardened and tempered conditions. The fracture toughness of both steels was enhanced by reducing the grain size and increasing the overall carbide volume in the matrix. The steel samples of average grain diameter => 40 mu m exhibit 2-3 MN/m exp 3/2 lower fracture toughness than samples of average grain diameter <= 15 mu m. A high content of retained austenite appears to raise the fracture toughness of as-hardened M2 steel. Tempering improved the fracture toughness of M2 and H13 steels. The present results are explained using observations of changes in the microstructure and the modes of fracture. 22 ref.--AA.

100. Okorafor, O. E. Some Aspects of the Fracture Behaviour of H13 and M2 Steels. Met. Forum. 1985 Jun; : 8, (1) 30-36; ISSN: 0160-7952.

Presented are the results of fracture toughness tests performed on commercial H13 hot-work die steel and M2 high-speed tool steel specimens of a variety of microstructures. Fracture behaviour was examined by means of three tests: the plane strain fracture toughness test, the dynamic tear test and the Charpy V-notch test. The variables studied include melting practice, heat treatment and microstructure. After failure, the fracture surfaces were examined metallographically and by means of the scanning electron microscope to relate microstructure and fracture mode. The major conclusions are: (i) For the H13 steels, increasing the austenitizing temp. increased hardness, decreased dynamic toughness, but had no significant effect on the plane strain fracture toughness. Variations in melting practice had no marked effect on these properties. (ii) For the M2 steels, increasing the austenitizing temp. resulted in a slight decrease in toughness. The electroslag remelted (ESR) and air-melted M2 steels had similar K sub Ic values for comparable heat treatments, but the ESR steel showed some improvement in dynamic tear properties. (iii) The volume fraction and distribution of undissolved carbides and retained austenite in the matrix greatly influenced the hardness, toughness and fracture behaviour of H13 and M2 steels. 6 ref.--AA.

101. Okuno, T. Effect of Microstructure on the Toughness of Hot Work Tool Steels, AISI H13, H10, and H19. Trans. Iron Steel Inst. Jpn. 1987 Jan; : 27, (1) 51-59; ISSN: 0021-1583.
Microstructures of hot work tool steels, AISI H13, H10 and H19, tempered after quenching at various cooling rates were studied for improvement of the toughness of these steels. It is found that the development of upper bainite with decreasing rate of quenching is accompanied by the following microstructural changes: (1) increase in the width and length of bainite grains and the effective grain size; (2) preferential precipitation of carbides along prior austenite grain boundaries; (3) dispersion of fine carbides in matrix. These microstructural changes lead to a reduction of the toughness in all the steels; deterioration occurs in H10 and H19 at a higher cooling rate than in H13. The toughness value reduces in the order of H13, H10, and H19, correlating with increasing order of the density of fine carbides in the matrix and the fraction of retained carbides. 22 ref.--AA.

102. OMSEN, ARNE; SKOOG, BENGT E. DIE BLOCKS OF FORGED H13 ARE TOUGH. METAL PROGR APR. 1970, 97, --4--, 75-76.

103. Orvar Supreme (Hot Work Tool Steel, AISI H13). Alloy Dig. ; 1988 Oct.
0002-614X. Orvar Supreme is a Cr--Mo--V alloyed steel. Special processing techniques and close control are responsible for its high purity and very fine structure. It has improved isotropic properties.

104. Pettersson, S. Sandberg ,. O. Johnson, B. (Uddeholm Tooling AB, Sweden). Designing the hardening practice for premium H13 die-casting dies. 1993; . CODEN: HTRMBS; ISSN: 0305-4829.
A practical investigation into the optimum procedure for heat treating premium-quality H13 has been undertaken with the assistance of leading heat treaters from several European countries. (Author abstract).

105. Philip T.V. and McCaffrey T.J. Ultrahigh-Strength Steels. 1990 Metals Handbook, 10th Ed. : ASM ; 1: 430-448.

106. Pickering, F. B. The Properties of Tool Steels for Mold and Die Applications. Proceedings of an International Conference on Tool Materials for Molds and Dies. : Colorado School of Mines; 1987 Oct.

107. Pina, J. Prata; Dias, A. Morao; Lebrun, J. L. Study of Residual Stresses and Cold Working Generated by Machining of AISI H13 Steel. International Conference on Residual Stress. ICRS 2. ; 1989.
Universidade de Coimbra, ENSAM. Attempts were made to study the influence of actual machining factors (polishing, grinding, milling, EDM) on residual stresses repartition, metallurgical structures and cold woking of H13 steel used for injection moulds. This study was mainly performed by X-ray diffraction method. Graphs. 8 ref.--AA.

108. Potomac M (Air-Hardening Hot Work Steel; AISI Type H13). Alloy Dig May 1977, (TS-318), 2 p.

109. Quaeyhaegens, C. Stals ,. L. M. Van Stappen, M. (Limburgs Univ Centrum, Belg). Texture analysis of martensitic hot-worked tool steel H13 coated with TiN by physical vapour deposition. 1991; . CODEN: MSAPE3; ISSN: 0921-5093.
With a theta -2 theta decoupled X-ray diffractometer, extended with a omega substrate rotation, it is possible to study the preferential orientation (texture) of polycrystalline materials in an experimental set-up which is comparable with the Field-Merchant configuration. After having established the preferential orientation of the substrates, which were made of martensitic hot-worked tool steel H13, they were coated with TiN by physical vapour deposition. Two layer thicknesses were deposited at two different bias voltages. Thin TiN layers with a thickness of 200-300 nm were polycrystalline while coatings with a layer thickness of 1400-1600 nm showed a preferential orientation of the (111) and (220) lattice planes parallel to the substrate surface. The (111) preferential orientation shows a decrease in mosaic spread with increasing bias voltage, but the mosaic spread of the (220) preferential orientation remains unchanged. (Author abstract) 15 Refs.

110. Quaeyhaegens, C.; D'Haen, J.; De Schepper, L.; Stals, L. M.; Van Stappen, M. (Limburgs Universitair Centrum). Correlation Between the Interface Structure and the Adhesion of Titanium Nitride and Ti/TiN Coated Martensitic Hot Work Steel AISI H13. IPAT 91. ; 1991.
A XTEM and TEM study of the structure of the interface between titanium nitride and martensitic tool steel AISI H13 is presented. When in the initial stage of the deposition process nitrogen atoms and ions are allowed to interact with the substrate material, twinning is observed. The (X)TEM results are correlated with the macroscopic adhesion features of titanium nitride on the substrate, studied by means of the scratch test method. By careful control

of the initial stage of the ion plating process, one is able to obtain a titanium nitride coating which has a better adhesion to martensitic tool steel AISI H13 even when no Ti intermediate layer is deposited, although in the literature it is generally accepted that deposition of a Ti intermediate layer is essential to obtain a good adhesion of titanium nitride on metallic substrates. These results point to the fact that the deposition process has to be very well controlled to obtain coatings with good functional properties.

111. Quaeyhaegens, C.; Stals, L. M.; Stappen, M. Van (Limburgs Universitair Centrum). Texture Analysis of Martensitic Hot-Worked Tool Steel H13 Coated With Titanium Nitride by Physical Vapour Deposition. Second International Conference on Plasma Surface Engineering. I. Materials Science and Engineering A. 1991 Jul 1; : A139, (1-2) 242-248; ISSN: 0921-5093.
With a theta -2 theta decoupled X-ray diffractometer, extended with a omega substrate rotation, it is possible to study the preferential orientation (texture) of polycrystalline materials in an experimental set-up which is comparable with the Field--Merchant configuration. After having established the preferential orientation of the substrates, which were made of martensitic hot-worked tool steel H13, they were coated with titanium nitride by physical vapour deposition. Two layer thicknesses were deposited at two different bias voltages. Thin titanium nitride layers with a thickness of 200-300 nm were polycrystalline while coatings with a layer thickness of 1400-1600 nm showed a preferential orientation of the (111) and (220) lattice planes parallel to the substrate surface. The (111) preferential orientation shows a decrease in mosaic spread with increasing bias voltage, but the mosaic spread of the (220) preferential orientation remains unchanged. Graphs. 15 ref.--AA.

112. Sandberg, O. and Roberts, W. Relation between Properties of Tool Steels and Mold/Die Performance. Proceedings of an International Conference on Tool Materials for Molds and Dies. : Colorado School of Mines; 1987 Oct.

113. Schindler A., Kulmberg A. and Stuhl J. H. Thermal Fatigue of H13 in Die Casting Applications. Proceedings of the 9th SDCE International Die Casting Exposition and Congress; 1977 Jun 6; Milwukee, Wisconsin. ; Paper No. G-T77-065.

114. Schmidt, M. L. Effect of Austenitizing Temperature on Laboratory Treated and Large Section Sizes of H-13 Tool Steel. Proceedings of an International Conference on Tool Materials for Molds and Dies. : Colorado School of Mines; 1987 Oct.

115. Schmidt, M. L. (Carpenter Technology). Testing Premium H13 Die Steels. Die Cast. Manage. 1989 Apr; : 7, (2) 24-27; ISSN: 0745-449X.
An evaluation of impact resistance of hot-worked die steels (H11 and H13) by Charpy V-notch test is preferable to Volkswagen test, where an unnotched sample is used which requires many more ft-lb of energy to break, often damaging the test maching by reaching its full capacity. The advantages of Charpy V-notch test over Volkswagen method are highlighted. Graphs.--B.C.

116. Schmidt, M. L. What Really Influences the Mechanical Properties of Premium H-13 Tool Steel? Transactions, NADCA 15th International Die Casting Congress and Exposition; 1989; St. Louis, MO. ; Paper No. G-T89-011.

117. Schruff I. Comparison of Properties and Characteristics of Hot-work Tool Steels x38CrMoV51 (Thyrotherm 2343), X40CrMoV51 (Thyrotherm 2344), X32CrMoV33 (Thyrotherm 2365) and X38CrMoV53 (Thyrotherm 2367). Thyssen Edelstahl. 1990 May(Special Issue): 32-44.

118. Schruff, I. Comparison of Properties and Characteristics of Hot-Work Tool Steels X38CrMoV51(Thyrotherm 2343), X40CrMoV51(Thyrotherm 2344), X32CrMoV33(Thyrotherm 2365) and X38CrMoV53(Thyrotherm 2367). Thyssen Edelstahl Technische Berichte. 1990 May: p. 32.

119. SDCE. Proceedings of the 9th International Die Casting Exposition and Congress; 1977 Jun 6; Milwuaukee, Wisconsin.

120. SDCE. Transactions of the 14th International Die Casting Congress and Exposition. Toronto, Ontario, Canada; 1987 May 11.

121. Seux, M.; Saint-Ignan, J. C.; Leveque, R. Improvement of Service Life for MPM H13 Mandrels. 30th Mechanical Working and Steel Processing Conference. Vol. XXVI. ; 1989.
C3F, UNIREC. MPM mandrels mainly fail because of thermal fatigue between 700-250 deg C. To improve thermal fatigue properties of MPM mandrels, an extensive research programme, based on specific laboratory equipment, was performed. Main conclusions are: oxidation of the base H13 material under chrome plating increases stresses at cracks tips; high impact values should be aimed at, rather than high hardness or UTS; and careful optimization of

chemical analysis, steel melting process forging and heat treating should be sought. Forgings manufactured according to these recommendations show an increased thermal fatigue resistance. Graphs, photomicrographs. 9 ref.--AA.

122. Shoaf, L. Improved Performance Through Design. Proceedings of the Symposium on Tools for Die Casting; Sunne, Sweeden. ; 1983.

123. Skidmore, K. F. The Selection of Premium Quality H13 Steel for Pressure Die Casting. Tools for Die Casting. ; 1983.

It is recommended that H13 steel die block quality always be ascertained prior to machining and heat treatment. A post-heat treated specimen examination is also desirable. The die that has been acceptance tested can withstand substantially more abuse than a die that would be considered unacceptable based upon the criteria that have been discussed. These conclusions and recommendations regarding H-13 steel selection are made based upon the state-of-the-art of steelmaking technology today and upon knowledge of the needs of the die-casting industry.--AA.

124. Skidmore, K. F. Selection of Premium Quality H13 Steel for Pressure Die Casting. Proceedings of the Symposium on Tools for Die Casting; Sunne, Sweeden. ; 1983.

125. Skoff J.V. Extended Die Life and Improved Performance Through Comprehensive Stress Texturing. Transactions, NADCA 15th International Die Casting Congress and Exposition; 1989; St. Louis, MO. ; G-T89-033.

126. Smith, W. Design and Fabrication of Quality Die Casting Dies. Proceedings of the Symposium on Tools for Die Casting; Sunne, Sweeden. ; 1983.

127. Smith, W. E. Design and Fabrication of Quality Die Cast Dies. Proceedings of an International Conference on Tool Materials for Molds and Dies. : Colorado School of Mines; 1987 Oct.

129. Stasko, W. Dorsch C. and Nichols H. P. Advances in the Development of Particle Metallurgy Hot Work Tool Steels. Transactions, NADCA 15th International Die Casting Congress

and Exposition; 1989; St. Louis, MO. ; Paper No. G-T89-051.

130. Sundqvist, Martin Hogmark ,. Sture (Univ of Karlstad, Karlstad, Sweden). Effects of liquid aluminum on hot-work tool steel. 1993; . CODEN: TRBIBK; ISSN: 0301-679X.
The effects of liquid aluminum on hot-work tool steel H13 have been studied using specimens in three different surface conditions: rough, polished and oxidized. The specimens were rotated around their own axes in molten aluminum at different temperatures and for different exposure times. Three intermetallic phases of Fe-Al which formed on the surface of the steel when submerged in liquid aluminum were identified. These were shown to grow as continuous layers or as cone-shaped dendrites, depending on the surface condition of the steel. The growth of these layers/cones was related to time and temperature. The formation of cones and their subsequent breaking is assumed to be an important factor in the erosion of die-casting dies. (Author abstract) 7 Refs.

131. Tabe, H. Thermal Shock Cracking of Tool Steels. Proceedings of an International Conference on Tool Materials for Molds and Dies. : Colorado School of Mines; 1987 Oct.

132. Tang, N. Y. Plumtree, A. (Univ of Waterloo, Waterloo, Ont, Can). Elevated temperature fatigue crack propagation in hot work tool steel. 1991; . CODEN: FFESEY; ISSN: 8756-758X.
Cyclic tests have been carried out on a hot work tool sheet (H13) over a range of temperatures using different waveforms. At a temperature of 125 degree C, a slow-fast wave resulted in lower crack propagation rates than those with a balanced (or symmetrical) waveform. However, at 500 degree C normal fatigue crack propagation behaviour was observed in which the slow- fast wave was more damaging than a balanced waveform at the same frequency. Dynamic strain aging is attributed to the reversed crack propagation effect at 125 degree C. (Author abstract) 17 Refs.

133. Tang, Nai Yong Niessen, Paul Plumtree, Alan (Univ of Waterloo, Waterloo, Ont, Can). Enhanced fatigue crack growth rate at elevated temperatures. 1991; . CODEN: ZEMTAE; ISSN: 0044-3093.
Fatigue crack propagation (FCP) rates in air for AISI type H13 hot work tool steel were measured over the temperature range of 300 to 600 degree C. The frequency-dependent apparent activation energy for thermally activated crack growth was found to be lower than that for oxygen diffusion in ferrite. It is shown that this is the consequence of stress gradients at the crack tip which cause diffusion processes to be position dependent. (Author abstract) 32 Refs.

134. The Society of Die Casting Engineers. Transactions of the 4th National Die Casting Congress ; 1966 Nov 14; Cleveland, Ohio.

135. Thomson, P. F. Surface damage in electrodischarge machining. 1989; . CODEN: MSCTEP; ISSN: 0267-0836.
The effect of pulse duration and electrode type (copper or graphite) on the pick-up of carbon in the surface of a die steel shaped using electrodischarge machining and on surface microcracks has been studied. The present work suggests that the number and the size of surface microcracks increase with pulse duration when machining with a copper electrode, but there is some evidence to suggest that, when using a graphite electrode, the number and the length of microcracks and the average thickness of the recast layer may be greatest at intermediate (75-150 mu s) pulse durations. Although no definite conclusion can be drawn from the results, it is suggested that this may be because the manner of decay of the temperature field after each pulse is determined by both electrode material and pulse duration. At high current densities and long pulse durations, the length and frequency of microcracks is increased greatly at the corners of specimens machined using a graphite electrode, but this occurred to a much lesser extent when using a copper electrode - a difference that would seem to reinforce the suggestion that the characteristics of the temperature field after each pulse depend on the electrode material. It was concluded that carbon was absorbed from the dielectric (paraffin) rather than from the electrode. The amount of copper absorbed did not depend on pulse duration. (Author abstract) 19 Refs.

136. Tonghe, Zhang Chengzhou ,. Ji Jinghua, Shen Jun, Chen Wenlian, Lin Fujin, Tan Yuzun, Gao (Beijing Normal Univ, Beijing, China). Annealing behaviour of H13 steel implanted with N, Ti and Ti plus N. 1993; . CODEN: SCTEEJ; ISSN: 0257-8972.
Ion implantation is a non-equilibrium process. After annealing, the process proceeds from its non-equilibrium state and the radiation-induced damage will be removed gradually. The hardness of Ti-, N- and Ti plus N-implanted layers of H13 steel as a function of the annealing temperature was obtained. The hardness increased with increasing annealing temperature ranging from 400 to 600 degree C. The maximum hardness was obtained when annealing at a temperature of 500 degree C for 20 min; this hardness is 62% greater than that of the unannealed specimens. The compounds Fe//2Ti and Fe//2N have been identified by X-ray diffraction and transmission electron microscopy. After annealing, the compounds still remain in the implanted layers. The H13 steel is strengthened by the compounds and the dislocations. (Author abstract) 12 Refs.

134. The Society of Die Casting Engineers. Transactions of the 4th National Die Casting Congress ; 1966 Nov 14; Cleveland, Ohio.

135. Thomson, P. F. Surface damage in electrodischarge machining. 1989; . CODEN: MSCTEP; ISSN: 0267-0836.
The effect of pulse duration and electrode type (copper or graphite) on the pick-up of carbon in the surface of a die steel shaped using electrodischarge machining and on surface microcracks has been studied. The present work suggests that the number and the size of surface microcracks increase with pulse duration when machining with a copper electrode, but there is some evidence to suggest that, when using a graphite electrode, the number and the length of microcracks and the average thickness of the recast layer may be greatest at intermediate (75-150 mu s) pulse durations. Although no definite conclusion can be drawn from the results, it is suggested that this may be because the manner of decay of the temperature field after each pulse is determined by both electrode material and pulse duration. At high current densities and long pulse durations, the length and frequency of microcracks is increased greatly at the corners of specimens machined using a graphite electrode, but this occurred to a much lesser extent when using a copper electrode - a difference that would seem to reinforce the suggestion that the characteristics of the temperature field after each pulse depend on the electrode material. It was concluded that carbon was absorbed from the dielectric (paraffin) rather than from the electrode. The amount of copper absorbed did not depend on pulse duration. (Author abstract) 19 Refs.

136. Tonghe, Zhang Chengzhou ,. Ji Jinghua, Shen Jun, Chen Wenlian, Lin Fujin, Tan Yuzun, Gao (Beijing Normal Univ, Beijing, China). Annealing behaviour of H13 steel implanted with N, Ti and Ti plus N. 1993; . CODEN: SCTEEJ; ISSN: 0257-8972.
Ion implantation is a non-equilibrium process. After annealing, the process proceeds from its non-equilibrium state and the radiation-induced damage will be removed gradually. The hardness of Ti-, N- and Ti plus N-implanted layers of H13 steel as a function of the annealing temperature was obtained. The hardness increased with increasing annealing temperature ranging from 400 to 600 degree C. The maximum hardness was obtained when annealing at a temperature of 500 degree C for 20 min; this hardness is 62% greater than that of the unannealed specimens. The compounds Fe//2Ti and Fe//2N have been identified by X-ray diffraction and transmission electron microscopy. After annealing, the compounds still remain in the implanted layers. The H13 steel is strengthened by the compounds and the dislocations. (Author abstract) 12 Refs.

137. Tonghe, Zhang Fuzhong ,. Wei Jun, Chen Huixing, Zhang Xioji, Zhang Ting, Lu (Beijing Normal Univ, Beijing, China). Ion implantation of Ti, Mo W, Mo plus C and W plus C in H13 steel and aluminum at elevated temperature. 1994; . CODEN: MRSPDH; ISSN: 0272-9172. The chemical change in the surface of H13 steel or aluminum is produced by implanting a reactive elements, such as Ti, Mo and W. The X-ray diffraction pattern shows that implanted Ti at 400 degree C has reacted with carbon(0.35 in wt.%) forming a second phase TiC. Auger analysis shows that the carbon atoms have been condensed in the Ti implanted region. Carbon peak concentration of 30 At.% is greater than Ti atom peak concentration of 12 At.%. Several second phases are formed during pulsed Mo ion implantation into aluminum with high ion flux of 50approx.80 mu A/cm**2 which raises the target temperature from 400 degree C to 600 degree C. More second phases are formed by dual Mo plus C implantation with high dose of 3approx.5 multiplied by 101**7/cm**2 and high flux of 50approx.75 mu A/cm**2. And the target temperature is raised from 400 to 600 degree C. The FeMo, Fe//3Mo//2, Fe//2MoC, MoC, Mo//2C, MoCx phases and iron carbides are identified by X-ray diffraction technique. (Author abstract) 8 Refs.

138. Tonghe, Zhang Fuzhong ,. Wei Jun, Chen Huixing, Zhang Xioji, Zhang Ting, Lu (Beijing Normal Univ, Beijing, China). Ion implantation of Ti, Mo W, Mo plus C and W plus C in H13 steel and aluminum at elevated temperature. 1994; . CODEN: MRSPDH; ISSN: 0272-9172. The chemical change in the surface of H13 steel or aluminum is produced by implanting a reactive elements, such as Ti, Mo and W. The X-ray diffraction pattern shows that implanted Ti at 400 degree C has reacted with carbon(0.35 in wt.%) forming a second phase TiC. Auger analysis shows that the carbon atoms have been condensed in the Ti implanted region. Carbon peak concentration of 30 At.% is greater than Ti atom peak concentration of 12 At.%. Several second phases are formed during pulsed Mo ion implantation into aluminum with high ion flux of 50approx.80 mu A/cm**2 which raises the target temperature from 400 degree C to 600 degree C. More second phases are formed by dual Mo plus C implantation with high dose of 3approx.5 multiplied by 1017/cm**2 and high flux of 50approx.75 mu A/cm2. And the target temperature is raised from 400 to 600 degree C. The FeMo, Fe//3Mo//2, Fe//2MoC, MoC, Mo//2C, MoCx phases and iron carbides are identified by X-ray diffraction technique. (Author abstract) 8 Refs.

139. Tonghe, Zhang Fuzhong ,. Wei Jun, Chen Huixing, Zhang Xioji, Zhang Ting, Lu (Beijing Normal Univ, Beijing, China). Tribological properties for pulsed W plus C and Mo plus C dual

implanted H13 steel. 1994; . CODEN: MRSPDH; ISSN: 0272-9172.
The tribological properties for pulsed W plus C and Mo plus C dual implanted H13 steel are given in this paper. The pulsed ion of W, Mo and C were implanted at 40KV to dose of (3to approx.12) multiplied by 1017/cm**2 with ion flux from 25 to 100 mu A/cm**2 using MEVVA implanter. The results show that the wear resistance life and hardness of the dual implanted H13 steel increase 2to approx.3 times. The comparison of dual implantation with single implantation shows that the dual implantation is better. The tribological properties of W plus C dual implanted H13 steel is better than Mo plus C dual implanted H13 steel. The TEM and X-ray diffraction analysis show that the super high hardening dispersed phases of MoC, MoCx, WC and W//2C were formed during ion implanting. The iron compounds of tungsten and molybdenum and iron carbides were obtained also. That is, the strengthening effect in H13 steel of phases MoC and WC is better than FeMo, Fe//3Mo//2, Fe//2W and Fe//7W//6. (Author abstract) 7 Refs.

140. Tonghe, Zhang Fuzhong ,. Wei Jun, Chen Huixing, Zhang Xioji, Zhang Ting, Lu (Beijing Normal Univ, Beijing, China). Tribological properties for pulsed W plus C and Mo plus C dual implanted H13 steel. 1994; . CODEN: MRSPDH; ISSN: 0272-9172.
The tribological properties for pulsed W plus C and Mo plus C dual implanted H13 steel are given in this paper. The pulsed ion of W, Mo and C were implanted at 40KV to dose of (3to approx.12) multiplied by 1017/cm**2 with ion flux from 25 to 100 mu A/cm**2 using MEVVA implanter. The results show that the wear resistance life and hardness of the dual implanted H13 steel increase 2to approx.3 times. The comparison of dual implantation with single implantation shows that the dual implantation is better. The tribological properties of W plus C dual implanted H13 steel is better than Mo plus C dual implanted H13 steel. The TEM and X-ray diffraction analysis show that the super high hardening dispersed phases of MoC, MoCx, WC and W//2C were formed during ion implanting. The iron compounds of tungsten and molybdenum and iron carbides were obtained also. That is, the strengthening effect in H13 steel of phases MoC and WC is better than FeMo, Fe//3Mo//2, Fe//2W and Fe//7W//6. (Author abstract) 7 Refs.

141. Tottempudi, S. Effect of Annealed Microstructure on the Final Heat Treated Properties of Premium Grade H-13 Tool Steel [Master Thesis]. Norman, Oklahoma: The University of Oklahoma; 1994.

142. Totten E. George (ed.). Quenching and Distortion Control, Proceedings of the First International Conference on Quenching and Control of Distortion; 1992 Sep 22; Chicago, Illinois. Metals Park, Ohio: ASM International; 1992.

143. Transactions, NADCA 15th International Die Casting Congress and Exposition; 1989; St. Louis, MO.

144. Transactions, NADCA 15th International Die Casting Congress and Exposition; 1989; St. Louis, MO.

145. Trejo-Luna, R. Zironi ,. E. P. Rickards, J. Romero, G. (Univ Nacional Autonoma de Mexico, Mexico City, Mex). Some features of low-temperature ion nitriding of steels. 1989; . CODEN: SCRMBU; ISSN: 0036-9748.
Nitriding was carried out on several commonly used commercial steels such as L6, W2, M2, H13, H12, H11, D2 and 4140 (AISI). The usefulness of the ion nitriding process at low temperatures was studied. The correlation of microhardness and nitrogen concentration was shown to be valid in these steels. For conventionally nitrided samples the microhardness profiles were fit using the same diffusion constant as the ion nitrided counterpart, indicating that the same mechanism is involved in the diffusion. All steels studied showed enhanced surface hardness when ion nitrided at low temperatures (150 degree C), although some conventionally nitrided ones showed no measurable effect. 5 Refs.

146. Uddeholm. Tools for Die Casting, Proceedings of a Symposium; 1983 Sep 26; Sunne, Sweeden. : Sweedish Institute for Metals Research.

147. Umemoto M., Ohtsuka H. and Tamura I. Transformation to Pearlite from Work-Hardened Austenite. Transactions of the Iron and Steel Institute of Japan. 1983 Sep; 23(9).

148. Vanadium Alloys Steel Corp. Vascojet 1000 for Ultra High Strength Structural Requirements. ; 1959.

149. VanEcho J. and Simmons W.F. Suppplemental Report on the Elevated Temperature Properties of Chromium-Molybdenum Steels. ; 1966 Jun; ASTM Data Series Publication No. DS

6S1.

150. Viscount 44 (Hot Work Die Steel, AISI Type H13). Alloy Dig. ; 1990 Mar.
0002-614X. Viscount 44 is a free machining "ready-to-use" Type H13 hot work die steel with good strength retention at 427-538 deg C. At the hardness range furnished by the mill (42-46Rc), machining of Viscount 44 is considerably more difficult than that of annealed tool steels. In turning, facing and shaping operations, reduced cutting speeds at normal feeds and depths of cut, with resultant decrease in metal removal rates of approx 30%, should be contemplated. Carbide tools are most commonly used but high-alloy grade high-speed steels (M3-3, T15, M42, or for short runs M2 or M7) are widely used for drills, die sinking cutters and taps. Applications include: grippers on straightening equipment, vice jaws, tool holders, punches, forming heads, shafts and many other general uses. It is highly adaptable to a wide range of engineering and maintenance applications.--AA.

151. Wallave J.F. and Hakulinen E. Influence of Cooling Rate on the Microstructure and Toughness of Premium Grade H-13 Die Steels. Transactions, NADCA 15th International Die Casting Congress and Exposition; 1989; St. Louis, MO. ; Paper No. G-T89-013.

152. White, C. V.; Luxon, J. T.; Zynda, L. M. Laser Surface Modification of H13 Hot Forming Tool Steel. Technology Vectors. ; 1984.
H13 tool steel is a thermal shock resistant tool steel used in a wide variety of hot forming applications including forming applications where water is used as a coolant. Failure of the tools is not well understood, but apparently is the result of thermal stress cracking and subsequent erosion by metal to metal sliding and escaping water and steam. It has been proposed that laser heat treatment and/or surface melting of the critical areas of certain tools could improve tool life. Placement of one or two 6 to 7 mm wide laser surface melted tracks on the high wear area of the selected hot forming tools has resulted in an increase in tool life by a factor of at least 2.5. Improved performance is the result of increased hardness and the homogenization of the melt layer.--AA.

153. Worzala F. J. and Shong D.S. Thermal Processing, Microstructure and Properties of H-13 Die Steels. Proceedings of an International Conference on Tool Materials for Molds and Dies. : Colorado School of Mines; 1987 Oct.

154. Yang, Jianhua Zhang ,. Tonghe (Nantong Textile Technology Inst, Nantong, China). RBS and TEM analysis of N plus implanted TiN layers. 1993; . CODEN: 001013; ISSN: 1003-3213. N plus ions with an energy of 100KeV were implanted in TiN layers plated on H13 steel. The RBS analysis of TiN layers illustrated that Fe and Ti atoms mixing on Fe-TiN interface can be resulted from ion implantation. The TEM analysis of the cross-section of implanted layers proved that N plus implantation can disperse the big Ti grains in the layer, make TiN grains small and also transfer alpha -Ti into delta -TiN and epsilon -Ti//2N mixing phase. Finally, the mechanism of the improvement of the wear resistance was given. (Edited author abstract) 2 Refs.

155. Zhang, T.; Ji, C.; Shen, J.; Chen, J.; Lin, W.; Tan, F.; Gao, Y. (Beijing Normal University). Annealing Behaviour of H13 Steel Implanted With Nitrogen, Titanium and Ti + N. Seventh International Conference on Surface Modification of Metals by Ion Beams. Surface and Coatings Technology. ; 1993 Jan 9: 56, (2) 143-149.
0257-8972. Ion implantation is a non-equilibrium process. After annealing, the process proceeds from its non-equilibrium state and the radiation-induced damage will be removed gradually. The hardness of titanium-, nitrogen and Ti + N-implanted layers of H13 steel as a function of the annealing temperature was obtained. The hardness increased with increasing annealing temperature ranging from 400-600 deg C. The maximum hardness was obtained when annealing at a temperature of 500 deg C for 20 min; this hardness is 62% greater than that of the unannealed specimens. The compounds Fe sub 2 Ti and Fe sub 2 N have been identified by X-ray diffraction and transmission electron microscopy. After annealing, the compounds still remain in the implanted layers. The H13 steel is strengthened by the compounds and the dislocations.

156. Zhang, T.; Ji, C.; Shen, J.; Chen, J.; Tan, F.; Gao, Y. (Beijing Normal University). The Influence of Titanium, Nitrogen and Titanium + Nitrogen Implantation on Phase Change, Microstructure, Growth of Metallic Compounds and Correlated Effects in Hardness and Wear Resistance in H13 Steel. Nuclear Instruments and Methods in Physics Research, Section B. 1992 Dec; : B72, (3-4) 409-420; ISSN: 0168-583X.
The lattice damage, small intermetallic-compound (Fe sub 2 Ti) and metallic-compound (titanium nitride, Fe sub 2 N) formation, and supersaturated solution of Ti or titanium + nitrogen-ion implanted into steel with various ion doses and energies were measured by TEM and X-ray diffraction. Formation and growth of the metallic compound was found to depend

on ion dose and energy. Changes of phases and microstructure were particularly enhanced with high dose and high energy. Metal hardening also increased with increasing ion dose, energy and the amount and size of metallic compounds. Specimens implanted at target temperatures ranging from 300-400 deg C (HT) or implanted at room temperature (RT) and then annealed at temperatures ranging from 300-500 deg C, showed significant increase in hardness. The wear resistance of high energy and high dose implanted steel is better than that of low energy and lower dose implantation. The wear rate decreases 2-2.6 times for low temperature implantation, 10.4 times for HT implantation and high energy implantation. The Fe sub 2 Ti and TiC precipitates, phase and microstructural changes in the implanted layer are responsible for such a drastic reduction in wear.

157. Zhang, Tonghe Ji ,. Chengzhou Yang, Jianhua Chen, Jun Shen, Jinghua Lin, Wenlian Gao, Yuzun Sun, Guiru (Beijing Normal Univ, Beijing, China). Formation of intermetallic compounds with a high flux pulse molybdenum ion beam in steel and aluminium. 1992; . CODEN: SCTEEJ; ISSN: 0257-8972.

Intermetallic compounds of molybdenum and tungsten implanted into H13 steel and aluminium were measured by transmission electron microscopy (TEM) and X- ray diffraction. Ions extracted from a metal vapor vacuum are source with around 25-100 keV energy and a dose range (1-5) multiplied by 10**17 cm minus 2 were used for implantation. The ion fluxes were 25, 47, 68 and 320 mu A cm minus 2. It was found from the results that the target temperature increases with increasing ion flux from 310 degree C (25 mu A cm** minus **2) to 580 degree C (68 mu A cm** minus **2). Intermetallic compounds such as FeMo, Al//2Mo, Al//1//2Mo, Fe//7W, Fe//2W and Al//5W, were easily observed by TEM and X-ray diffraction when the flux was greater than 47 mu A cm** minus **2. In situ observation in a high voltage transmission electron microscope (HVEM) was used to investigate the structure and formation of intermetallic compounds of molybdenum-implanted H13 steel. The electron diffraction pattern of FeMo precipitates appeared at 500 degree C. Recrystallization and grain growth occurred at 650 degree C. (Author abstract) 8 Refs.

158. Zhang, Tonghe Ji ,. Chengzhou Shen, Jinghua Chen, Jun Lin, Wenlian Sun, Guiru Gao, Yuzun (Beijing Normal Univ, Beijing, China). Influence of target temperature and dose on metallic strengthening for titanium implantation into steel. 1992; . CODEN: SCTEEJ; ISSN: 0257-8972.

The formation of intermetallic compounds on titanium implantation into H13 steel at different

target temperature (minus 196, 150 and 400 degree C) is studied. The steel strengthening mechanism of titanium impl antation with different doses and target temperatures was discussed. The titanium ions are implanted in the energy range from 100 to 300 keV and dose range from 1 multiplied by 10**1**7 to 5.5 multiplied by 10**1**7 cm** minus **2. The observations of phase change, microstructure and intermetallic compounds were carried out by high voltage (1 MV) electron microscopy and X-ray diffraction analysis. The hardness of the implanted layer increases one to 2.5 times for low temperature (minus 196 and 150 degree C) implantation, two to three times for moderate temperature (MT) (400 degree C) implantation. The wear rate decreases two to 2.6 times for low temperature implantation and ten times for MT implantation. The influence of target temperature and dose on metallic strengthening is discussed. (Author abstract) 10 Refs.

159. Zlepping, W. Schindler ,. A. and Kogler E. Research Knowledge Helps Die Steel Selection in Dayly Practice. Proceedings of an International Conference on Tool Materials for Molds and Dies. : Colorado School of Mines; 1987 Oct.